Title
GRAIN BOUNDARY STRUCTURE IN BODY-CENTERED CUBIC MATERIALS

Author
Kamenetzky, E.A.

Publication Date
1985-10-01

Lawrence Berkeley Laboratory
UNIVERSITY OF CALIFORNIA

Materials & Molecular Research Division

GRAIN BOUNDARY STRUCTURE
IN BODY-CENTERED CUBIC MATERIALS

E.A. Kamenetzky
(Ph.D. Thesis)

October 1985

Prepared for the U.S. Department of Energy under Contract DE-AC03-76SF00098

DISCLAIMER

GRAIN BOUNDARY STRUCTURE IN BODY-CENTERED CUBIC MATERIALS

Eduardo Alberto Kamenetzky

Ph. D. Thesis

Materials and Molecular Research Division
Lawrence Berkeley Laboratory
and
Department of Materials Science and Mineral Engineering
University of California
Berkeley, CA 94720

October 1985

This work was supported by the Director, Office of Energy Research, Office of Basic Energy Sciences, Materials Science Division of the U.S. Department of Energy under Contract No. DE-AC03-76SF00098.

GRAIN BOUNDARY STRUCTURE IN BODY-CENTERED CUBIC MATERIALS

Eduardo Alberto Kamenetzky

ABSTRACT

A method has been developed to study the atomic structure of grain boundaries in BCC materials. Rigid body displacements between two grains are calculated. These displacements result in groups of atoms that retain first or second-nearest neighbor distances across the boundary. After further individual atom relaxations, the atoms at the boundary form distorted polyhedra whose edges have the length of the first or second-nearest neighbor distances. The boundary structure can be described by these structural units. Certain favored boundaries are composed of only one type of polyhedron while intervening boundaries are composed of mixtures of the polyhedra of the favored boundaries.

Several structural unit descriptions are possible for each boundary. The most likely structure is chosen on the basis of the criteria of highest symmetry, maximum coordination and minimum excess volume at the boundary. A study of the symmetry of the grain boundaries in terms of color symmetry groups is given. Some structures are related by the addition of one layer of atoms parallel to the boundary, or, since the excess volume is equal for those boundaries, by an in-plane displacement. Possible transformations between these structures have important implications in the phenomena of grain boundary segregation. The crystallographic concepts to study rigid-body translations and their equivalent in-plane displacements are described in detail.

It is shown that the structure of the boundaries as given by the structural unit model agree well with high-resolution electron microscopy observations.

TABLE OF CONTENTS

page

1. INTRODUCTION

1.1. Objective

Grain boundaries affect the physical properties of polycrystalline materials. The relationships between grain boundary structure and grain boundary phenomena are not well established due to a lack of data on the atomic structure of grain boundaries. In particular, very little work has been done on the characterization of atom positions at grain boundaries in body-centered cubic (BCC) materials. In this investigation, an effort has been made to model the atomic structure of BCC grain boundaries in a way which is consistent with the available experimental data. A method to study the structural features of grain boundaries has been developed in order to better understand the systematic variations in structure which appear in BCC symmetrical tilt boundaries. The results have been generalized to other geometries and the implications of the atomistic description on interfacial phenomena have been examined.

1.2. Grain Boundaries in Metals

A grain boundary is the region where two crystals, differing only in orientation, are in contact with each other. For materials that are used in polycrystalline form, grain boundaries influence a number of chemical, kinetic, magnetic, electronic, and mechanical properties. The experimental characterization of these effects constitutes a significant portion of the metallurgical literature. In order to characterize grain boundary effects systematically a number of grain boundary properties have been defined and studied, these are: energy, segregation, diffusion, migration, and sliding. The two categories of migration and sliding refer to movement of the boundary normal or parallel to itself. Historically, these concepts are associated with recrystallization and

creep, respectively. Modern views of the fundamental mechanisms underlying migration and sliding contend that they both occur by the interaction of point defects, crystal dislocations and grain boundary dislocations. In general, the accommodation of deformation at grain boundaries under a wide variety of internal and external conditions occurs by the interaction of the defects mentioned above. The other important physical entity to describe is the grain boundary structure. Without this knowledge any grasp of electronic and magnetic properties is entirely impossible. In addition, knowlege of the grain boundary structure leads to a better understanding of all grain boundary properties and their inter-relationships.

As the crystal systems of two grains are related by an orthogonal transformation, the simplest way to define the crystallography consists of the axis (the real eigenvector) which is the the direction in the two crystals that remains unchanged, and the angle which describes the rotation around that axis. This description is usually referred to as the axis-angle pair $[hkl]/\theta$. In addition one can define the indices of the grain boundary plane. This simple description will suffice for now. The next chapter is entirely dedicated to crystallographic studies of grain boundary structure.

The 1957 comprehensive review of the experimental literature by McLean reached no definitive conclusion on the structure of grain boundaries. [1] However, it disproved a number of early models and it inferred that the atomic arrangements are such that some order exists at the interface and atomic bonding is not substantially different from that in the crystal. Grain boundaries are usually divided into small-angle and large-angle categories according to the magnitude of the angle of misorientation. When the misorientation is small ($\theta < 10^\circ$), the rotation can be decomposed into small translations and the boundary is described as a network of dislocations. [2] The

structure of a small-angle interface has patches of perfect crystal structure and regions of disregistry at the core of dislocations. The experimental evidence for this model was reviewed in 1959. [3] This model does not apply to large-angle boundaries because the dislocations are so close that the cores overlap. The next important concept to be developed was that of the coincidence-site lattice (CSL). This was a concept first introduced by Friedel [4] for the analysis of twin structures. For certain misorientations about rational axes there exist superlattices on which a fraction $1/\Sigma$ of the lattice points of either crystal lie. Each of these lattices is designated by the letter Σ and the value of the fraction; for example the misorientation [100]/36.9° produces a $\Sigma 5$. Coincidence-site lattices are discussed in detail in section 2.2. The concept of the CSL was reintroduced on the belief that large angle misorientations that have a corresponding CSL would have grain boundaries that show good atomic fit.[5] The best fit and hence the lowest energy would occur when the interface follows a plane containing a high density of coincidence sites. These ideas where greatly expanded by Bollmann[6] who generalized the concept of CSL to a lattice that is now continuous in the misorientation by extending coincidence to internal positions within the unit-cell. But most important he defined a set of translations that can preserve a CSL for small deviations from a perfect CSL misorientation. In 1972 Gleiter and Chalmers published an extensive review of large angle grain boundary properties.[7] They gave account of a series of systematic experiments performed by the French group at Saint Etienne that showed that some CSL grain boundaries had special properties.[8] Pumphrey reviewed the properties of these special large-angle grain boundaries a few years later, but there was still no clue as to why certain boundaries show special behavior and others do not.[9]

This brief historical review has already introduced some of the key questions that this work addresses. Given that the boundary region is ordered, is there a way to base the atomic structure of the interface on some simple geometrical parameters? Would that description be unique? Could boundaries with special properties be predicted? These questions will be addressed throughout this work.

Over the last ten years there has been a substantial amount of theoretical and experimental work on the structure and properties of grain boundaries. The heart of this research activity is reviewed periodically in international conferences and meetings. [10] [11] One of the important theoretical developments is the use of computer simulation methods based on interatomic potentials which are functions only of the atomic nuclei coordinates. This assumption greatly simplifies the solution of the mathematical problem which is the many-body time-dependent relativistic wave equation. An array of atoms is initialized (position and velocity) and the evolution of the array as the atoms interact according to the given force law is observed. In principle, a minimum energy configuration for each physical situation can be obtained. Starting from a CSL misorientation, the relaxation to a minimum energy configuration is usually described as a combination of a rigid body translation of one crystal with respect to the other and further individual atom relaxations. A detailed description and critique of these methods are presented in chapter 3. The atomistic calculations suggest the existence of certain structural units at the boundary which are compact polyhedral arrangements of atoms. [12] A simpler procedure is to consider the packing of atoms in bicrystals made up of hard spheres. The conclusions of this work for face-centered cubic materials (FCC) is exactly the same as the atomistic calculations.[13] The author has extended the hard-sphere model to the case of body-centered cubic (BCC)

materials and has made the analysis systematic. The analytical procedure and computer code are presented in chapter 3. The character of the polyhedral arrangements are also discussed in that chapter. The resulting grain boundary structures are described in chapter 4. None of these models provide complete answers to the questions stated above. However, the models presented in this work offer significant insight into the structure and physical behavior of grain boundaries. Thus, the implications of our present work are discussed in chapter 6.

Experimentally, the most significant progress in understanding grain boundary structure was made by advanced transmission electron microscopy (TEM) techniques. Standard TEM allows the determination of the orientation of abutting crystals by several diffraction techniques, and the study of the displacement field of grain boundary dislocations by dynamical strong and weak beam techniques. The author has used these techniques to study the accommodation of deformation at BCC grain boundaries. [14] Analytical electron microscopy has been used to study the modulation of segregation along a grain boundary, [15] to study the relationship between the amount of segregation and structure, [16] and to study the variations of concentration across a grain boundary in a number of materials. [17] Several techniques are available to measure relative rigid-body displacements between grains. For example, the intensity profiles of the stacking-fault like fringes formed at inclined CSL interfaces can be measured and compared with simulated images. [18] Present day electron microscopes are capable of directly resolving the atomic structure of boundaries by phase contrast imaging. [19] The atomic arrangements can be deduced from the images, and a simple measurement of lattice- or moiré-fringe displacement between two points across the boundary gives a more accurate estimate of the rigid body displacement than the

technique mentioned above. [20] Details of high-resolution electron microscopy (HREM) studies are discussed in chapter 5. The technique of preparing specimens suitable for HREM are presented, and the results are analyzed in detail. Image simulation procedures used in the interpretation are also discussed in that chapter. These image simulation techniques also indicate the potential of HREM techniques to study grain boundary segregation.

This brief historical perspective has indicated the points in grain boundary research that this work addresses. Hopefully, it has given the reader a sense of where this work fits in the overall area of research in grain boundary structure and properties, and it has also given the reader an overall plan of the presentation. The questions that are sketched here are discussed in detail throughout this work.

1.3. Special Boundaries

The author has taken the view that a detailed knowledge of grain boundary structure will lead to qualitative predictions on grain boundary properties which could have significant implications on the engineering of materials. Thus, this work is not *in vacuo* and has to relate and explain the available experimental data. The most important sets of experimental grain boundary property data that relate to this work are reviewed here; they all point to the existence of certain boundaries that have special properties. This data will serve the purpose of defining some grain boundary properties, and of explaining the selections of particular types of grain boundaries to be studied. Most of the experimental data available is on FCC materials; this is one of the reasons why the author has embarked on the study of the BCC grain boundaries.

A thermodynamic approach is a global approach that allows the description of macroscopic situtations close to the actual phenomena in terms of state variables. In order to introduce a surface between two bodies at the same temperature, same pressure, and same composition, a state variable is defined which is the energy of the interface. The corresponding intensive parameter γ can be regarded as an energy per unit area or a force per unit length of perimeter of the surface A. The total energy variation for such a system is

$$dE = T \cdot dS - P \cdot dV + \sum_i \mu_i \cdot dN_i + \gamma \cdot dA \tag{1.3.1}$$

where all symbols have their standard thermodynamic meaning. The quantity γ is then the work (change in free energy) necessary to enlarge an interface by an unit area at constant temperature, pressure, and number of atoms.

$$\gamma = \left.\frac{\partial F}{\partial A}\right|_{T,V,N_i} \tag{1.3.2}$$

Equilibrium considerations show that grain boundary energies at a grain boundary junction are related to the dihedral angles by [21]

$$\frac{\gamma_{23}}{\sin\phi_1} = \frac{\gamma_{13}}{\sin\phi_2} = \frac{\gamma_{12}}{\sin\phi_3} \tag{1.3.3}$$

An experimental method to measure relative grain boundary energies is to use a three-grain flat specimen with orientation of the grains so chosen that the junction line of the three grains will be straight throughout the thickness and perpendicular to the surface of the specimen. [22] The orientations of the specimen can be determined by reorientation and growth of seed crystals. The relative energies can be measured using Eqn. 1.3.3. The results for a systematic study of misorientations around a [110] [23] and a [100] [24] axis in Fe+3.5%Si are shown in Figures 1.3.1 and 1.3.2 respectively. The results indicate a cusp in the energy curve at the twin boundary $\Sigma 3$ for the [110] boundaries and in the vicinity of $\Sigma 5$ or $\Sigma 29$ for the [100] case. The use of the axis/angle pair as the sole indication of the crystallography is not sufficient, as will be discussed in section 2.2. The means of determining the crystallography for this set of experiments were not very precise and so the position of the cusps is within ± 2 °. The [110] series was reexamined by the technique of thermal etching pits which gives a quantitative value of the boundary energy. [25] In this case a measurement of the dihedral angles at the intersection of a bicrystal with the surface enables the grain boundary energy to be related to the surface energy. Again, using Eqn. 1.3.3 a quantitative estimate of the boundary energy can be obtained since the surface energies are known quantities. The results indicate additional cusps at orientations corresponding

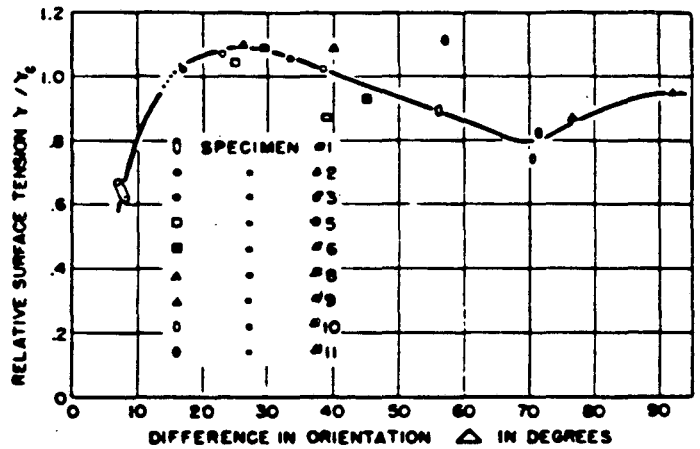

Fig. 1.3.1 Variation of relative surface tension with difference in misorientation for [110] tilt boundaries (from Dunn and Lionetti, *op.cit.*).

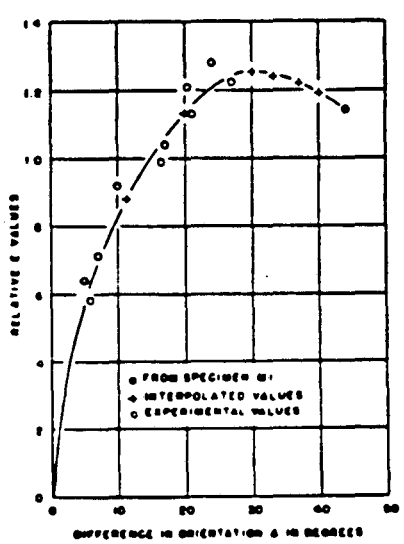

Fig. 1.3.2 Variation of relative surface tension with difference in misorientation for [100] tilt boundaries (from Dunn, Daniels and Bolton, *op.cit.*).

to $\Sigma 51$, $\Sigma 19$, and $\Sigma 9$ in order of increasing angle.

Crystallographically the orientation of the boundary plane is important since even by thermodynamic considerations the shape of an interface is not given by T and P alone, because the area can also change. The equilibrium form is such that $\int_S \gamma \cdot dA$ is a minimum. Faceting of grain boundaries is commonly observed, and the variations of energy with grain boundary orientation can be described with the aide of a Wulff plot. From Eqn. 1.3.1 written for a dilute binary system, and making some reasonable approximations, it may be shown that the excess solute at the grain boundary Γ_b at constant temperature is given by [26]

$$\Gamma_b = -\frac{1}{RT}\frac{d\gamma}{d\ \ln X_c} \tag{1.3.4}$$

where X_c is the solute molar content. Experimentally a measure of γ as a function of X_c can be obtained. The thermodynamic approach regards the grain boundary as a black box but provides insight into the phenomena of faceting and segregation.

A powerful technique to study naturally occurring low energy boundaries is the formation of small bicrystal particles that result from a chemical reaction. Bicrystals result from the deposition on a container wall of single and bicrystals of iron 10-50 μ in size after the reduction of iron chloride in hydrogen at 680 °C. The crystals grow isolated from each other so that a bicrystal forms by the nucleation of one of the crystals on the surface of the other. The relative orientation was measured by electron channeling patterns; the frequency of occurance of bicrystals with a common [100] axis is shown in Figure 1.3.3. [27] The numbers on the vertical lines are Σ values of coincidence systems; the existence of dense parallel planes is also indicated. The histogram

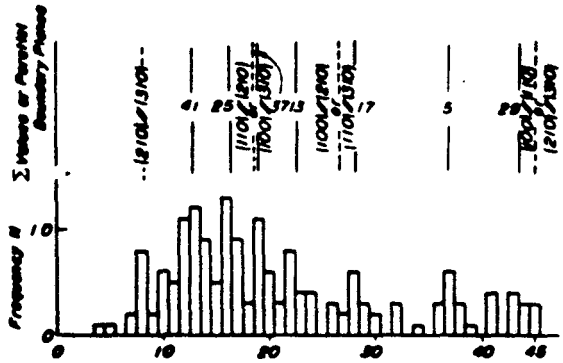

Fig. 1.3.3 Histogram of rotation angle about [100] axis for deposited bicrystals of iron. Solid lines indicate CSLs while broken lines indicate two densely packed lattice planes parallel (from Ishida and Yamamoto, *op.cit.*).

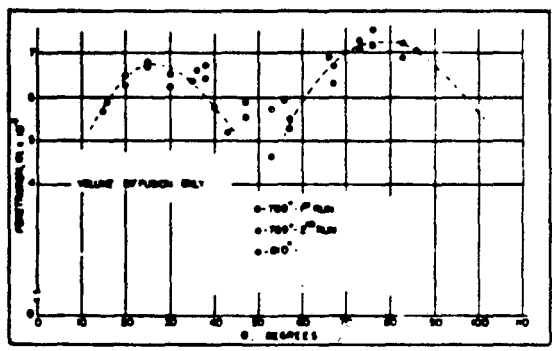

Fig. 1.3.4 Depth of grain boundary penetration as a function of angle of misorientation for [110] tilt boundaries (from Haynes and Smoluchowski, *op.cit.*).

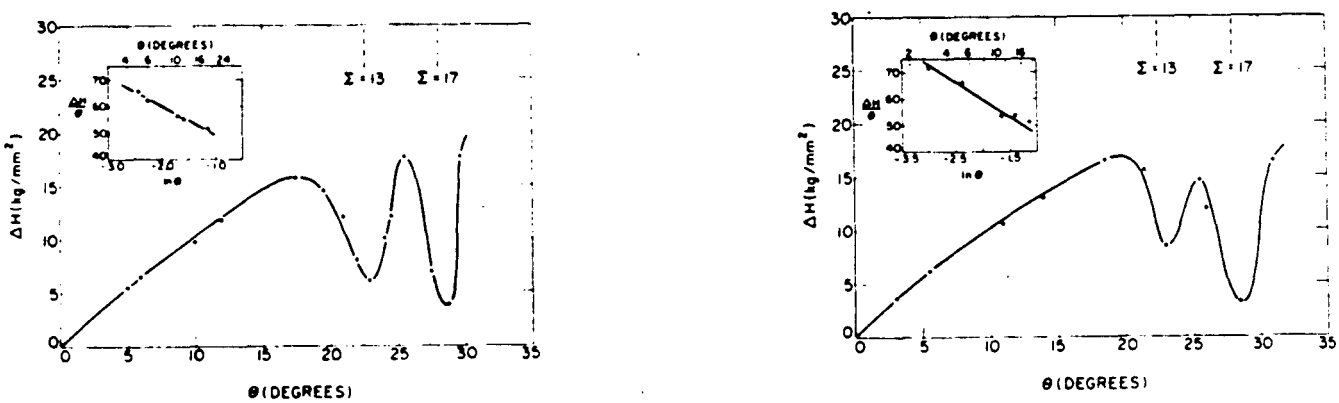

(a) (b)

Fig. 1.3.5 Variation of relative hardness ($\Delta H = H_b - H_c$) with misorientation angle; (a) (010)/[100] symmetrical tilt boundaries; (b) $(01\bar{1})$/[100] symmetrical tilt boundaries (from Chou, Cai, Romig and Lin, *op.cit.*).

shows that coincidence and near-coincidence boundaries occur more frequently than others. In a detailed analysis of these experiments it was shown that 90% of the boundaries were symmetrical tilt boundaries when the rotation angle is less than 30° and only 10% when the rotation angle is over 37°. [28] The boundaries near a misorientation of 45° are mostly asymmetrical.

Because the structure of the boundary is more open than the lattice, very high atomic mobility exists at the interface compared to that in the bulk. Grain boundary short circuit diffusion plays a crucial role in the kinetics of microstructural changes. To model this phenomenon the grain boundary is thought to be a slab of uniform thickness (2a). The change of concentration inside the slab results from the divergence of a flux with diffusion coefficient D_b and from exchanges with the lattices at the end of the slab. The concentration inside the slab is uniform. Fick's law inside the slab is written as

$$\frac{\partial c_b}{\partial t} = D_b \frac{\partial^2 c_b}{\partial y^2} + \frac{D}{a}\frac{\partial c}{\partial x}\bigg|_{x=a+\epsilon} \tag{1.3.5}$$

where all symbols have their standard meaning. This equation has an exact solution which allows one to compare experimental data with calculated profiles and thus estimate the grain boundary diffusion coefficient. [29] Experimentally, the penetration depth of a tracer element can be used as a measure of the grain boundary diffusivity. The exact determination of the interfacial diffusion coefficient requires complete information on the isoconcentration contours. Haynes and Smoluchowski conducted a series of experiments in [110] bicrystals of silicon iron and found that the penetration depth changed with the misorientation angle. [30] Figure 1.3.4 illustrates their data. The data indicates that the twin boundary, $\Sigma 3$, and the $\Sigma 19$ boundary are open

structures. This is contrary to other experimental data that indicates that the ideal twin boundary does not show preferential diffusion, and it seems to indicate a twin orientation with an asymmetrical boundary plane. Minimal grain boundary diffusivity occurs in the vicinity of $\Sigma 11$ indicating a close structure. The lack of crystallographic data on the boundary planes implies that this data should be taken only as an indication of the existence of special boundaries and it does not give rise to a systematic trend.

Similarly, because of the openess of the interfacial structure, the mechanical properties of a bicrystal are different than that of a single crystal. Chou *et.al.*, report on microhardness measurements of controlled bicrystals. [31] The boundary hardness is usually higher than the crystal because of segregation which also causes embrittlement. In these experiments the entire crystallography was well defined and the mean boundary plane was kept constant (this concept is discussed in section 2.2). Thus two sets of data for [100] bicrystals are shown in Figures 1.3.5, one for (010) and one for $(01\bar{1})$ mean boundary plane. The data indicates that the low Σ CSL boundaries are low energy configurations which show a relatively small amount of hardening at the interface. Similar experiments on the groove depth after a nitric-hydrofluoric etch show a minimum at the same boundaries as in Figure 1.3.5. [32]

The data presented in this section shows the existence of CSL related grain boundaries with special properties but no apparent correlation with CSL crystallography in their behavior. The author's studies are concerned with the structure of CSL grain boundaries. In an effort to relate his observations with available experimental data the boundaries chosen for these studies were selected based on this data. *The ranges of interest for the study of variations of structure with misorientation angle are from*

$\Sigma 3$ to $\Sigma 1$ for the [110] boundaries and from $\Sigma 5$ to $\Sigma 1$ for the [100] boundaries.

The crystallography of these boundaries is studied in chapter 2. The method of calculation of structure is detailed in chapter 3 and results presented in chapter 4. Experimental observations are discussed in chapter 5, and the implications of this work close the presentation.

1.4. References

[1] D. McLean, *Grain Boundaries in Metals* , Oxford U. Press, Oxford, 1957.

[2] W. T. Read, *Dislocations in Crystals* , McGraw-Hill, New York, 1953.

[3] S. Amelinckx and W. Dekeyser, *Solid State Phys.* **8** ,325 (1959).

[4] J. Friedel, *Lecons de Cristallographie* , Blanchard, reprint of 2nd. ed., Paris, 1964.

[5] M. L. Kronberg and F. H. Wilson, *Trans. A.I.M.E.* **185** ,501 (1949).

[6] W. Bollmann, *Phil. Mag.* **16** ,363 and 383 (1967).

[7] H. Gleiter and B. Chalmers, *Prog. Matls. Sci.* **16** ,(1972).

[8] G. Hasson, J.-Y. Boos, I. Herbeuval, M. Biscondi, and C. Goux, *Surf. Sci.* **31** ,115 (1972).

[9] P. H. Pumphrey, in *Grain Boundary Structure and Properties* , G. A. Chadwick and D. A. Smith (eds.), Academic Press, New York, 1976.

[10] *Grain Boundary Structure and Kinetics* , ASM Matls. Sci. Sem. 1979, ASM, Metals Park, Ohio, 1980.

[11] *Structure et Proprietes des Joints Intergranulaires* , J. de Physique **C6** , 1982.

[12] V. Vitek, A. P. Sutton, D. A. Smith, and R. C. Pond, in *Grain Boundary Structure and Kinetics* , ASM Matls. Sci. Sem. 1979, ASM, Metals Park, Ohio, 1980, p.115.

[13] H. J. Frost, M. F. Ashby and F. Spaepen, *Grain Boundary Structure and Kinetics* , ASM Matls. Sci. Sem. 1979, ASM, Metals Park, Ohio, 1980, p.149.

[14] E. A. Kamenetzky and R. Gronsky, *Res Mechanica* **8** ,185 (1982).

[15] J. Briceno Valero and R. Gronsky, in *Solid-Solid Phase Transformations* , H. I. Aaronson *et.al.* (eds.), The Metall. Soc. of AIME, Warrendale, PA, 1982, p.439.

[16] J. H. Rose and R. Gronsky, *Appl. Phys. Lett.* **41** ,993 (1982).

[17] J. B. Vander Sande, A. J. Garrat-Reed, Y.-M. Chiang and T. Thorvaldsson, *Ultramicros.* **14** , 65 (1984).

[18] R. C. Pond, *J. Micros.* **116** ,105 (1979).

[19] R. Gronsky, in *Grain Boundary Structure and Kinetics* , ASM Matls. Sci. Sem. 1979, ASM, Metals Park, Ohio, 1980, p.45.

[20] G. J. Wood, W. M. Stobbs, and D. J. Smith, *Phil.Mag.* **A50** ,375 (1984).

[21] J. P. Hirth and J. Lothe, *Theory of Dislocations* 2nd. ed., J. Wiley, New York, 1982, pp.698-699.

[22] C. G. Dunn, *J. Metals* **1** ,72 (1949).

[23] C. G. Dunn, and F. Lionetti, *J. Metals* **1** ,125 (1949).

[24] C. G. Dunn, F.W. Daniels and M.J. Bolton, *J. Metals* **2** ,1245 (1950).

[25] Y. S. Avraamov, A. G. Gvozdev, and V. M. Kutsak, *Phys. Metals. Metallog.* **36** , no.5, 198 (1973).

[26] M. P. Seah, *J. Phys. F* **10** ,1043 (1980).

[27] Y. Ishida, T. Yamamoto, and S. Kimura, *Proc. Eighth. Intl. Congr. Electron Micros.* , Canberra, 1974, p.596.

[28] Y. Ishida and T. Yamamoto, *Trans. Jap. Inst. Met.* **18** ,221 (1977).

[29] G. Martin and B. Perraillon, in *Grain Boundary Structure and Kinetics* , ASM Matls. Sci. Sem. 1979, ASM, Metals Park, Ohio, 1980, p.239.

[30] C. W. Haynes, and R. Smoluchowski, *Acta Met.* **3** , 130 (1955).

[31] Y. T. Chou, B. C. Cai, A. D. Romig, and L.S. Lin, *Phil. Mag.* **A47** ,363 (1983).

[32] X. R. Qian and Y. T. Chou, *Phil. Mag.* **A45** ,1075 (1982).

2. THE CRYSTALLOGRAPHY OF GRAIN BOUNDARIES

2.1. Introduction: Geometrical Models of Grain Boundaries

The geometrical models of grain boundary structure are at the heart of current thinking on the structure and properties of grain boundaries. Although the actual atomic arrangements are quite different from what these models would predict, the geometrical models provide a way to study the crystallography and symmetry of grain boundaries. All of the current studies on grain boundary phenomena use the geometrical models in their analysis. The actual atomic arrangements have come to be seen as a deviation from the structure predicted by geometrical means. It is the purpose of this chapter then to introduce these concepts which allow us some insight into the crystallography of grain boundary structure. As in the study of a single crystal much can be learned from the analysis of a perfect unit cell . Once this ideal block has been determined, it becomes apparent that a number of properties depend on the deviation from a perfect crystal, the imperfections or defect structure. Later in this thesis, variations on the analysis established in this chapter are considered. But there is a twist: these deviations constitute a defect structure for the crystal itself, while on top of it a grain boundary defect structure will be added that results from the interaction of crystal defects with the grain boundary. The categories in the analysis of grain boundary structure are perhaps best illustrated in Fig. 2.1.1.

The two most important concepts in the analysis of interfaces in general are the coincidence-site lattice and the displacement-shift-complete lattice. These two concepts were presented in detail in a previous publication, [1] and in several current reviews of the grain boundary literature. [2],[3] For the sake of completeness, the basic

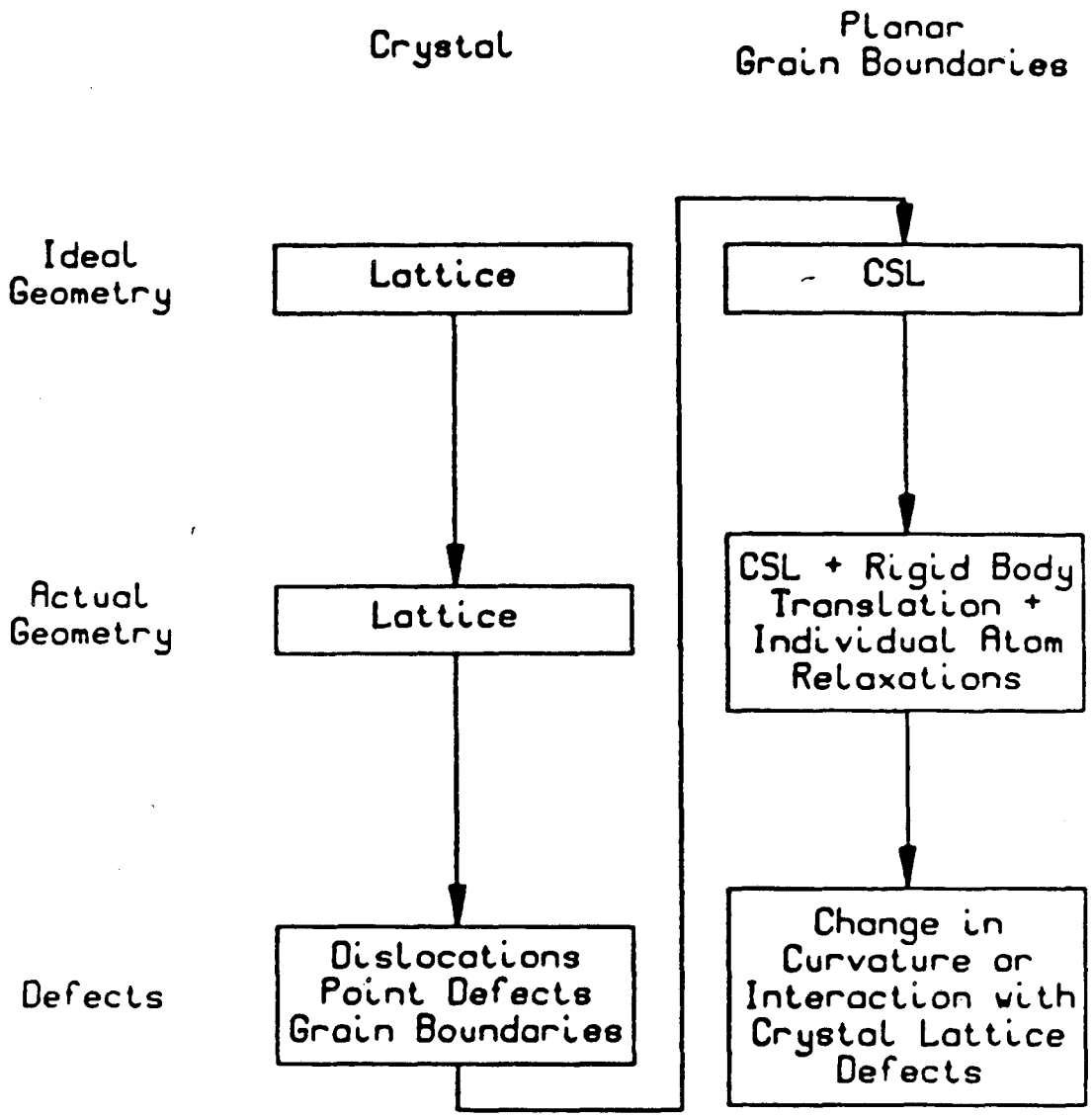

Fig. 2.1.1 Categories used in structural studies of perfect crystals and grain boundaries. Arrows indicate the way the analysis proceeds.

properties of these two lattices will be briefly reviewed in the next section. The later sections of this chapter deal with more advanced concepts of the geometrical models which are not treated in detail in the references above or the grain boundary literature in general. These concepts are essential in the development of the arguments in this thesis, and thus are explained in detail. The first quantity to be studied (section 3) is the planar density of coincidence sites. This quantity is thought to have an important bearing on the physical properties of grain boundaries, although no definite correlation exists. However, the second crystallographic concept presented, the cell of non-identical diplacements, depends critically on the planar density of coincidence sites as is shown in section 4. This cell encloses the set of smallest equivalent translations away from a common origin coincidence-site lattice.

The last two sections introduce symmetry considerations that have significant bearing on the study and physical properties of grain boundaries. An introduction to the colored symmetry groups used in these sections is given. Next, the dichromatic pattern corresponding to the CSL is derived. By introducing planar cuts in the dichromatic pattern, the symmetry of an ideal maximum symmetry interface will be obtained. The last section considers the change in symmetry that occurs by a displacement of the black lattice; all possible variations are considered. Relaxational variants arise because of the multiple ways in which a relaxed structure can be obtained from the original maximum symmetry interface. The multiplicity and structure of these variants is shown to be related to the symmetry elements lost in the relaxation.

2.2. The Coincidence-Site Lattice and its Displacement Lattice

The idea of a coincidence-site lattice is best illustrated graphically as in Figure 2.2.1. Two simple cubic lattices misoriented by the rotation indicated in the upper right hand corner are shown extended through space and interpenetrating. If two lattice points, one from each crystal, are brought into coincidence by a rigid translation a three-dimensional lattice of coincidence sites forms. This lattice is known as the coincidence-site lattice and it will be noted as CSL throughout the discussion. The volume density of coincidence sites is denoted by $1/\Sigma$. The CSL will be denoted in calculations as the structure matrix $\mathbf{C}$ which has as columns the basis of its lattice. The degree of coincidence Σ is also a qualitative indication of the size of the CSL but the actual volume of the unit cell of the CSL is given by the determinant of $\mathbf{C}$. For the case of Figure 2.2.1

$$\mathbf{C} = \begin{bmatrix} 1 & 2 & 0 \\ \overline{2} & 1 & 0 \\ 0 & 0 & 1 \end{bmatrix} \tag{2.2.1}$$

A grain boundary is a two dimensional cut through the interpenetrating lattices. Atoms on one side of the boundary belong to crystal 1 (also designated as the upper crystal throughout the discussion) and on the other side to crystal 2 (designated as the lower crystal). This two-dimensional cut is also a cut through the CSL and thus it contains a two-dimensional net of coincidence sites which gives two-dimensional periodicity to the grain boundary structure. That is, the boundary can be regarded as consisting of identical periods each of which is one unit of the two-dimensional grain boundary structure. Obviously the size of this period is dependent on the size of the CSL, and on the orientation of the cut.

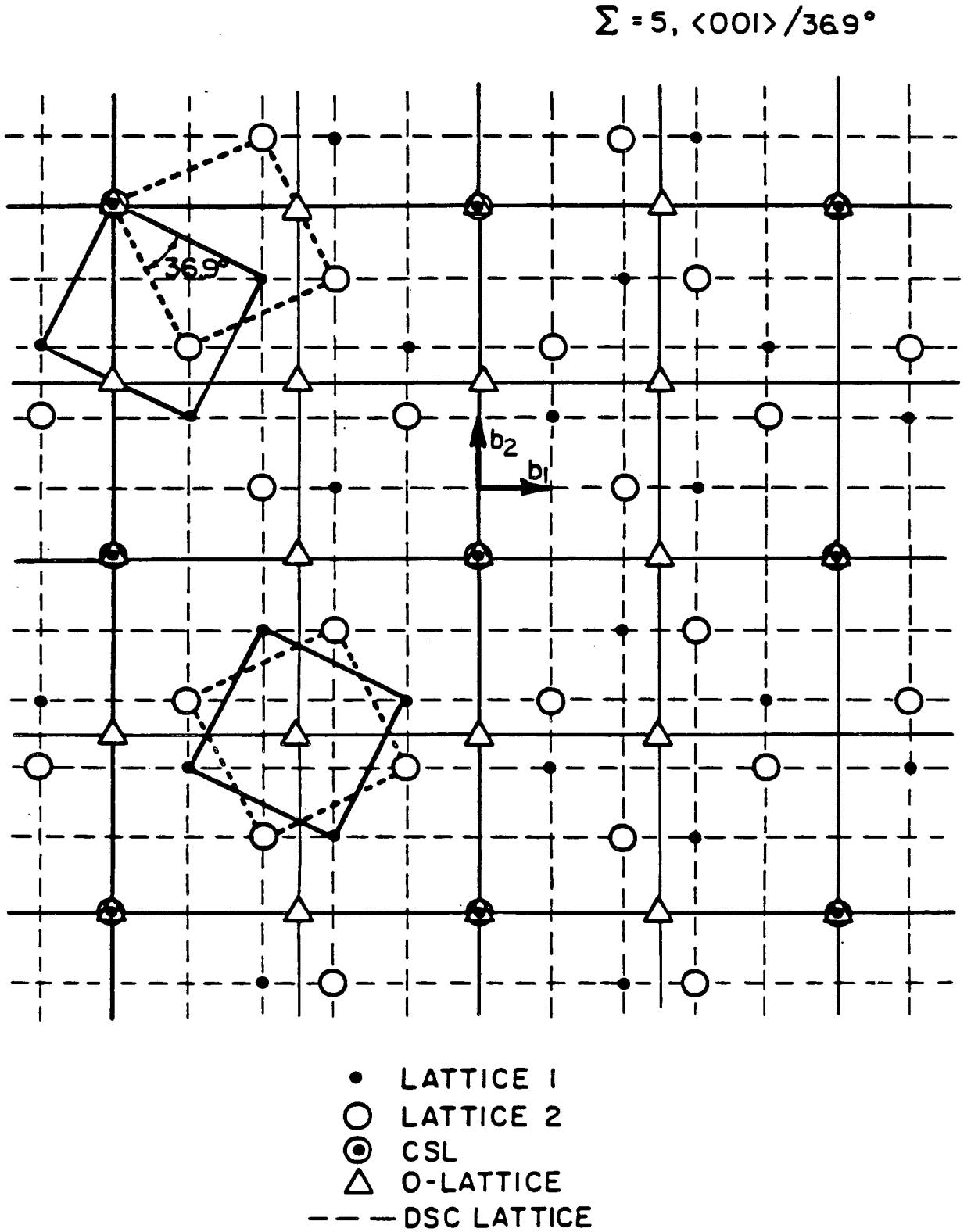

Fig. 2.2.1 The O-lattice, CSL, and DSCL of a Σ5 bicrystal for a simple cubic structure. The basis of the DSCL is $\mathbf{b}_1$ and $\mathbf{b}_2$.

The rotations that lead to a CSL are given by rotation matrices of the form

$$\mathbf{R}^{CSL} = \frac{1}{S} a_{ij} \tag{2.2.2}$$

such that there is no integral factor common to the positive integer S and the integers a_{ij}. The degree of coincidence Σ is equal to the largest odd factor of S and is the least common denominator of the matrix elements of R. [4]

$$\Sigma = \frac{S}{\alpha} \qquad \Sigma \; odd, \qquad \alpha = 1,2,or\; 4 \tag{2.2.3}$$

The misorientations for which CSLs occur can be obtained from a generating function [5] or from number theory. [6] There are several forms of the generating function, the first one given by Ranganathan. [7] In its more complete form the generating function is given by Grimmer. [8] The quadruples or quaternions $[m, U, V, W]$ with m positive give rise to a rotation matrix

$$\mathbf{R} = \frac{1}{S} \begin{bmatrix} m^2+U^2-V^2-W^2 & 2(UV-mW) & 2(UW+mV) \\ 2(UV+mW) & m^2-U^2+V^2-W^2 & 2(VW-mU) \\ 2(UW-mV) & 2(VW+mU) & m^2-U^2-V^2+W^2 \end{bmatrix} \tag{2.2.4}$$

$$S = m^2+U^2+V^2+W^2$$

The rotation axis is $[U, V, W]$ and the rotation angle is given by

$$\tan\frac{\theta}{2} = \frac{(U^2+V^2+W^2)^{1/2}}{m} \tag{2.2.5}$$

These equations allow us to study systematic variations of grain boundary structure with for example a fixed tilt axis. In particular, in this work we will be concerned with the quaternions of the type [m,1,0,0] and [m,1,1,0]. This point will be retaken later on since now a brief and necessary disgression on the physical significance of the CSL is

needed.

The actual atomic configurations are different than the atomic positions in the ideal bicrystal described above. The forces that are set in the ideal bicrystal and produce a rearrangement have the periodicity of the grain boundary plane through the CSL. It is in principle possible to calculate the structure of the boundary by some physical principle for only one segment, and then to assume a repetition of this calculated structure. Saint-Venant's principle states that the strains that are produced in a body by the application to a small part of its surface of an equilibrated system of forces are of negligible magnitude at distances which are large compared with the linear dimensions of the part.[9] Applied to the case of the ideal semi-infinite bicrystal with length equal to one period this indicates that the distortions in one crystal will extend into the crystal to a distance comparable with the periodicity. The conclusion is then that the energy is smaller when the grain boundary period is smaller. Special grain boundary planes are expected to be low-index planes of the CSL that produce periodic structures with relatively small repeat cells. A higher planar density of coincidence sites implies a shorter period. A procedure to calculate the planar density of coincidence sites for a given plane in a given CSL is given in the next section. The physical significance of the CSL was initially attributed to the fact that an atom in the boundary which is in a coincidence site is in a region of good fit because it belongs to both crystal lattices. It was assumed then that the higher the density of these sites the better the fit and the lower the energy of the boundary region. [10] ,[11] The significance of these physical criteria will be discussed later. For now, it should be stated that the physical significance of the CSL is that a boundary which is parallel to a rational plane of the CSL has a periodic structure.

A grain boundary where the the grain boundary plane is normal to the axis of rotation is a twist boundary. A grain boundary where the axis of rotation is contained in the boundary plane is a tilt boundary. This work is entirely concerned with the study of tilt grain boundaries because their atomic structure can be studied by high-resolution electron microscopy as it will be shown later. However, the implications and applicability of this study to twist and mixed boundaries will be discussed later on.

In a systematic study of grain boundary structure the first objective is to reduce the numbers of degrees of freedom. A grain boundary has five degrees of freedom: two for the rotation axis, 1 for the rotation angle and two for the grain boundary plane. By restricting the study to one of the quaternions mentioned above, the two degrees of freedom for the rotation axis are eliminated. Next, if an angle is picked, two degrees of freedom remain for the boundary plane. If a symmetrical boundary plane exists for that angle, it is unique and then these two degrees of freedom are eliminated. So by restricting the study to symmetrical grain boundary planes around a low index axis of rotation a systematic study of variation of structure with respect to the angle of misorientation can be carried out.

Boundary plane normals $\mathbf{p}_1$ and $\mathbf{p}_2$ by convention are always defined in both grains going from the lower to the upper grain. The Miller indices are then in the relation

$$h_1^2 + k_1^2 + l_1^2 = h_2^2 + k_2^2 + l_2^2 \tag{2.2.6}$$

This ensures that the areas of the two-dimensional unit cells are in an integral ratio so that coincidence of atomic sites can exist in the grain boundary plane. Note that for the above condition to be true a multiple of the lowest index representation of $\mathbf{p}_1$ or

$\mathbf{p}_2$ might be necessary. An equivalent to the CSL cut is the cut and weld procedure of a single crystal which is illustrated for a tilt boundary in Figure 2.2.2 a and b. The arrows indicate the sense of rotation after the cuts are made; the shaded volume is thrown away.

The lowest index crystal plane with indices multiple of $\mathbf{p}_1+\mathbf{p}_2$ is defined as the mean boundary plane. The period vectors parallel to the boundary plane are $\mathbf{q}_1$ and $\mathbf{q}_2$ and have the same magnitude as per Eqn. 2.2.6. By definition the mean period vector is defined as $\mathbf{q}_1+\mathbf{q}_2$; it bisects the angle between $\mathbf{q}_1$ and $\mathbf{q}_2$.

A [100] tilt boundary could have mean boundary plane (001) and mean period vector $[0\bar{1}0]$. By varying the the angle θ and using the construction shown in Figure 2.2.2.c, all boundaries with mean bounary plane (001) can be built. Alternatively, one could choose a mean boundary plane (011) and mean period vector $[01\bar{1}]$. In general for any tilt axis, the boundary plane normal lies in the zone of the axis so that there are two independent indices (h_m and k_m) prescribing the mean boundary plane. The parameter $\xi = k_m/h_m$ characterizes all boundaries with the same mean boundary plane [12] There are equivalent ξ systems that are related by the symmetry operators of the point group 432 in the coordinate systems. In the two cases mentioned above $\xi=\infty$, but in general equivalent systems can have different values of ξ.

For a particular ξ system, if the mean boundary plane is a crystal mirror plane or the mean period vector is an even-fold symmetry axis then all boundaries in that system are symmetrical. In cubic crystals either the mean boundary plane is {110} or {100} or the mean period vector is <110> or <100>. [13] For example a system of symmetric tilt boundaries exists for a [112] tilt axis since we can choose a mean boun-

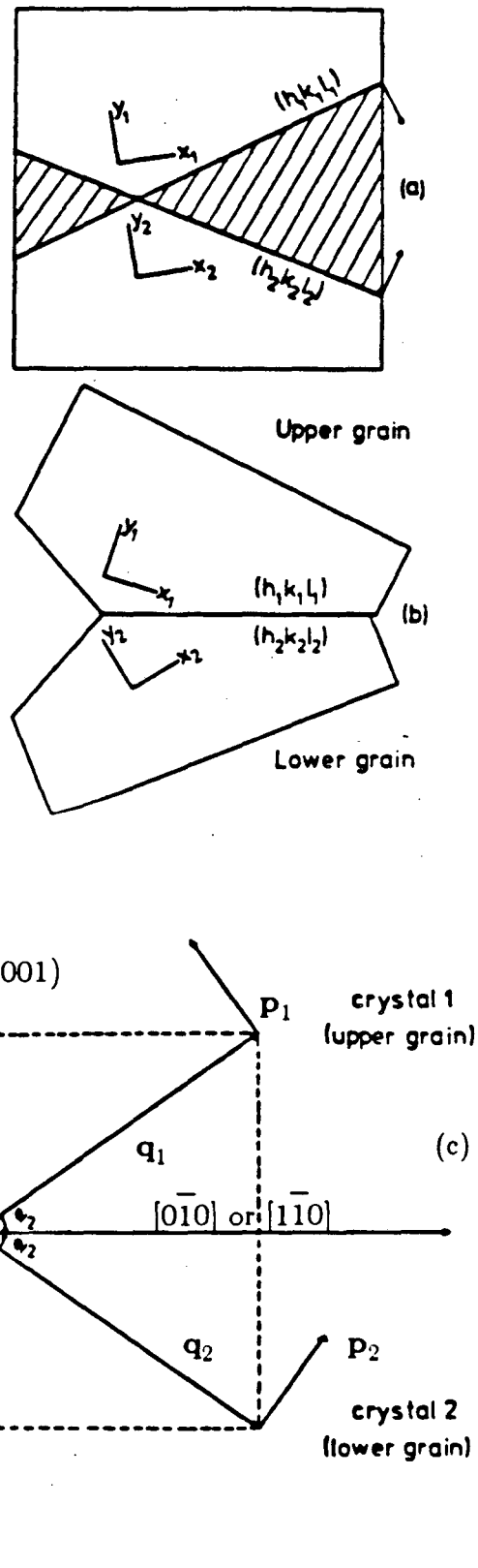

Fig. 2.2.2 The construction of a tilt boundary: (a) before; (b) after rotation; (c) with a given mean boundary plane (after A.P. Sutton, Ph.D. Thesis, University of Pennsylvania, 1981).

dary plane of $[1\bar{1}0]$. In this work, as it was mentioned above, the author has chosen to study [110] and [100] tilt boundaries. A list of symmetric grain boundaries in both systems is shown in Table 2.2.1. The [110] boundaries have mean boundary plane (001) and mean period vector $[1\bar{1}0]$. The Σ notation follows that of Mykura. [14] In the table the indices are chosen to be consistent and indicate the boundaries that will be studied in the next sections. Notice that the examples used in this chapter do not belong to any of the particular choices indicated in Table 2.2.1. This has been done somewhat in order to show that changes in coordinates ultimately produce the same atomic configuration. However, consistency in crystallographic manipulations is extremely important. Lack of it can lead to errors in the analysis. The choice of (001) as the mean boundary plane was based on the fact that large angle tilt boundaries show only one set of dislocations with $<100>$ Burgers vectors[15] and that the twinning plane for BCC is of the $<112>$ type. Choosing the same mean boundary plane for both systems will allow us in the future to study the change in boundary structure with a change of axis of misorientation. Other descriptions (ξ) are possible and equivalent but this one seems physically more meaningful. The description adopted depends ultimately then on crystal structure.

Bollman has generalized the concept of the CSL to coincidence of interior cell points. [16] These are points that do not have atom positions associated with them. These generalized coincidence points form the O-lattice. The importance of the O-lattice is that whereas the CSL changes discontinuously, following an infinitesimal change in the relative orientation of the two crystal lattices, the O-lattice changes smoothly. In addition the O-lattice theory provides a formal discrete dislocation model of an interface. The elements of the lattice (points, lines, or planes) are separated by

Cubic CSL
Symmetric Grain Boundaries

<110>			<100>		
Σ	θ	Grain Boundary Plane	Σ	θ	Grain Boundary Plane
1	0°	{001}	1	0°	{001}
33a	20.05°	$\{\bar{1}18\}$	41a	12.68°	{019}
19a	26.53°	$\{\bar{1}16\}$	25a	16.25°	{017}
27a	31.58°	$\{\bar{1}15\}$	37a	18.92°	{016}
9	38.94°	$\{\bar{1}14\}$	13a	22.62°	{015}
11	50.48°	$\{\bar{1}13\}$	17a	28.07°	{014}
41c	55.88°	$\{\bar{3}38\}$	5	36.87°	{013}
33c	58.98°	$\{\bar{2}25\}$	29a	43.61°	{025}
3	70.53°	$\{\bar{1}12\}$			
17b	86.63°	$\{\bar{2}23\}$			
—	—	—	—	—	—
17b	93.37°	$\{\bar{3}34\}$			
3	109.47°	$\{\bar{1}11\}$			
33c	121.02°	$\{\bar{5}54\}$	29a	46.39°	{037}
41c	124.12°	$\{\bar{4}43\}$	5	53.13°	{012}
11	129.52°	$\{\bar{3}32\}$	17a	61.93°	{035}
9	141.06°	$\{\bar{2}21\}$	13a	67.38°	{023}
27a	148.42°	$\{\bar{5}52\}$	37a	71.08°	{057}
19a	153.47°	$\{\bar{3}31\}$	25a	73.75°	{034}
33a	159.95°	$\{\bar{4}41\}$	41a	77.32°	{045}
1	180°	$\{\bar{1}10\}$	1	90°	{011}

Table 2.2.1

cell walls and the lack of registry between the two lattices can be considered to be concentrated into discontinuities at the cell walls. When an interface is introduced the intersections of the cell walls with the interface becomes a network of line defects or the interfacial dislocation network. The author has used with success the O-lattice formalism in the analysis of small-angle grain boundaries,[17] [18] but its use in the study of large-angle grain boundaries is cumbersome and lacks the physical significance of the concept that we discuss next.

Just as a large-angle boundary with Burgers vectors equal to a lattice translation accomodates a deviation from a perfect crystal, a network of dislocations could accomodate a deviation from coincidence in order to preserve the coincidence orientation. What is needed is the set of all translations of lattice 2 with respect to the fixed lattice 1 so that after every translation, the same CSL reappears. The positions of the coincidence positions do not have to be the same. The lattice of all these translations is the Displacement Shift Complete lattice (DSCL). If a particular CSL represents an energy minimum, a structure that deviates slightly from this CSL would tend to preserve the arrangement of the CSL. This is done by means of a dislocation network. The Burgers vectors of these dislocations must be DSC translations. An example of the DSC lattice for a rotation in a simple cubic bicrystal is given in Figure 2.2.1. The strucutre matrix for this DSC lattice is given by

$$\mathbf{D} = \frac{1}{5}\begin{bmatrix} 1 & 2 & 0 \\ \overline{2} & 1 & 0 \\ 0 & 0 & 5 \end{bmatrix} \tag{2.2.7}$$

The DSCL can be defined as the coarsest possible lattice which contains crystal lattices 1 and 2 as sublattices; in other words, the lattice into which crystal lattices 1 and

2 are embedded. As we can see from the figure, the DSC lattice is the lattice of the difference vectors between the two crystal lattices. On the other hand the CSL is the finest lattice which is contained in crystal lattice 1 as well as in crystal lattice 2.

The DSCL and CSL are reciprocally related in simple cubic structures by [19]

$$\mathbf{C}\,\mathbf{D}^T = \mathbf{I} \tag{2.2.8}$$

where $\mathbf{I}$ is the identity matrix. In general the DSCL is the reciprocal lattice of the coincidence lattice formed by the two reciprocal crystal lattices. The volume of the DSCL unit cell goes as $1/\Sigma$ while the volume of the CSL goes as Σ. For the primitive cubic structure, the reciprocal unit cell is the same as the crystal unit cell. The DSCL is then the reciprocal of the CSL and is given by Eqn. 2.2.8. The procedures for calculating the CSL have been mentioned before; the DSCL for the primitive cubic structures are calculated using Eqn. 2.2.8. Appropiate centering for FCC and BCC structures is carried out using procedures that stem from number and set theory. [20]

A grain boundary with $\Sigma 3$ is commonly referred to in the metallurgical literature as a twin. A misorientation of 180° about a rational direction is a possible twin description of the grain boundary. Not all grain boundaries have twin descriptions. Of all grain boundaries with a twin description, $\Sigma 3$ is the most important in FCC and BCC crystals because of its role in a number of metallurgical phenomena. Twin boundaries may be formed by shear forces during deformation or heat treatment. They interfere with the slip process and increase the strength of a part. The movement of the boundary can cause the part to deform. Twinning is a mode of deformation which is particularly important in BCC materials. Because of its importance a twin grain boundary in a BCC bicrystal has been chosen to illustrate the crystallographic con-

cepts introduced in the next two sections. Several twin grain boundaries are shown in Figure 2.2.3. The twin grain is entirely surrounded by the matrix in order to illustrate the structure of different grain boundary planes. The axis/angle pair can be given as $[01\bar{1}]/70.53\,^{\circ}$ or, equivalently, by the disorientation (minimum angle axis/angle pair), $[111]/60\,^{\circ}$. A $[01\bar{1}]$ projection is used for the purposes of illustration. The rotation matrix is given by

$$\mathbf{R} = \frac{1}{3}\begin{bmatrix} 1 & 2 & 2 \\ \bar{2} & 2 & \bar{1} \\ \bar{2} & \bar{1} & 2 \end{bmatrix} \tag{2.2.9}$$

This matrix is also a structure matrix in that it contains the coordinates in crystal 1 of the basis of crystal 2. The CSL is given by

$$\mathbf{C} = \frac{1}{2}\begin{bmatrix} 1 & 2 & \bar{2} \\ 1 & 0 & 2 \\ 1 & \bar{2} & 0 \end{bmatrix} \tag{2.2.10}$$

This CSL is hexagonal. The CSL is indicated in Figure 2.2.3 and subsequent figures by the filled atom positions. In order to make the actual atom arrangements at different facets more visible, the interpenetrating lattices are not plotted in this case. The DSCL is given by

$$\mathbf{D} = \frac{1}{6}\begin{bmatrix} 1 & 2 & \bar{2} \\ 1 & 2 & 4 \\ 1 & \bar{4} & \bar{2} \end{bmatrix} \tag{2.2.11}$$

This structure matrix represents also an hexagonal lattice.

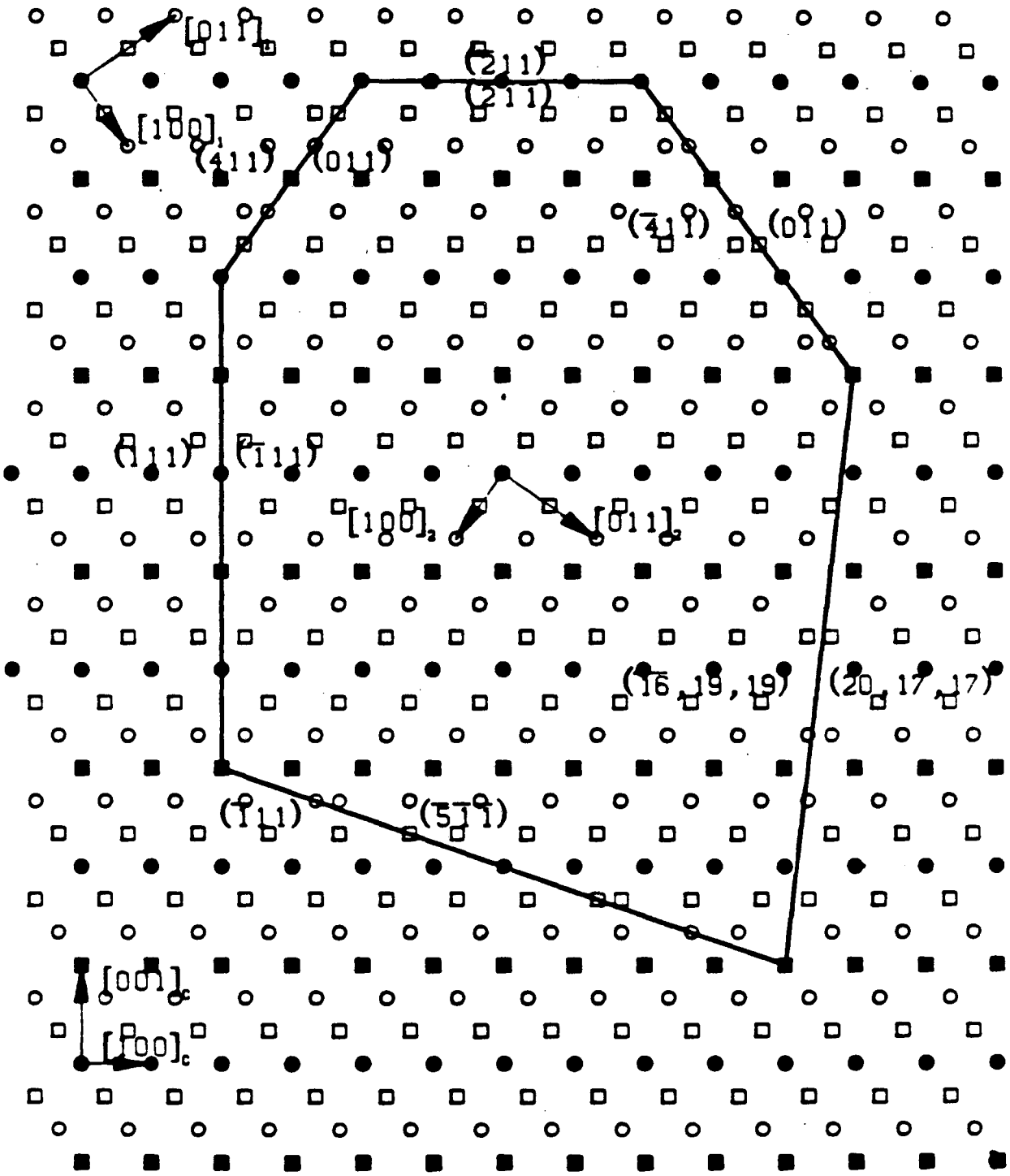

Fig. 2.2.3 Projection along (01$\bar{1}$) of a BCC twin grain and matrix in the relative position which forms a CSL. Squares and circles represent the ABAB.. stacking along [01$\bar{1}$]. Filled symbols represent coincidence sites. All indices inside the twin grain are in the coordinate system of the twin grain, all indices outside are in the coordinate system of the matrix.

2.3. Planar Density of Coincidence Sites

As pointed out earlier, the volume ratio of crystal lattice sites to coincidence sites is Σ . However, the physical properties of a planar grain boundary depend on the density of coincidence sites contained in the boundary plane. A simple procedure for calculating the ratio of coincidence sites to atomic sites ρ in a planar grain boundary is given in this section. For a crystal which has a volume per atom υ, the number of atoms in a slab of thickness d and area A is $n_T = (d\ A)/\upsilon$. In general for any lattice in any of its various descriptions, the planar density of atomic sites is given by

$$n_D = \frac{n_T}{A} = \frac{d_{hkl}}{\upsilon} \tag{2.3.1}$$

wher d_{hkl} is the spacing of the plane (hkl).

A plane (hkl) in the crystal has an equivalent description $(h'k'l')$ on the basis of the CSL. Then ρ is simply given by

$$\rho = \frac{n_D^{CSL}}{n_D^{cryst}} = \frac{d_{h'k'l'}^{CSL}\ \upsilon^{cryst}}{d_{hkl}^{cryst}\ \upsilon^{CSL}} \tag{2.3.2}$$

If we use the primitive unit cells of the crystal and the CSL, and their respective reciprocal lattices, Eqn. (2.3.2) becomes

$$\rho = \frac{|\,\mathbf{g}_{hkl}\,|\ \ |\,\mathbf{C}\,|}{|\,\mathbf{g}_{h'k'l'}\,|\ \ |\,\mathbf{S}\,|} \tag{2.3.3}$$

where **C** and **S** are the structure matrices with the basis of the primitive CSL and the primitive crystal structure unit cells. The spacings of lattice planes are given by the recripocal of the magnitude of their respective reciprocal lattice vectors, and the volumes per atom are given by the determinants of the structure matrices.

If $(h'k'l')$ is a primitive lattice vector of the CSL, its spacing is equal to that of (hkl) and ρ is given by the volume ratio, $\rho = 1/\Sigma$. If $(h'k'l')$ is an integer multiple p of a primitive reciprocal lattice vector, then $\rho = p/\Sigma$. The reciprocal quantity $1/\rho$ can have the value of Σ or one of its factors down to one. For a particular coincidence site relationship the value of ρ is the same for a particular plane in all three cubic Bravais lattices.

Consider as an example the twin boundary $\Sigma 3$ shown in Figure 2.2.3. In this particular case $\rho = 1/3$ or $\rho = 1$. The quantity ρ will be calculated for the planes $(\bar{1}11)$ and $(\bar{2}11)$ which will be used in the discussion later on in this chapter. For a bcc crystal the volume per atom is $v^{cryst} = a^3/2$ (two atoms per unit cell), and the spacing between planes is

$$d = \frac{a}{\sqrt{h^2+k^2+l^2}} = \frac{a}{\sqrt{3}} \tag{2.3.4}$$

But since this is a body-centered structure and (h+k+l) is odd, the spacing indicated in Eqn. (2.3.4) is actually twice the spacing [21] so that

$$d_{hkl}^{cryst} = \frac{a}{2\sqrt{3}} \tag{2.3.5}$$

The indices of the normal in the CSL are given by

$$[h'k'l']^T = \mathbf{C}^{-1}\,[hkl]^T \tag{2.3.6}$$

since C is the structure matrix of the CSL.[22]

$$\frac{1}{3}\begin{bmatrix} 2 & 2 & 2 \\ 1 & 1 & \bar{2} \\ \bar{1} & 2 & \bar{1} \end{bmatrix}\begin{bmatrix} \bar{1} \\ 1 \\ 1 \end{bmatrix} = \begin{bmatrix} 1 \\ \bar{1} \\ 1 \end{bmatrix} \tag{2.3.7}$$

These indices remain the same in the standard hexagonal notation (just a reordering of the columns in C). The plane $(hkil)$ normal to the direction $[uvtw]$ is given by [23]

$$(h, k, i, l) = (u, v, t, \lambda^2 w) \tag{2.3.8a}$$

where

$$\lambda^2 = \frac{2}{3}\left[\frac{c}{a_h}\right]^2 \tag{2.3.8b}$$

in this case $c = 1/2\sqrt{3}\,a$, $a_h = 1/2\sqrt{8}\,a$, $(c/a_h)^2 = 3/8$, and $\lambda^2 = 1/4$, so that

$$(h'k'l') = (4\bar{4}1) \tag{2.3.9}$$

The spacing of planes in the hexagonal lattice is

$$\frac{a_h{}^2}{d^2} = \frac{4}{3}(h^2 + hk + k^2) + \left(\frac{a_h}{c}\right)^2 l^2 \tag{2.3.10}$$

Or, in this particular case

$$d_{h'k'l'}^{CSL} = \frac{a}{2\sqrt{3}} \tag{2.3.11}$$

The atomic volume in the CSL is given by the volume of the CSL unit cell since there is one atom per unit cell. The volume of an hexagonal lattice unit cell is

$$v^{CSL} = \frac{\sqrt{3}}{2}\,a_h{}^2\,c = \frac{3}{2}\,a^3 \tag{2.3.12}$$

Using Eqns.(2.3.12), (2.3.11) and (2.3.5) in Eqn. (2.3.2) we obtain

$$\rho = \frac{1}{3} \tag{2.3.13}$$

This procedure, using Eqn. (2.3.2), although general in nature, requires parameters that have to be calculated for each particular boundary plane, for each grain boundary disorientation and each CSL. It also requires knowledge of the symmetry of each CSL. The procedure indicated above was first suggested by Tu[24] and utilized by

Acton and Bevis in a more systematic way to develop tables of planes with a high density of coincidence sites for boundaries with Σ up to 31.[25] Using the equivalent Eqn. (2.3.3) a more straightforward procedure can be developed that can easily be carried out on a computer. A simple program has been developed to use the procedure described below in our investigations. All it requires as input are the indices of the plane whose ρ is desired and the structure matrix of the CSL for that particular misorientation. The procedure is general in nature and can be used for grain boundaries in other crystal structures.

As an example, consider the same case of a $(\bar{1}11)$ in a $\Sigma 3$ boundary. The normal vector $\mathbf{n} = [1\bar{1}1]$ is transformed into the coordinate system of the CSL and the crystal recriprocal lattices. For this transformation the transformation matrix is just the transpose of the structure matrix.[26]

$$\mathbf{g}_{h'k'l'} = \mathbf{C}^T \ \mathbf{n} \tag{2.3.14}$$

and

$$\mathbf{g}_{hkl} = \mathbf{S}^T \ \mathbf{n} \tag{2.3.15}$$

where

$$\mathbf{S} = \frac{1}{2} \begin{bmatrix} 1 & \bar{1} & 0 \\ 1 & 1 & 0 \\ 1 & 1 & 2 \end{bmatrix} \tag{2.3.16}$$

is the structure matrix of a particular choice of primitive unit cell for the bcc lattice. These vectors have to be simplified so that their coordinates become integers with no common divisor. The $\mathbf{g}$ vectors are $\mathbf{g}_{h'k'l'} = [1\bar{4}4]$,and $\mathbf{g}_{hkl} = [132]$. The spacings then are given by the reciprocal of the magnitude of these $\mathbf{g}$ vectors. The length of a vector $\mathbf{v}$ is given by means of the metric tensor $\mathbf{G}$ as

$$| \mathbf{v} | = (\mathbf{v}^T \ \mathbf{G} \ \mathbf{v})^{1/2} \tag{2.3.17}$$

where **G** is expressed in reciprocal space as

$$\mathbf{G} = (\mathbf{M}^T \mathbf{M})^{-1} \tag{2.3.18}$$

and **M** is a structure matrix.[27] By using Eqns. (2.3.17) and (2.3.18) in the CSL and crystal structures we obtain $d_{h'k'l'} = d_{hkl} = 1/2\sqrt{3}$. Using all this information in Eqn. (2.3.3), the planar density of coincidence sites results as before $\rho = 1/3$.

Using the same procedure for a (111) or $(\bar{2}11)$ plane would show that the planar density of coincidence sites in both cases is $\rho = 1$. The planar density of coincidence sites depends on the grain in which it is measured. The procedure described above can also be used in the other grain. All the planar densities of coincidence sites mentioned in this section are for the upper crystal (crystal 1). For symmetrical grain boundaries the planar density of coincidence sites is the same in both grains. This method was first suggested by H. Grimmer *et.al.* [28] in their studies of the properties of the CSL and DSC lattice using number theory. This procedure is general in nature and thus a computer program was developed to utilize it in this investigation.

2.4. Cell of Non-Identical Displacements

Up until now the two grains have been considered to have undergone a translation such that at least two atoms coincide and a rotation that produces a CSL. Since atoms at the grain boundary plane are crowded, as can be seen in Figure 2.3.3., the energy of the boundary can be decreased by translating one of the grains, the lower grain by convention. The overall translation $\mathbf{t}$ is comprised of two components. The component $\mathbf{t}_p$ corresponds to movements parallel and/or perpendicular to the boundary that restore perfect crystal density (no excess volume). For example, if an integral number of atomic planes parallel to the boundary are removed, a perpendicular displacement is needed to preserve crystal density. It should be pointed out that although certain atoms are crowded at a CSL boundary, the density of the ideal bicrystal is equal to the perfect crystal density. The second component $\mathbf{t}_e$ corresponds to a displacement normal to the grain boundary plane that leads to the creation of excess volume. The overall translation is then

$$\mathbf{t} = \mathbf{t}_p + \mathbf{t}_e \tag{2.4.1}$$

It is assumed that $\mathbf{t}_p$ is the minimum representation of the set of equivalent translations $\mathbf{t}_p + \mathbf{d}^{SC}$. In other words, $\mathbf{t}_p$ is specified in the Wigner-Seitz cell of the DSCL. In this section it will be shown that $\mathbf{t}_p$ can be transformed into an in-plane formulation and the cell of the minimum in-plane translations ($\mathbf{t}_i$) will be defined. It will also be shown that the planar density of coincidence sites influences the characteristics of this cell of non-identical displacements (CNID). These concepts were first introduced by Pond. [29] The last part of this section shows how to use the in-plane analysis to calculate the steps associated with DSC grain boundary dislocations and the Burgers

vector of partial grain boundary dislocations.

First, consider the variation of grain boundary structure with location of the boundary for a fixed translation $\mathbf{t}_p$. Figures 2.4.1.a and 2.4.2.a show the grain boundary structure of a $(\bar{2}11)$ and $(\bar{1}11)$ grain boundary plane in the $\Sigma 3$ boundary shown in Fig. 2.2.3. As stated previously, the $(\bar{2}11)$ plane has ρ=1. This plane is one of the observed twinning planes in BCC crystals. As shown in Fig 2.4.1.a ρ is 1 only at every third plane. As indicated in Fig.2.4.1.c , e, g and i, the structure changes with the boundary location. Thus the structure of a ρ=1 type boundary varies, cyclically repeating every Σth plane. For the case of the $(\bar{1}11)$ plane ρ=1/3 and, as indicated in Fig. 2.4.2.a, c, and d, the structure of the boundary is independent of boundary location, i.e. the planar density of coincidence sites is the same for all boundary locations.

All the structures indicated in Figures 2.4.1 and 2.4.2 can be created at a fixed boundary location by relative translations parallel to the boundary plane. It will be indicated in our discussion as the in-plane translation $\mathbf{t}_i$. Note that $\mathbf{t}_i$ is a member of the family of equivalent translations $\mathbf{t}_p + \mathbf{d}^{SC}$. In order to change to an in-plane displacement, it is only necessary to transform the component of $\mathbf{t}_p$ perpendicular to the boundary. This component is $n\,\mathbf{p}$ where $\mathbf{p}$ is a vector normal to the grain boundary plane and having magnitude equal to its interplanar spacing. In an asymmetrical boundary there will be two vectors $\mathbf{p}_U$ and $\mathbf{p}_L$ since the interplanar spacings are different in each grain. The in-plane displacement is simply given by the addition of a crystal lattice vector $\mathbf{b}_C^{SC}$ which is also a DSC vector. The vector $\mathbf{b}_C^{SC}$ has to be a crystal lattice vector rather than just a DSC vector, otherwise it would relocate the boundary plane of the initial structure. [30], [31] Thus

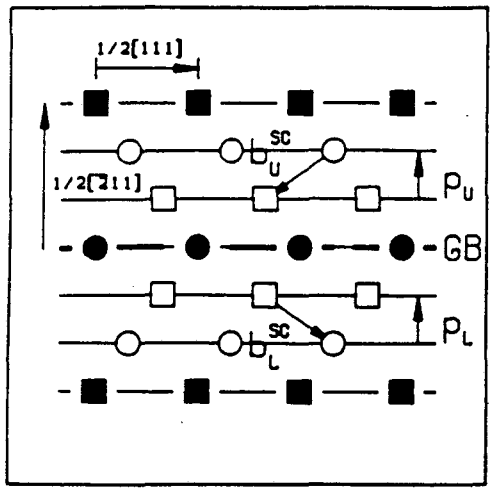

(a)

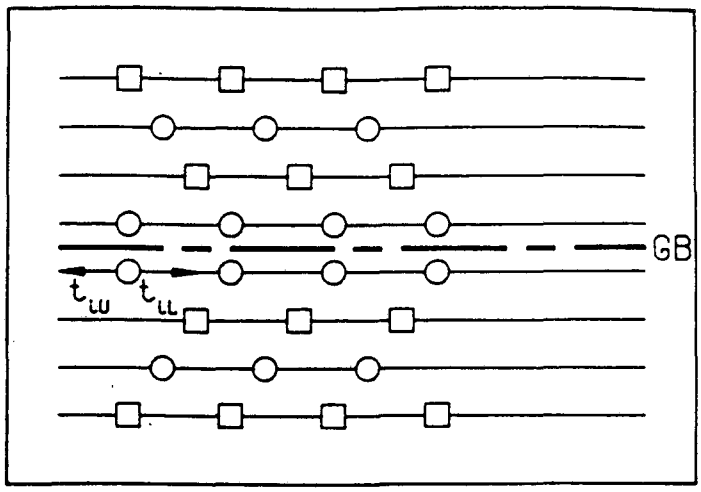

(b)

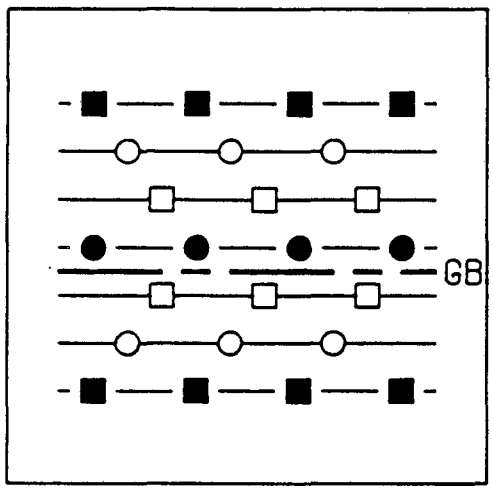

(c)

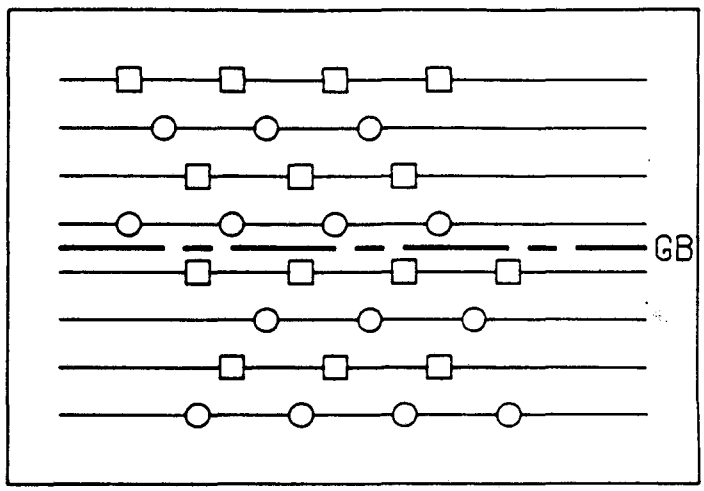

(d)

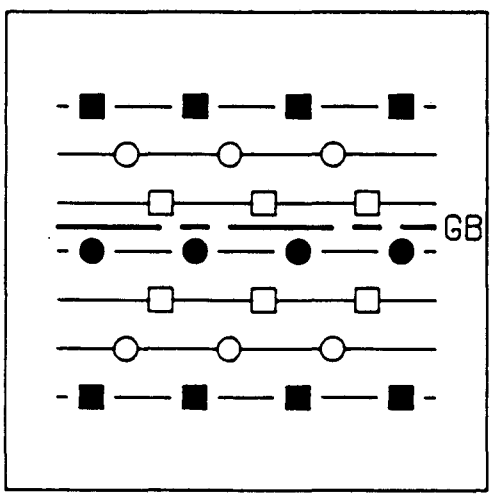

(e)

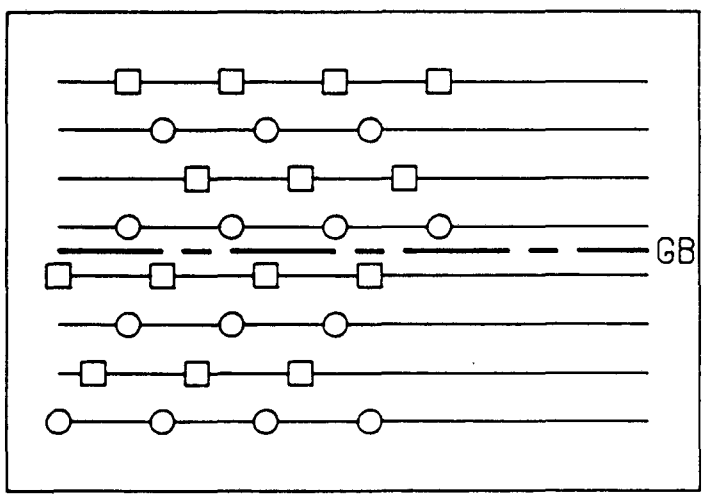

(f)

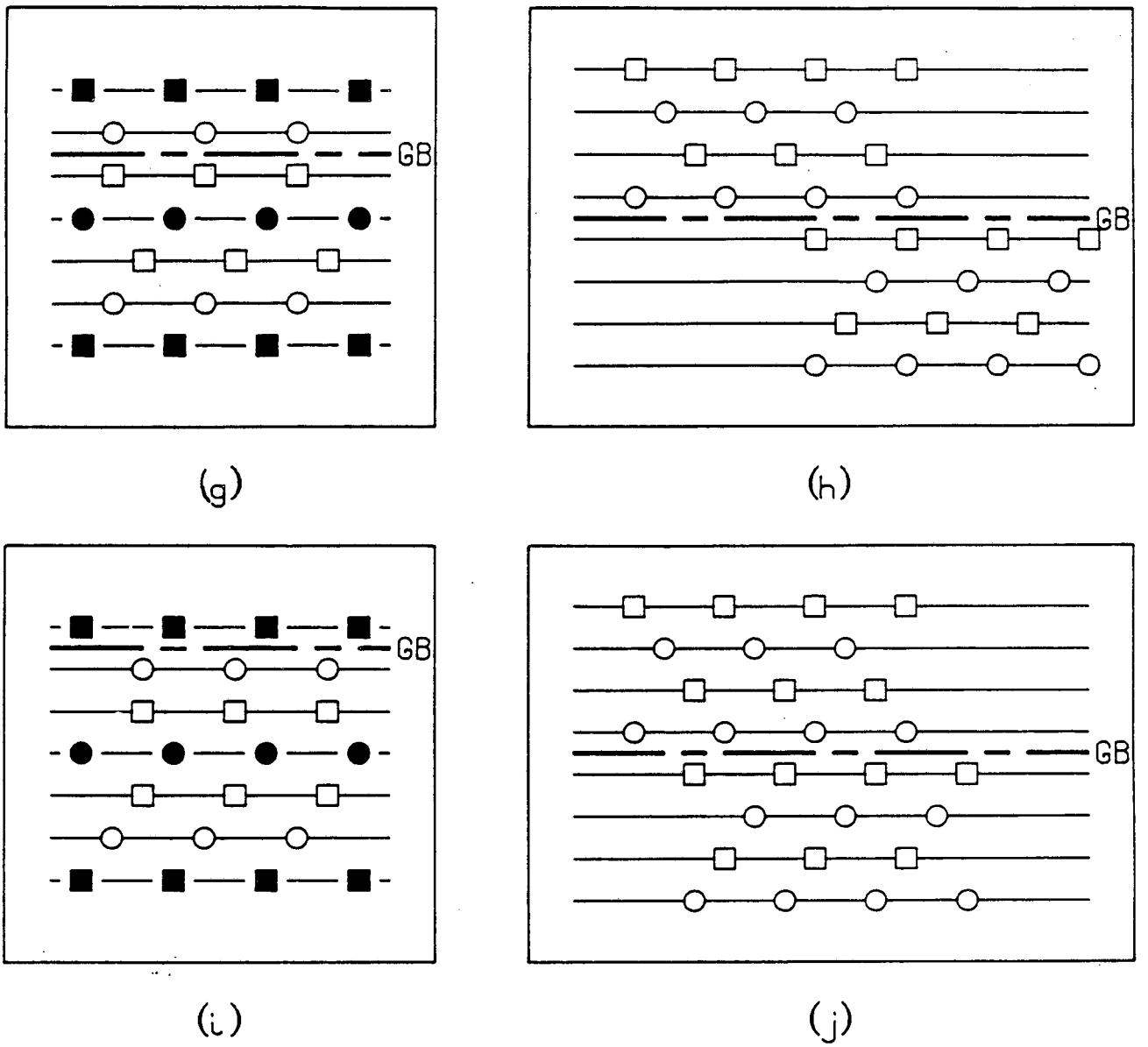

Fig. 2 . 4. 1 Grain boundary translations and in-plane translations for a $\Sigma 3$ $[01\bar{1}]/70.53^{\circ}$ $(\bar{2}11)$; (a) the structure of the boundary in the coincidence translation ; (b) reference state for in-plane translations; (c) and (d) boundary structure in the starting configuration and its corresponding in-plane (fixed boundary) displacement; (e) and (f) boundary structure after a translation $\mathbf{t}_p = \mathbf{p}_u$ and its corresponding in-plane displacement; (g) and (h) $\mathbf{t}_p = 2\mathbf{p}_u$; (i) and (j) $\mathbf{t}_p = 3\mathbf{p}_u$.

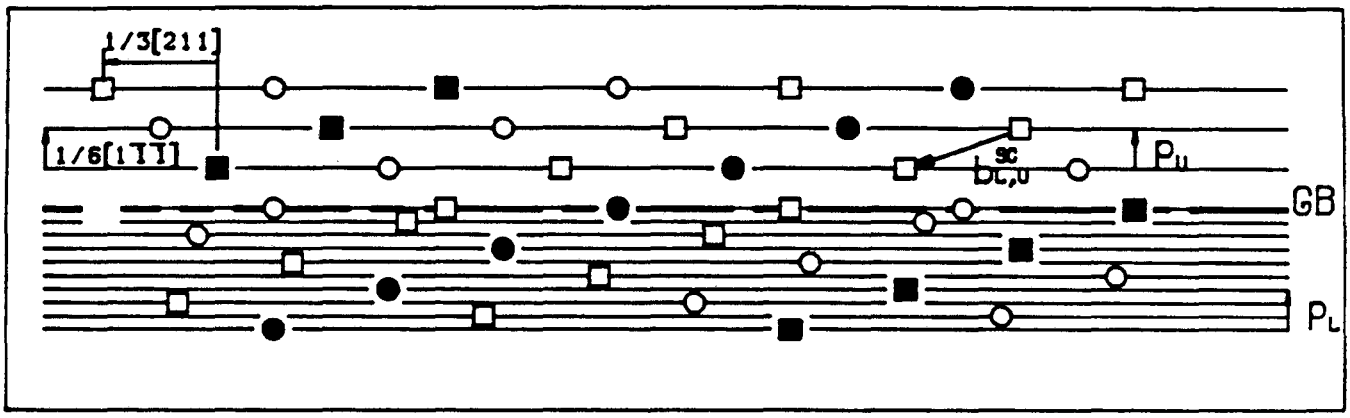

(a)

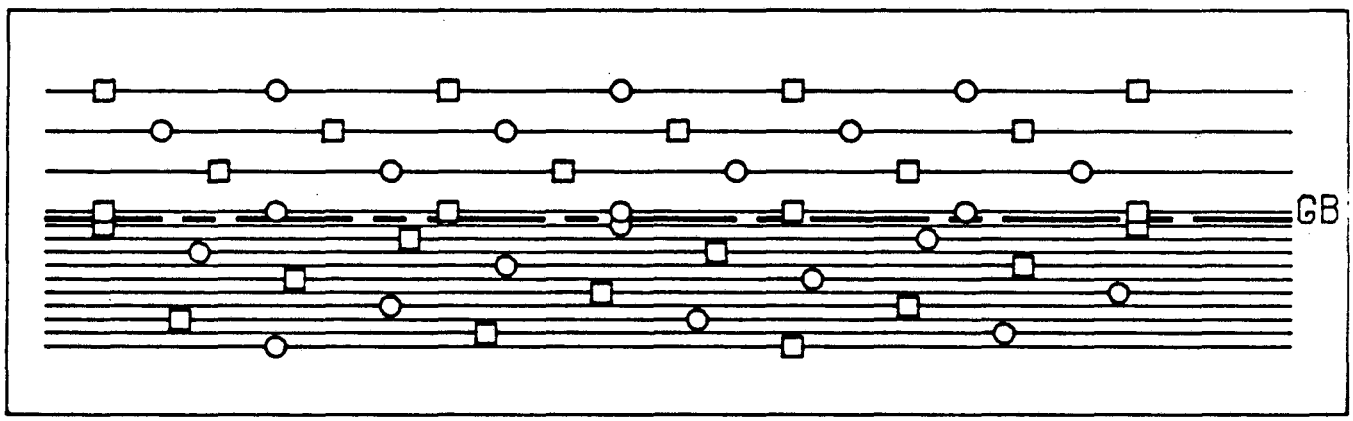

(b)

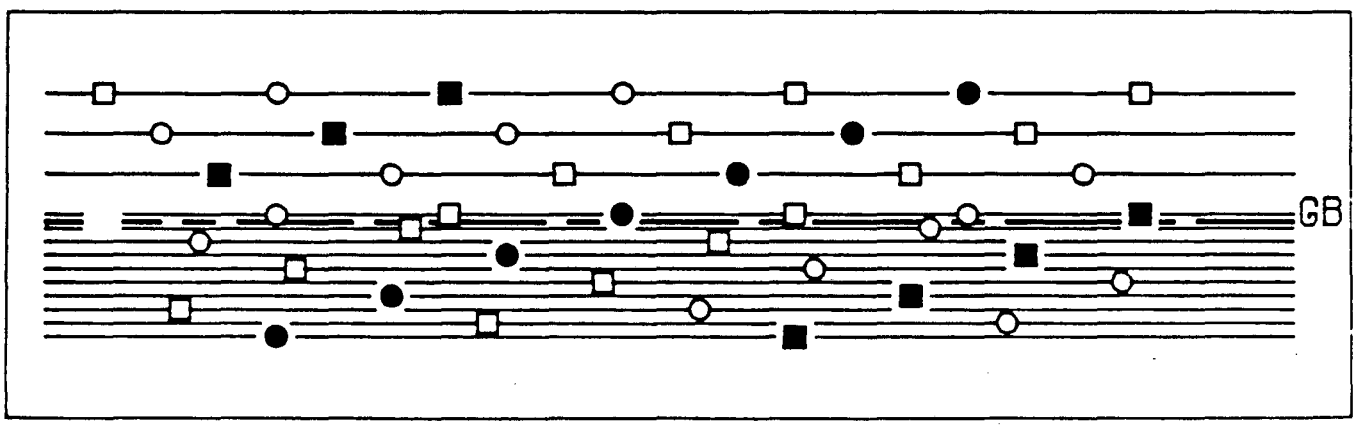

(c)

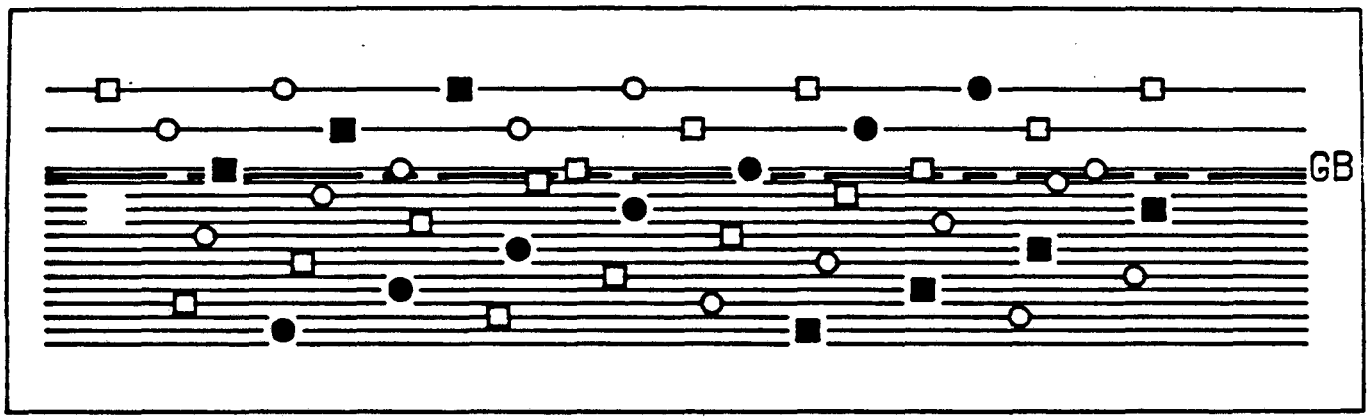

(d)

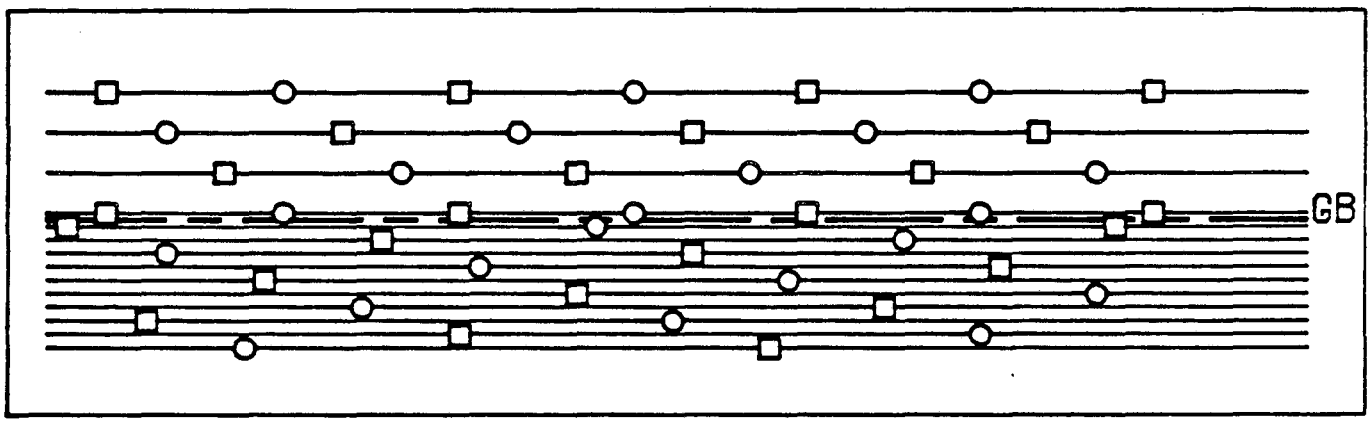

(e)

Fig. 2.4.2 Grain boundary translations and in-plane translations for a $\Sigma 3$ $[01\bar{1}]/70.53^{\circ}$ $(\bar{1}11)$; (a) the structure of the boundary in the coincidence translation ; (b) reference state for in-plane translations; (c) and (e) boundary structure in the starting configuration and its corresponding in-plane (fixed boundary) displacement; (d) boundary structure after a translation $\mathbf{t}_p = \mathbf{p}_u$, the corresponding in-plane displacement is also (e).

$$\mathbf{t}_i = \mathbf{p}_C + \mathbf{b}_C^{SC} \tag{2.4.2}$$

The subscript C takes the values U and L for upper and lower crystal. By convention $\mathbf{p}_C$ is always pointing towards the upper grain and $\mathbf{b}_C^{SC}$ is chosen so as to close the translation perpendicular to the boundary. In Fig. 2.4.1 the in-plane translation that corresponds to a shift of the boundary plane by one interplanar distance is

$$\mathbf{t}_{iU} = \frac{1}{6}[\bar{2}11] - \frac{1}{2}[011] \pm \frac{1}{2}[01\bar{1}] = \frac{-1}{3}[111] + \frac{1}{2}[01\bar{1}] = \frac{1}{6}[\bar{2}1\bar{5}] \tag{2.4.3}$$

or for the case where the lower grain is shrinking in size

$$\begin{aligned} \mathbf{t}_{iL} &= \frac{1}{6}[\bar{2}1\bar{1}]_L + \frac{1}{2}[011]_L \pm \frac{1}{2}[01\bar{1}]_L = \frac{1}{3}[\bar{1}11]_L - \frac{1}{2}[01\bar{1}]_L \\ &= \frac{1}{3}[111] - \frac{1}{2}[01\bar{1}] = \frac{1}{6}[2\bar{1}5] \end{aligned} \tag{2.4.4}$$

In a symmetric tilt boundary with ρ=1 , $\mathbf{t}_{iU} = \mathbf{t}_{iL}$ because the interplanar spacings are the same.

Consider the different boundary locations shown in Figs. 2.4.1.c, e, g, and i. This sequence of structures can also be created by in-plane translations $\mathbf{t}_i$. The reference structure for the in-plane description can not be the coincidence position. The reference structure for this particular boundary is shown in Fig. 2.4.1.b. It corresponds to a displacement $\mathbf{t}_p = \mathbf{p}_U$. The plane of coincidence atoms belongs to both the upper and lower grain in the reference state. In the coincidence position it is not clear to which grain the boundary plane belongs. The two different positions of the boundary plane shown in Figs. 2.4.1.c and e can be created from the reference state by a translation of $\mathbf{t}_{iL}$ and $\mathbf{t}_{iU}$ respectively as shown in Figs. 2.4.1.d and f. Consider the growth of the lower grain by a movement of the boundary plane from Fig. 2.4.1.c to Fig. 2.4.1.e. This translation $\mathbf{t}_p = 1/6[\bar{2}11]$ is equal to the in-plane translation

$$\mathbf{t}_i = \mathbf{t}_{iU} - \mathbf{t}_{iL} = \frac{1}{3}[\bar{2}1\bar{5}] \tag{2.4.5}$$

$-\mathbf{t}_{iL}$ takes us back to the reference and $\mathbf{t}_{iU}$ to the new boundary structure. In general, for a relocation by one interplanar spacing,

$$\mathbf{t}_i = \pm(\mathbf{t}_{iU} - \mathbf{t}_{iL}), \tag{2.4.6}$$

depending on the sense of relocation. The positive quantity indicates growth of the lower grain and is indicated by $\mathbf{t}_{i1}$, in this case $\mathbf{t}_{i1} = 1/3[\bar{2}1\bar{5}]$. $\mathbf{t}_{i1}$ is independent of the choice of reference translation since it is the difference of two relative translations. Consider again the three different grain boundary structures Figs. 2.4.2.c, e, and g. Since the relative displacement in the sequence is always $\mathbf{t}_p = 1/6[\bar{2}11]$ it follows that *the in-plane displacement* $\mathbf{t}_{i1}$ *is a* $\mathbf{d}^{SC}$ *vector with the same periodicity as* $\mathbf{t}_p$. In this case

$$\mathbf{t}_{i1} = 4\mathbf{b}_1 - \mathbf{b}_2 - \mathbf{b}_3 = \mathbf{d}^{SC} \tag{2.4.7}$$

It has been pointed out before that a DSC translation which is not a crystal lattice vector relocates the boundary plane of the initial structure. Starting from Fig. 2.4.1.c the sequence of structures is obtained by equivalent in-plane translations $\mathbf{t}_i = \mathbf{t}_{iL}$ (Fig.2.4.1.d), $\mathbf{t}_i = \mathbf{t}_{iL} + \mathbf{t}_{i1}$ (Fig.2.4.1.f), $\mathbf{t}_i = \mathbf{t}_{iL} + 2\mathbf{t}_{i1}$ (Fig.2.4.1.h). The structure of Fig. 2.4.1.i is the same as that of Fig. 2.4.1.c and can be generated by the translation $\mathbf{t}_i = \mathbf{t}_{iL} + 3\mathbf{t}_{i1}$ or $\mathbf{t}_i = \mathbf{t}_{iL}$ as indicated in Fig. 2.4.1.j. This is because

$$\Sigma \cdot \mathbf{t}_i = 3.\frac{1}{3}[\bar{2}1\bar{5}] = [\bar{2}1\bar{5}] \tag{2.4.8}$$

is a lattice vector and in this case the structures are identical. In genereal for a ρ=1 boundary the sequence of structures repeats at each Σth location because $\mathbf{t}_{i1}$ has the form of a DSC vector or $\mathbf{t}_{i1} = \frac{a}{\Sigma}[lmn]$ where [lmn] is a lattice vector. As the

boundary keeps on moving, the in-plane translations can be reduced to the smallest magnitude $\mathbf{t}_i$ by subtracting lattice vectors which are multiples of $\Sigma \cdot \mathbf{t}_{i1}$. *The cell of non-identical displacements for a ρ=1 boundary is the cell of smallest crystal lattice vectors in the boundary plane.*

Consider now the ρ=1/3 $(\bar{1}11)$ boundary shown in Fig. 2.4.2.a. In this case since the boundary structure is the same regardless of position, $\mathbf{t}_{iU} = \mathbf{t}_{iL}$.

$$\mathbf{t}_{iU} = \frac{1}{6}[1\bar{1}\bar{1}] + \frac{1}{2}[111] = \frac{1}{3}[211] \tag{2.4.9}$$

$$\mathbf{t}_{iL} = \frac{3}{54}[\bar{5}\bar{1}\bar{1}]_L + \frac{1}{2}[\bar{1}11]_L = \frac{1}{18}[4,10,10]_L = \frac{1}{3}[211] \tag{2.4.10}$$

The vectors $\mathbf{t}_{iU}$ and $\mathbf{t}_{iL}$ are given by the vector $\mathbf{p}$ of magnitude equal to the spacing of the crystal planes with the highest spacing in the asymmetrical boundary. Notice that $\mathbf{t}_{iU}$ and $\mathbf{t}_{iL}$ are not integral DSC vectors

$$\mathbf{t}_{iU} = \mathbf{t}_{iL} = \frac{1}{3}[\, 8\mathbf{b}_1 + \mathbf{b}_2 - \mathbf{b}_3 \,] \tag{2.4.11}$$

The GB structure shown in Fig. 2.4.2.c is obtained from the reference structure Fig. 2.4.2.b by a translation equal to 1/3 of $\mathbf{t}_{iU}$ because the spacing of the two crystals at the reference state is one interplanar distance of the planes with lower spacing, in this case those of the lower grain. However, any growth or shrinkage of a grain occurs by a multiple of the interplanar distance of the planes with the highest spacing, in this case those of the upper grain. The in-plane translation is null because

$$\mathbf{t}_{i1} = \mathbf{t}_{iU} - \mathbf{t}_{iL} = 0 \tag{2.4.12}$$

This is illustrated in Figs. 2.4.2.c and d, which have the same in-plane translation Fig. 2.4.2.e. *The cell of non-identical displacements for a ρ=1/Σ boundary is the Wigner-*

Seitz cell of the smallest DSC vectors parallel to the boundary plane.

The shift of the origin of the CSL caused by the relative displacement of the crystal lattices by a DSC vector usually has a component **h** normal to the boundary plane. The corresponding grain boundary dislocation is associated with a step in the boundary plane of height $|h|$. The steps are denoted climb ledge and glide ledge (according to the type of movement of the grain boundary dislocation in the boundary plane) so as to differentiate them from a pure ledge or step without dislocation character. [32] Imagine a glissile dislocation with a Burgers vector **b** moving along the boundary plane. Since **b** is in the plane of the boundary, $\Delta \mathbf{t}_i = \mathbf{b}$ for the case where no boundary relocation occurs. In addition there is an effective change of boundary structure. The change in boundary structure would occur since only an in-plane lattice Burgers vector $\mathbf{b}_i^L$ would conserve the structure. It follows that in order to preserve grain boundary structure

$$\Delta \mathbf{t}_i = \mathbf{b}_i^L = \mathbf{b} + n\,\mathbf{t}_{i\,1} \tag{2.4.13}$$

and the physical dislocation has an associated step $n\,\mathbf{p}_1$. At ρ=1/Σ boundaries, $\mathbf{t}_{i\,1}$=0 and movement of glissile grain boundary dislocations does not involve migration. The shortest vector joining equivalent sites after a DSC shift of crystal 2 with respect to crystal 1 is defined as the step vector **s**. [33] For a pure ledge the step vector is a CSL vector while for a step associated with a dislocation it is a DSC vector which is not a CSL vector. King has tabulated step vectors in cubic crystals. [34] Alternatively, the DSC translations can be defined as a group and analytical solutions to the step vector can be obtained from the matrix representation of the group. [35] The author finds this procedure considerably more cumbersome but more elegant in nature.

These considerations are important in discussing steps at grain boundary dislocation reactions and the migration of boundaries by a dislocation mechanism. [36]

Finally, the in-plane analysis can be used to define the Burgers vector of partial grain boundary dislocations that separate boundary regions with different translations. The Burgers vector is defined as the difference between these translations or in the in-plane form

$$\mathbf{b} = \Delta \mathbf{t}_i \tag{2.4.14}$$

Partial grain boundary dislocations exist at facet intersections and separate regions of symmetry related structures.

2.5. The Symmetry of the CSL: The Dichromatic Pattern

In order to study the symmetry of ideal bicrystals a classification system is needed which is equivalent to the conventional point or space groups that describe the symmetry of ideal single crystals. A bicrystal is a three-dimensional object that contains a unique plane (the interface) in which there may be two, one, or perhaps no translational axes. In this and the next section a systematic procedure to analyze the symmetry of bicrystals is described. The procedure, which is general in nature and can be used to study all types of interphase interfaces, has been developed over the last few years independently by several groups. [37] [38] [39] The analysis presented in this section is specific to grain boundaries and the examples, as in previous sections, correspond to cases that will be studied later. Many of the concepts used in this and the next section have been developed and systematized by Shubnikov and Kopstik; reference will be made when needed to their classic book. [40]

Consider first the homogeneous composite made of two interpenetrating lattices in the coincidence orientation. The principle of symmetry superposition of composites states that for homogeneous composites the symmetry of the composite is given by the intersection of the groups of its components and can be extended by a symmetrizing operation. [41] Except for this symmetrizing operation there is a dissymetrization on going from the two individual components to the composite. The general procedure for studying the symmetry of bicrystals is to find the group of maximum symmetry and then study the operations of dissymetrization in the order that they preserve symmetry. The procedure is shown in Figure 2.5.1 and is discussed next. $\Phi^*(\lambda)$ and $\Phi^*(\mu)$ are the holosymmetric space groups of the lattices of the two crystals. In the discussion that follows one of the lattices will be designated white and will be

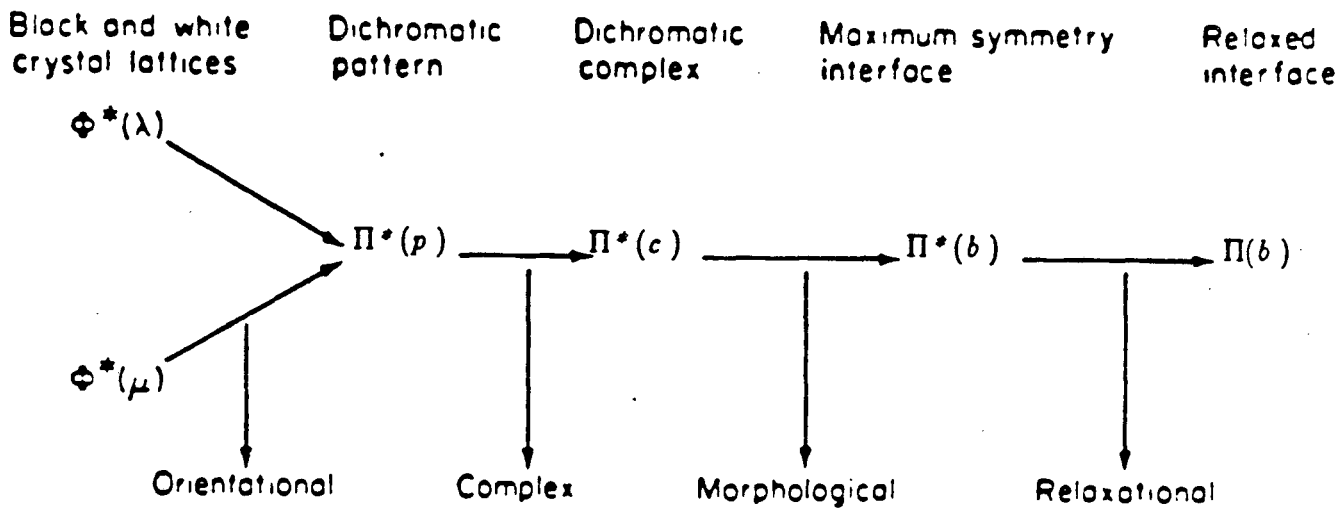

Fig. 2.5.1 Schematic of the methodology used in the analysis of the symmetry of bicrystals. The origin of the various types of variants of interfacial structure are indicated (from R. C. Pond [44]).

considered fixed while the other, designated the black lattice, will be free to translate and relax. The composite of these two lattices forms a dichromatic pattern $\Pi^*(p)$. The chosen origin of this pattern is a coincident black and white lattice point. For each crystal operation that is suppressed in going from one stage to the next a multiplicity of variants occur as indicated in Fig. 2.5.1. Orientational variants arise from the fact that the rotation matrix has alternative descriptions. It can be shown that the set of color symmetry operations is given by the set of alternative descriptions of the rotation matrix obtained by automorphic transformations of the dichromatic pattern.[42] Thus it is immaterial which of these descriptions is chosen. If the crystals are non-holosymmetric (the crystal has less symmetry than the lattice) or non-symmorphic (the crystal symmetry includes mirror glide planes or screw axes), the dichromatic complex $\Pi^*(c)$ has to be taken into account. A lattice complex is the set of points obtained by carrying out on a chosen point all the symmetry operations of the crystal's space group. [43] The pattern created by superimposing the black and white lattice complexes in the appropiate orientation is called the dichromatic complex. Complex variants produce equivalent dichromatic complexes that would ultimately produce equivalent interfacial structures that would be separated at the interface by defects of different character than those that have already been mentioned. [44] In the case of holosymmetric symmorphic crystals the dichromatic pattern and dichromatic complex are identical and so the dichromatic complex and complex variants are of no interest for our discussion. A bicrystal can now be created by introducing a mathematical plane into the dichromatic pattern in the orientation and position of the chosen interface, and locating white atoms at the positions of the white lattice on one side of the interface and black atoms at the positions of the black lattice on the other

side. For the grain boundary planes considered in this work, the resulting spatial group $\Pi^*(b)$ are the maximum symmetry interface. Morphological variants arise since different cuts of the dichromatic complex produce different bicrystal spatial groups; these will be discussed briefly. Finally the interface is allowed to relax by rigid-body translations that produce the boundary structure spatial group $\Pi(b)$. Relaxational variants occur since each translation produces a boundary with different symmetry.

The general procedure discussed above indicates that the steps that are needed to define the symmetry of the boundary structures to be studied are the following: to define the dichromatic pattern, to define the maximum symmetry interface (and morphological variants), and to define and study relaxed interfaces and relaxational variants. The first two steps are studied in this section while the last aspect is reserved for the next section of this chapter.

It has been mentioned that one of the components of the dichromatic composite is regarded white and the other black. The point and space groups of such composites are expressed by using color symmetry groups. Symmetry relationships between the two components are expressed by color-reversing symmetry operations while the symmetry between parts of the same crystal are given by ordinary symmetry elements. A pattern is said to have dichromatic symmetry if a change in color occurs in conjunction with one or more of its symmetry elements. For example the colored point group $4'$ consists of: two right angles, and colored rotations through one right angle and three right angles. Colored symmetry elements are indicated by a prime ($'$) or by the operator R_c. Thus g' denotes the action of a glide g followed by a change of color and similarly m' is a mirror symmetry followed by a change of color. The symmetry

operation t' denotes a translation of one-half the repeat distance in any direction, followed by a change of color. The dichromatic pattern symmetry group is one of the Shubnikov (colored) point and space groups. Bradley and Cracknell divide Shubnikov space groups into the four categories given next. [45] Type I are the ordinary Fedorov space groups G. A type II Shubnikov group M is given by $M = G + R_c G$. For example the two-dimensional space group pmm transforms to the gray group $pmm21'$. Type III are black and white space groups based on ordinary Bravais lattices. A type III space group is given by $M = H + R_c(G - H)$ where H is a halving subgroup of the Fedorov space group and $(G - H)$ contains no pure translations. Type III Shubnikov groups lack antitranslation and anti-identity operators but contain antisymmetry operators. For example the two-dimensional Fedorov group pmm gives rise to pmm' and $pm'm'$. There are 674 type III Shubnikov groups. Type IV Shubnikov groups are given by Fedorov groups augmented by an equal number of colored operations that are the result of multiplying an element in G by the antitranslation operator; $M = G + t'G$. For example the two-dimensional space group pmm gives rise to $p_b'mm$ and $p_c'mm$ where the subscripts b and c indicate the direction in which the change of color occurs. There are 517 type IV space groups. A systematic list of the Shubnikov space groups is given in Shubnikov and Belov. [46] The dichromatic patterns have Shubnikov type III symmetry groups.

However, dichromatic patterns can have translation symmetry in zero, one, two or three dimensions. The symmetry of a dichromatic pattern with no translation symmetry is given by the colored point group. The symmetry of a dichromatic pattern with one-dimensional translation symmetry is given by colored rod groups. A rod is an infinite periodic body related to a singular axis lying in the body. Many examples of

rod groups have been investigated in nature (for example the double helix of DNA). An international nomenclature and complete listing does not exist although Shubnikov and Kopstik mention many examples. [47] Rod groups can contain non-crystallographic rotation operations (including roto-inversion and colored rotations). Axes with 8- and 12- fold symmetry will be encountered later on; these rod groups are treated in detail by Vlachavas. [48] For cubic lattices, two-dimensional translation symmetry is not possible since a periodicity in two directions **u**,**v** implies a periodicity in $\mathbf{u}\times\mathbf{v}$. Finally, dichromatic patterns in three dimensions have Shubnikov type III symmetry groups.

The dichromatic pattern symmetry group is composed of ordinary symmetry elements and color reversing symmetry elements. Ordinary symmetry elements occur when identical symmetry elements of the white and black lattices are coincident. In the following discussion groups are denoted by G and elements in the group by g; subscripts w, b, and c indicate the white lattice, the black lattice and the composite, respectively. Subgroups are designated D with elements d and subscripts o for ordinary and c for color. The black lattice is considered to be generated from the white lattice by the operation of the rotation matrix and a color reversal (operator R). The elements of D_o are elements of G_w such that

$$d_{oi} = R d_{oi} R^{-1} \tag{2.5.1}$$

A white lattice point can be generated from a black lattice point by an operator $g_w R^{-1} d_o$. In addition another operation d_o can be effected on the white lattice. The color reversal operations are then given by

$$d_{ci} = d_{ok}\ g_{wi}\ R^{-1}\ d_{oi} \tag{2.5.2}$$

If g_{wi} is a member of D_o then $d_{ci} = d_{oi}\ R^{-1}$; otherwise, $d_{ci} = g_{wi}\ R^{-1}$. By adding

$D_o + D_c$ a table of antysimmetry groups formed by the superposition of two identical point groups can be developed (Table 2.5.1). [49]

It should be remembered that what is needed is the dichromatic pattern of the lattice that in the uncolored version is a CSL. For quaternions {m,1,0,0} it can be shown that the CSL is tetragonal, and for quaternions {m,1,1,0} the CSL is orthorhombic except for {1,1,1,0} ($\Sigma 3$) where the CSL is hexagonal. [50] In Table 2.5.1. there are three colored point groups that are derived from tetragonal lattices ($8'/mmm'$, $4'/mmm'$ and $4/mm'm'$). All the <100> CSLs examined have colored symmetry $I4'/mmm'$ as shown for example in Figure 2.5.2.a. Notice that in this figure the translation-bearing symmetry elements are omitted for simplicity. The colored rod group $8'/mmm'$ arises at the unique rotation [100]/45° (not a CSL rotation); this is an example of extension of the dichromatic pattern by a symmetrizing operation. An angle of 45° is outside the angular range of interest in this research and thus this particular colored group is of no interest at present. Similarly, there is only one hexagonal colored group $6'/m'mm'$ which is the colored group of the twin boundary shown in Figure 2.5.2.b.; this twin boundary has been discussed previously, but notice that the projection in this figure is [111]. There is only one orthorhombic colored group $mm'm'$. It appears in [110] boundaries as either C-centered or F-centered, as shown in Figure 2.5.2.d and e. *It has been established then that the dichromatic patterns of interest are* $I4'/mmm'$ *for [100] tilt boundaries;* $P6'/m'mm'$ *for the twin boundary; and* $Cmm'm'$ *or* $Fmm'm'$ *for the other [110] boundaries.*

The dichromatic pattern having been established, there is now a dilution of symmetry as the degrees of freedom are reduced (moving to the right in Fig. 2.5.1). The

Table 2.5.1 Antysimmetry point groups formed by the superposition of two identical point groups with common origin (from reference [49]).

Point group of components	Antisymmetry point group of composite
1	$11'$ $\bar{1}'$ $2'$ m'
$\bar{1}$	$\bar{1}1'$ $2'/m'$
2	$21'$ $2/m'$ $22'2'$ $2m'm'$ $4'$ $\bar{4}'$ $2'$ m'
m	$m1'$ $2'/m$ $2'mm'$ $2'$ m'
$2/m$	$2/m1'$ $mm'm'$ $4'/m$ $2'/m'$
222	$2221'$ $m'm'm'$ $4'22'$ $\bar{4}'2m'$ $22'2'$ $2m'm'$ $2'$ m'
$2mm$	$2mm1'$ mmm' $4'mm'$ $\bar{4}'2'm$ $22'2'$ $2m'm'$ $2'mm'$ $2'$ m'
mmm	$mmm1'$ $4'/mmm'$ $mm'm'$ $2'/m'$
4	$41'$ $4/m'$ $42'2'$ $4m'm'$ $8'$ $\bar{8}'$ $2'$ m'
$\bar{4}$	$\bar{4}1'$ $4'/m'$ $\bar{4}2'm'$ $2'$ m'
$4/m$	$4/m1'$ $4/m'm'm'$ $8'/m$ $2'/m'$
422	$4221'$ $4/m'm'm'$ $8'22'$ $\bar{8}'2m'$ $42'2'$ $4'22'$ $4m'm'$ $\bar{4}'2m'$ $22'2'$ $2m'm'$ $2'$ m'
$4mm$	$4mm1'$ $4/m'mm$ $8'mm'$ $\bar{8}'2'm$ $42'2'$ $4m'm'$ $2'mm'$ $2'$ m'
$\bar{4}2m$	$\bar{4}2m1'$ $4'/m'mm'$ $4'22'$ $\bar{4}'2m'$ $\bar{4}2'm'$ $22'2'$ $2m'm'$ $2'mm'$ $2'$ m'
$4/mmm$	$4/mmm1'$ $8'/mmm'$ $4'/mmm'$ $4/mm'm'$ $mm'm'$ $2'/m'$
3	$31'$ $\bar{3}'$ $32'$ $3m'$ $6'$ $\bar{6}'$ $2'$ m'
$\bar{3}$	$\bar{3}1'$ $\bar{3}m'$ $6'/m'$ $2'/m'$
32	$321'$ $\bar{3}'m'$ $6'22'$ $\bar{6}'2m'$ $32'$ $3m'$ $22'2'$ $2m'm'$ $4'$ $\bar{4}'$ $2'$ m'
$3m$	$3m1'$ $\bar{3}'m$ $6'mm'$ $\bar{6}'2'm$ $32'$ $3m'$ $2'mm'$ $2'$ m'
$\bar{3}m$	$\bar{3}m1'$ $6'/m'mm'$ $\bar{3}m'$ $4'/m$ $2'/m'$ $mm'm'$
6	$61'$ $6/m'$ $62'2'$ $6m'm'$ $\underline{12}'$ $\overline{\underline{12}}'$ $2'$ m'
$\bar{6}$	$\bar{6}1'$ $6'/m'$ $\bar{6}2'm'$ $2'$ m'
$6/m$	$6/m1'$ $6/mm'm'$ $\underline{12}'/m$ $2'/m'$
622	$6221'$ $6/m'm'm'$ $\underline{12}'22'$ $\overline{\underline{12}}'2m'$ $62'2'$ $6m'm'$ $4'22'$ $\bar{4}'2m'$ $22'2'$ $2m'm'$ $2'$ m'
$6mm$	$6mm1'$ $6/m'mm$ $\underline{12}'mm'$ $\overline{\underline{12}}'2'm$ $62'2'$ $6m'm'$ $2'mm'$ $2'$ m'
$\bar{6}m2$	$\bar{6}m21'$ $6'/mmm'$ $\bar{6}2'm'$ $4'mm'$ $\bar{4}'2'm$ $22'2'$ $2m'm'$ $2'mm'$ $2'$ m'
$6/mmm$	$6/mmm1'$ $\underline{12}'/mmm'$ $6/mm'm'$ $4'/mmm'$ $mm'm'$ $2'/m'$
23	$231'$ $m'3'$ $\bar{4}'3m'$ $4'32'$ $32'$ $3m'$ $6'$ $\bar{6}'$ $22'2'$ $2m'm'$ $2'$ m'
$m3$	$m31'$ $m3m'$ $\bar{3}m'$ $6'/m'$ $mm'm'$ $2'/m'$
432	$4321'$ $m'3'm'$ $8'22'$ $\bar{8}'2m'$ $6'22'$ $\bar{6}'2m'$ $4'22'$ $42'2'$ $4m'm'$ $\bar{4}'2m'$ $32'$ $3m'$ $22'2'$ $2m'm'$ $2'$ m'
$\bar{4}3m$	$\bar{4}3m1'$ $m'3'm$ $6'mm'$ $\bar{6}'2'm$ $\bar{4}2'm'$ $32'$ $3m'$ $2'mm'$ $2'$ m'
$m3m$	$m3m1'$ $8'/mmm'$ $6'/m'mm'$ $4'/mmm'$ $4/mm'm'$ $\bar{3}m'$ $mm'm'$ $2'/m'$

(a) [100]/36.9 °, Σ5, $I\,4/mm'm'$

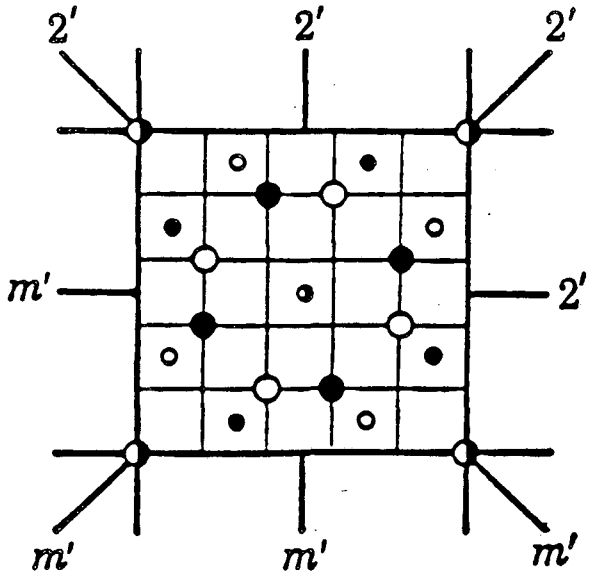

(b) [111]/60.0 °, Σ3, $P\,6'/m'm'm$

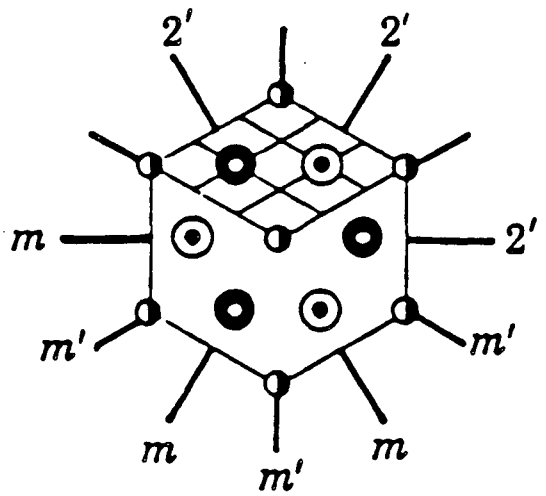

Fig. 2.5.2 See caption on next page.

(c) [110]/38.9 °, Σ9, *Fmm'm'*

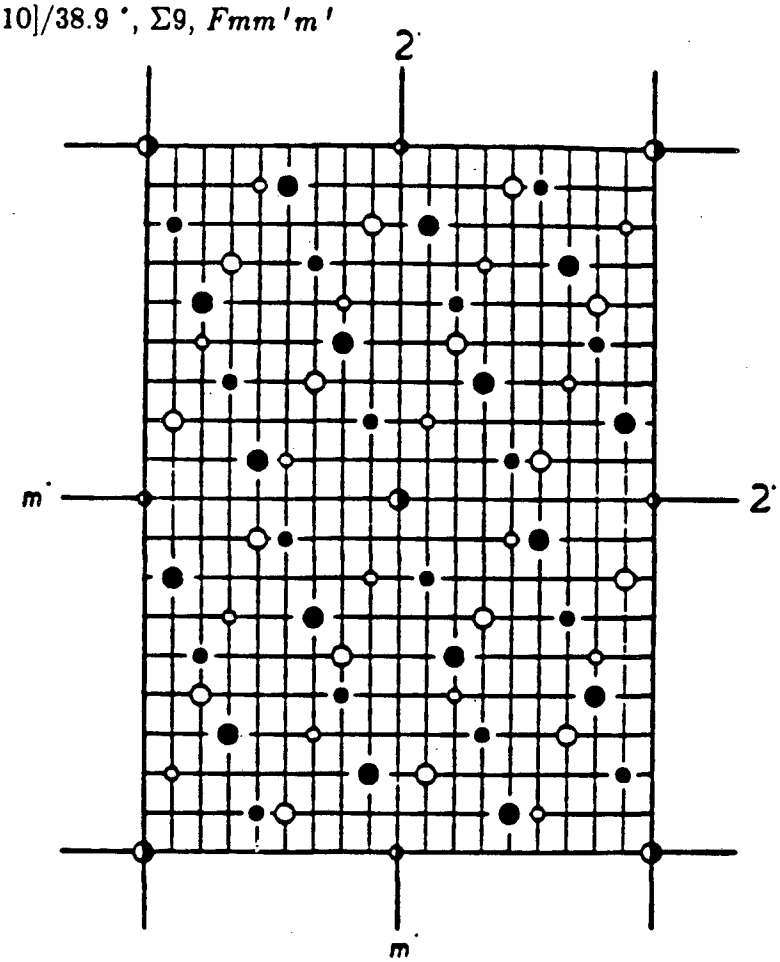

(d) [110]/50.47 °, Σ11, *Cmm'm'*

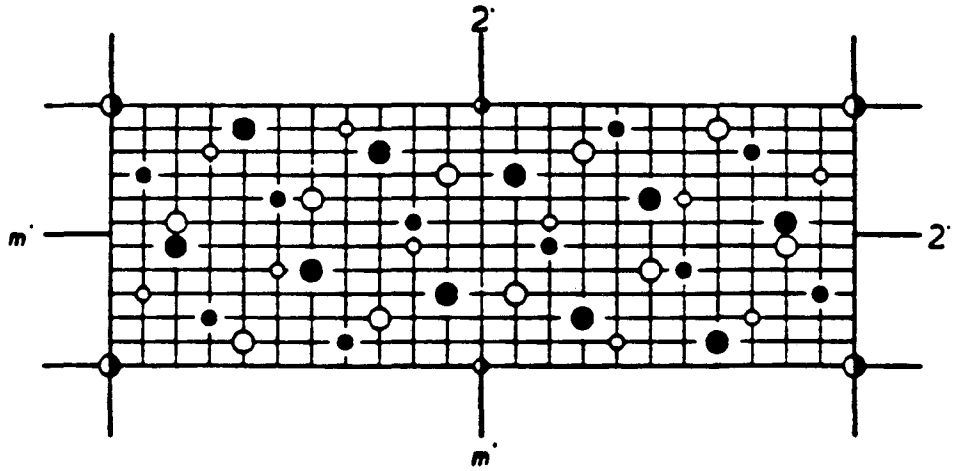

Fig. 2.5.2 Projections along the tilt axis of dichromatic patterns formed by body-centered cubic lattices. The size of the symbols at atom positions represent the stacking along the tilt axis (a and b from Pond and Bollman, *op.cit.*).

reduction in symmetry is given by a crystallographic theorem; [51] a crystallographic space group G can be decomposed into left cosets with respect to a subgroup H by

$$G = H + g_1H + g_2H + \cdots + g_{n-1}H \tag{2.5.3}$$

where n is defined as the index of H in G and g_i are operators in G which do not belong to H. The elements g_i are such that g_i is contained only in the coset g_iH. The index n has geometric significance; the number of variants (see Fig. 2.5.1) of the structure H is equal to n. The loss of symmetry occurs in three forms:

(1) by reducing the order of the point group. These are sometimes referred to as *Zellengleich* subgroups, [52] but the new international convention of referring to them as *translationengleich* or t-subgroups is used here. These subgroups conserve all translations of the space group.

(2) by loss of translations. The point group of H is the same as that of G and the crystal class is unchanged. These are defined as *klassengleich* or k-subgroups.

(3) by a combination of 1 and 2.

The point group of a bicrystal is a subgroup of that for the dichromatic pattern. For CSL based dichromatic patterns the bicrystal symmetry class is that of a layer. Layer groups are simply the two-dimensional color groups derived from the two-dimensional plane groups; a listing of these colored groups is given by Belov and Tarkhova. [53] The symmetry elements of a bicrystal depend on the orientation of the interface. For example in Fig. 2.5.2.a a twist boundary with boundary plane $(100)_c$ or $\{100\}$ in the crystals has space group $p\,42_1{}'2'$. The subscript c indicates a plane of the CSL; the [100] direction of the CSL is normal to the page and the [010] direction is along a line of text. Tilt boundaries with planes $(010)_c$, $(001)_c$, $(011)_c$ or $(0\bar{1}1)_c$ (

{013} and {012}) have symmetry $p\,2'mm'$. A boundary $(0rs)_c$, {0lm} conserves the mirror plane normal to the tilt axis and thus has symmetry $p\,1m\,1$. There are other possible bicrystals. However, it is not possible to obtain bicrystals with point symmetries belonging to all subgroups of $4/mm'm'$. *The maximum point symmetry of a tilt boundary is $2'mm'$, and this is the point symmetry of all the symmetrical tilt boundaries in our study.* This is regardless of the original dichromatic pattern. This is why the unrelaxed bicrystal pattern is designated as a maximum symmetry interface in Figure 2.5.1.

Morphological variants are the result of the constraint imposed by the interface. Morphological variants are crystallographically equivalent interfacial cuts of the dichromatic pattern. The number of morphological variants of a maximum symmetry interface is given by the index of H in G. For example the dichromatic pattern $[4/mm'm'$ gives rise to the maximum symmetry interface $p\,2'mm'$ by the cut $(010)_c$, {013}. The point group decomposes as

$$\begin{aligned}\{4/mm'm'\} &= \{2'mm'\} + 4^1_{100}\,\{2'mm'\} + 2^1_{100}\,\{2'mm'\} + 4^3_{100}\,\{2'mm'\} \\ &= \{4\}\,\{2'mm'\}\end{aligned} \tag{2.5.4}$$

Consequently there are 4 crystallographically equivalent morphological variants which can be seen as the cuts $(010)_c$, $(0\bar{1}0)_c$, $(001)_c$, $(00\bar{1})_c$. The cuts of the type $(011)_c$ also have maximum interface symmetry $2'mm'$ but the two cuts are crystallographically non-equivalent.

2.6. Variations of Bicrystal Symmetry with Translations of the Black Lattice

It is possible now to examine the last step in Figure 2.5.1, the loss of symmetry that occurs due to a rigid body displacement of the black lattice. It should be pointed out that it is immaterial whether relaxations of the maximum symmetry interface are viewed as the last step, or translations of the dichromatic pattern are taken into account before a cut to that pattern produces a bicrystal. [54] The later procedure is more cumbersome. Consider for a moment the displacements of the dichromatic pattern. The translation vectors of the DSCL preserve the symmetry of the dichromatic pattern, and thus they are also Displacement Symmetry Conserving. [55] This implies that only the reduced displacements inside the Wigner-Seitz cell of the DSCL should be considered. As an illustration examine the loss of symmetry with displacements of the black lattice in Fig.2.5.2.a. For displacements $(x\,00)_c$ along the tilt axis the ordinary mirror plane is lost, the color four-fold axis is lost, and the color mirror planes are transformed into color two-fold rotations; the resulting space group is $I\,42'2'$. For a displacement $(0y\,0)_c$ normal to the tilt axis, the mirror planes that are not normal to the displacement are lost while the mirror plane that is normal to the mirror plane is translated by $x/2$, and the ordinary mirror plane is conserved; the resulting space group is $Im'm\,2'$. However, when $x = 1/2$ the colored mirror plane parallel to the translation is transformed into a colored glide reflection a' ; the resulting space group is now $Imm'a'$. These examples illustrate some of the different principles that will be developed in the following systematic treatment.

Figure 2.6.1 illustrates the cells of the layer groups $pm\,2'm'$ and $cm\,2'm'$ with their respective symmetry elements. Notice that the position of the symbols in the

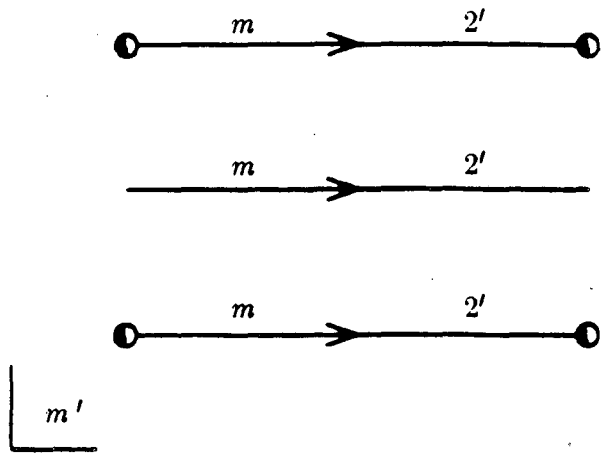

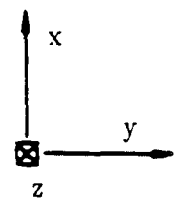

Subgroups of $pm\,2'm'$

t-subgroups
Type I: $pm\,11$, $p\,12'1$, $p\,11m'$, $p\,1$
k-subgroups
Type IIa: none
Type IIb: $cm\,2'm'$, $cm\,2'n'$, $pb\,2_1'm'$, $pm\,2_1'b'$, $pb\,2'b'$, $pm\,2_1'n'$, $pb\,2'n'$, $pm\,2'a'$, $pb\,2_1'a'$

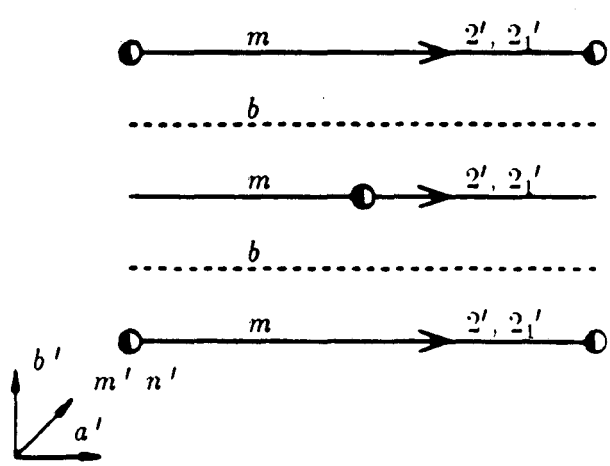

Subgroups of $cm\,2'm'$

t-subgroups
Type I: $cm\,11$, $c\,12'1$, $p\,11m'$, $p\,1$
k-subgroups
Type IIa: $pm\,2'm'$, $cm\,2'g'$, $pb\,2_1'm'$, $pm\,2_1'b'$, $pb\,2'b'$, $pm\,2_1'g'$, $pb\,2'g'$, $pm\,2'a'$, $pb\,2_1'a'$
Type IIb: none

Fig. 2.6.1Symmetry Elements of CSL Symmetrical Boundaries

layer group have been changed to correspond to the axis convention used throughout this work : x is the tilt axis, the y axis is parallel to the boundary plane and the z axis is normal to the boundary plane. In figure 2.6.1 the graphical symbol conventions of the International Tables for Crystallography are used, and in addition, the letter notation is given to differentiate color and ordinary symmetry elements. [56] The colored mirror plane (m') has as subelements the colored diagonal glide plane (n') or two glide planes normal to each other (a' and b', denoted in one symbol as g'). The colored two-fold rotation axis ($2'$) has as subelement the colored screw axis ($2_1'$). The atom positions indicated really correspond to the reference structures such as Figures 2.4.1.b and 2.4.2.b except that now the plane of the page is the boundary plane; there is a plane of black atoms on the top side of the boundary plane and a plane of white atoms on the back side.

An important aspect of the procedure used in this section is to determine the subgroups of the space groups $pm\,2'm'$ and $cm\,2'm'$. In deriving these subgroups reference will be made to definitions and procedures described in the International Tables for Crystallography. The point group of the layer cell characterizes the t-subgroups of the layer group. [57] There are 31 layer cells [58] and the one of interest here is $m\,2'm'$. The multiplication tables of this layer point group are simple enough so that the t-subgroups can be readily determined and are indicated in Fig. 2.6.1; listings are also available. [59] The subgroups will be referred to in an unconventional Herman-Maugin symbol as in the International Tables for regular uncolored crystallography; [60] the conventional groups can be easily derived. The k-subgroups are of three types: [61] for type IIa the unit cell size is conserved, for type IIb the unit cell size is a derivative lattice and for type IIc the unit cell size is also a derivative lattice and the

subgroup is the maximal isomorphic subgroup. The sets of type IIb and IIc are infinite so some restrictions are imposed. First it is noted that a plane rectangular primitive lattice can have either a primitive or centered sublattice. Similarly a plane rectangular centered lattice can have a primitive or centered sublattice. All sublattices (derivative lattices) of indices higher or equal to 4 are ignored since the first few sublattices give the different symmetries and cell multiplicities are of no interest. The derivative lattices are used as a way to find the symmetries of the subgroups. Thus the maximal isomorphic subgroups and the other isomorphic groups (type IIc) are left out because they are totally equivalent to the original structure.[62] In order to get the subgroups of type IIa and IIb it is best to look at a listing of plane groups arranged by common point groups and cell size, for example that by Lockwood and Macmillan. [63] If any of the plane groups of the same plane point group can be obtained by the arrangement in the proper order of elements and subelements of the parent group G then that indicates a subgroup H of G. For the layer groups, subelements of m' are n', b', a', g'; the subelement of m is b; the subelement of $2'$ is $2_1'$. At once the k-subgroups of $pm\,2'm'$ are all of type IIb and they are: $cm\,2'm'$, $cm\,2'n'$, $pb\,2_1'm'$, $pm\,2_1'b'$, $pb\,2'b'$, $pm\,2_1'n'$, $pb\,2'n'$, $pm\,2'a'$, $pb\,2_1'a'$. Similarly the k-subgroups of $cm\,2'm'$ are all type IIa and they are the same as above except that $cm\,2'm'$ becomes $pm\,2'm'$ and the symbol n' should be replaced by g' to indicate a glide in x and a glide in y, but not a diagonal glide. A theorem due to Herman states that a maximal subgroup of a space group G is either a t-subgroup or a k-subgroup of G. [64] Additional general subgroups exist that are the k-subgroups of the t-subgroups of G. [65] Since the maximal subgroups are the ones of interest the general subgroups were not investigated. The subgroups worked out in this paragraph are

listed for convenience in Figure 2.6.1.

Symmetry operations can be denoted by their Seitz symbol $S \equiv (\mathbf{S}/\tau)$. S is a 3×3 matrix and τ is the vector that represents the translation part of the symmetry operation. For example the colored two-fold screw axis operator, $2_1'$ is given by

$$(2_{[010]} / [0,1/2,0])' \cdot \mathbf{r} = \begin{bmatrix} \bar{1} & 0 & 0 \\ 0 & 1 & 0 \\ 0 & 0 & \bar{1} \end{bmatrix}' \begin{bmatrix} x \\ y \\ z \end{bmatrix} + \begin{bmatrix} 0 \\ 1/2 \\ 0 \end{bmatrix} \tag{2.6.1}$$

The multiplication rule of these operators is simply

$$(\mathbf{S}_2/\tau_2) \cdot (\mathbf{S}_1/\tau_1) = (\mathbf{S}_1\mathbf{S}_2 / (\mathbf{S}_2\tau_1+\tau_2) \tag{2.6.2}$$

The identity operator is (I,0).

Upon translation of the black lattice there are six types of transformation on a symmetry element; these are shown in Table 2.6.1. The equivalent of cases 4 and 6 for ordinary symmetry elements are not possible because they correspond to a change of symmetry of one of the components, in other words, a change of crystal structure.

Table 2.6.1
Spatial Symmetry Variations

Case	Before	After	Conservation Equation
1	Ordinary tf†	Ordinary tf	2.6.6
2	Ordinary tb	Ordinary tb	2.6.10
3	Colored tf	Colored tf	2.6.6
4	Colored tf	Colored tb	2.6.13
5	Colored tb	Colored tb	2.6.10
6	Colored tb	Colored tf	2.6.14

† tf = translation-free , tb = translation-bearing

It is now possible to examine the changes in bicrystal symmetry caused by rigid-body translations. First the spatial variation for each symmetry element is examined (as in Table 2.6.1). Let us first examine the cases where a translation-free element remains translation-free as in cases 1 and 3 of Table 2.6.1. In the particular case of layer groups, anti-identity, inversion and anti-inversion centers do not exist. Ordinary symmetry elements occur in a bicrystal because of spatial coincidence of identical operations of the two components. Consequently, a displacement **t** conserves an ordinary translation-free symmetry element only if it leaves these operations in coincidence. Before the translation, two points in the same lattice are related by

$$\mathbf{S}_o \cdot \mathbf{r}_b = \hat{\mathbf{r}}_b \tag{2.6.3}$$

and similarly for the white lattice. The hat over a vector position indicates the vector after a symmetry operation. After the translation

$$\mathbf{S}_o \cdot (\mathbf{r}_w - \mathbf{t}/2) = \hat{\mathbf{r}}_w - \mathbf{t}/2 \tag{2.6.4}$$

and

$$\mathbf{S}_o \cdot (\mathbf{r}_b + \mathbf{t}/2) = \hat{\mathbf{r}}_b + \mathbf{t}/2 \tag{2.6.5}$$

In these equations the displacement **t** is thought to occur by a displacement $-\mathbf{t}/2$ of the white lattice and $\mathbf{t}/2$ of the black lattice. The conservation equation is then

$$\mathbf{S}_o \cdot (\mathbf{t}/2) = \mathbf{t}/2 \tag{2.6.6}$$

It should be remembered that positions are expressed here in the coordinates of the dichromatic pattern or CSL. For example for the mirror plane $m_{[100]}$

$$\begin{bmatrix} \bar{1} & 0 & 0 \\ 0 & 1 & 0 \\ 0 & 0 & 1 \end{bmatrix} \begin{bmatrix} 0 \\ t_2/2 \\ t_3/2 \end{bmatrix} = \begin{bmatrix} 0 \\ t_2/2 \\ t_3/2 \end{bmatrix} \tag{2.6.7}$$

The following general rule can be stated: *an ordinary two-fold axis or mirror plane is conserved only by displacements parallel to this axis or plane of symmetry.* In the original dichromatic bicrystal a colored translation-free symmetry element is given by

$$\mathbf{S}_c \cdot \mathbf{r}_w = \mathbf{r}_b \tag{2.6.8}$$

After displacement the symmetry relationship becomes

$$\mathbf{S}_c \cdot (\mathbf{r}_w - \mathbf{t}/2) = \mathbf{r}_b + \mathbf{t}/2 \tag{2.6.9}$$

The conservation equation is given then by

$$\mathbf{S}_c \cdot (-\mathbf{t}/2) = \mathbf{t}/2 \tag{2.6.10}$$

For the colored mirror plane $m'_{[001]}$

$$\begin{bmatrix} 1 & 0 & 0 \\ 0 & 1 & 0 \\ 0 & 0 & \bar{1} \end{bmatrix}' \begin{bmatrix} 0 \\ 0 \\ -t_3/2 \end{bmatrix} = \begin{bmatrix} 0 \\ 0 \\ t_3/2 \end{bmatrix} \tag{2.6.11}$$

The following rule can be stated: *a color-reversing axis $2'$ or plane m' is conserved by displacements which are perpendicular to the rotation axis or symmetry plane.* Using type 1 and 3 symmetry variations the rigid body relaxations 1-5 in Table 2.6.2 are possible. For each subgroup the displacement conserves all the symmetry operations in the subgroup. The spatial symmetry for a displacement with no changes in the type of symmetry element is always given by a t-subgroup.

There are no translation bearing symmetry elements in the bicrystal layer group $pm2'm'$. Thus cases 2, 5 and 6 in Table 2.6.2 are of no concern for the relaxation of

this bicrystal. The layer group $cm\,2'm'$ has both ordinary and colored translation-bearing symmetry elements. The preservation of these elements (cases 2 and 5) occurs by an equation such as 2.6.6 and 2.6.10. If the relaxation of this dichromatic bicrystal is of interest then all cases in Table 2.6.2 should be taken into account.

Next, displacements that transform translation-free rotation axes or mirror planes of the original bicrystal into screw axes or glide planes, and vice versa, are considered (cases 4 and 6). These displacements are referred to as special because they are given by a vector of specific magnitude, whereas the displacements already obtained in the paragraphs above maintain the symmetry of the relaxed bicrystal over wide limits of translations. The translation-free symmetry element is denoted by $(\mathbf{S}_c/0)$ and the translation-bearing symmetry element by $(\mathbf{S}_c/\tau)$. In the original bicrystal Eqn. 2.6.8 holds. After displacement

$$(\mathbf{S}_c/\tau)\cdot(\mathbf{r}_w-\mathbf{t}/2) \equiv \mathbf{S}_c\cdot(\mathbf{r}_w-\mathbf{t}/2)+\tau = \mathbf{r}_b+\mathbf{t}/2 \qquad (2.6.12)$$

or

$$\mathbf{S}_c\cdot(-\mathbf{t}/2)+\tau = \mathbf{t}/2 \qquad (2.6.13)$$

Similarly for case 6 a nonsymmorphic colored operation is transformed to its symmorphic part by

$$\mathbf{S}_c\cdot(-\mathbf{t}/2)-\tau = \mathbf{t}/2 \qquad (2.6.14)$$

The periodicities of the maximum symmetry interface in the x,y,z axes will be denoted as a_c, b_c, c_c. Consider the transformation of $2'_{|010|}$ to $2_{1,}'_{|010|}$

$$\begin{bmatrix} \bar{1} & 0 & 0 \\ 0 & 1 & 0 \\ 0 & 0 & \bar{1} \end{bmatrix}' \begin{bmatrix} -t_1/2 \\ -\frac{1}{2} b_c/2 \\ -t_3/2 \end{bmatrix} + \begin{bmatrix} 0 \\ b_c/2 \\ 0 \end{bmatrix} = \begin{bmatrix} t_1/2 \\ \frac{1}{2} b_c/2 \\ t_3/2 \end{bmatrix} \tag{2.6.15}$$

The displacement can be written as $\mathbf{t} = (x\,0z) + (0,b_c/2,0)$. The following rule can be stated: *color reversing screw diads* $2_1'$ *or glide reflection planes* b', a', n', g' *are created from* $2'$ and m' *by displacements which are the sum of a displacement that leaves* $2'$ *or* m' *invariant and a displacement parallel to* $2'$ *or* m' *which is equal to the translation part of* $2_1'$, b', a', n', *or* g' .

The subgroups that correspond to the spatial symmetry of a special displacement are a k-subgroups. In order to find the displacement that produces a particular k-subgroup one looks, using the rules and equations in this section, for a displacement that will produce all the elements in the subgroup from the elements in the original maximum symmetry interface; b', a', g', n' come from m' (or vice versa); $2_1'$ from $2'$; b from m ; m', $2'$, *and/or* m can be conserved.

The special subgroups (6-8) are listed in Table 2.6.2. The coordinates used in Table 2.6.2 are fractional coordinates of the periodicities in the plane of the boundary.

The fact that all displacements show z variable comes from treating a quasi-two-dimensional problem as three-dimensional. It implies also that the component $\mathbf{t}_e$ of $\mathbf{t}$ (Eqn. 2.4.1) does not affect the bicrystal symmetry. It was also shown in section 2.4 that the component $\mathbf{t}_p$ can be reduced to an in-plane displacement within the CNID. This implies that *the variations of bicrystal symmetry with relative displacement can be determined from the position of the in-plane displacements within the CNID.*

The CNID of a $\Sigma 17$ (014) boundary is shown in Figure 2.6.2. All of the the symmetrical tilt boundaries studied are ρ=1 boundaries and their CNID is given by the

Table 2.6.2
Variations in Bicrystal Symmetry with Relative Displacements

#	Displacement	Symbol	Relaxed Bicrystal Symmetry	
			from $pm\,2'm'$	from $cm\,2'm'$
1	(0,0,0)	O	$pm\,2'm'$	$cm\,2'm'$
2	(0,y,z)	α	$pm\,11$	$cm\,11$
3	(x,0,z)	β	$p\,12'1$	$c\,12'1$
4	(x,y,z)	λ	$p\,1$	$p\,1$
5	(0,0,z)	δ	$pm\,2'm'$	$cm\,2'm'$
6	(1/2,0,z)	A	$pm\,2'a'$	$cm\,2'g'$
7	(0,1/2,z)	B	$pm\,2_1'b'$	$cm\,2'g'$
8	(1/2,1/2,z)	C	$pm\,2_1'n'$	$cm\,2'm'$

cell of smallest crystal lattice vectors in the boundary plane. The CNID of a $\Sigma 5$ (013) boundary is shown in Figure 2.6.3. This is a centered boundary and consequently the shape of the CNID is different. The reference structure is represented by the point O at the center of the cell, which also represents the translations δ normal to the boundary plane. The different displacements in table 2.6.2 are also ploted in Figures 2.6.2 and 2.6.3. Equivalent structures are indicated but they are not differentiated except for the displacement λ in Figure 2.6.2 whose variants are discussed next.

Relaxational variants (see Figure 2.5.1) can be analyzed by superimposing on the CNID the symmetry elements of Figure 2.6.1. The number of equivalent structures of a particular relaxed bicrystal is equal to the number of equivalent points in the CNID. For example consider the structure designated λ in Figure 2.6.2. There are three additional equivalent structures obtained from λ as indicated in Figure 2.6.4. The

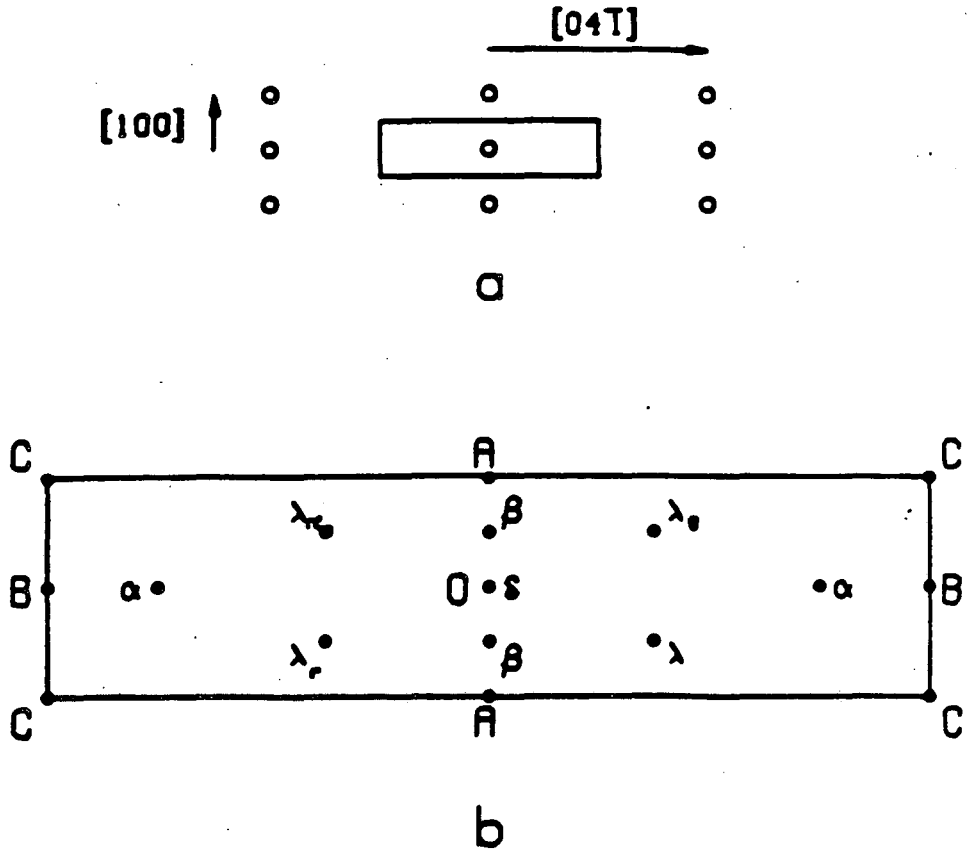

Fig. 2.6.2 CNID and displacements for a Σ17 (014) tilt boundary; (a) the position of the CNID in the boundary plane is indicated ; (b) relative displacements shown within the CNID.

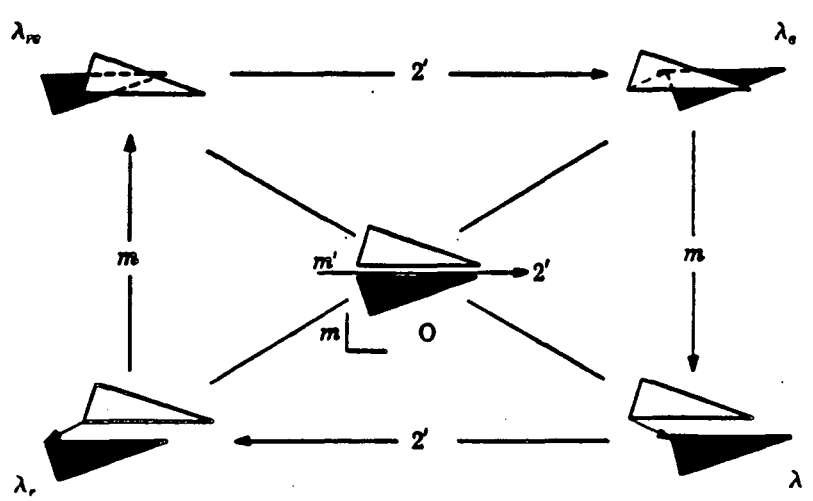

Fig. 2.6.3 Schematic representation of four equivalent bicrystal structures for a displacement with rank 4 in a symmetrical tilt boundary. The reference structure and the symmetry elements relating the structures are also shown (after Pond and Bollman, *op.cit.*) .

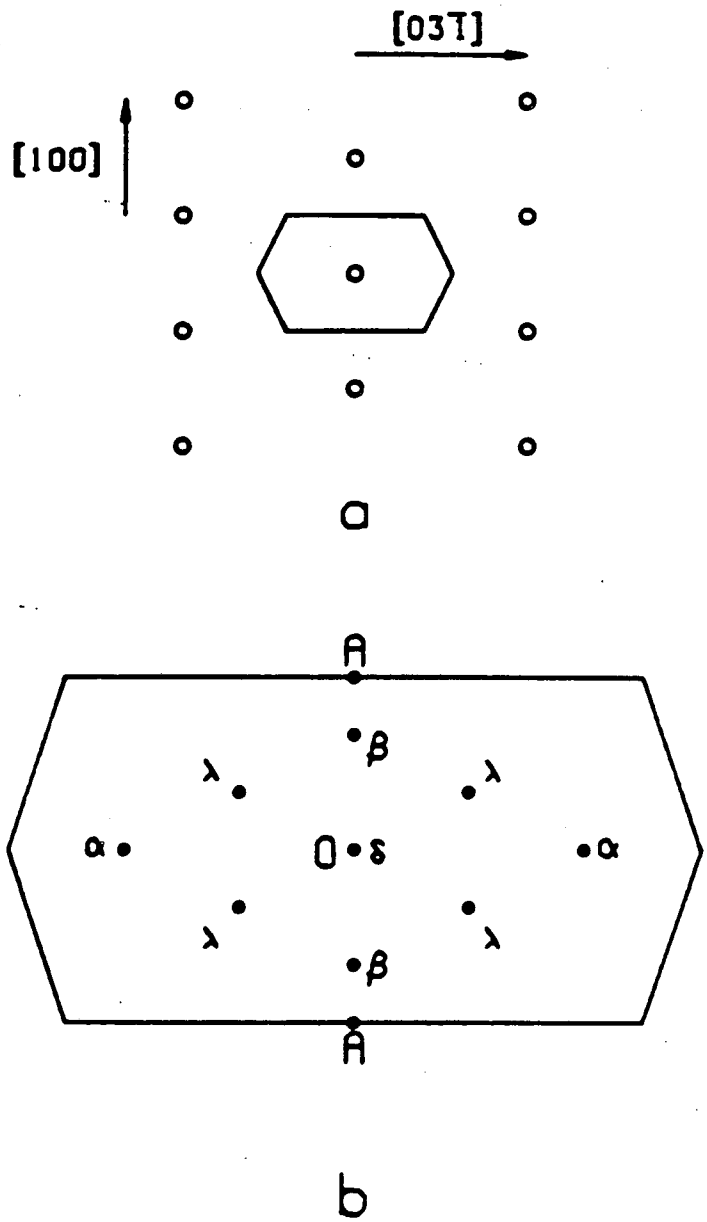

Fig. 2.6.4 CNID and displacements for a Σ5 (013) tilt boundary; (a) the position of the CNID in the boundary plane is indicated ; (b) relative displacements shown within the CNID.

structure λ_e is obtained from λ by the ordinary mirror plane operator. Notice that the superposition of the figures indicates the sense of the translation vector in the direction of the tilt axis, and that the axis of the mirror plane is fixed at the origin of the white lattice. The structure λ_r can be obtained from λ by applying the colored operation $2'$; this is perhaps visualized best if the transformation is thought to occur in three steps: two-fold rotation, color reversal and change of translation vector so as to correspond to a displacement of the black lattice. If m is applied to λ_r the structure λ_{re} is obtained. The number of relaxational variants is defined as the rank of a structure. The rank of a structure r_r is related to the order of the relaxed symmetry group n_r and the order of the bicrystal group n_b by [66]

$$n_r \times r_r = n_b \tag{2.6.16}$$

The previous discussion has important implications on the physical behavior of grain boundaries. The most general principle is the equivalent of the Neumann principle of crystal physics: [67] *The symmetry elements of any physical property of a bicrystal must include the symmetry elements of the point group of the bicrystal.* This implies that the nature of individual atom relaxations depends on the starting relative translation. The symmetry of the force field, i.e the pair-potential interactions, must be at least as high as the bicrystal symmetry. Symmetry considerations show that, in general, the structure of grain boundary dislocations with opposite Burgers vectors are generally different except at some rank 1 structures (for example the λ structure discussed above). [68] The variations of boundary energy $\gamma(\mathbf{t})$ with relative displacement describes a Wulff plot with point group symmetry $m\,2'm'$. Special displacements correspond to either local maxima or local minima; the character of the extrema has to

be decided by computation or physical experiment. Most computer calculations seem to indicate that the special translations correspond to local minima. [69] The few examples mentioned here show the importance of symmetry considerations in the analysis of the physical properties of grain boundaries.

2.7. References

[1] E. A. Kamenetzky, *The Mechanisms of Accommodation of Deformation at Grain Boundaries in BCC Materials* , M.S. Thesis, University of California, Berkeley, LBL - 14613, 1982.

[2] A. P. Sutton, *International Metals Rev.* **29** , 377 (1984).

[3] R. W. Balluffi and G. B. Olson, *Met. Trans.* **16A** ,529 (1985).

[4] D. H. Warrington and P. Bufalini, *Scripta Met.* **5** , 771 (1971).

[5] H. Grimmer, *Acta Cryst.* **A40** ,108 (1984).

[6] H. Grimmer, W. Bollmann and D. H. Warrington, *Acta Cryst.* **A30** , 197 (1974).

[7] S. Ranganathan, *Acta Cryst.* **A21** , 197 (1966).

[8] H. Grimmer, *op.cit.*

[9] A. E. H. Love, *A Treatise on the Mathematical Theory of Elasticity* ,Dover, New York, 1944, p.132.

[10] D. G. Brandon, B. Ralph, S. Ranganathan, and M. S. Wald, *Acta Met.* **12** , 813 (1964).

[11] D. G. Brandon, *Acta Met.* **14** ,1479 (1966).

[12] A. P. Sutton and V. Vitek, *Phil. Trans. R. Soc. Lond.* **A309** , 37 (1983).

[13] M. A. Fortes, *Rev. Fis. Quim. Engen.* **A7** ,7 (1972).

[14] H. Mykura, in *Grain Boundary Structure and Kinetics* , ASM Matls. Sci. Sem. 1979, ASM, Metals Park, Ohio, 1980, p.445.

[15] J. M. Penisson, R. Gronsky, and J. B. Brosse, *Scripta Met.* **16** ,1239 (1982).

[16] W. Bollmann, *Crystal Defects and Crystalline Interfaces* , Springer-Verlag, Berlin, 1970.

[17] E. Kamenetzky, *op.cit.*

[18] E. Kamenetzky, in *Proc. El. Micros. Soc. Am 40th Meet.* G. W. Bailey, ed., Claitor's Publishing, 1982, p.624.

[19] H. Grimmer, *Scripta Met.* **13** , 161 (1974)

[20] H. Grimmer, W. Bollmann, and D. H. Warrington, *op.cit.*

[21] A. Kelly and G. W. Groves, *Crystallography and Crystal Defects* , Addison-Wesley, Reading, MA, 1970, p.399.

[22] W. Bollmann, *Crystal Lattices, Interfaces, Matrices* , published by the author, Geneva, 1982, p.277.

[23] G. Thomas and M. J. Goringe, *Transmission Electron Microscopy of Materials* , John Wiley, New York, 1979, p.277.

[24] K. N. Tu, *Scripta Met.* **5** , 537 (1971).

[25] A. F. Acton and M. Bevis, *Acta Cryst.* **A27** , 175 (1971).

[26] W. Bollmann, *op.cit.* , p.276.

[27] *Ibid.* , pp. 26-30.

[28] H. Grimmer, W. Bollmann and D. H. Warrington, *op.cit.*

[29] R. C. Pond, *Proc. R. Soc. Lond.* **A357** ,471 (1977).

[30] W. Bollmann, *Crystal Defects and Crystalline Interfaces* , Springer Verlag, New York, 1970, pp. 207-209.

[31] D. A. Smith and R. C. Pond, *International Metals Rev.* **205** , 61 (1976).

[32] J. P. Hirth and R. W. Balluffi, *Acta Met.* **21** , 929 (1973).

[33] A. H. King and D. A. Smith, *Acta Cryst.* **A36** , 335 (1980).

[34] A. H. King, *Acta Met.* **30** , 419 (1982).

[35] A. Brookman, *Acta Cryst.* **A37** , 500 (1981).

[36] C. M. F. Rae and D. A. Smith, *Phil. Mag.* **A41** ,477 (1980).

[37] R. C. Pond and D. S. Vlachavas, *Proc. R. Soc. Lond.* **A386** ,95 (1983).

[38] D. Gratias and R. Portier, *J. de Physique* **C6-43** , 15 (1982).

[39] G. Kalonji and J. W. Cahn, *J. de Physique* **C6-43** ,25 (1982).

[40] A. V. Shubnikov and V. A. Kopstik, *Symmetry in Science and Art* ,Plenum Press, New York, 1977.

[41] A. V. Shubnikov and V. A. Kopstik *op. cit.*

[42] R. C. Pond and D. S. Vlachavas, *op. cit.*

[43] W. Fischer and E. Koch, *Lattice Complexes* , in *International Tables for Crystallography* , Vol. A, D. Reidel Publ. Co., Boston, 1983.

[44] R. C. Pond, *Phil. Mag.* **A47** , L49 (1983).

[45] C. J. Bradley and A. P. Cracknell, *The Mathematical Theory of Symmetry in Solids. Representation Theory for Point Groups and Space Groups* , Clarendon Press, Oxford, 1972, p. 575.

[46] A. V. Shubnikov and N. V. Belov, *Colored Symmetry* ,Pergamon Press, New York, 1964.

[47] A. V. Shubnikov and V. A. Kopstik, *op.cit.*

[48]. D. S. Vlachavas, *Acta Cryst.* **A40** ,221 (1984).

[49] D. S. Vlachavas, *Acta Cryst.* **A40** ,213 (1984).

[50] H. Grimmer, *Acta Cryst.* **A40** ,108 (1984).

[51] H. Wondratscheck, *Introduction to Space Group Symmetry* , in *International Tables for Crystallography* , Vol. A, D. Reidel Publ. Co., Boston, 1983.

[52] J. V. Smith, *Geometrical and Structural Crystallography,* J. Wiley, New York, 1982, p.293.

[53] N. V. Belov and N. A. Tarklova, *Dichromatic Plane Groups* ,in A. V. Shubnikov and N. V. Belov, *op.cit.*

[54] D. S. Vlachavas, *Acta Cryst.* **A40** ,200 (1984).

[55] R. C. Pond and W. Bollmann, *Philos. Trans. R. Soc. Lond.* **292** , 449 (1979).

[56] T. Hahn (ed.), *International Tables for Crystallography* ,Vol. A, D. Reidel Publ. Co., Boston, 1983, pp.7-10.

[57] T. Hahn (ed.), *op. cit.* ,p.736.

[58] N. V. Belov and T.N. Tarkhova, *op. cit.*

[59] E. Ascher and A. Janner, *Acta Cryst.* **18** ,325 (1965).

[60] T. Hahn (ed.), *op. cit* , p.32.

[61] T. Hahn (ed.), *op.cit.* , sections 6 and 7.

[62] Y. Billiet and E. F. Bertaut, *Isomorphic Subgroups of Space Groups* , in *International Tables for Crystallography* , Vol. A, D. Reidel Publ. Co.,Boston, 1983, p 809.

[63] E. H. Lockwood and R. H. Macmillan, *Geometric Symmetry* , Cambridge U. Press, Cambridge, 1978, pp.139-141.

[64] T. Hahn (ed.), *op.cit* , p.727.

[65] W. T. Holser, *Z. Kristallogr.* **110** ,266 (1958).

[66] R. C. Pond, in *Grain Boundary Structure and Kinetics* , ASM Matls. Sci. Sem. 1979, ASM, Metals Park, Ohio, 1980, p.13.

[67] J. F. Nye, *The physical properties of crystals* , Oxford U. Press, Oxford, 1969, p.20

[68] A. P. Sutton, D. A. Smith, and V. Vitek, *J. Micros.* **116** ,97 (1979).

[69] D. Schwartz, V. Vitek, and A. P. Sutton, *Phil.Mag.* **A51** ,499 (1985).

3. STRUCTURAL UNITS AND COMPUTATIONAL PROCEDURES

3.1. Limitations of the CSL-DSCL Model

Our discussion on the previous chapter was limited to the crystallography of CSL boundaries. It was shown in section 1.2 that these boundaries have special properties, and that the range over which these special properties extends is a few degrees from the CSL misorientation. The structures of these near-coincidence boundaries can be thought of as the CSL boundary plus an array of DSC dislocation wich preserve the CSL structure. This model is then an extension of the dislocation theory of small-angle grain boundaries. There is extensive experimental evidence that the model predicts correctly the dislocation content of the near-coincidence boundaries. Balluffi and his coworkers performed a series of experiments in FCC twist bicrystals of controlled misorientation and observed by TEM diffraction contrast that the spacing of the dislocations corresponds to that predicted by this model. [1] The experiments were later extended to larger deviations from coincidence by an improved diffraction contrast technique that included reflections due to the periodicity of the boundary. [2] Because of the difficulty of detecting small Burgers vectors in diffraction contrast the best conclusion that these studies could reach was that the observations were consistent with a relaxation to the nearby CSL.

An additional problem arises because of the multiplicity of dislocation descriptions of a particular boundary. Let the transformation relating two crystals $\mathbf{R}$ be a composite of the transformation to an ideal interface $\mathbf{R}_C$ and an additional transformation $\mathbf{R}_L$. The transformation $\mathbf{R}_L = \mathbf{R} \cdot \mathbf{R}_C^{-1}$ specifies the deviation to be accommodated by the secondary grain boundary dislocation array. The dislocation description

of the boundary is then given by the equivalent of Frank's formula for small-angle boundaries

$$\mathbf{b}^{SC} = \left[\mathbf{I} - \mathbf{R}_L^{-1}\right]\mathbf{p} \tag{3.1.1}$$

which indicates the total content of DSC dislocations crossing a vector $\mathbf{p}$ in the boundary plane. Clearly a different choice of unit cell or a symmetry operation would leave the boundary structure unchanged. To affect changes of unit cell in crystals 1 and 2 the corresponding transformation matrix would have to be modified by the corresponding unimodular lattice invariant shears $\mathbf{U}_2\mathbf{R}\mathbf{U}_1$. This would change $\mathbf{R}_L$ and consequently change the dislocation content of the interface. A symmetry operation would affect the dislocation content in exactly the same maner; the matrices $\mathbf{U}$ have to be replaced by the operations of the point group. For static properties of the grain boundaries any dislocation description is appropiate since they should all predict the same properties. Thus, one usually adopts the dislocation description that correspond to the largest spacing between dislocations or the rotation matrix that corresponds to the smallest angle of rotation (referred to as the misorientation throughout the text) and a unimodular transformation that relates nearest neighbors. On the other hand dynamical experiments on migrating boundaries could distinguish between different descriptions because the changes in shape of a bicrystal would be different for each description. Washburn and Parker conducted experiments in a tilt boundary in zinc which indicated clearly that the boundary was composed of a wall of edge dislocations. [3]

An additional problem in the dislocation description of grain boundaries is the difficulty in distinguishing extrinsic and intrinsic dislocations for particular geometries.

An extrinsic dislocation is associated with a long-range stress field and it is pressumed to enter the boundary from the crystal or to originate in grain boundary sources. These dislocations have been observed by the author using TEM diffraction contrast techniques. The extrinsic dislocations retain their identity in the boundary as trapped dislocations or dissociate into DSC dislocations. [4] Intrinsic dislocations have a short-range stress field and are part of the equilibrium structure of the boundary. However, Chou has proved based on symmetry arguments that an extrinsic dislocation in a dislocation wall at a symmetrical tilt boundary would have the same characteristics as that in a homogeneous single crystal. [5] In other words, the extrinsic dislocation has no long-range stress field and it cannot be distinguished from the intrinsic dislocations.

The worst problem arises due to the multiplicity of the choice of reference structure. No boundary in a cubic material is more than about 2° away from a CSL with $\Sigma<150$. There is then an obvious problem in deciding which is the reference structure for a particular boundary. A cutoff at some arbitrary Σ value would be totally arbitrary. One requirement would be that the minimum spacing of the secondary dislocations precludes reference structures with periodicty larger than that spacing. This criteria is invalidated as soon as dislocations with multiple DSC Burgers vectors are considered. For near-coincidence symmetrical tilt boundaries there is always a large number of reference structures that are possible.

The simple CSL model presented here has been extended on the basis of some physical arguments on the nature of the expected relaxations from coincidence. [6] A continuity in boundary description is obtained by using relaxations centered on O-lattice elements. This approach circumvents some of the objections mentioned above, but it is not quantitative and does not lead to the precise calculation of structures.

3.2. Atomistic Calculations: A Review and Critique

All atomistic calculations of grain boundary structure make use of a central force approximation whereby the interaction between atoms in an assembly occurs pairwise. For this assumption the energy of an assembly of N atoms is given by [7]

$$E = N \cdot U(\Omega) + \frac{1}{2} \sum_{\substack{i,j=1 \\ i \neq 1}}^{N} \Phi(r_{ij}) \tag{3.2.1}$$

where U is the part of the energy that depends only on the average volume per atom Ω, and Φ is the central force potential. The potential depends on the separation between atoms r_{ij} but also on Ω. The cohesive energy is described by the first term while the second term gives the energy change associated with changes in the relative positions of the atoms in the ensemble. The energy given by 3.2.1 is equivalent to a quantum mechanical second order perturbation expansion. The first term is an entirely arbitrary parameter which is fitted to give the appropiate elastic constants. This is an approximation which is justifiable for calculations of atomic arrangements but precludes the use of atomistic calculations for surface problems or problems involving point defects. Furthermore, a linear dependence of U on Ω is assumed so that the calculations carried at constant pressure and constant volume are equivalent. [8] The assumptions mentioned above imply that calculations can be carried out for problems where the local environments do not deviate appreciably from the perfect crystal. This is the case of grain boundary structures where only small and slowly varying changes of the density occur. However, it precludes the study of grain boundary point deffects, diffusion and crack nucleation. A simple potential that consists of a cohesive potential and the usual repulsive core-core interaction has been developed for transition metals. [9] This potential overcomes the restriction mentioned above but

to our knowledge it has not yet been used in atomistic calculations of grain boundary structure.

The BCC structure is stable under central forces in which the contributions of the first- and second- nearest neighbors are of the same magnitude. The atomic potential used in the calculations has to satisfy this requisite. Most atomistic calculations use empirical potentials which are analytical expressions with one or more parameter to be adjusted to some experimental observation. Almost all atomistic calculations for BCC structures were carried using the Johnson potentials for iron. Several Johnson potentials are shown in Figure 3.2.1. The original Johnson potential [10] J_o consists of three splines each of which has the form

$$\Phi(r_{ij}) = Ar^3 + Br^2 + Cr + D \tag{3.2.2}$$

fitted at their junction to provide continuity. The inner portion (up to 1st neighbor distance) is fitted to the threshold energy for radiation damage. The middle portion (up to just beyond the 2nd neighbor) is fitted to the elastic constants, and the third portion is chosen to go smoothly to zero just between the 2nd and 3rd neighbors. The other potentials are variations of the Johnson potential which include additional splines so that additional constants are fitted to energy of a generalized stacking fault. [11] The potential J_o has the peculiarity that the density dependent term of Eqn. 3.2.1 is null. One of the striking characteristics of atomistic simulations is that for a given metal all grain boundary structures calculated using different potentials are the same. Some material properties such as point defect formation and activation energies and the energy of stacking faults are known to be extremely sensitive to the empirical potential parameters. To the authors knowledge there is no detailed account as to why

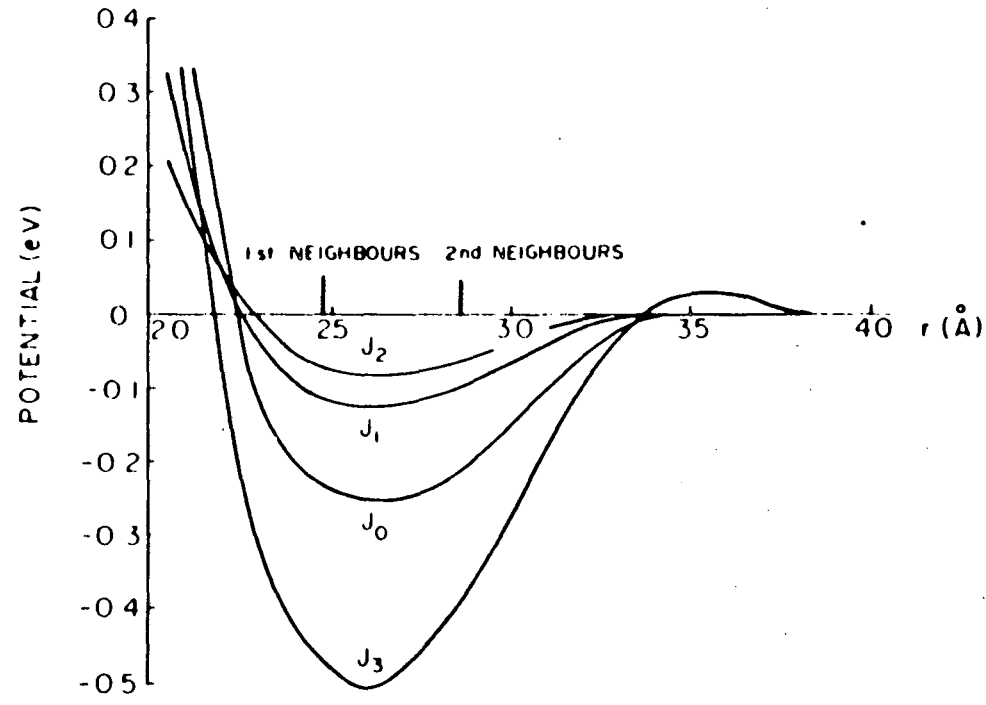

The Johnson-type potentials for b.c.c. iron used in the present work. The first- and second-nearest-neighbour separations are marked. J_0 is the original Johnson potential and J_1, J_2 and J_3 potentials constructed by Duesbery *et al.* (1973).

XBL 833-8735

Fig. 3.2.1 from V. Vitek, D. A. Smith and R. C. Pond, Phil. Mag. 41, 649 (1980).

the structure of the boundary should be insensitive to the variations in the empirical potential. Moreover, an extensive number of calculations seem to indicate that the structure of the boundary is very similar for metals within the same crystal class. The electronic states of atoms at a metal grain boundary may differ considerably from the corresponding state of the atom in the bulk crystal. [12] The use of the central potentials fitted to single crystal properties is then of limited significance. For example, the value of the energy of a particular structure should not be taken as a quantitative result. However, there is some agreement that the atomistic calculations give the general features of the structure of a grain boundary. [13],[14]

The basic principle of the atomistic calculations is to establish a suitable unit cell which has the defect in its center, and then to relax the structure following a suitable scheme of minimization of the energy of the starting block. One approach is simply to minimize the second term in Eqn. 3.2.1. This static method is equivalent to minimization of the internal energy at 0 °K. The starting block is equal to one period of the CSL extending a large number of layers perpendicular to the boundary plane and including a few atomic layers in the direction of the tilt axis. The method of relaxation which is always used is the steepest gradient method whereby each atom is moved incrementally in the direction of the force that acts on it by a distance proportional to that force. Each research group uses different detailed procedures. Vitek and his coworkers use a modified steepest gradient method in which the relaxation parallel and perpendicular to the boundary for each plane parallel to the boundary (referred to as a layer) is carried out independently. [15] This procedure minimizes the energy of the boundary with respect to both the relative displacement of the two grains and the local atom positions at the same time. Since the calculations are

carried out at constant volume because the outer layers are fixed the local expansion at the boundary is calculated by extrapolating the normal displacements of the last relaxed layers back to the interface. [16] This displacement is then the local expansion at the boundary. The objective of maintaining fixed border conditions is to keep the average density constant. The end result of such a constraint is a region with local expansion at the boundary and regions of compression at the borders. However, the potential varies significantly with local density and the constant volume trick does not help in this respect.

Another important aspect of the static calculations is the relative translation of the grains in the starting configuration. Since existence of a number of local minima is very likely the calculations are carried out starting from a number of different translations. This is usually accomplished by the removal of one layer and the corresponding shift normal to the boundary. It was shown in section 2.4. that this is equivalent to a shift parallel to the boundary. However, also by the discussion of section 2.4, this limits the starting configurations to displacements that are periodic. More important yet is that the stable structure has to be chosen from all the obtained structures purely on the basis of the energy which has been shown to be an unreliable quantitative parameter. The symmetry of the relaxed structure can not be higher than the starting configuration, and in fact investigators find that the individual atomic relaxations tend to preserve the symmetry elements of the starting configuration. [17] Because of the limitations of the starting configuration to layer remouval some of the translated states indicated in Table 2.6.2 can not be achieved, in particular those that do not contain the ordinary mirror plane, like β and λ. It is surprising to the author then that some investigators assign particular significance to the fact that the ordinary

mirror is conserved in all relaxed structures[18] since it is just an artifact of the calculation.

Other relaxation procedures exist and are reviewed here only briefly because the results that are of interest for this research were obtained mostly by the static procedure described above. In dynamical simulations the evolution of the system of particles as a function of time is computed. Each atom is assigned a velocity in order to simulate a given temperature. The starting configuration is a statically relaxed structure. The time evolution of the system itself equilibrates the kinetic and potential energy in a time usually equivalent to two atomic vibrations. The final temperature is usually one-half of the initial kinetic energy. Obviously the details of the calculations are very numerous and important to the outcome and have been reviewed recently. [19] The basic output of such studies are particle positions and velocities as a function of time. These are the solutions to Newton's equation where the force is just given by the gradient of the potential.

$$m \cdot \frac{d^2 \mathbf{r}_i}{dt^2} = -\sum_{j \neq i}^{N} \frac{\partial \Phi}{\partial \mathbf{r}_i}(\mathbf{r}_i - \mathbf{r}_j) \tag{3.2.3}$$

In this equation m is the atom mass. In Monte Carlo calculations the evolution of the system is purely stochastic, so that the velocities are not calculated. The system evolution is followed only in configuration space. The molecular dynamics and Monte-Carlo simulation give in principle the same results. [20] Molecular dynamics is an extremely useful technique in that it allows the calculation of thermodynamic properties such as the entropy [21] and the stress tensor, [22] and other grain boundary properties such as coupled sliding and migration [23] and vacancy migration. [24] It should be pointed out that the authors of the molecular dynamics studies have carried out these

simulations only using model potentials. The investigations point out the potential of molecular dynamics techniques but this group of investigators feels that the empirical potentials available are not good enough to carry out calculations for specific metals and obtain quantitative or qualitative answers. For example, the molecular dynamic technique could study variations in grain boundary structure with temperature. Only recently has this group started assessing the use of empirical potentials, but this work is in progress.

Two computational methods have emerged recently that have significant potential applications in the studies of grain boundaries. Kikuchi and Cahn have used the cluster variational approximation to look at changes in boundary width as a function of temperature and report on grain boundary melting below the temperature of crystal melting. [25] A totally different approach is the use of the self-consisten-field X-α scattered wave method to study electron energies and densities in polyhedral arrangements. [26] The types of polyhedra and their relation to grain boundary structure are described in the next section. This method has the potential of providing enough information on the electronic structure of these polyhedra so that accurate empirical potentials can be developed. A discussion of either of the methods presented in this paragraph is quite beyond the possibilities of this brief review, but they are mentioned here because significant contributions from these fields are expected in the next few years.

A variant of the static approach is the molecular static method whereby atoms are allowed to move if they have non-zero forces acting on them; only the individual atom relaxations are carried out by molecular dynamics and the kinetic energy is quenched at each step. This technique has been used in the simulation of FCC[27] and

BCC[28] grain boundaries. In the way the technique has been implemented all of the restrictions mentioned for the purely static calculations have been circumvented except of course for the validity of the empirical potentials at the grain boundaries.

The results of the atomistic calculations are reviewed next. The following is a review of a series of calculations, using the static approach, conducted over the last ten years by V. Vitek and coworkers. [29],[30] Other researchers have made significant contributions and they are mentioned in the reviews quoted above. The results using molecular dynamics, molecular statics and the other techniques mentioned above are very few and as yet not systematic like the ones whose results are discussed now. It should be mentioned that all calculations were carried out for FCC materials.

For some certain low Σ boundaries the structure is comprised of a uniform array of a single type of structural unit. A structural unit is defined as a group of atoms arranged in a polyhedral configuration. The characteristics of these units are discussed in the next section. These favored boundaries are extremely uniform in structure and the resulting stress field is highly localized and relatively weak. For these calculations the axis of misorientation and mean boundary plane are kept fixed. Boundaries whose misorientation is in between favored boundaries are composed from mixtures of the units of the two favored boundaries. If the structure of the favored boundaries are composed of type A and type B structural units respectively, the structure of a boundary whose misorientation is close to A is composed of units of B in an array of a large number of A units. The B units are the core of a grain boundary dislocation whose Burgers vector belongs to the DSCL of the A boundary. The cores of these grain boundary dislocation are also narrow and retain their identity at small spacings. A complication arises when the favored boundary can exist in a number of

different configurations. These different configurations arise from symmetry related structures (discussed in section 2.6) or from metastable configurations with different energies. The intervening boundaries have then a multiplicity of possible structures.[31]

3.3. Structural Units

The structural unit model for FCC boundaries can be developed in a much simpler way from hard-sphere models of the grain boundary structure. The metallic bond tends to favor well-defined nearest neighbor distances due to repulsive interactions at small interatomic distances. In other words the minima of the interatomic potentials are very sharp in particular for FCC metals. In addition, metal ions have spherical symmetry and they can be considered hard in the sense that no substantial changes to their dimensions are expected in any crystal packing. Maximum cohesion requires then optimal packing of such spheres. The concept optimal is made more precise by the three Laves rules. [33] A *Space Principle* requires the most efficient space filling. A *Symmetry Principle* requires the highest symmetry. A *Connection Principle* requires the highest coordination. The three geometrical principles compete with each other. These principles have been successfully applied to the study of alloy phases and their use in the study of grain boundary structure is just an extension of their applicability. A justification for the use of hard-sphere models in BCC structures is made in the next section. The individual atom relaxations can be neglected then if a model can be developed where the atoms across the boundary retain the interatomic distances of the crystal and maximize the coordination. This is the basic purpose of the hard-sphere models.

A structural unit description can also be derived purely on the basis of geometry. Bishop and Chalmers developed this first structural unit model based on a ledge description of the CSL grain boundary structure. [34] They pointed out that a continuous description of structure exists because the ledge structure of a high Σ boundary is composed of ledges of its respective low Σ favored boundaries. Furthermore, they

show that some simple translations which are carried out by removing the first layer increase the number of coincident atoms in the boundary plane. Thus, their model emphasizes boundary coincidence rather than lattice coincidence.

The problem of arrangements of spheres has been divided by Coxeter into *packings* where no point is inside more than one sphere and *coverings* where no point is outside every sphere. [35] For FCC crystals the problem of interest is the packing of spheres such that all spheres touch their neighbors. A space filling (regular packing) in three dimensions is given by stacking close packed {111} planes in any form such as FCC, HCP, stacking faults, polytypes, etc. Of particular interest are solids which do not fill space on their own but that could exist as the core of defects such as a grain boundary. The polyhedra of interest are polyedra holes. Crystal structures can be described as regular packing of polyhedra holes; for example the FCC structure can be described as packing of octahedra and tetrahedra that surround the corresponding interstitial sites. The coordination polyhedron of such a hole would have to be made of equilateral triangle faces and be convex. The number of possible configurations for this particular problem are limited. These polyhedra were denominated deltahedra by Cundy [36] who listed them; Bernal selected those that do not admit another sphere inside and the five resulting solids are usually known as the Bernal polyhedra or canonical holes. [37] The solids where used for a model of the structure of liquids as mixtures of canonical holes. [38] The geometry of the canonical holes is described next.

The five canonical holes are: the tetrahedron, the octahedron, the tetragonal dodecahedron, the capped trigonal prism and the capped Archimedian antiprism. These are shown in Figure 3.3.1 together with other polyhedra that appear in grain boundaries; these polyhedra are also discussed below. The convex deltahedra with the

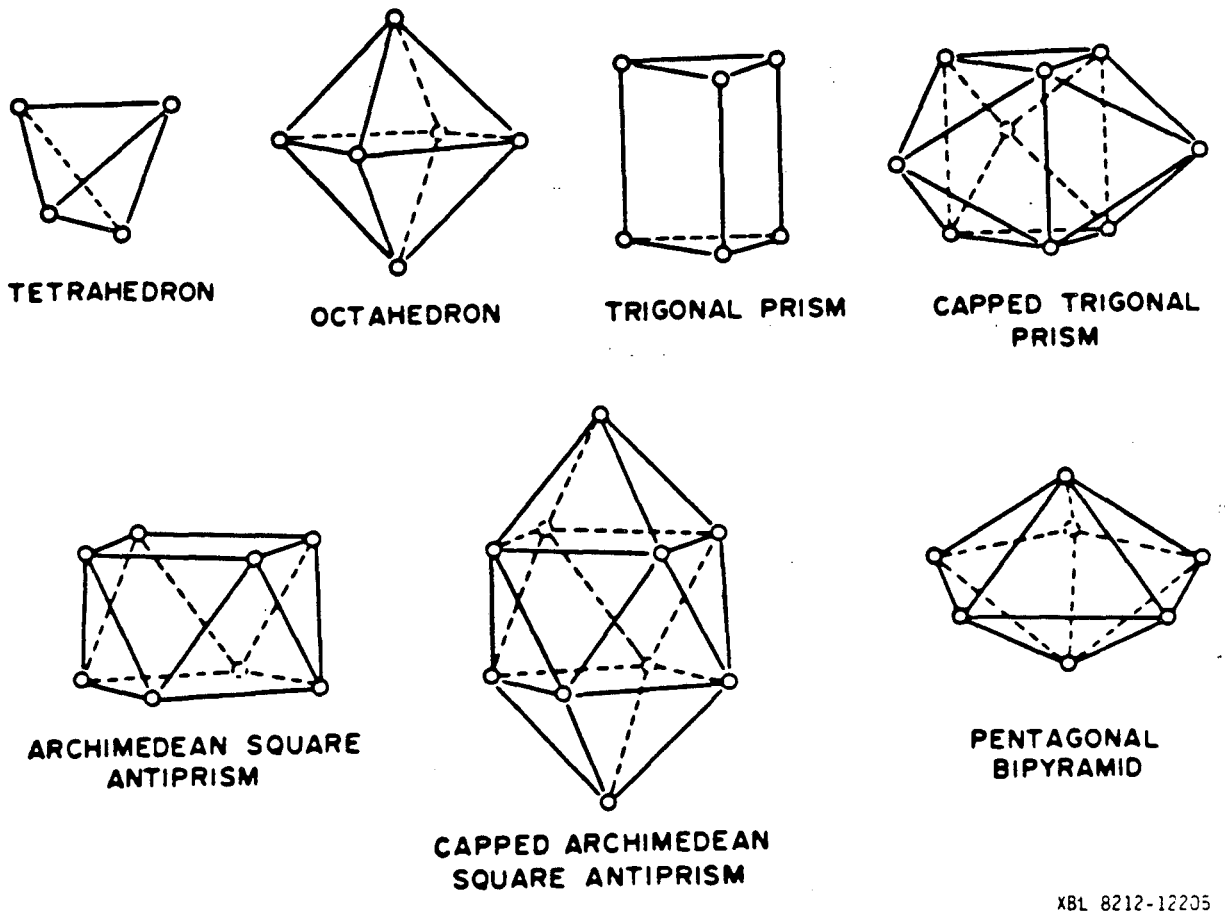

Fig. 3.3.1. Polyhedra occurring as structural units in grain boundaries (from V. Vitek, A. P. Sutton, D. A. Smith and R. C. Pond, *op.cit.*).

smallest number of vertices is the tetrahedron with 4 of them. A figure with 5 vertices is simply two terahedra which share a face, no new canonical hole is formed then. The figure with 6 vertices is the regular octahedron. The FCC structure can be thought as space filling of a combination of regular tetrahedra and octahedra surrounding the corresponding interstitial sites. The BCC structure is similarly described as space filling of distorted octahedra surrounding the interstitial site. Four edges of the distorted octahedron have the length of the second-nearest neighbor separation and the remaining have the length of the first nearest neighbor separation. The octahedron and the polyhedron are expected to occur frequently at grain boundaries, in particular at small angle grain boundaries, as the polyhedra in regions where the crystal structure is preserved. The symmetry elements of the tetrahedron and polyhedron are showed in Figures 3.3.2 and 3.3.3 respectively. The symmetry elements in these and the next figures are shown first in the plane and then normal to the most appropiate projection plane for each figure. As is expected, these polyhedra contain 3 and 4-fold rotation axes typical of the cubic structures. The figure with 7 vertices is the pentagonal bipyramid which is equivalent to a ring of five tetrahedra. Thus, it is not a new canonical hole but it is included in Figure 3.3.1 because it appears frequently at [110] tilt boundaries as it will be shown in the next chapter. This polyhedra can be looked at as a very particular arrangement of tetrahedra at the grain boundary. Following the symmetry considerations of last chapter, the elements of interest in each polyhedra are its symmetry elements and the way they could be stacked along the tilt axis. In the case of [110] and [100] tilt boundaries the polyhedra should be able to stack in an ABAB.. sequence. Similarly the symmetry elements of interest are two-fold axis and mirror planes; once they fit into the boundary these symmetry elements could become

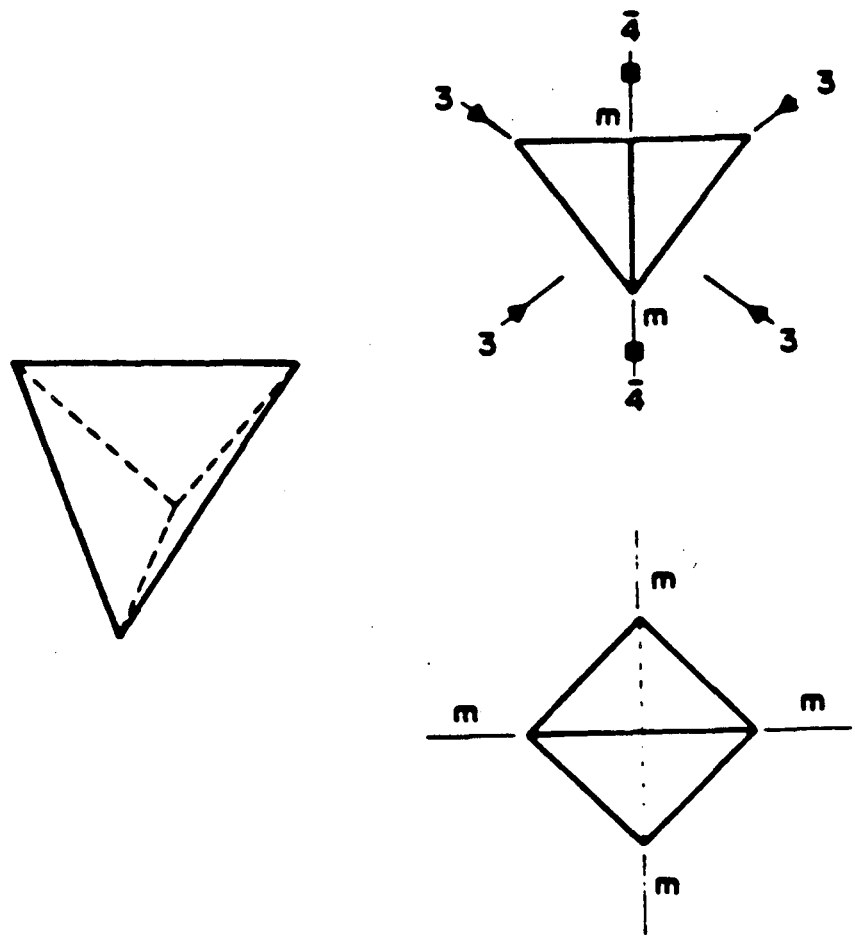

XBL 8212-12211

Fig. 3.3.2 Symmetry elements of a tetrahedron (from M. F. Ashby, F. Spaepen, and S. Williams, *op.cit.*).

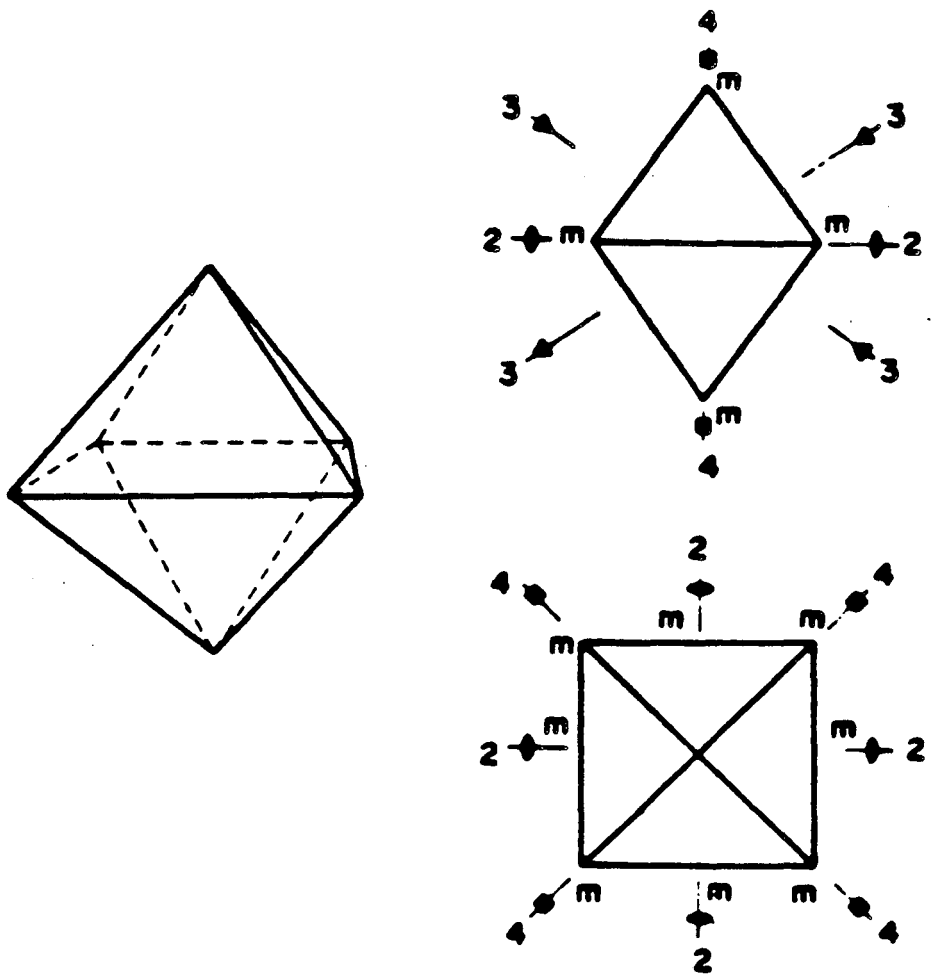

XBL 8212-12210

Fig. 3.3.3 Symmetry elements of an octahedron (from M. F. Ashby, F. Spaepen, and S. Williams, *op.cit.*).

their corresponding colored symmetry element. The symmetry elements of the pentagonal bipyramid are shown in Figure 3.3.4. As it can be seen this polyhedra is ideally suited for symmetric tilt boundaries since it contains all the symmetry elements of the point group $m\,2'm'$ when the five-fold axis is along the tilt axis. In addition in this orientation an AB stacking is possible. The figure with 8 vertices is the tetragonal dodecahedron. Although it has some of the symmetry elements required, it can not be stacked in an AB sequence and thus it does not show in the structures discussed in the next chapter. The figure with 9 vertices is the capped trigonal prism. As shown in Figure 3.3.5 with the 6-fold axis along the tilt axis this polyhedra is ideally suited for tilt boundaries. The capped regions are half an octahedron and thus they sometimes fit exactly in the crystal structure. Thus, the trigonal prism can exist on its own, as shown in Figure 3.3.1 or with 1,2 or 3 capped regions. The figure with 10 vertices is the capped Archimedian antiprism whose symmety elements are shown in Figure 3.3.6. A uniform antiprism consists of two regular n-polygons (bases) connected by 2n equilateral triangles. The octahedron is an antiprism with triangular base n=3. When n=4 the resulting antiprism can be capped with a half an octahedron and results in the capped Archimedian antiprism. This polyhedron is ideally suited for twist boundaries. The holosymmetric point group of the highest symmetry twist bicrystal is $42'2'$. With the eight fold axis along the twist axis the capped Archimedian antiprism provides a quantized rotation of 45 °. This polyhedron has been observed in a detailed atomistic x-ray diffraction study of a $\Sigma 13$ boundary in gold. [39] The Archimedian square antiprism can exist in the twist boundary by itself (as shown in Figure 3.3.1) or with 1 or 2 capped regions.

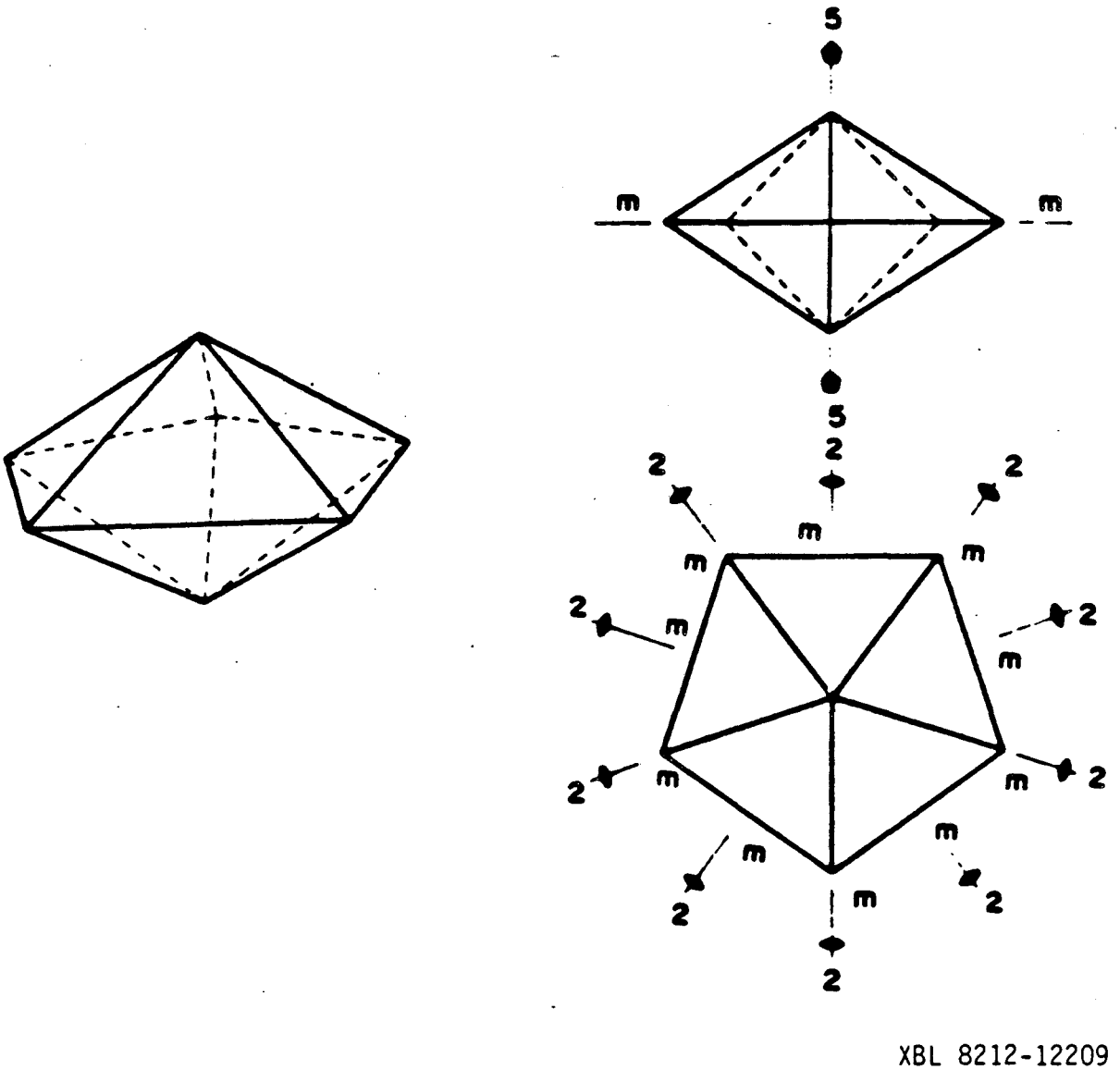

Fig. 3.3.4 Symmetry elements of a pentagonal bipyramid (from M. F. Ashby, F. Spaepen, and S. Williams, *op.cit.*).

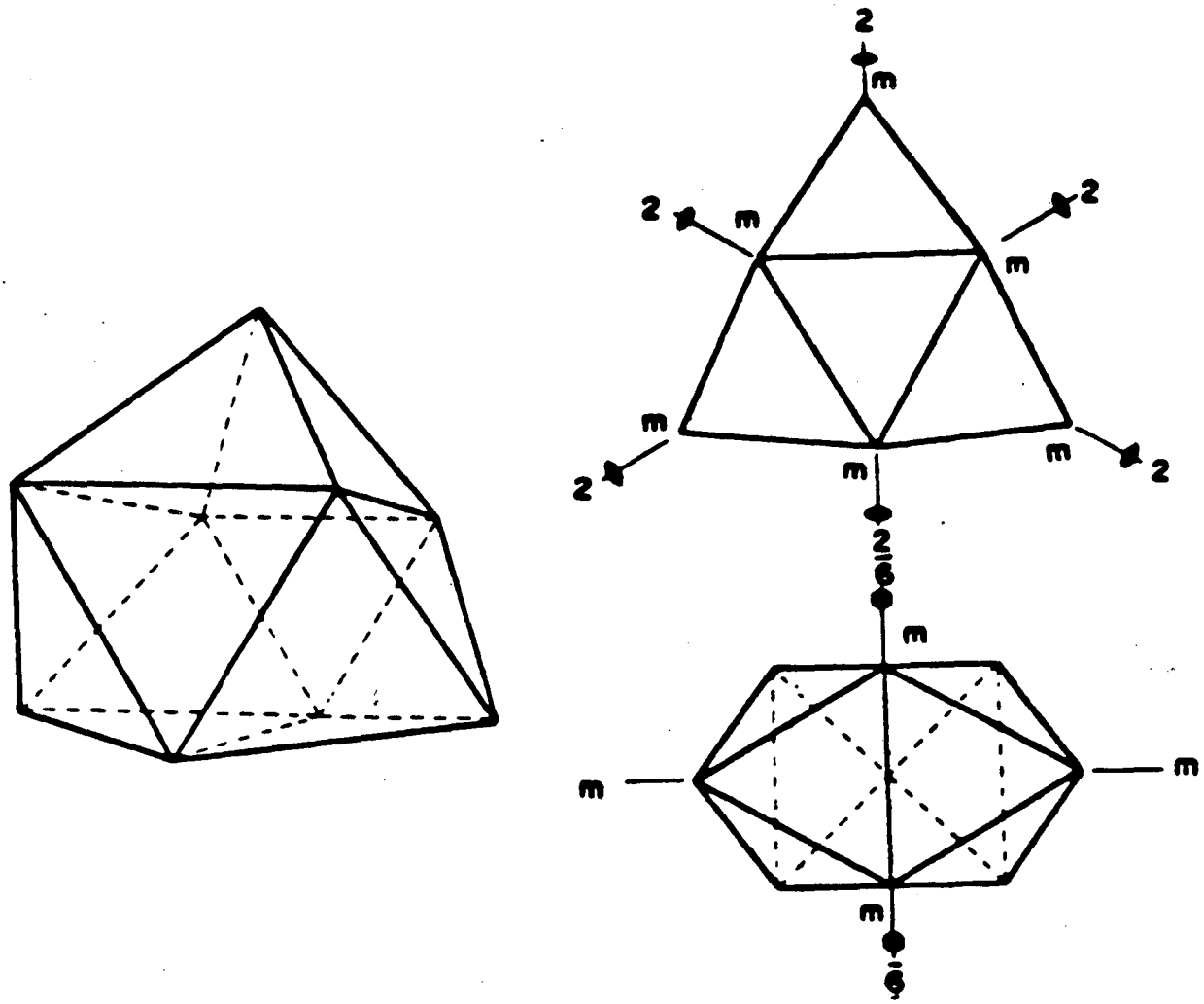

Fig. 3.3.5 Symmetry elements of a capped trigonal prism (from M. F. Ashby, F. Spaepen, and S. Williams, *op.cit.*).

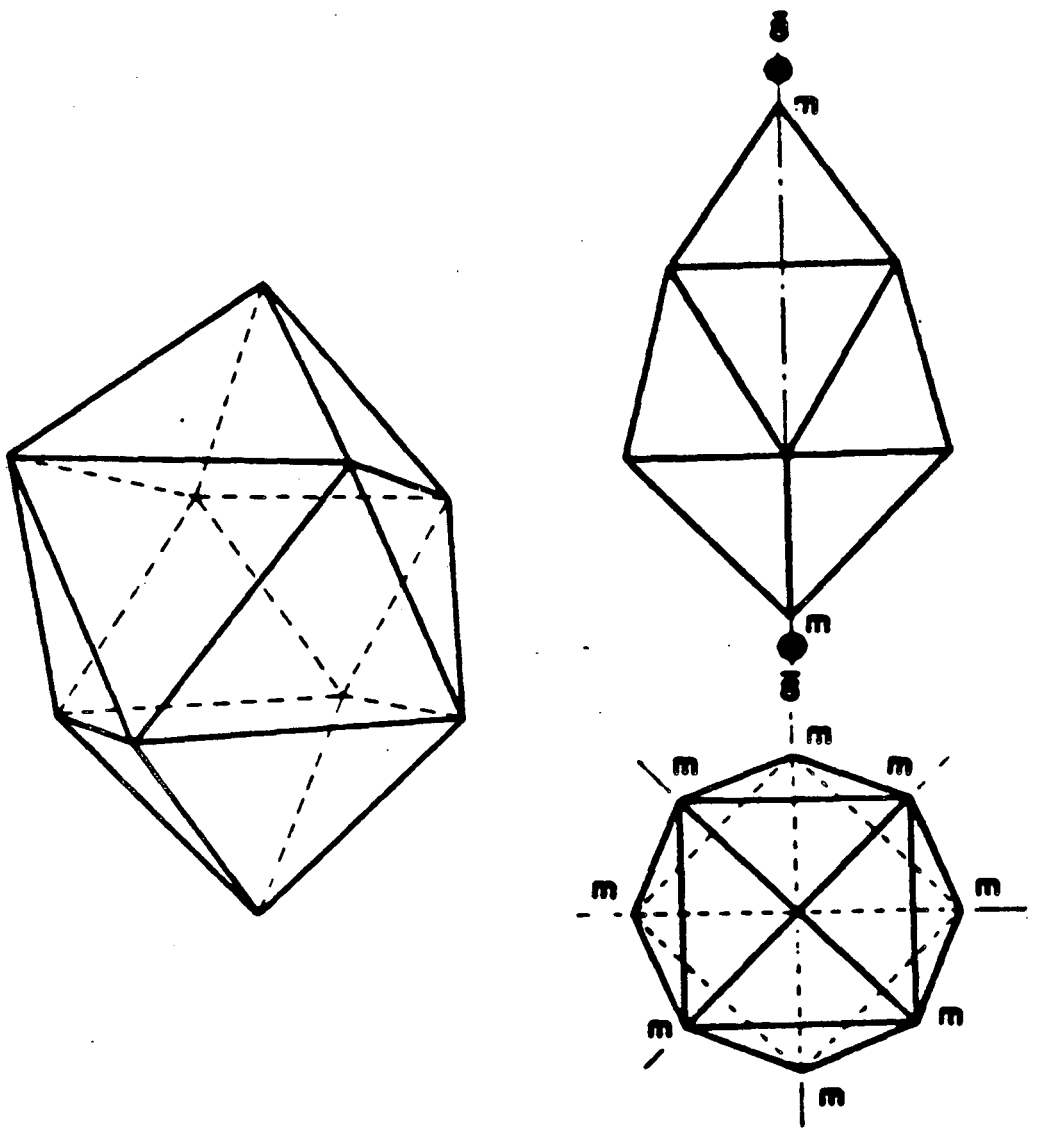

XBL 8212-12206

Fig. 3.3.6 Symmetry elements of a capped Archimedian antiprism (from M. F. Ashby, F. Spaepen, and S. Williams, *op.cit.*).

The pentagonal bipyramid, the capped trigonal prism and the capped Archimedian antiprism lack the symmetry that would enable them to form regular structure by themselves, although in regular combination with others they can occur in crystal structures. By combining these polyhedra with tetrahedra and octahedra crystal coordination can be conserved at the grain boundary. This model of packing of polyhedra at grain boundaries was first developed by Ashby, Spaepen and Williams.[40] The atomistic structure of the grain boundary can be described by these finite number of structural units and different combinations of these can produce a continuous change of boundary structure with a change in macroscopic parameters such as the misorientation angle or rotation axis. This would occur by embedding units with quantized misorientations in combination with tetrahedra and octahedra along the grain boundary. For example the trigonal prism with one capped region in one crystal and the other capped region in the other crystal provides a quantized rotation of 60 °. The favored structures are then $\Sigma 1$ and the boundaries that are composed of only one of these quantized rotation deltahedra.

The first systematic studies of hard-sphere grain boundaries were carried out by Frost and coworkers. [41] Two symmetrical half-crystals were translated graphically with respect to each other until a mechanically stable structure wich maximized the density was found. The method is not systematic and since examining all possible translations is cumbersome some translations might have been overlooked. An analytical procedure has been proposed recently and it is extended to the calculation of BCC structures in the next section. [42] The results of Frost and coworkers are important in two respects. First, they point out that a relationship between the excess volume and the area of the repeat unit in the boundary. [43] This result is important because other

physical properties of the grain boundary can be correlated with the excess volume. This point will be discussed again in chapter 6. Second, the structure developed on the basis of the hard-sphere model are shown to be very similar to the structures calculated using static atomistic calculations.[44] The same conclusion is reached in our studies (chapter 4). The procedure to carry out systematic hard-sphere modelling of grain boundary structure in BCC materials is described next.

3.4. Hard Sphere Models of Symmetrical BCC Grain Boundaries: Computational Procedure

It has already been mentioned that the BCC structure is stable under bonding which is equivalent to central forces in which the contribution of the first- and second-nearest neighbors are equally important. This is illustrated by the shape of the empirical potential well in Figure 3.2.1. The effective coordination from the point of view of atomic interactions is 14 rather than 8 which is the number of first-nearest neighbors. This coordination affects the structure of the grain boundary in ways which are discussed in this section and the next two chapters. In particular the preferred atom spacings in the distorted canonical holes are going to be the first-nearest neighbor spacing $\frac{\sqrt{3}}{2}a$ and the second-nearest neighbor spacing a. *Throughout the rest of this work all units of distance unless specified are multiples of a the lattice parameter.* For example, the first-nearest neighbor distance will be simply indicated as .866 . The model developed in this section takes into account the considerations discussed above.

The graphical procedure used by the researchers mentioned in the last section is used as an introduction to the problem. Figure 3.4.1.a shows the typical arrangement of the first layer of atoms in a symmetrical tilt boundary. The key element of this figure is the existence of the colored mirror plane. The problem of finding the translation that preserves in the case of FCC metals the first-nearest neighbor distance is that of finding the translation **u** in the plane of the boundary for which the separation **d** is a minimum. The upper crystal is considered fixed as in the convention that has been used throughout this work. The distance $d_A{}'$ at which atom A can be placed

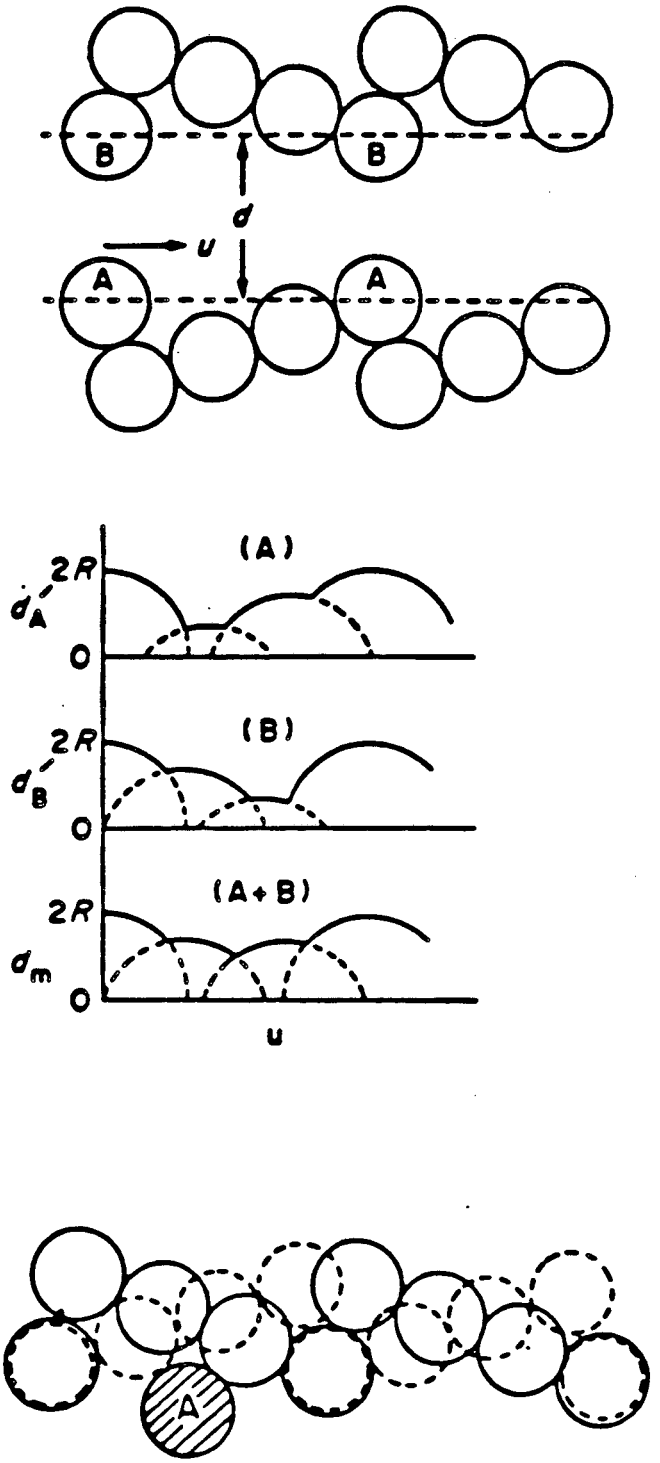

Fig. 3.4.1 Calculation procedures for grain boundary displacements; (a) and (b) graphical procedure: (a) is a plan view along the tilt axis and (b) shows the separation versus displacement curves; (c) superimposed crystal blocks forming the calculation surface for the analytical procedure described in the text (from M. Koiwa, *et. al., op. cit.*).

without overlapping with the upper block is plotted for each displacement **u**. The same procedure can be carried out for atom B in the upper block and both curves can be added as shown in the last curve of Figure 3.4.1.b. The minimum separation d_m can be obtained from the composite curve; this separation maximizes the density. The solution is not analytical and it is rather cumbersome since half of the area of the grain boundary repeat unit has to be covered.

Consider the way the first two-curves in Figure 3.4.1.b are drawn. Because of the mirror symmetry the arrangement that atom A sees in the upper crystal is the same than the arrangement that atom B sees in the lower crystal. The curves have mirror symmetry about a plane that contains the tilt axis and at half the repeat period in the boundary plane normal to the tilt axis. This is just a consequence of the symmetry related displacements shown in Figure 2.6.3. where the displacements **t** and **–t** are symmetry related and thus the resulting structures are equivalent. This fact can be used to develop an equivalent procedure. Instead of overlapping the displacement curves, the atom arrangements can be overlapped as shown in Figure 3.4.1.c. The atomic arrangement of the first layer of the upper crystal remains as is, and the first layer of the lower crystal has been redrawn as seen by atom B of the upper crystal. Notice that the atoms that mark the period of the boundary coincide as in the CSL orientation. *The problem then has been reduced to the problem of positioning an atom sphere relative to a superposed arrangement of atoms.* The set of atoms corresponding to the lower crystal can be produced from the first layer of the lower crystal by the symmetry operation of the two-fold colored axis normal to the boundary plane and the colored mirror plane at the boundary plane; this can be visualized in Figure 2.5.2.a.

The CSL and DSCL of a $\Sigma 17$ boundary are shown in Figure 3.4.2 together with the atom positions of the interpenetrating lattices. The atoms numbered in this figure are the atom positions used in the calculations. The symmetry considerations of the previous paragraph can also be appreciated in this figure. The problem of interest is then to place an atom in the surface composed of the atom positions numbered. *The position of the new atom defines a possible translation at the grain boundary. Thus, the position of the new atom is written as* (t_x, t_y, t_z). The coordinate frame is such that x is parallel to the tilt axis, y is normal to the tilt axis and contained in the boundary plane and z is normal to the boundary plane and pointing towards the upper crystals. This implies that all possible translations have t_z negative. If two atoms in the calculation surface are selected then a new sphere can be fitted within an arc of circle with radius r equal to the required interatomic distance. This situation is illustrated in Figure 3.4.3. The arc is part of a circle that lies on a plane normal to the vector that joins both spheres at the contact point. The circle of solutions is limited to an arc because of the presence of other layers of atom planes normal to the tilt axis. If the repeat distance for an AB stacking along the tilt axis is r_{AB}, the new atom t_z coordinate is restricted to

$$\frac{-r_{AB}}{2} \leq t_z \leq \frac{r_{AB}}{2} \tag{3.4.1}$$

because otherwise overlap would occur with the equivalent surface atom positions with $x = -r_{AB}$ or $x = r_{AB}$. *Because of the mirror symmetry of the problem only translations with* $0 \leq t_z \leq \frac{r_{AB}}{2}$ *are studied.* This restriction then limits the circle of solutions to an arc of possible solutions.

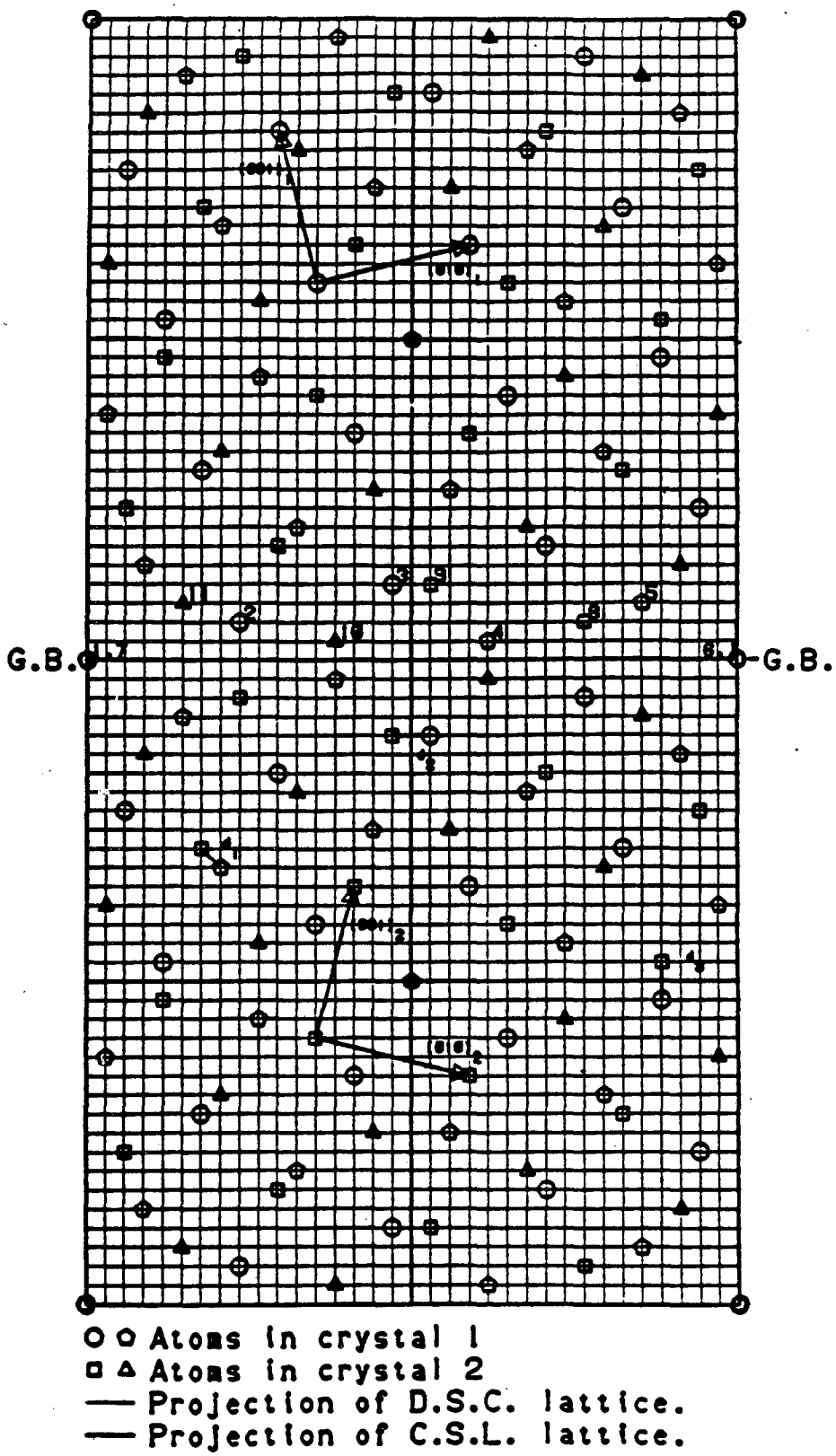

Fig. 3.4.2 The CSL and DSCL for a Σ17 [100]/(014) BCC grain boundary. The atoms numbered are the ones used in the calculations.

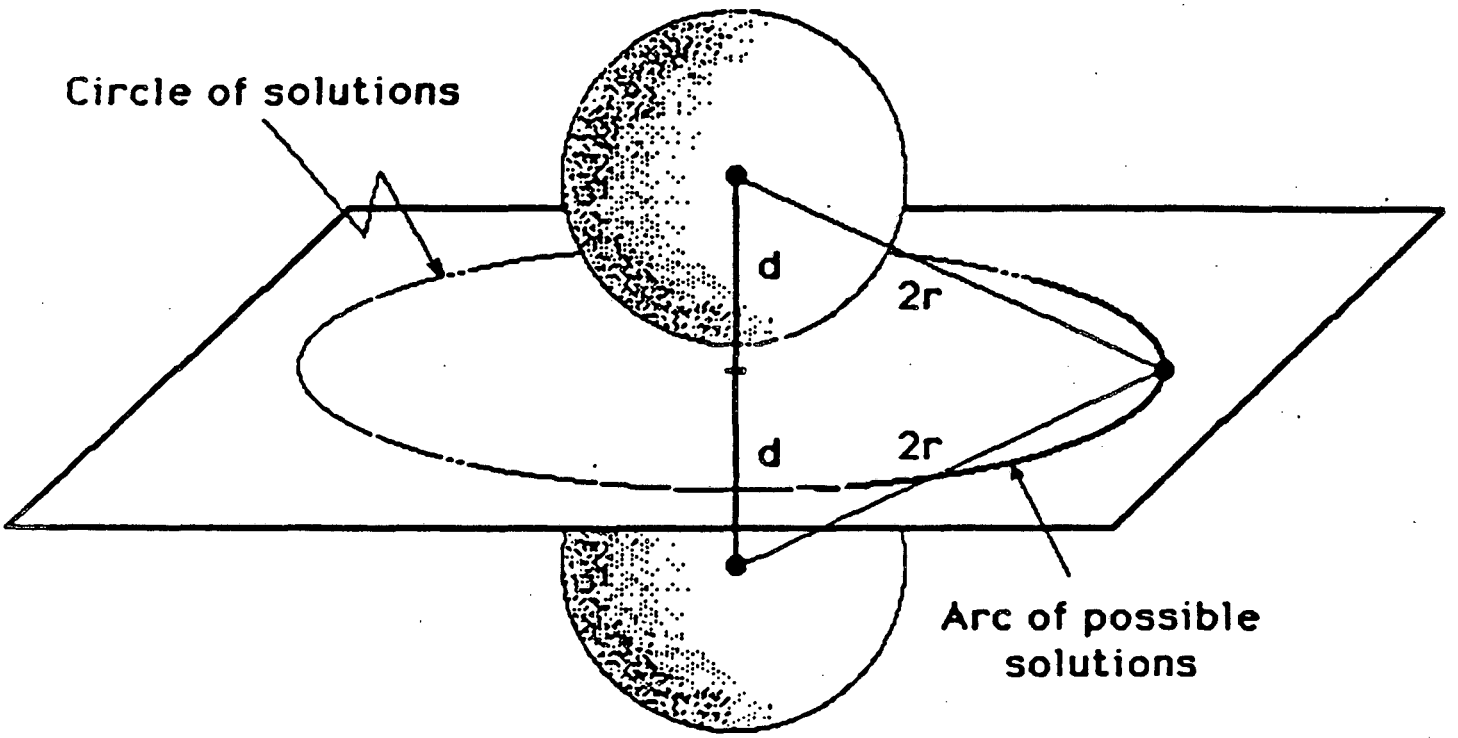

Solutions for a two sphere problem.

Figure 3.4.3

The first nearest-neighbor distance is indicated as D_1 and the second-nearest neighbor distance as D_2 and similarly for the corresponding radius. Consider first the FCC case where all atoms are equidistant. As it has been discussed above the two-sphere problem has an infinite set of solutions (all contained in the arc of possible solutions). This implies that any given solution is mechanically unstable since there are other possible solutions in the immediate vecinity. A mechanically stable solution requires at least three contacts across the boundary per repeat unit of the boundary. A third atom is chosen and the center of a new sphere circumscribing simultaneously the other three is calculated. Of course, the new sphere can not overlap with any of the atom positions in the calculation surface. For each set of three atoms the coordinate frame is translated such that the origin coincides with the center of the circle in Figure 3.4.3. and the y axis is along the vector that joins any two of the positions in the set of three. In this coordinate frame the new sphere center is given by

$$\begin{aligned} (t_x')^2 + (t_z')^2 + d^2 &= 4R_1^2 \\ (x_1' - t_x')^2 + (z_1' - t_z')^2 + (y_1')^2 &= 4R_1^2 \end{aligned} \tag{3.4.2}$$

where the prime indicates the new reference frame, and the third atom in the set, not shown in Fig. 3.4.3, is indicated by (x_1, y_1, z_1).

The solutions to Eqn. 3.4.2 are discussed briefly. The displacement in the primed x direction is given by

$$t_x' = \frac{m - 2z_1' t_z}{2x_1'} \tag{3.4.3}$$

where

$$m = (x_1')^2 + (y_1')^2 + (z_1')^2 - d^2 \tag{3.4.4}$$

The displacement in the primed z direction is given by the negative solution to the quadratic equation

$$\left[\frac{(z_1')^2}{(x_1')^2} + 1\right](t_z')^2 + \left[\frac{-mz_1'}{(x_1')^2}\right]t_z' + \left[\left(\frac{m}{2x_1'}\right)^2 + d^2 - 4R_1^2\right] = 0 \tag{3.4.5}$$

A special case occurs when all three atoms are in the same layer, i.e. $x_1'=0$. In this case,

$$t_z' = \left[4R_1^2 - \left(\frac{m}{2z_1'}\right)^2 - d^2\right]^{-\frac{1}{2}} \tag{3.4.6}$$

and

$$t_z' = \frac{m}{2z_1'} \tag{3.4.7}$$

A difficulty arises when two of the atoms coincide. Consider the set of atoms 1,2,7 in Figure 3.4.2. Atoms 1 and 7 coincide but they are two different objects, and upon translation they exist as two different atom positions. However, from a mathematical point of view we are back to the two-sphere problem. In order to solve this problem the displacement in the direction of the tilt axis is set arbitrarily to be equal to $\frac{r_{AB}}{2}$. This distance is indicated in the equations as m_x. With the origin of the coordinate system at the coinciding atoms a set of equations similar to equation 3.4.2 can be set-up. The solutions to these equations are

$$t_z' = \frac{p - t_y' y_1'}{z_1'} \tag{3.4.8}$$

where

$$p = \frac{1}{2}\left[(y_1')^2 + (z_1')^2 + (m_x - x_1')^2 - m_x^2\right] \tag{3.4.9}$$

and

$$\left[1+\frac{(y_1')^2}{(z_1')^2}\right](t_z')^2 + \left[\frac{-2py_1'}{(z_1')^2}\right]t_z' + \left[m_x^2 + \frac{p^2}{(z_1')^2} - 4R_1^2\right] = 0 \tag{3.4.10}$$

This particular choice of the displacement in the direction of the tilt axis minimizes the excess volume and conserves the ordinary mirror symmetry. Obviously, these displacements occur in all symmetrical tilt boundaries and their particular role in grain boundary structure is discussed in chapter 5.

The considerations of geometry and symmetry in the discussion presented here have reduced a problem with infinite solutions to a problem with analytical solutions. Up until now the discussion has been limited to the FCC case; the extension to the BCC case is straightforward and is discussed next.

Consider again the form of Equations 3.4.2. There are no restrictions on the values of the required distances which are given by the right hand side of the equations. In particular it is easy to require that the first-nearest neighbor distance be satisfied with two of the atoms in the set of three and that the second-nearest neighbor distance be satisfied with the remaining atom position.

$$\begin{aligned} (t_x')^2 + (t_z')^2 + d^2 &= 4R_1^2 \\ (x_1' - t_x')^2 + (z_1' - t_z')^2 + (y_1')^2 &= 4R_2^2 \end{aligned} \tag{3.4.11}$$

There are 8 cases for BCC calculations which are equivalent to Eqns. 3.4.11. These occur because for a given set of three atoms, there are $\binom{3}{2} = 3$ combinations of the three atoms taken R_1 at a time, and an equal number for R_2. In addition the new

atom might be equidistant to all three in the set by either R_1 or R_2. These 8 cases are tabulated as programmed in Table 3.4.1. The solutions marked standard are the ones that have already been discussed in this section. All other solutions are just variations of these solutions and are discussed here. The solutions for case 5 are marked Standard‡ because the only modification necessary is to replace R_1 by R_2 in every equation. The solutions marked Modify† have for the regular cases

$$m = (x_1')^2 + (y_1')^2 + (z_1')^2 - d^2 + 4R_1^2 - 4R_2^2 \tag{3.4.12}$$

or for the coinciding cases

$$p = \frac{1}{2}\left[(y_1')^2 + (z_1')^2 + (m_x - x_1')^2 - m_x^2 + 4R_1^2 - 4R_2^2\right] \tag{3.4.13}$$

The solutions for the regular case are given as before by Eqns 3.4.3, 5, 6, and 7, and

Table 3.4.1
BCC Analytical Solutions

Case	Distance to Positions			Comments on Solutions	
#	1	2	3	Regular	Coinciding
1	R_1	R_1	R_1	Standard	Standard
2	R_2	R_1	R_1	Modify†	Modify†
3	R_1	R_1	R_1	Modify†	Not Possible
4	R_1	R_2	R_1	Modify†	Not Possible
5	R_2	R_2	R_2	Standard‡	Standard‡
6	R_1	R_2	R_2	Modify§	Modify§
7	R_2	R_2	R_1	Modify§	Not possible
8	R_2	R_1	R_2	Modify§	Not possible

The comments on the type of solutions are discussed in the text

the solutions for the coinciding case are given by Eqns. 3.4.8 and 10. For the solutions marked Modify§ m is given by

$$m = (x_1')^2 + (y_1')^2 + (z_1')^2 - d^2 + 4R_2^2 - 4R_1^2 \tag{3.4.14}$$

and p by

$$p = \frac{1}{2}\left[(y_1')^2 + (z_1')^2 + (m_x - x_1')^2 - m_x^2 + 4R_2^2 - 4R_1^2\right] \tag{3.4.15}$$

The solutions for the regular cases and coinciding case are given by the same equations mentioned above except that R_1 has to be changed to R_2. Finally the coinciding solutions that are marked Not Possible in Table 3.4.1 can not occur because the atom positions 2 and 3 are always chosen as the coinciding positions by a subroutine ORDER that is described below. The new atom position then cannot be at two different distances from the same calculation surface position.

The program developed for these calculations is described next.

The first part of the program generates all the geometrical data from a few parameters that are particular for each boundary. A simple procedure to generate all grain boundary CSL structures is used. Any symmetrical tilt boundary can be described by a set of three vectors $\mathbf{d}_i^*$ where $\mathbf{d}_1^*$ is along the tilt axis and the other two vectors are contained in the crystallographic plane normal to the tilt axis. The vector $\mathbf{d}_2^*$ is usually along the boundary plane and is equal to 1/4,1/2, or the full length of the boundary period depending on the boundary. The vector $\mathbf{d}_3^*$ is parallel to the mean period vector (see section 2.2). Only the atoms in the upper crystal need to be defined since the atoms positions corresponding to the lower crystal at the calculation surface are obtained by symmetry operations. The atom positions in the upper

crystal are then given by

$$\mathbf{r} = l\,\mathbf{d}_1^* + m\,\mathbf{d}_2^* + n\,\mathbf{d}_3^* \tag{3.4.16}$$

For example for the $\Sigma 17$ boundary shown in Fig. 3.4.2 the starred base vectors are $\mathbf{d}_1^* = 1/2[100]$, $\mathbf{d}_2^* = 1/2[04\bar{1}]$, and $\mathbf{d}_3^* = 1/2[010]$. A vector equivalent to $\mathbf{d}_3^*$ in the lower block is defined by the twinning matrix on the plane (HKL)

$$\mathbf{R}_{180} = \frac{1}{H^2+K^2+L^2}\begin{bmatrix} H^2-K^2-L^2 & 2HK & 2LH \\ 2HK & K^2-L^2-H^2 & 2KL \\ 2LH & 2KL & L^2-H^2-K^2 \end{bmatrix} \tag{3.4.17}$$

For the $\Sigma 17$ boundary this vector $\mathbf{d}_l^*$ is $1/34[0,15,\bar{8}]$. The geometry defined above is given in the coordinate system of crystal 1 since all the vectors in the starred system are defined in the coordinate frame of this crystal. In order to change to the coordinate system used in the calcualtions and the presentation of results, half of a rotation matrix operation is applied to the geometry. For [100] boundaries and (0KL) boundary plane this rotation is

$$\mathbf{R}_h = \begin{bmatrix} 1 & 0 & 0 \\ 0 & FL & -FK \\ 0 & FK & FL \end{bmatrix} \tag{3.4.18}$$

$$F = 1/\sqrt{K^2+L^2}$$

And for the [110] boundaries with $(\bar{H}HL)$ boundary plane

$$\mathbf{R}_h = \begin{bmatrix} F_1 & F_1 & 0 \\ -F_2L & F_2L & 2F_2H \\ F_3H & -F_3H & F_3L \end{bmatrix} \tag{3.4.19}$$

where

$$F_1 = 1/\sqrt{2}$$

$$F_2 = 1 \,/\, \sqrt{2(2H^2+L^2)} \tag{3.4.20}$$

$$F_3 = 1 \,/\, \sqrt{2H^2+L^2}$$

All the atom positions are now expressed in the coordinate frame used throughout the rest of this work.

The main DO loops of the program go through all possible sets of three atoms where 2 atoms belong to one crystal and the remaining to the other. On the basis of geometry some sets are discarded because a solution does not exist for that particular group. These are sets where two atoms are too far to possibly give a solution or where all three atoms belong to the same lattice. For each three atom set that can possibly give a solution the following subroutines are called.

Subroutine ORDER takes the three atom set and orders them such that atoms 2 and 3 are in the same layer and atom 2 is further from the boundary than 3. Under this order of the three atom set the solutions to the problem take the forms discussed in this section and sumarized in Table 3.4.1. Subroutine NEWSPHERE produces the change of coordinates indicated in Figure 3.4.3 and discussed in the text. The solutions to the problem are obtained in this prime coordinate frame and then back-transformed to the original coordinate system. Subroutine CHECK checks the solution obtained by NEWSPHERE so that no overlap with other atoms in the calculation surface occurs. In addition the new solution is compared with the solutions already obtained since different atom sets can give the same solution. This indicates a particularly stable translation since additional redundant bonds across the boundary occur.

For each boundary translation the atom positions can be plotted as shown in Figure 3.4.4.a for a translation $t_x = .5$, $t_y = .59$, $t_z = -.64$, of the $\Sigma 17$ boundary shown in Figure 3.4.2. Notice that this boundary has mean boundary plane (011) and so it is different than the [100] tilt boundaries discussed in the next section. It is used here for the purpose of illustration. From this atom positions a very distorted picture, Figure 3.4.4.b, of the boundary in terms of polyhedra appears. However, individual atom relaxations that would produce additional bonds of the required length are evident as shown in Figure 3.4.4.c. The structural unit description then is shown in Figure 3.4.4.d. The graphical procedure of obtaining the individual atom relaxations is entirely justifiable since at present the atomistic calculations can not claim to be more accurate. In addition the atomistic calculations give as result only one minima of the energy function, and in order to obtain other possible structures the calculations have to be restarted from a different initial configuration. In the systematic procedure described here all possible minima of the energy function are generated at once with considerable savings of computational effort.

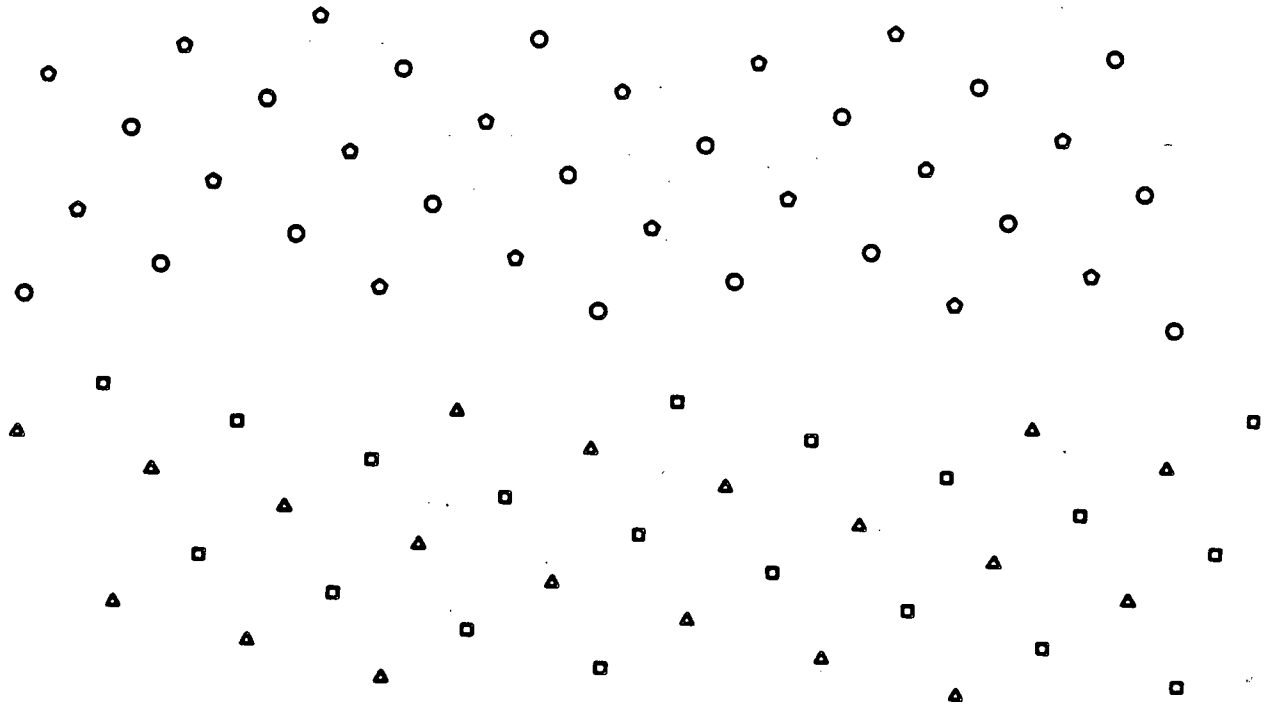

(a)

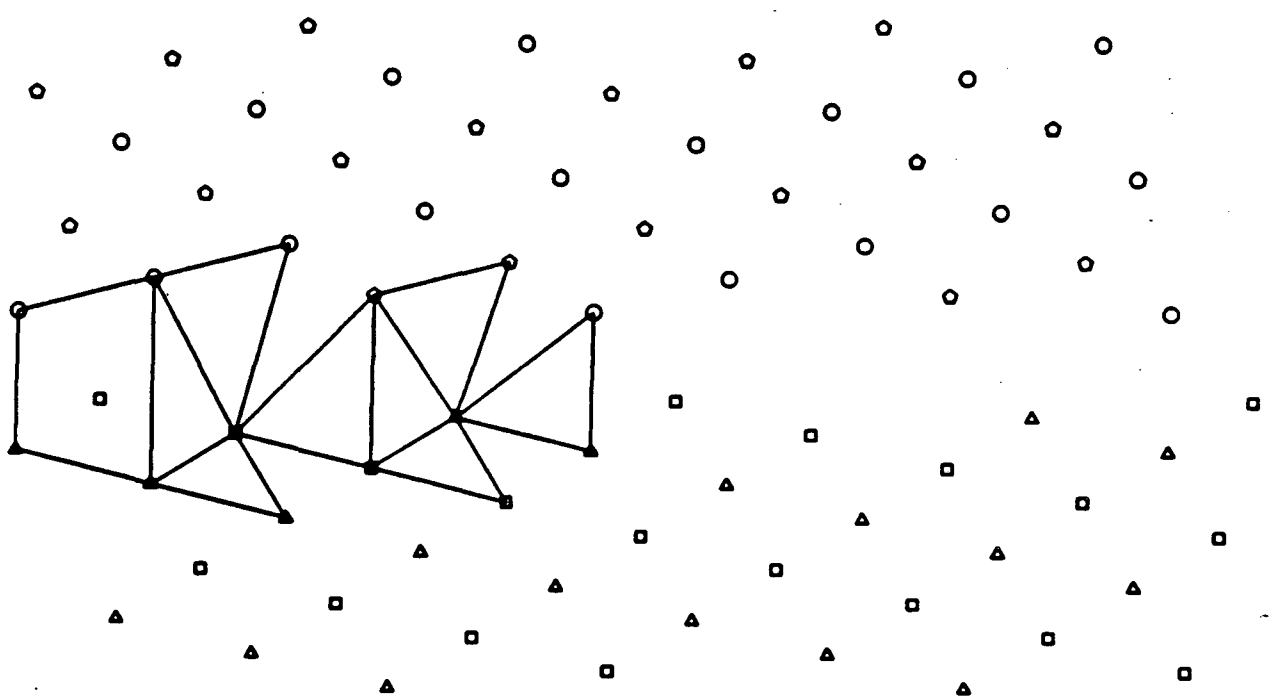

(b)

Fig. 3.4.4 See caption on next page

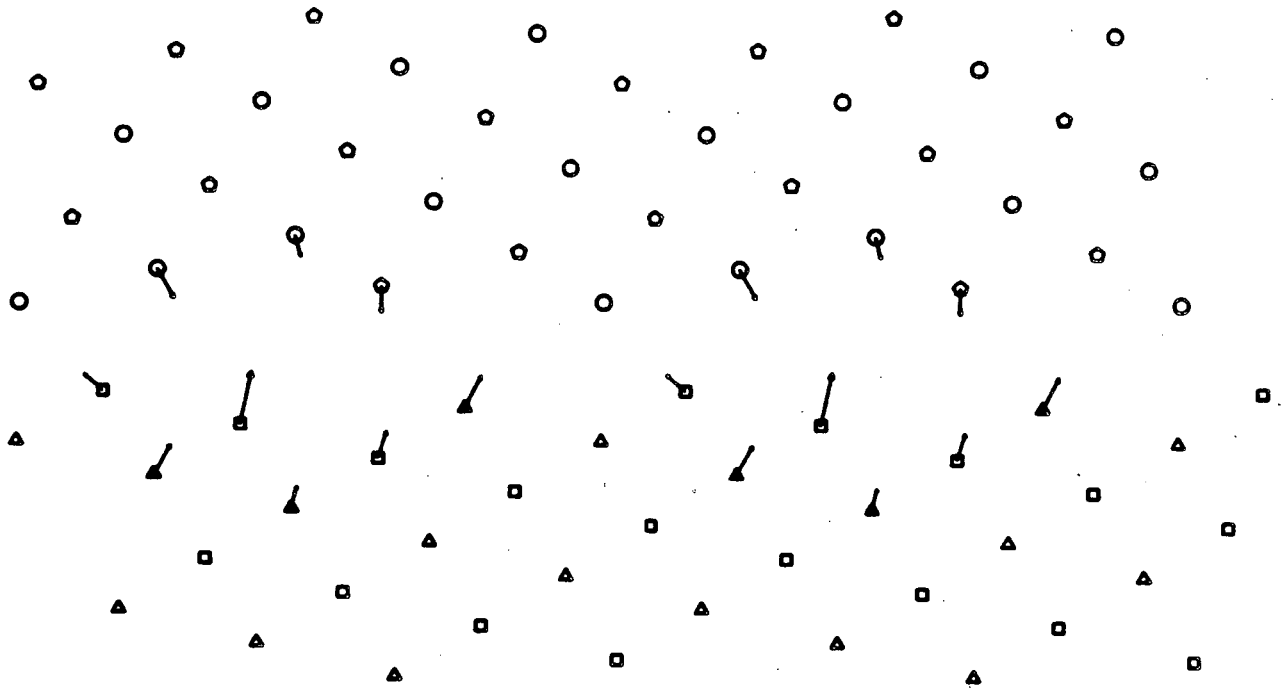

(c)

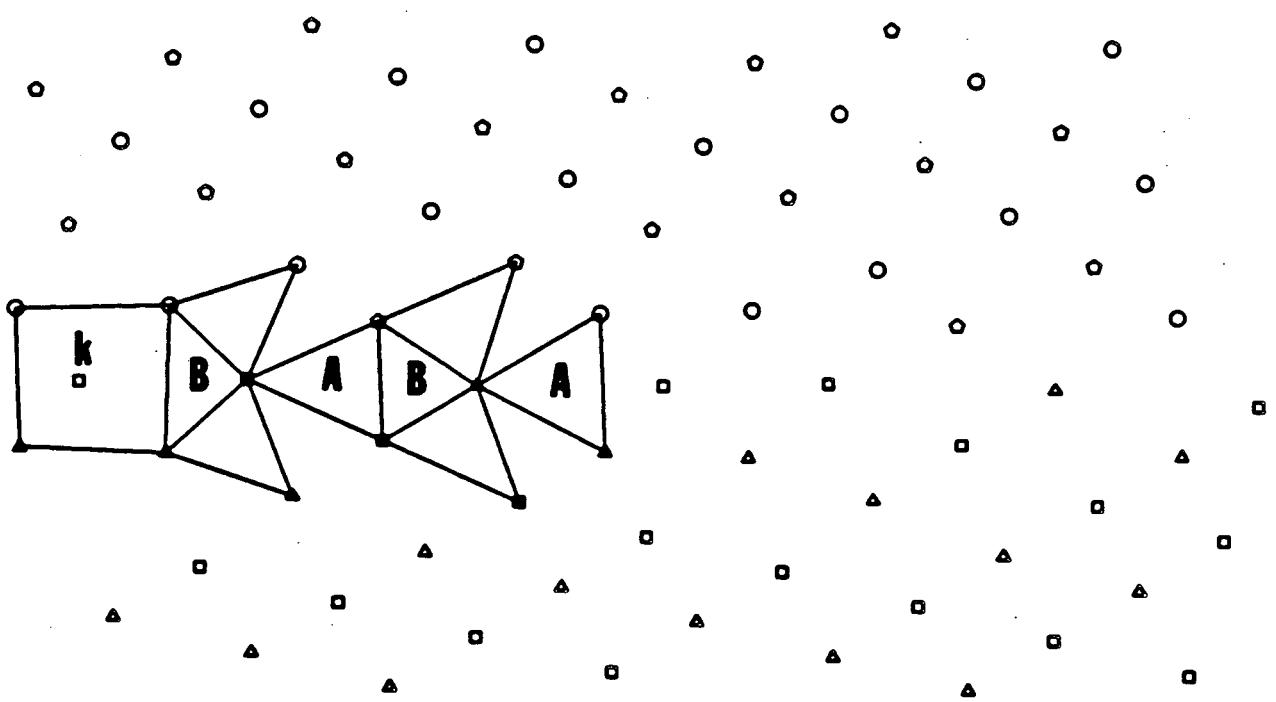

(d)

Fig. 3.4.4 Atom positions for a hard sphere Σ17 boundary; (a) ater a translation $t_x = .5$, $t_y = .59$, $t_z = -.64$; (b) distorted structural units for (a); (c) individual atom relaxations are indicated; (d) structural units in the grain boundary after individual atom relaxations.

3.5. References

[1] R. W. Balluffi, Y. Komem and T. Schober, *Surf. Sci.* **31** ,68 (1972).

[2] T. Y. Tan, S. L. Sass and R. W. Balluffi, *Phil. Mag.* **31** , 575 (1975).

[3] C.H. Li, E. H. Edwards, J. Washburn and E. R. Parker, *Acta Met.* **1** ,223 (1953).

[4] E. A. Kamenetzky and R. Gronsky, *Res Mechanica* **8** ,185 (1982).

[5] Y. T. Chou, *Scripta Met.* **10** ,331 (1976).

[6] A. Brokman and R. W. Balluffi, *Acta Met.* **29** ,1703 (1981).

[7] W. A. Harrison, *Pseudopotentials in the Theory of Metals* , Benjamin/Cummings, Menlo Park, CA, 1966.

[8] K. Maeda, V. Vitek, and A. P. Sutton, *Acta Met.* **30** ,2001 (1982).

[9] V. Vitek, A. P. Sutton, D. A. Smith and R. C. Pond, in *Grain Boundary Structure and Kinetics* ,ASM Matls. Sci. Sem. 1979, ASM, Metals Park, Ohio, 1980, p.115.

[10] M. W. Finnis and J. E. Sinclair, *Phil. Mag.* **A50** ,45 (1984).

[11] R. A. Johnson, *Phys. Rev.* **134** ,A1329 (1964).

[12] M. S. Duesbery, V. Vitek and D. K. Bowen, *Proc. R. Soc. Lond.* **A332** ,85 (1973).

[13] M. Hashimoto, *et. al., Surface Sci.* **144** ,182 (1984).

[14] V. Vitek and Y. Minonishi, *Surface Sci.* **144** ,196 (1984).

[15] R. J. Harrison, *Surface Sci.* **144** ,215 (1984).

[16] V. Vitek, R. C. Pond and D. A. Smith, *Proc. Int. Conf. Computer Simulation for Materials Application, Nuclear Metallurgy,* **20** ,265 (1976).

[17] P. D. Bristowe and A. G. Crocker, *Phil. Mag.* **A38** ,487 (1978).

[18] P. D. Bristowe and A. G. Crocker, *op.cit.*

[19] R. C. Pond and V. Vitek, *Proc. R. Soc. Lond.* **A357** ,453 (1977).

[20] G. H. Bishop, R. J. Harrison, T. Kwok and S. Yip, in *Prog. Matls. Sci., Chalmers Anniversary Vol.,* Pergamon, New York, 1981, p.49.

[21] S. Yip, *Comments Sol. St. Phys.* **XI** ,125 (1984).

[22] R. J. Harrison, J. A. Cox, G. H. Bishop and S. Yip, *Proc. Int. Conf. Computer Simulation for Materials Application, Nuclear Metallurgy,* **20** ,604 (1976).

[23] J. A. Cox, G. H. Bishop, R. J. Harrison and S. Yip, *Proc. Int. Conf. Computer Simulation for Materials Application, Nuclear Metallurgy,* **20** ,434 (1976).

[24] G. H. Bishop, R. J. Harrison, T. Kwok, and S. Yip, in *Grain Boundary Structure and Kinetics* ,ASM Matls Sci. Sem. 1979, ASM, Metals Park, Ohio, 1980, p.373.

[25] T. Kwok, P. S. Ho and S. Yip, *Surface Sci.* **144** ,44 (1984).

[26] R. Kikuchi and J. W. Cahn, *Phys. Rev.* **B21** ,1893 (1980).

[27] C.L. Briant and R. P. Messmer, *Phil. Mag.* **B42** ,569 (1980).

[28] M. Hashimoto, Y. Ishida, R. Yamamoto and M. Doyama, *J. Phys. F* **10** ,1109 (1980).

[29] M. Hashimoto, Y. Ishida, R. Yamamoto and M. Doyama, *Acta Met.* **32** ,1 (1984).

[30] V. Vitek, A. P. Sutton, D. A. Smith and R. C. Pond, *op.cit.*

[31] A. P. Sutton and V. Vitek, *Phil. Trans. R. Soc. Lond.* **A309** ,1 (1983).

[32] G. J. Wang, A. P. Sutton and V. Vitek, *Acta Met.* **32** ,1093 (1984).

[33] C. S. Barrett and T. B. Massalski, *Structure of Metals* , Pergamon Press, New York, 3rd. ed., 1980, p. 373.

[34] G. H. Bishop and B. Chalmers, *Scripta Met.* **2** ,133 (1968).

[35] H. S. M. Coxeter, *Acta Math. Acad. Sci. Hungaricae* **5** , 263 (1954).

[36] H. M. Cundy, *Math. Gaz* **36** , 263 (1952).

[37] J. D. Bernal, *Scient. Am.* , 125 (1960).

[38] J. D. Bernal, *Proc. Roy. Soc. Lond.* **280A** , 299 (1964).

[39] P. D. Bristowe and S. L. Sass, *Acta Met.* **28** , 575 (1980).

[40] M. F. Ashby, F. Spaepen, and S. Williams, *Acta Met.* **26** ,1647 (1978).

[41] H. J. Frost, M. F. Ashby and F. Spaepen, *Scripta Met.* **14** ,1051 (1980).

[42] M. Koiwa, H. Seyazaki and T. Ogura, *Acta Met.* **32** ,171 (1984).

[43] H. J. Frost, F. Spaepen and M. F. Ashby, *Scripta Met.* **16** ,1165 (1982).

[44] H. J. Frost and F. Spaepen, *J. de Physique* **C6-43** ,73 (1982).

4. THE STRUCTURE OF TILT GRAIN BOUNDARIES

4.1. Analysis of the Structures of Σ17

The calculation procedure described in section 3.4 results in a set of possible translations for each symmetrical tilt grain boundary studied. Each of these translations represents a possible structure for that particular grain boundary. In this section, all the possible structures for a particular grain boundary, Σ17, are analyzed. This detailed procedure has been carried out for the coincidence boundaries with tilt axis [100] and [110]. The grain boundaries of interest have already been indicated in Table 2.2.1 and the ranges of misorientation were selected in section 1.2. For the [100] grain boundaries, the range of interest is between Σ5 and the perfect crystal. A structural unit description of this set of boundaries is given in the second section of this chapter. It is shown that this sequence of structures can be described by a combination of structural units of the favored Σ5 boundary and distorted units representative of the perfect crystal coordination. The analysis of the [110] boundaries starts with a description of the possible translation states of the twin boundary in the third section of this chapter. Finally, the [110] sequence is described in the last section in the same manner as the [100] sequence, although the types of structural units present are different. For this chapter, since there is a large amount of data, most tables and all figures are presented at the end of the corresponding sections.

The result of the calculations described in section 3.4 is an interlocking group of 3 or 4 atoms. Starting with the coincidence boundary, the atom in the lower grain at the coincidence position is translated to the newly calculated atomic center and forms a group of atoms that retains the interatomic distances of the crystal. The set of all possible translations for the Σ17 grain boundary are shown in Table 4.1.1 in order of

increasing z component. The atom positions in the CSL and the set of atoms used in the calculations are shown in Figure 4.1.1. The AB stacking is indicated by open and filled circles; for the calculation-atoms corresponding to the lower grain a circle with a + inside it corresponds to the level of a filled circle and a circle with an x inside it corresponds to an open circle. Because of the symmetry of the atom calculation set about the half period, similar translations result from, for example, the sets 1,2,11 and 6,5,8. For a given case in Table 3.4.1 the translation that results from 1,2,11 corresponds to **t** while the translation obtained from 6,5,8, corresponds to –**t**. Only the positive translations are indicated in Table 4.1.1. Equivalently, the calculations could be carried out only for half a period or for one quarter of the period for the case of centered boundaries. The coordinate axes are as follows : *the y axis is along the grain boundary in the plane of the paper, starting from the atom numbered 1 towards the other atoms in the calculation set, the z axis is normal to the boundary and into the upper grain, the x axis is along the tilt axis and its direction is chosen to form a right-handed coordinate system. All numerical values of position are given in units of the lattice parameter.* Once the rigid-body translation is accomplished, further individual atom relaxations are evident that form additional groups of atoms that retain the interatomic distances of the crystal. The resulting structures for all possible translations are shown in Figures 4.1.2 to 18 in the same order as Table 4.1.1; the figure number for the corresponding translation is one higher. The upper grain atom positions are shown in filled circles (atoms at 0.) and open circles (atoms at .5). The lower grain atom positions are shown in the same way when the x-component of the translation is 0. or close to 0. (for example Fig.4.1.9) and by changing filled circles to open circles and viceversa when the x-component is equal to .5 or very close to .5 (for exam-

ple Fig. 4.1.5). The structure of these boundaries can be readily interpreted as an AB stacking along the tilt axis. When the x-component of the translation is different than 0 or .5 a new set of symbols (filled squares and open squares) is used. The following notation is used to describe a given structure: C is a capped trigonal prism, K is a unit of BCC crystal, and T and O stand for a tetrahedron and an octahedron respectively. In all cases, the individual atom relaxations are large ($>.25$) only for 2 or 3 atoms per period. Thus, other than the distorted structural units shown at the grain boundary, additional tetrahedra, octahedra and BCC unit cells occur within 3 lattice parameters normal to the boundary.

Some translations produce a structure that can be described as a sequence of polyhedra that repeats with the period of the boundary. For example, the translations 5,7,14, result in the sequence CTCTK while the translations 1,2,4,11,17 result in the sequence CTCOT. These translations have a component parallel to the tilt axis close or equal to 0 or .5, as a result the ordinary mirror plane is conserved and the translations correspond to type α in Table 2.6.2. Notice that that the capped trigonal prisms are capped on two sides only. However, some translations form only a few structural units between the atoms in the set that originated that particular translation. For example, the translations 3,9,10,12,13,15, and 16 result in a group of two or three tetrahedra near the origin but it was impossible to relax the boundary further and create additional structural units. Particularly interesting sets of translations are 7 and 8. The y component of the translation moves the lower grain to one-half of the period of the boundary which is equal to 4.14. Because of the symmetry of the calculation set about the half-period (see Fig. 4.1.1), these translations are the result of a number of different atom sets and, in particular, translation 7 is the result of a Case 2

and a Case 7 (see Table 3.4.1). The boundary structure as shown in Figures 4.1.8 and 4.1.9 includes two capped trigonal prisms but the rest of the boundary cannot be relaxed to give additional structural units. Because of the symmetry of the calculation set the centers of the trigonal prisms are separated by half the period of the boundary. Notice that in this case the capped trigonal prisms are capped on three sides. The translations that result in incomplete structural unit descriptions have a component parallel to the z axis which is different than .0 or .5. For these translations all symmetry elements are destroyed and thus they correspond to type λ in Table 2.6.2.

In order to choose a favored structure among all the possible translations for this particular boundary the three Laves rules (see section 3.3) and the minimization of the free volume are followed. Aaron and Bolling have shown that minimization of the grain boundary free volume is a good criterion for evaluating grain boundary models.[1] However, the properties of a given grain boundary depend on the distribution of the free volume along the grain boundary. In order to calculate the excess volume, a parallelepiped box is constructed with vertices at atom centers well within the perfect crystal and with two of its faces parallel to the boundary plane. In the coincidence position, the volume of this solid is

$$V_{pc} = A \cdot N_p \cdot d_p \tag{4.1.1}$$

where A is the grain boundary area, N_p is the number of planes parallel to the boundary plane, and d_p is the corresponding interplanar spacing. The density of the solid in the coincidence position is equal to the crystal density. Upon a translation, the volume of the parallelepiped whose vertices are fixed increases so that the same number of atoms are included in the solid. The volume of this solid is

$$V_{gb} = A \cdot N_p \cdot d_p + A \cdot (t_z - d_p) \tag{4.1.2}$$

The excess volume is then simply

$$V_{ex} = V_{gb} - V_{pc} = A \cdot (t_z - d_p) \tag{4.1.3}$$

The excess volume is linearly related to the z-component of the translation and thus to minimize the excess volume the lowest t_z is required. Notice that the excess volume is really given by the excess of t_z over d_p; this quantity is usually referred to as the *expansion* . For the (014) boundary $d_p = .243$ so that for translation number 1 the expansion is .239.

The criteria that have been stablished in order to obtain the most likely occuring boundary structure are to look for the structure with the highest coordination and with the minimum excess volume. Of the two continuous structures indicated above, the one with the highest coordination is the structure CTCTK. This occurs because the atom positions are distorted in the structure CTCOT in such a way that the octahedral atoms inside crystals 1 and 2 have coordination 12 instead of coordination 14 (see Figs. 4.1.3 and 5) . Thus, the most likely structure of the $\Sigma 17$ boundary is translation 5, illustrated in Figure 4.1.6 .

There are a number of grain boundaries that cluster in groups whose excess volume does not differ by more than 5%. One of these clusters is formed by the first 7 boundaries in table 4.1.1. The translations of some of these boundaries are very close and thus the resulting structures are similar, for example, translations 5 and 6 and translations 1,2, and 4. Another important phenomenon that occurs for translations with similar z-component is the transformation between structures with different overall translation. These transformations occur by the addition or removal of a layer

of atoms parallel to the boundary and the subsequent shift by d_p of the lower grain. For ρ=1 symmetrical boundaries this represents the addition or removal of one atom per boundary period. It was shown in the description of the concept of the CNID that the addition or removal of one layer parallel to the boundary plane is equivalent to an in-plane displacement. Thus, the difference between the in-plane components $t_{x\,1}, t_{y\,1}$ and $t_{x\,2}, t_{y\,2}$ is approximately equal to the crystallographic in-plane displacement corresponding to layer addition or removal. An example of such a transformation is the addition of one layer to translation 5 which transforms the most likely structure into the structure of translation 8. These transformations are extremely important in the description of grain boundary phenomena such as segregation. The change in structure of a grain boundary as the level of segregation increases occurs by transformations among the possible structures of a grain boundary. This point is discussed in detail in section 6.2.

Some of the translations are exactly equal to a DSCL translation. For example translation 14 is equal to $1/2[11\bar{1}]$ which is a crystal lattice translation and also a DSCL translation. The resulting structure is the same as the most likely structure but the excess volume is much larger indicating that in order to obtain this particular structure larger individual atom relaxations are required. The structure that is obtained by a DSCL translation can also be obtained by removing an equivalent number of layers from the zero translation CSL structure. This was shown in the discussion in section 2.4. In this case the removal of five layers parallel to the boundary from Figure 4.1.1 will give the structure of Figure 4.1.15. Some of the most likely structures for boundaries other than $\Sigma 17$ are the result of DSC translations and thus this point is retaken in the next section.

TABLE 4.1.1
GB Translations for a BCC Σ=17 [100]/(014) Tilt Boundary

#	Translations in order of increasing z component (lattice parameter a=1.0)			New atom center at this position is distant to the atom centers indicated † by					
				.866a			a		
1	.4355	.7815	-.4819	11	2	-	10	-	-
2	.4242	.7653	-.4841	11	2	-	1	7	-
3	.3309	.6366	-.4850	11	2	1	-	-	-
4	.5000	.7099	-.4960	11	-	-	1	7	-
5	.5000	.5038	-.4961	11	7	1	-	-	-
6	.4922	.5108	-.4969	11	1	7	2	-	-
7	.1377	2.0616	-.4980	10	4	-	3	-	-
				10	-	-	9	3	-
8	.0320	1.9327	-.5143	10	-	-	3	4	-
9	.3762	1.0257	-.5355	2	10	-	11	-	-
10	.1111	.6544	-.5562	2	1	7	11	-	-
11	.5000	.6566	-.5647	-	-	-	2	7	1
12	.2846	.8880	-.5712	2	-	-	11	10	-
13	.2136	.7884	-.5768	2	-	-	11	1	7
14	.5000	.3638	-.6063	1	7	-	11	-	-
15	.2909	.5395	-.6118	1	7	-	11	2	-
16	.3916	.6724	-.6281	-	-	-	11	2	1
17	.5000	.5878	-.6360	-	-	-	11	7	1

† Three atom sets are used in the calculations. If a fourth center is indicated, it is redundant. Only one set is shown; there are other sets of atoms that produce the same translation. These other sets are obvious from the symmetry of the grain boundary.

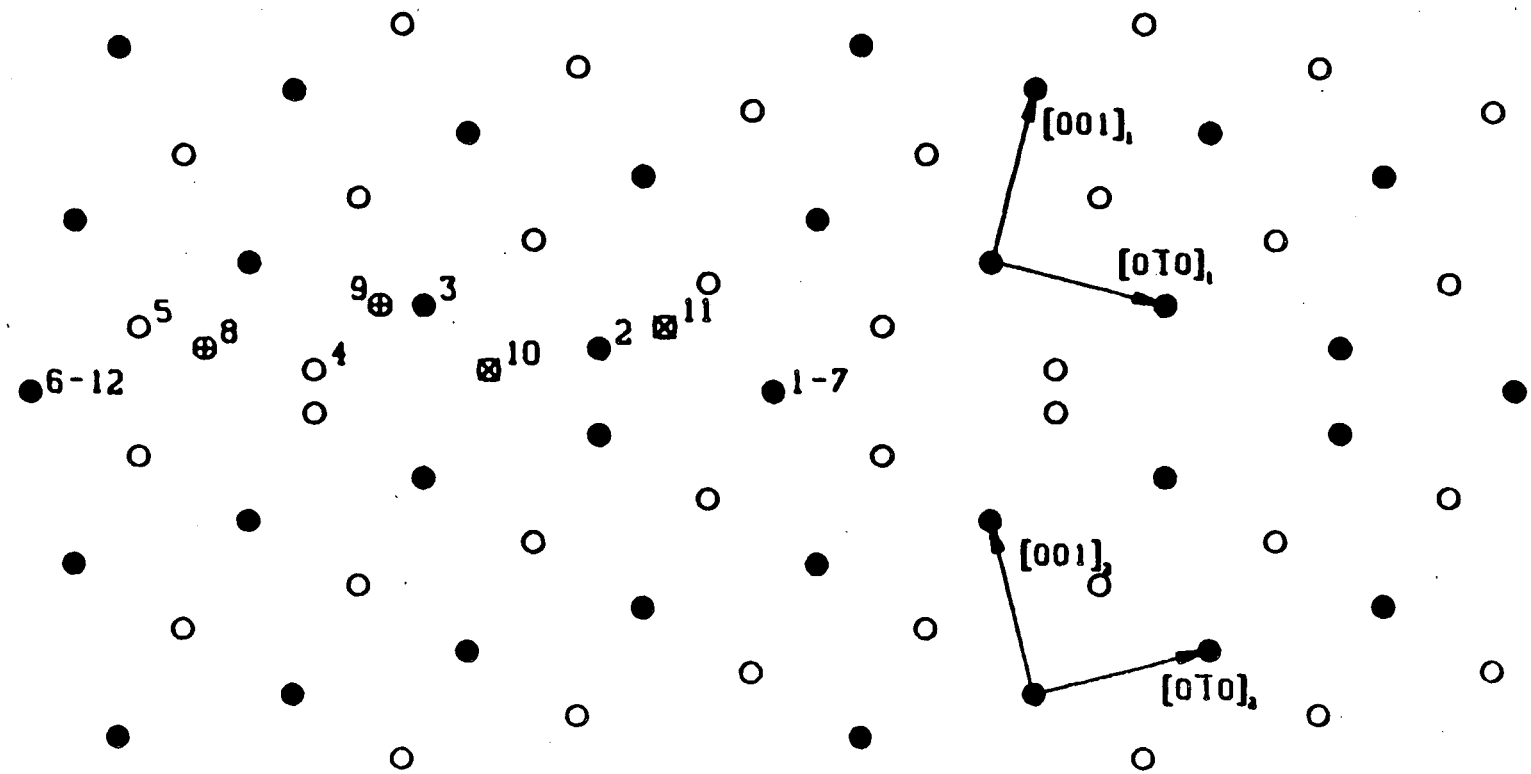

FIGURE 4.1.1 STRUCTURE OF Σ17 CSL BOUNDARY

T_x=0.435 T_y=0.781 T_z=-0.482

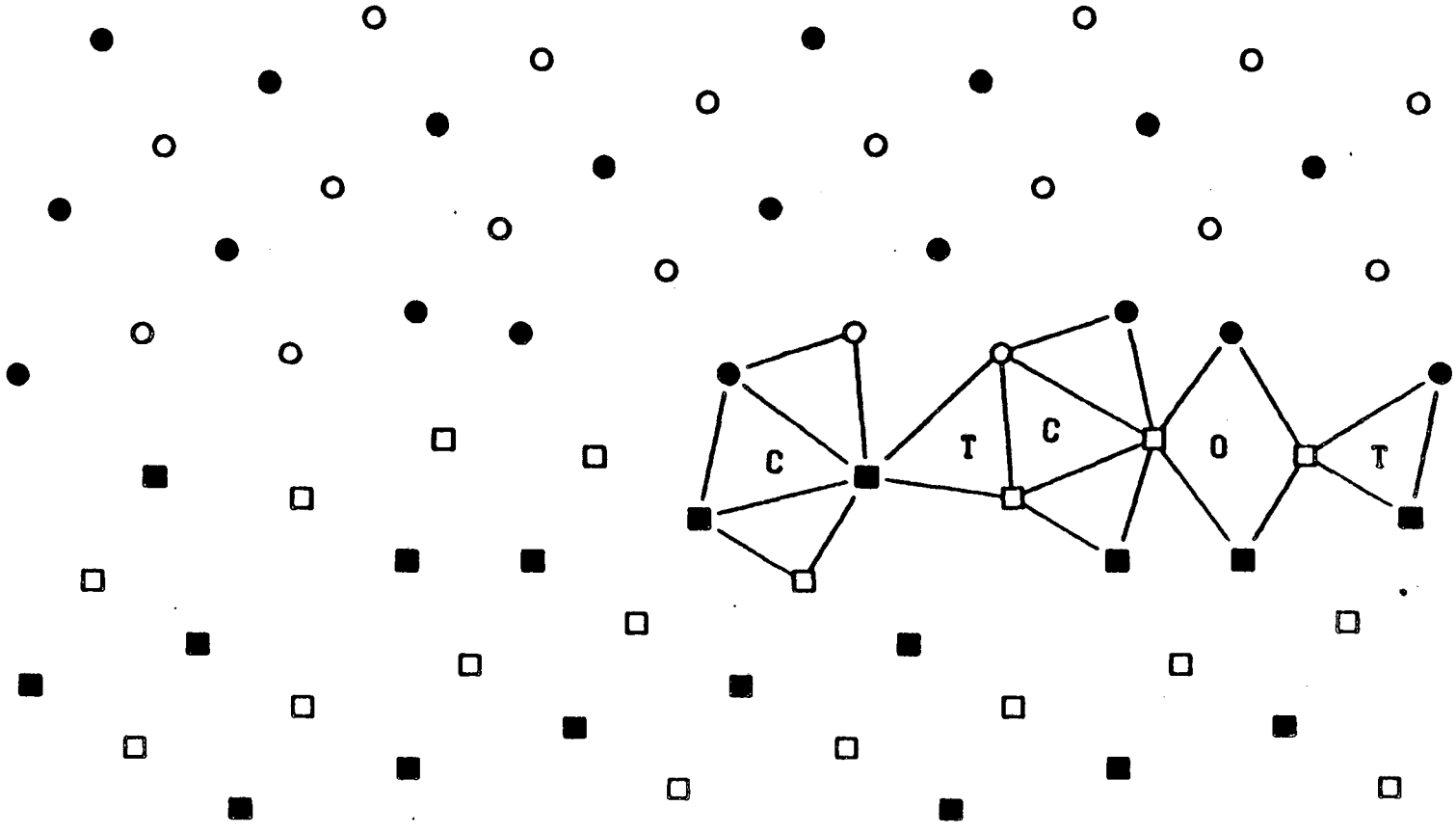

FIGURE4.1.2 Σ17 STRUCTURAL UNITS

T_x=0.424 T_y=0.765 T_z=-0.484

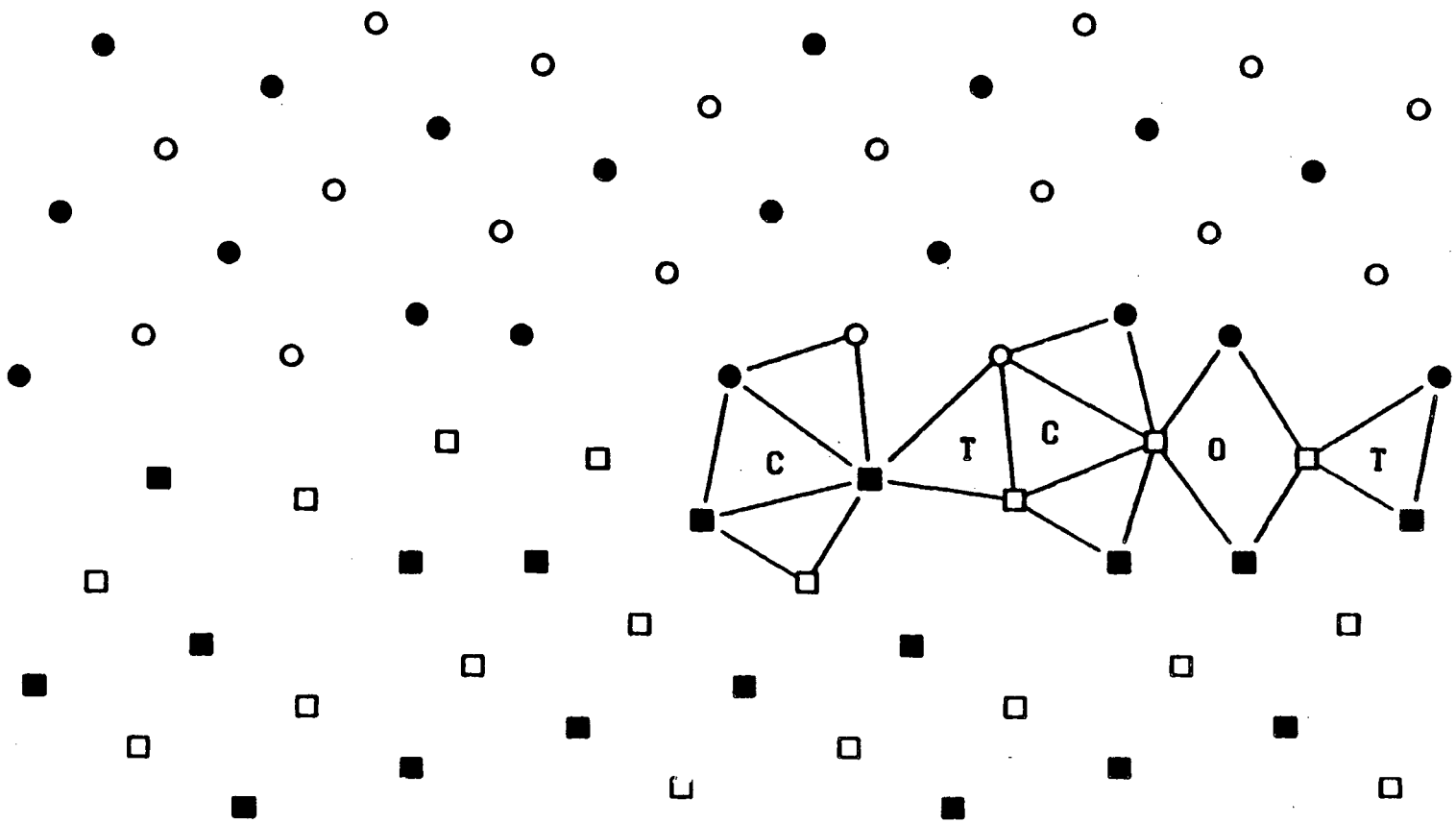

FIGURE4.13 Σ17 STRUCTURAL UNITS

T_x=0.331 T_y=0.637 T_z=-0.485

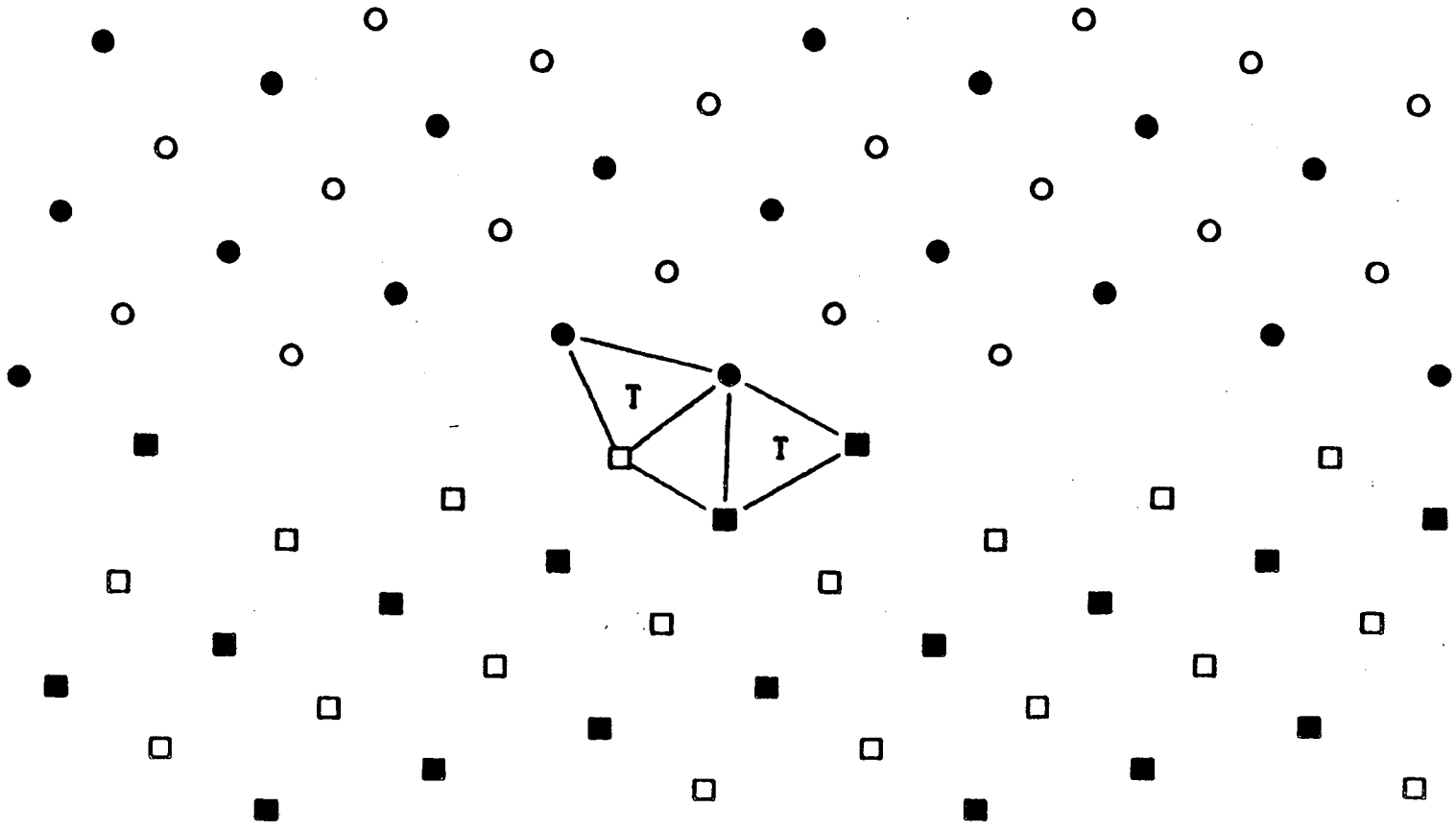

FIGURE 4.1.4 Σ17 STRUCTURAL UNITS

T_x=0.500 T_y=0.710 T_z=-0.496

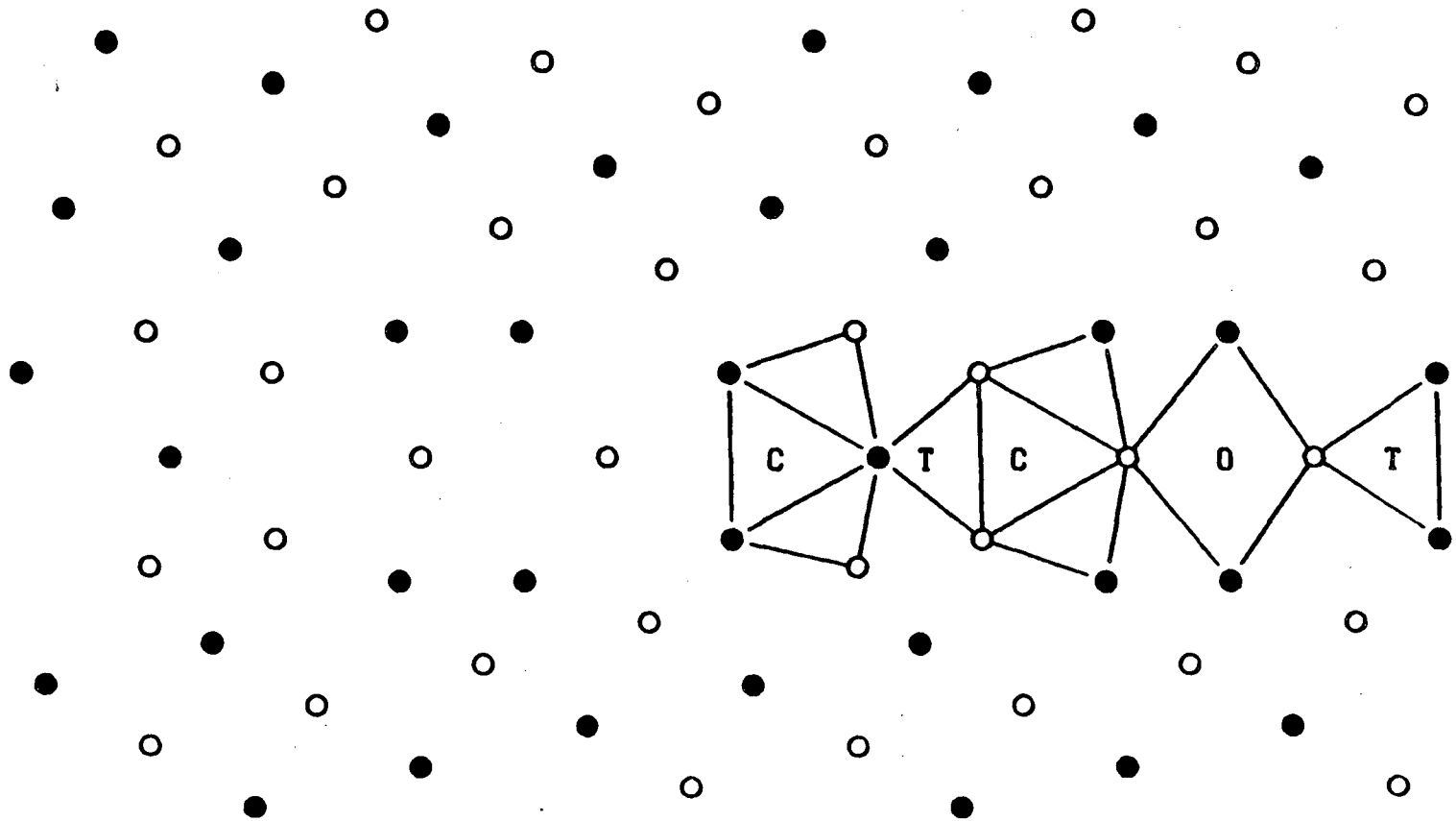

FIGURE 4.15 Σ17 STRUCTURAL UNITS

T_x=0.500 T_y=0.504 T_z=-0.496

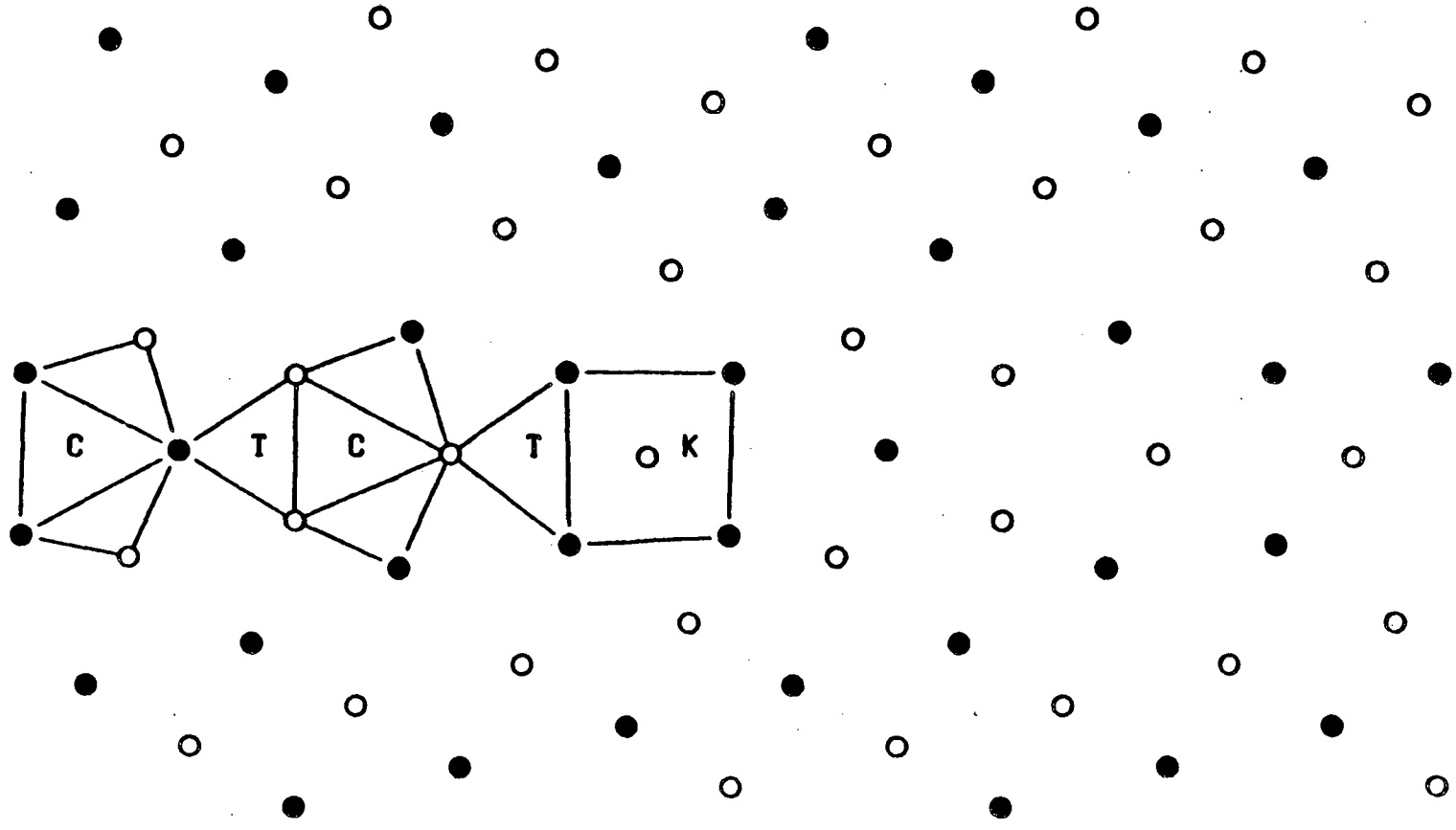

FIGURE 4.1.6 Σ17 STRUCTURAL UNITS

T_x=0.492 T_y=0.511 T_z=-0.497

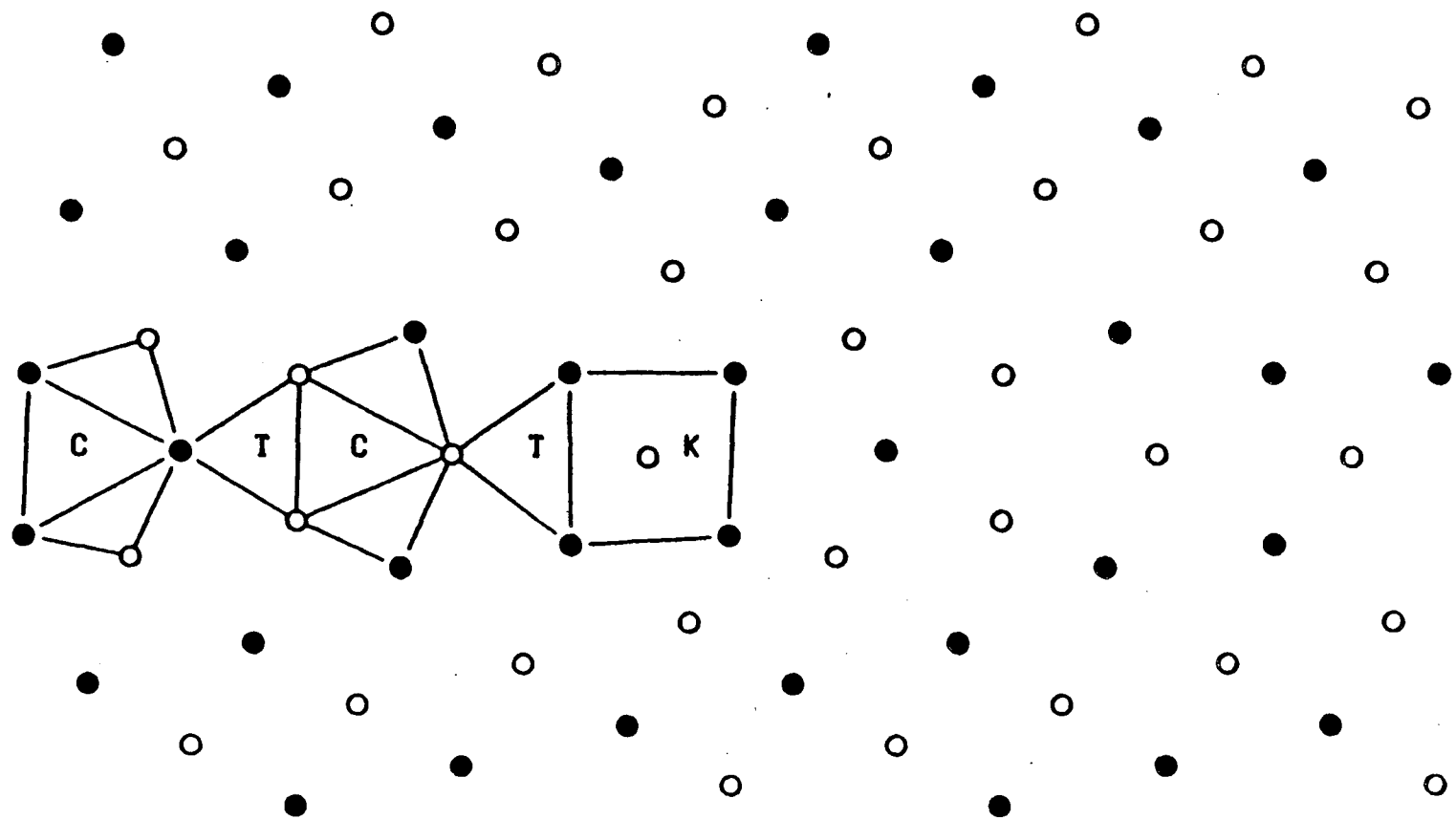

FIGURE4.17 Σ17 STRUCTURAL UNITS

T_x=0.138 T_y=2.062 T_z=-0.498

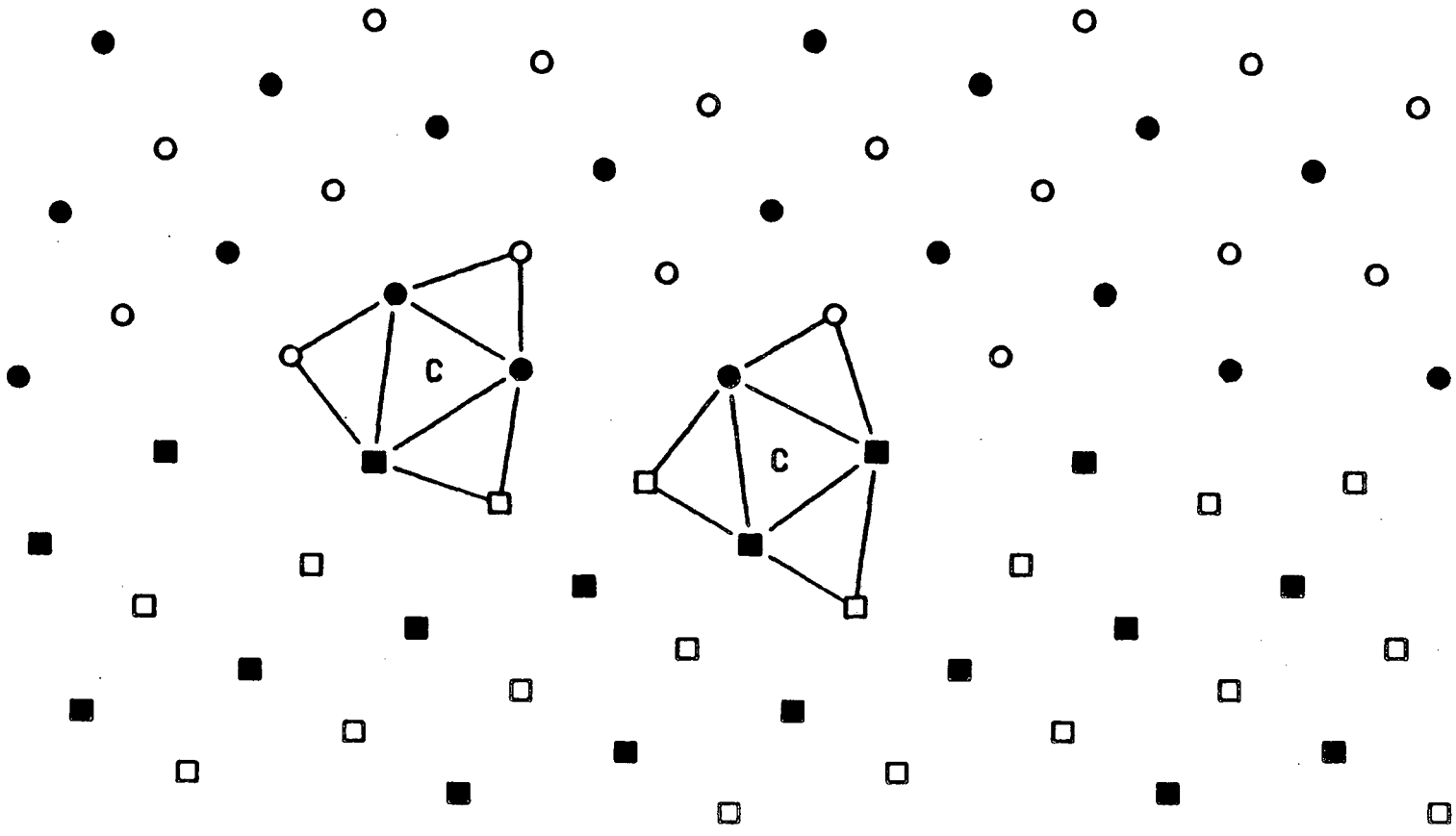

FIGURE4.1.8 Σ17 STRUCTURAL UNITS

T_x=0.032 T_y=1.933 T_z=-0.514

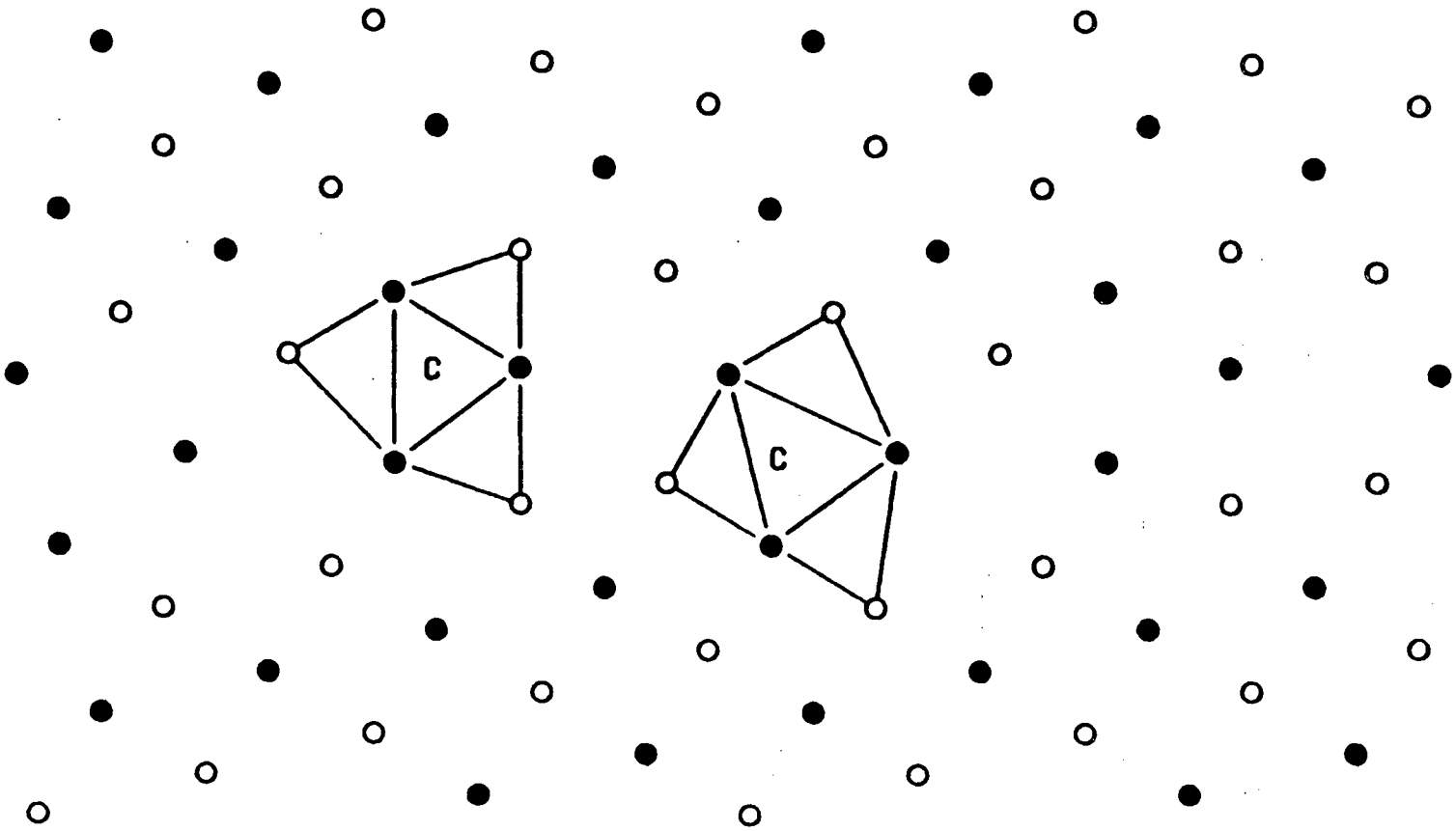

FIGURE 4.1.9 Σ17 STRUCTURAL UNITS

T_x=0.376 T_y=1.026 T_z=-0.536

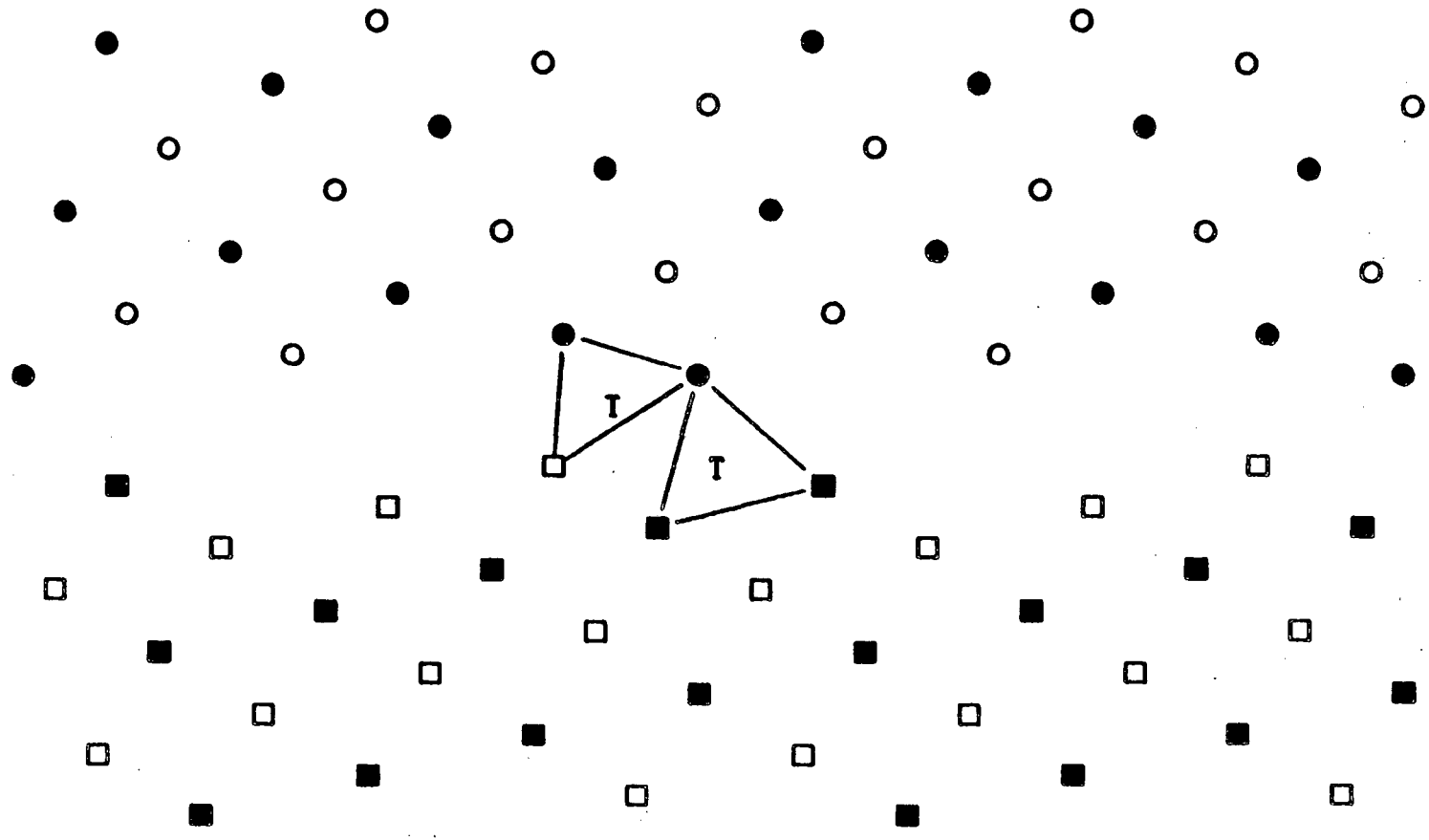

FIGURE 4.1.10 Σ17 STRUCTURAL UNITS

T_x-0.111 T_y-0.654 T_z--0.556

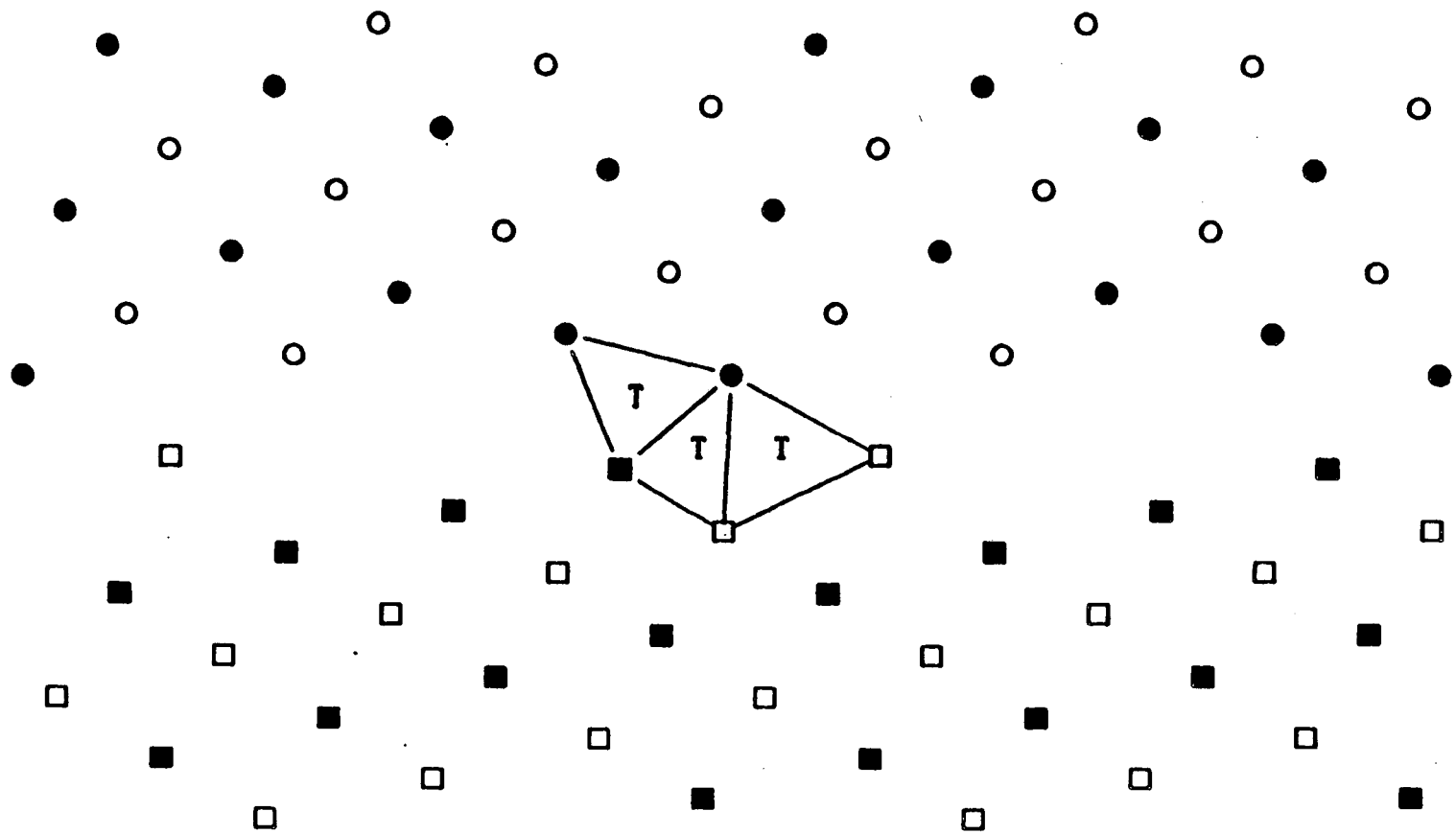

FIGURE 4.11 Σ17 STRUCTURAL UNITS

T_x=0.500 T_y=0.657 T_z=-0.565

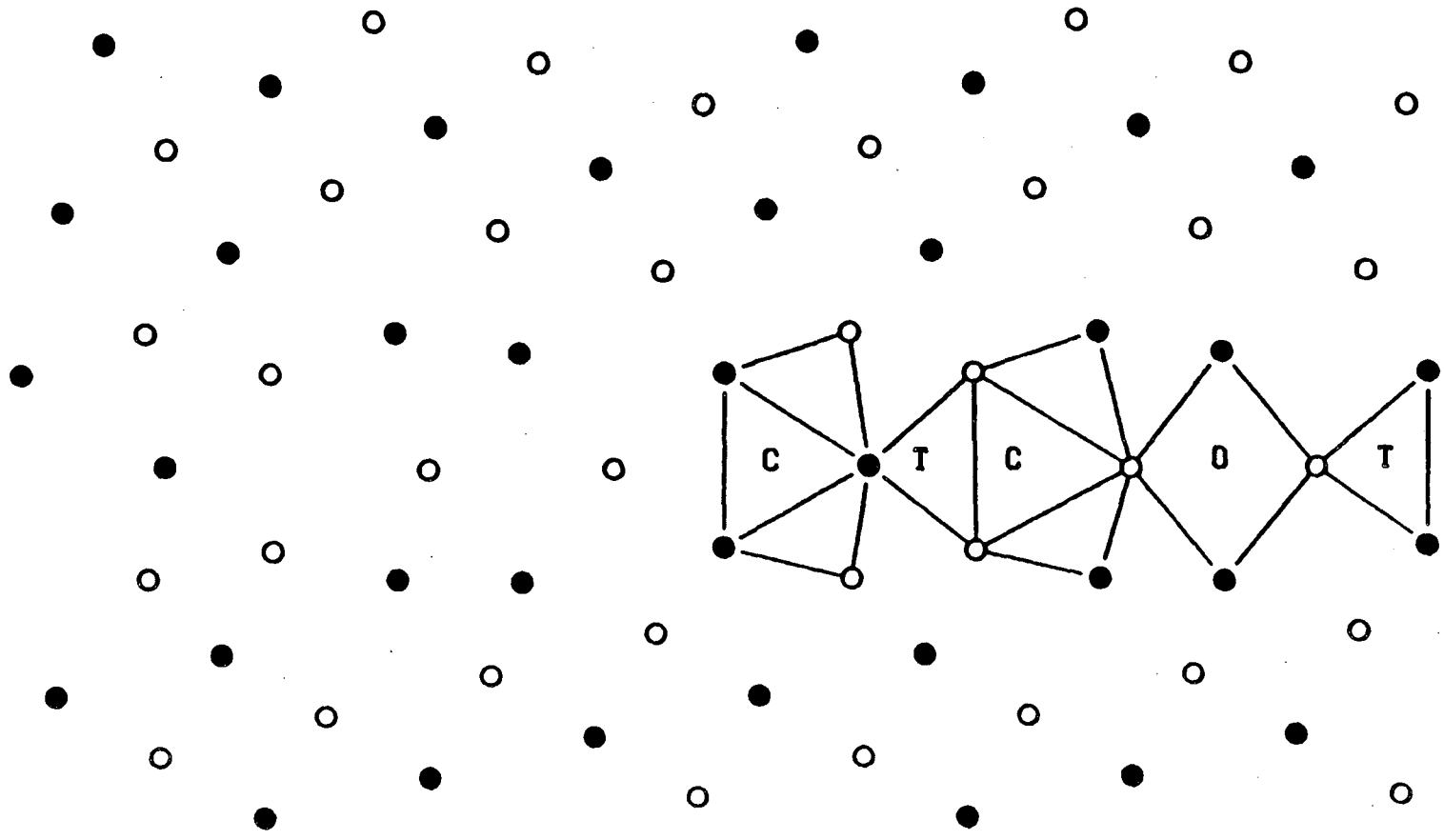

FIGURE4.1.12Σ17 STRUCTURAL UNITS

T_x=0.285 T_y=0.888 T_z=-0.571

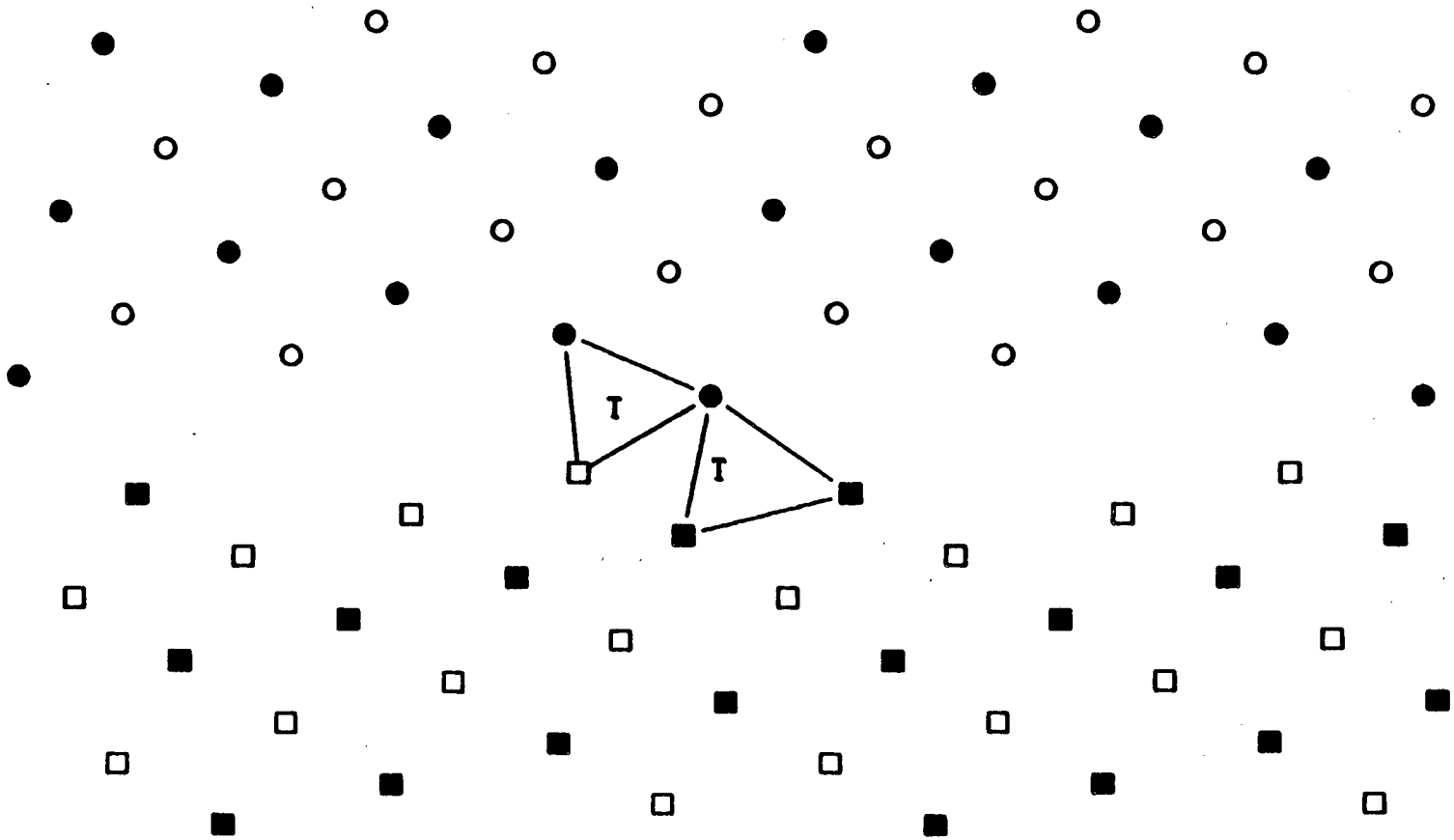

FIGURE 4.1.13 Σ17 STRUCTURAL UNITS

T_x=0.214 T_y=0.788 T_z=-0.577

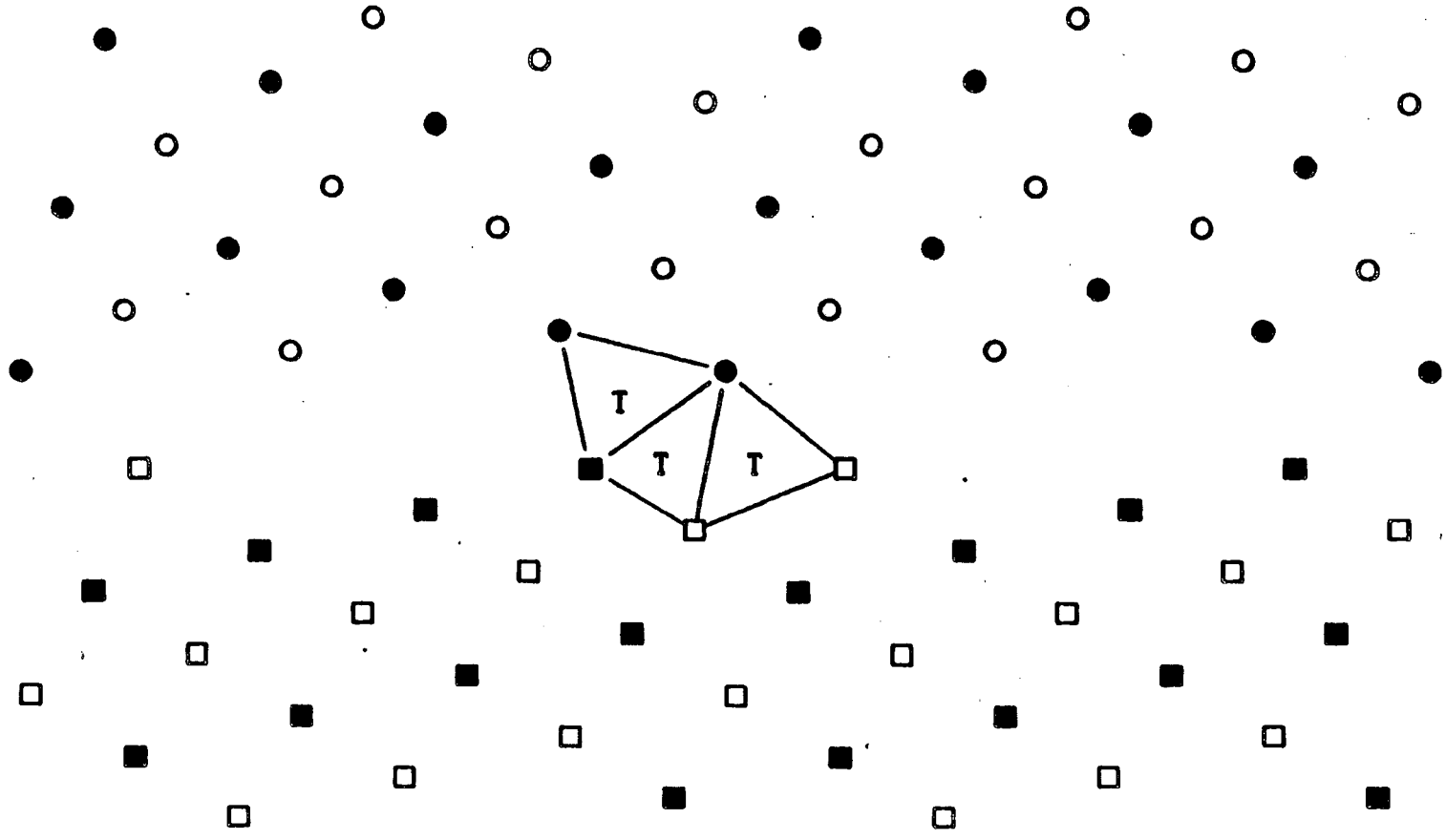

FIGURE4.1.14Σ17 STRUCTURAL UNITS

T_x=0.500 T_y=0.364 T_z=-0.606

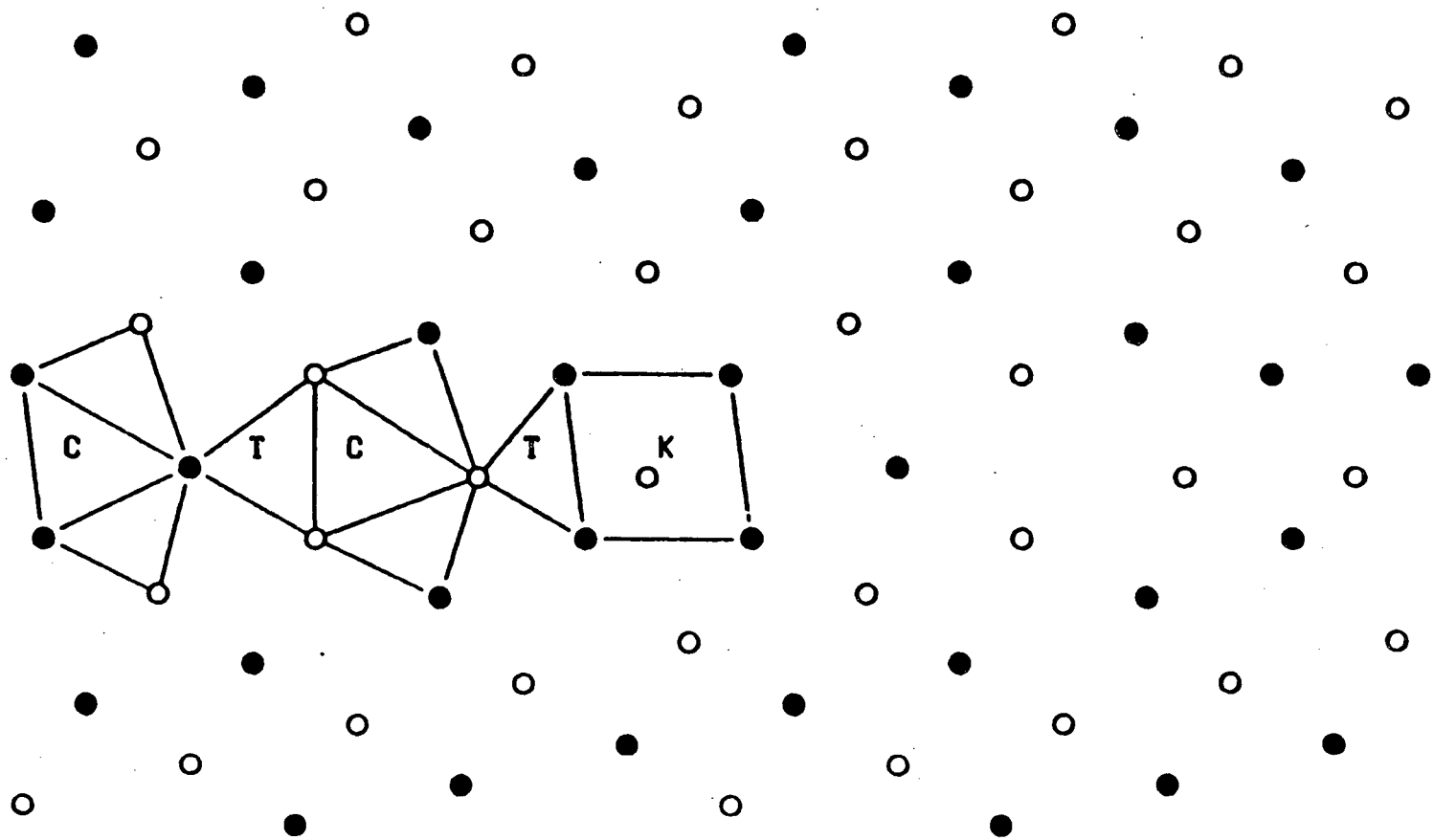

FIGURE 4.1.15 Σ17 STRUCTURAL UNITS

T_x=0.291 T_y=0.539 T_z=-0.612

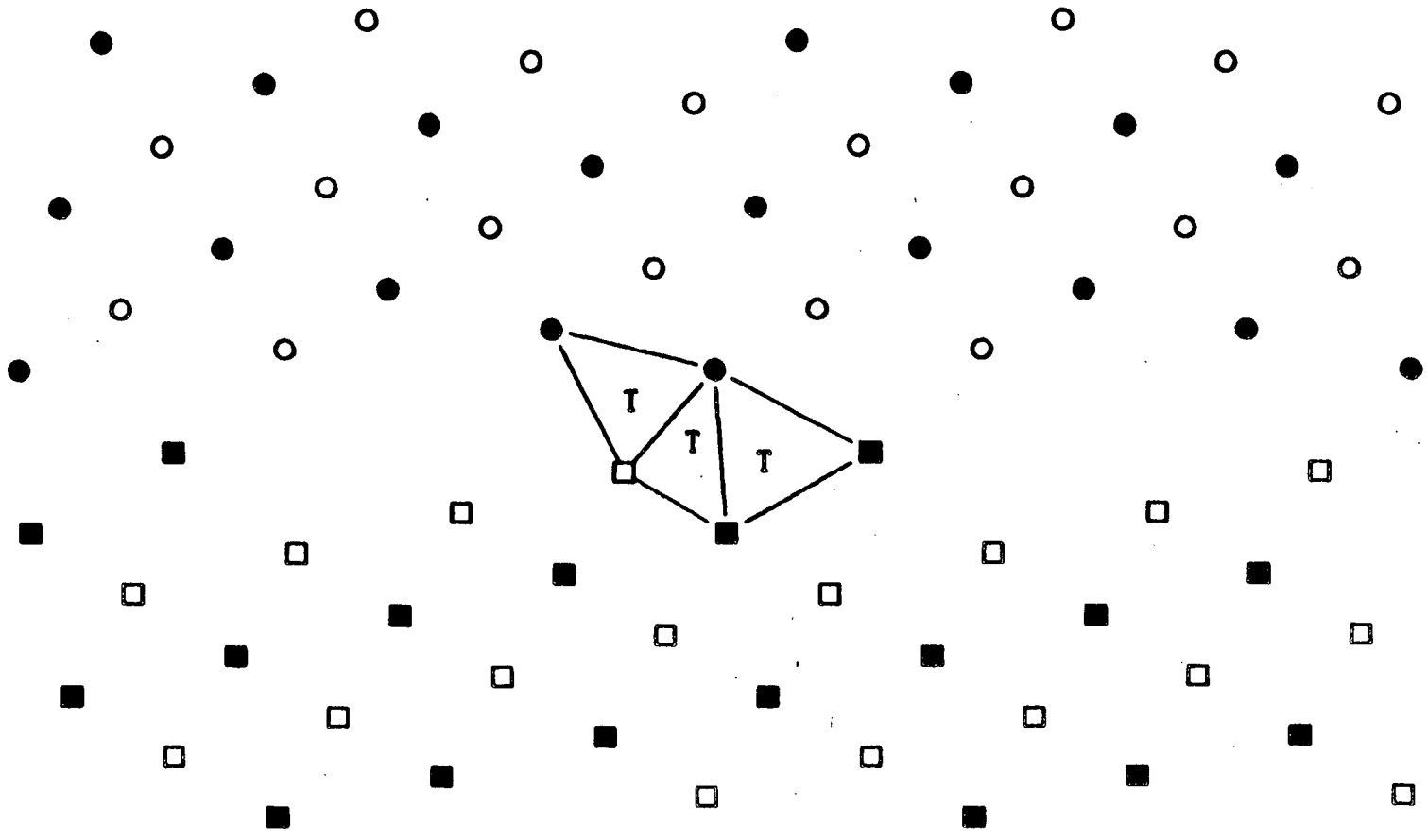

FIGURE 4.1.16Σ17 STRUCTURAL UNITS

T_x=0.392 T_y=0.672 T_z=-0.628

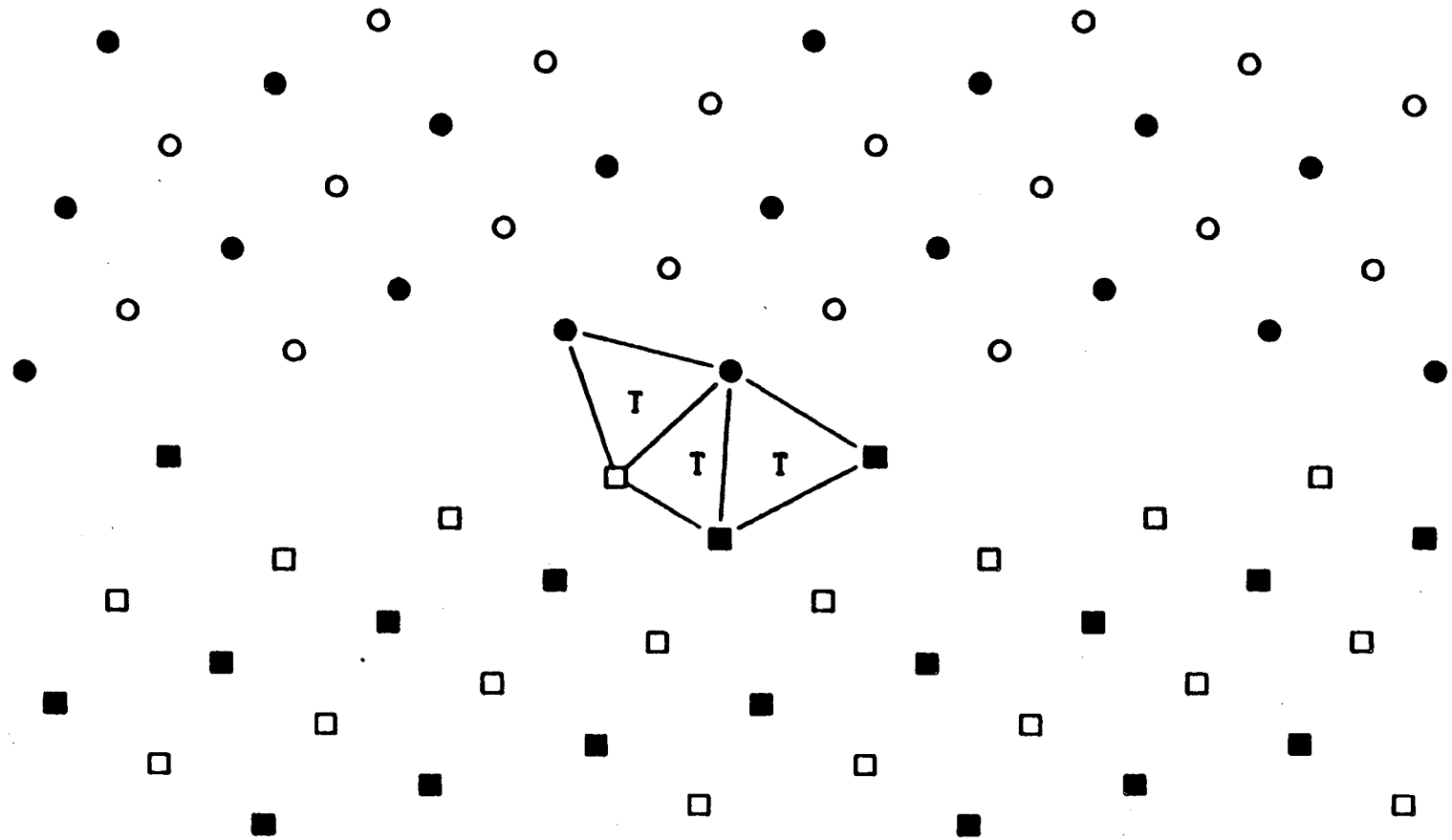

FIGURE4.1.17Σ17 STRUCTURAL UNITS

T_x=0.500 T_y=0.588 T_z=-0.636

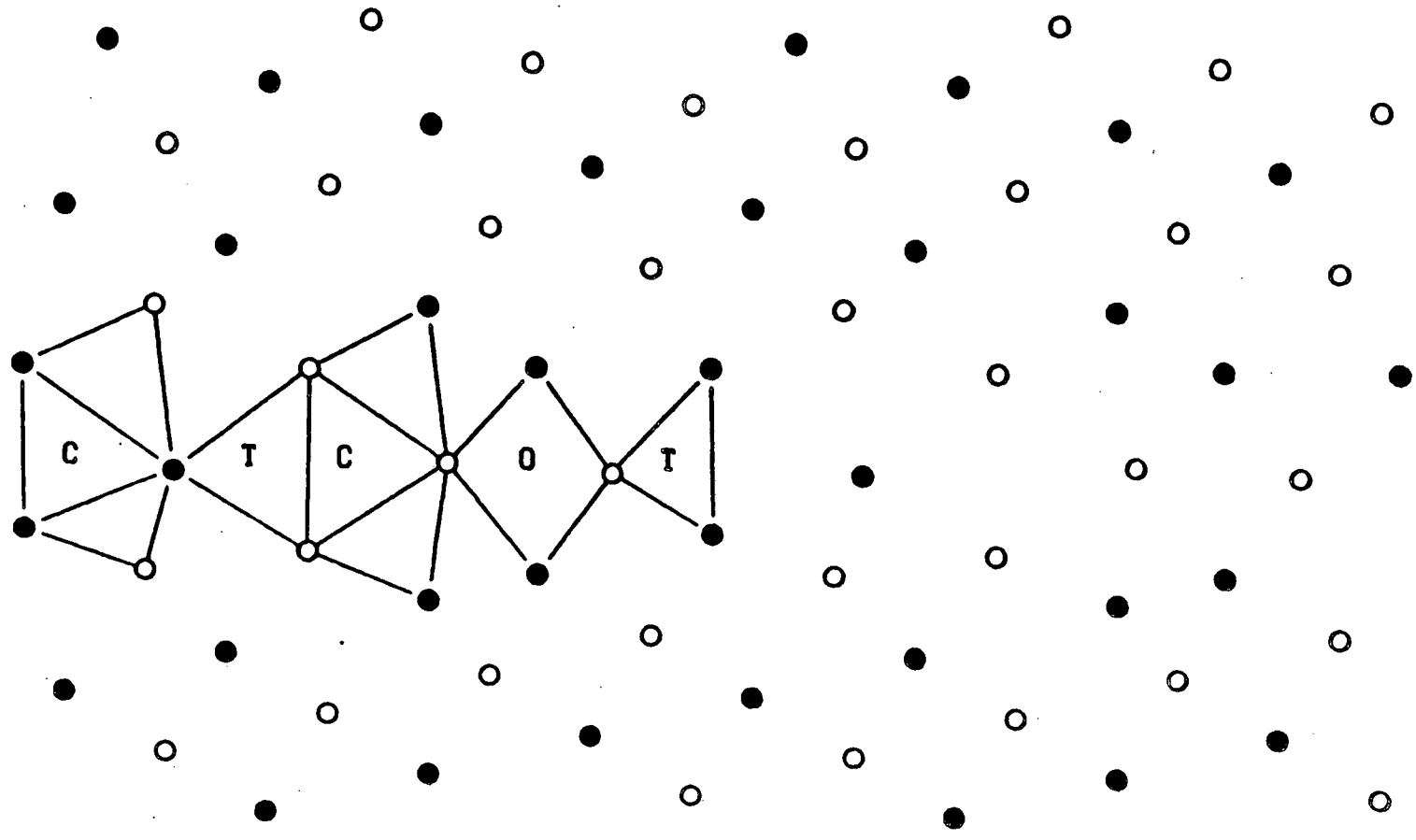

FIGURE 4.1.18 Σ17 STRUCTURAL UNITS

4.2. [100] Symmetrical Tilt Boundaries

Each boundary in the sequence of [100] symmetrical tilt grain boundaries between Σ5 and the perfect crystal was studied as the Σ17 boundary described in the previous section. The crystallographic data for these boundaries is shown in Table 4.2.3. The basis for the CSL and DSCL for each boundary is indicated. For each boundary, the following tables and figures are included: a table with all the possible translations, a figure of the boundary in the CSL position and a figure of the atom positions in the grain boundary for the most likely translation state. For the later figures the structural units at the grain boundary are indicated for one period of the boundary. The grain boundary data are included in order of decreasing degree of coincidence.

This sequence of boundaries can be described by a mixture of structural units of the Σ5 boundary and the perfect crystal. The sequence of structural units for each boundary is shown in Table 4.2.1

TABLE 4.2.1
Structural Unit Description of [100] Symmetrical Tilt Boundaries

Σ	*Angle*	*Plane*	*Structural Unit Sequence*
1	0	(001)	K,K,....
41	12.68	(019)	CTKKK-CTKKK,CTKKK-CTKKK,....
25	16.26	(017)	CTKK-CTKK,CTKK-CTKK,....
37	18.92	(016)	CTKKCTK,CTKKCTK,....
13	22.62	(015)	CTK-CTK,CTK-CTK,....
17	28.07	(014)	CTCTK,CTCTK,....
5	36.89	(013)	CT-CT,CT-CT,....

C = distorted capped triangular prism
T = distorted tetrahedron
K = perfect or distorted bcc unit cell

The $\Sigma 5$ boundary is termed the favored boundary because it is composed of only one type of structural unit, if the capped trigonal prism and tetrahedron are considered as a single unit. A [100] symmetrical tilt boundary is centered when the boundary plane (0hk) has both h and k odd. Thus the size of the structural unit of $\Sigma 5$ is $1/2[03\bar{1}]$. The capped trigonal prisms form the core of two terminating (002) planes (one in each crystal) and thus the favored boundary can be described as an array of primary lattice dislocations. Consider next the primitive (non-centered) boundary $\Sigma 17$. Its period can be decomposed as

$$[04\bar{1}] = 2 \cdot 1/2[03\bar{1}] + [010] \tag{4.2.1}$$

This boundary has two alternative dislocation descriptions. The two capped trigonal prisms are at the core of two terminating (002) planes per unit. Thus, as before, the boundary can be described as an array of primary dislocations. Alternatively, each distorted lattice unit can be considered as the core of two terminating (013) planes. The boundary can then be considered as a $\Sigma 5$ boundary plus a superimposed array of DSC dislocations $2/10[013]$. The spacing of the DSC dislocations is equal to one period of the $\Sigma 17$ boundary. The structure of the $\Sigma 41$ boundary shows three distorted lattice units that separate capped trigonal prisms. There are two terminating (002) planes per prism and thus the boundary can be described as an array of primary dislocations. The structure of the other boundaries can be described in the same manner as those already discussed. The $\Sigma 13$ boundary is the intermediate boundary having one unit of $\Sigma 5$ boundary and one unit of perfect crystal. For the boundaries with small misorientation, a primary lattice description is preferred, while for the case of boundaries with large misorientations close to $\Sigma 5$ the DSC dislocation array is preferred. It should be pointed out that mathematically a primary dislocation array or a

DSC dislocation array are equivalent descriptions of a grain boundary. The distinction can be made only on the basis of dynamical physical experiments as pointed out in section 3.1.

A simpler description of this sequence of structures can be given in terms of the structural units indicated in Table 4.2.1. The favored boundaries consist of only one type of structural unit; these are the $\Sigma 5$ and $\Sigma 1$ boundaries. The structure of the intermediate boundaries is derived from a simple rule of mixing of the units of the favored boundaries. In the case of intermediate boundaries with misorientation close to $\Sigma 5$, the structure consists of K units embedded in an array of a large number of CT units. In the case of intermediate boundaries with small misorientations, the structure consists of CT units embedded in an array of a large number of K units. The $\Sigma 13$ boundary represents the 1:1 mixture of favored boundary structural units. The construction of each boundary is illustrated for the case of the $\Sigma 37$ boundary. The procedure was first proposed by Sutton, *et.al.* [2] The period of the boundary is $[06\bar{1}]$. As in the case of the $\Sigma 17$ boundary this period is decomposed as follows

$$[06\bar{1}] = 2 \cdot 1/2[03\bar{1}] + 3[010] \tag{2.1.2}$$

In order to find a structure composed of two CT units and three K units, higher ratio ligaments are combined. A 1:1 ligament is equal to CTK , a 1:2 ligament is equal to CTKK, etc. The 2:3 ligament is equal to 1:2+1:1 and thus the structure is CTKKCTK which is confirmed by Figure 4.1.8.

A similar structural unit description of grain boundaries in FCC materials arises from a systematic study, using molecular static computations, of symmetric [3] and asymmetric tilt boundaries, [4] and of twist boundaries. [5] Balluffi and Bristowe have

critically reviewed the calculations mentioned above. [6] They suggest that there are a number of choices for the description of a range of boundaries. The entire range of [100] tilts can be described by considering the favored boundaries Σ1-Σ5-Σ5-Σ1 as has been done for the BCC case above (see Table 2.2.1). Alternatively, Balluffi and Bristowe point out that the same sequence of boundaries can be described by mixtures of the Σ1-Σ1 sequence. Thus the problem of the multiplicity of descriptions that was brought up in section 3.1. arises again. However, the distortions of the structural units are shown to be systematic and a simple model has been derived to study core properties.[7] The model depends on understanding the properties of the delimiting boundaries and thus, due to the multiplicity of choices, the structural unit model can not be used to predict properties in a quantitative manner.

The BCC tilt grain boundaries were also studied by Vitek, *et.al.* using molecular statics with the Johnson potentials illustrated in Figure 3.2.1. [8] The structure of the boundaries calculated agree very well with the structures shown in this section. Although only the Σ41, Σ25, Σ17 and Σ5 boundaries are discussed, the translation states for each boundary in the range are given. Table 4.2.2 gives a comparison of the translation states given by Vitek *et.al.* and the values obtained in this investigation. The equivalent atomistic values are necessary to compare with this investigation because only positive translations have been tabulated and studied. Thus for the Σ41 and Σ25 boundaries the x-component of the atomistic translation changes to .5 because these are centered boundaries and the y-component is equal to half the period minus the value given. For the Σ13 and Σ5 boundaries the translations given are DSC translations and the equivalent values are equivalent DSC translations with positive components. This indicates that for these two boundaries, the rigid body

TABLE 4.2.2
In Plane Translations and Expansions for BCC [100] Tilt Boundaries

Designation	Atomistic Calculation†		Equivalent Atomistic		Hard Sphere Model		Expansion	
							Atomistic	Sphere
Σ41	.0	-4.09	.5	.43	.5	.44	.30	.44
Σ37	.0	2.07	.0	2.07	.0	1.94	.29	.38
Σ25	.0	-3.12	.5	.41	.5	.42	.27	.42
Σ17	.5	.58	.5	.58	.5	.50	.29	.25
Σ13	.0	-.98	.5	.39	.5	.48	.19	.31
Σ5	.0	.0	.0	.95	.0	.91	.19	.23

† V.Vitek, D. A. Smith and R. C. Pond, *Phil.Mag.* **41A**, 649 (1980).

relaxation was carried out by layer removal. Since the hard sphere calculations do not allow for layer removal, a rigid body translation always exists. The values of the expansion are usually higher in the hard-sphere calculations since the atomistic calculations are carried out at constant volume and the expansion is obtained by the interpolation procedure described in section 3.3. In spite of these differences the hard sphere calculations show a remarkable similarity with the atomistic calculations in the structures that they predict. The structural unit analysis of grain boundaries is extended to [110] boundaries in the fourth section of this chapter.

TABLE 4.2.3
BCC [100] Tilt Grain Boundaries Between Σ=1 and Σ=5.

Designation	Boundary Plane	Angle (degrees)	CSL Unit Vectors (columns*1/2)†			DSC Unit Vectors (columns*1/2*Σ)†		
Σ1	001	0.0	1	$\frac{1}{1}$	1	1	$\frac{1}{1}$	1
			1	1	$\frac{1}{1}$	1	1	$\frac{1}{1}$
			1	1	1	1	1	1
Σ41	019	12.68	2	1	1	41	0	$\frac{0}{8}$
			0	$\frac{9}{1}$	1	1	10	
			0		9	9	8	10
Σ25	017	16.26	2	1	1	25	0	$\frac{0}{6}$
			0	$\frac{7}{1}$	1	1	8	
			0		7	7	6	8
Σ37	016	18.92	2	1	1	37	0	0
			0	$\frac{5}{7}$	7	$\frac{5}{7}$	$\frac{12}{2}$	2
			0		5			12
Σ13	015	22.62	2	1	1	13	0	0
			0	$\frac{5}{1}$	1	$\frac{5}{1}$	$\frac{4}{6}$	6
			0		5			4
Σ17	014	28.07	2	1	1	17	0	0
			0	$\frac{3}{5}$	5	5	$\frac{8}{2}$	2
			0		3	3		8
Σ5	013	36.89	2	1	1	5	0	0
			0	$\frac{3}{1}$	1	$\frac{3}{1}$	$\frac{2}{4}$	4
			0		3			2

† Cubelike forms with unit vectors close to the coordinate system used in the calculations.

TABLE 4.2.4
GB Translations for a BCC Σ=5 [100]/(013) Tilt Boundary

#	Translations in order of increasing z component (lattice parameter a=1.0)			New atom center at this position is distant to the atom centers indicated † by					
				.866a			a		
1	.1864	.6900	-.4890	1	2	5	-	-	-
2	.2714	.7568	-.4967	2	5	-	1	-	-
3	.5000	.6980	-.5127	-	-	-	1	2	4
4	.5000	.4643	-.5333	1	4	5	-	-	-
5	.3991	.7434	-.5367	2	5	-	1	3	-
6	.3631	.5743	-.5369	1	5	-	2	-	-
7	.0310	.7416	-.5423	2	-	-	1	5	-
8	.4482	.7087	-.5449	5	-	-	2	1	-
9	.5000	.6698	-.5490	5	-	-	4	1	-
10	.1290	.5992	-.6118	1	-	-	2	5	-
11	.5000	.3163	-.6325	4	1	-	5	-	-
12	.2175	.7394	-.6371	-	-	-	1	2	5
13	.5000	.5373	-.6792	-	-	-	1	4	5

† Three atom sets are used in the calculations. If a fourth center is indicated, it is redundant. Only one set is shown; there are other sets of atoms that produce the same translation. These other sets are obvious from the symmetry of the grain boundary.

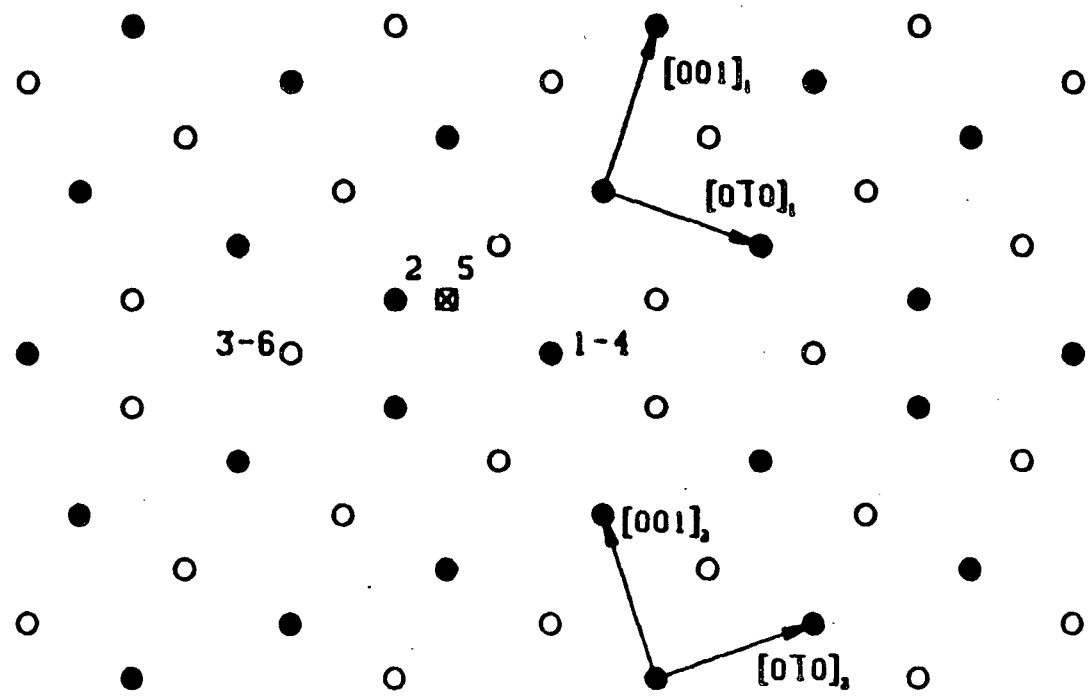

FIGURE 4.21 STRUCTURE OF Σ5 CSL BOUNDARY

T_x=0.000 T_y=0.911 T_z=-0.549

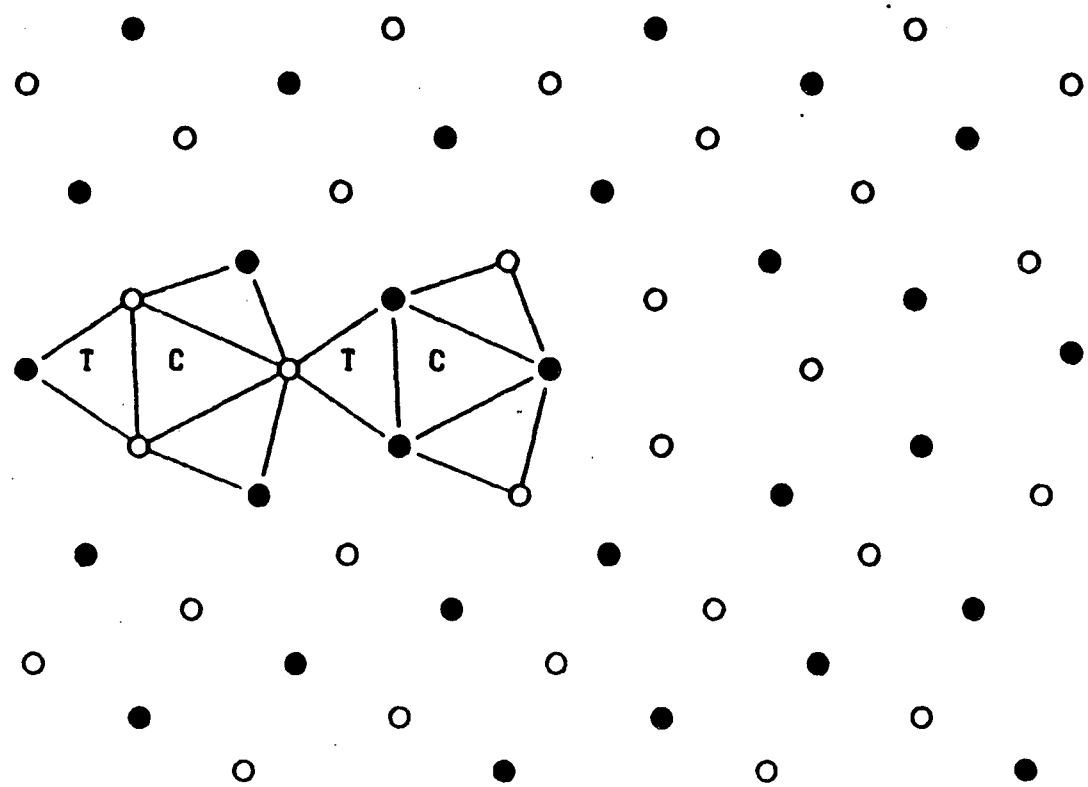

FIGURE 4.2.2 Σ5 STRUCTURAL UNITS

TABLE 4.2.5
GB Translations for a BCC Σ=13 [100]/(015) Tilt Boundary

#	Translations in order of increasing z component (lattice parameter a=1.0)			New atom center at this position is distant to the atom centers indicated † by					
				.866a			a		
1	.5000	.7304	-.4653	2	-	-	1	5	-
2	.4074	.6036	-.4687	1	2	7	-	-	-
3	.5000	.5269	-.4716	1	5	7	-	-	-
4	.5000	.4853	-.5143	1	5	-	2	-	-
5	.4300	.9094	-.5523	6	-	-	2	3	-
6	.2098	.6227	-.5641	1	2	-	7	-	-
7	.3168	.7528	-.5770	2	-	-	1	7	-
8	.5000	.3922	-.5883	1	5	-	7	-	-
9	.5000	.6290	-.5953	-	-	-	1	2	5
10	.3775	.5017	-.5965	1	-	-	2	7	-
11	.4832	.6312	-.6067	-	-	-	1	2	7
12	.5000	.6174	-.6073	-	-	-	1	5	7

† Three atom sets are used in the calculations. If a fourth center is indicated, it is redundant. Only one set is shown; there are other sets of atoms that produce the same translation. These other sets are obvious from the symmetry of the grain boundary.

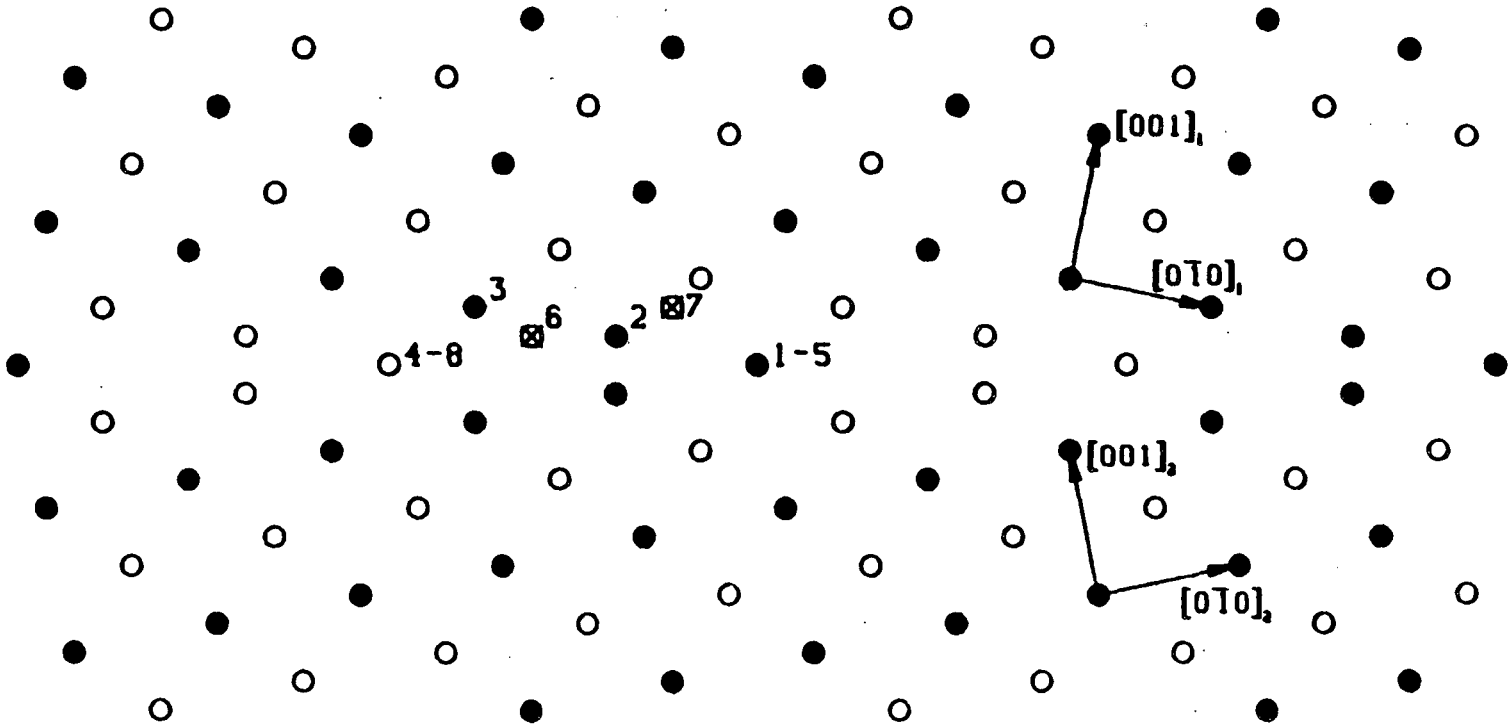

FIGURE 4.23 STRUCTURE OF Σ13 CSL BOUNDARY

T_x=0.500 T_y=0.485 T_z=-0.514

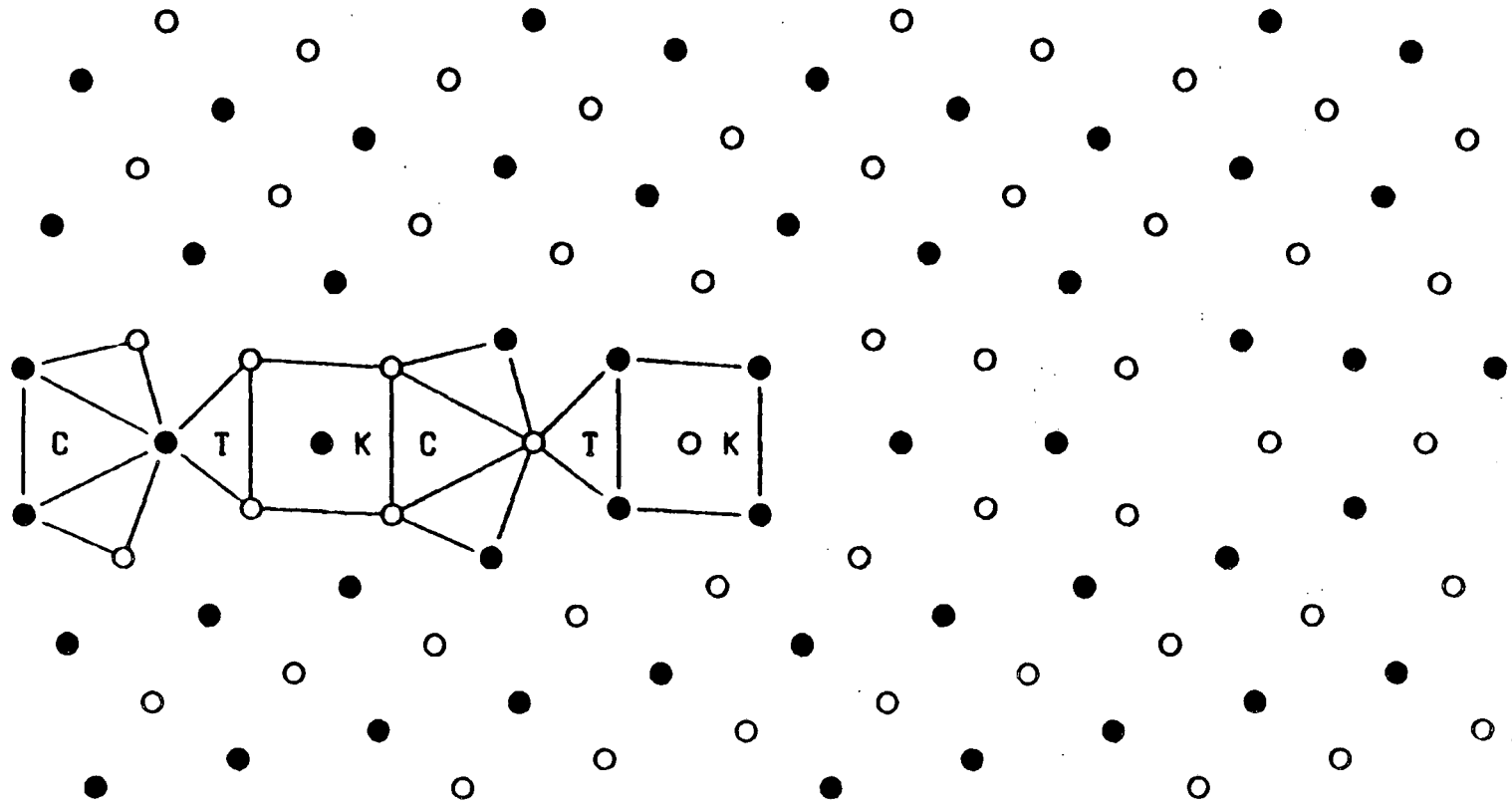

FIGURE4.24 Σ13 STRUCTURAL UNITS

TABLE 4.2.6
GB Translations for a BCC Σ=25 [100]/(017) Tilt Boundary

#	Translations in order of increasing z component (lattice parameter a=1.0)			New atom center at this position is distant to the atom centers indicated † by					
				.866a			a		
1	.4819	.5682	-.4416	1	2	9	-	-	-
2	.5000	.5522	-.4417	1	6	9	-	-	-
3	.0941	1.5840	-.4816	2	3	8	-	-	-
4	.5000	.7035	-.5051	2	-	-	1	6	-
5	.2054	1.7152	-.5157	3	8	-	2	-	-
6	.2440	1.4661	-.5396	2	8	-	3	-	-
7	.5000	.4560	-.5404	1	6	-	2	-	-
8	.3116	.5847	-.5576	1	2	-	9	-	-
9	.4217	.7116	-.5619	2	-	-	1	9	-
10	.5000	.4243	-.5657	1	6	-	9	-	-
11	.4626	.4602	-.5695	1	-	-	2	9	-
12	.3548	1.5966	-.5699	8	-	-	2	3	-
13	.5000	.6501	-.5722	-	-	-	1	6	9
14	.5000	.5950	-.6293	-	-	-	1	2	6
15	.1130	1.6064	-.6379	-	-	-	2	3	8

† Three atom sets are used in the calculations. If a fourth center is indicated, it is redundant. Only one set is shown; there are other sets of atoms that produce the same translation. These other sets are obvious from the symmetry of the grain boundary.

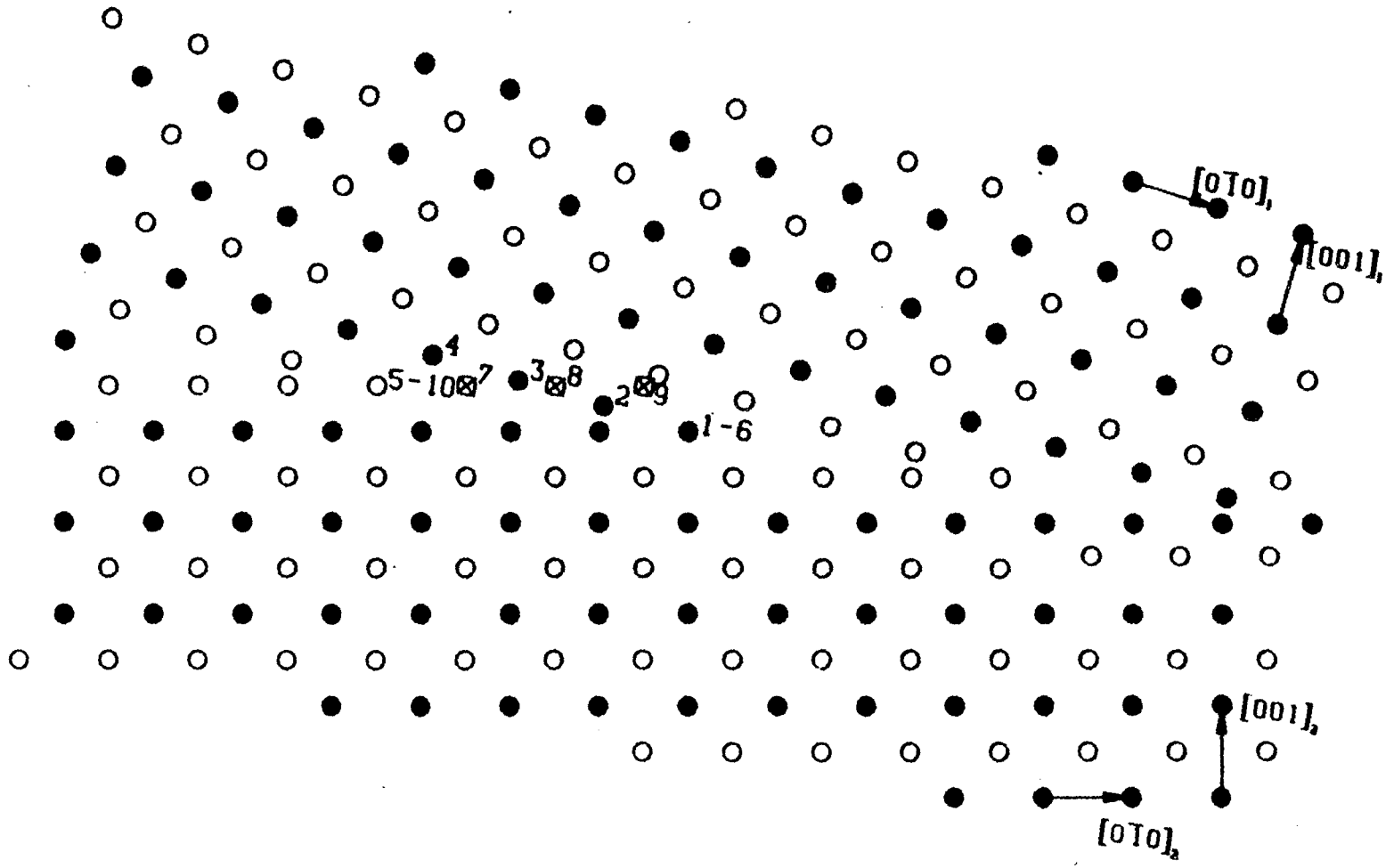

FIGURE 4.25 STRUCTURE OF Σ25 CSL BOUNDARY

T_x=0.500 T_y=0.424 T_z=-0.566

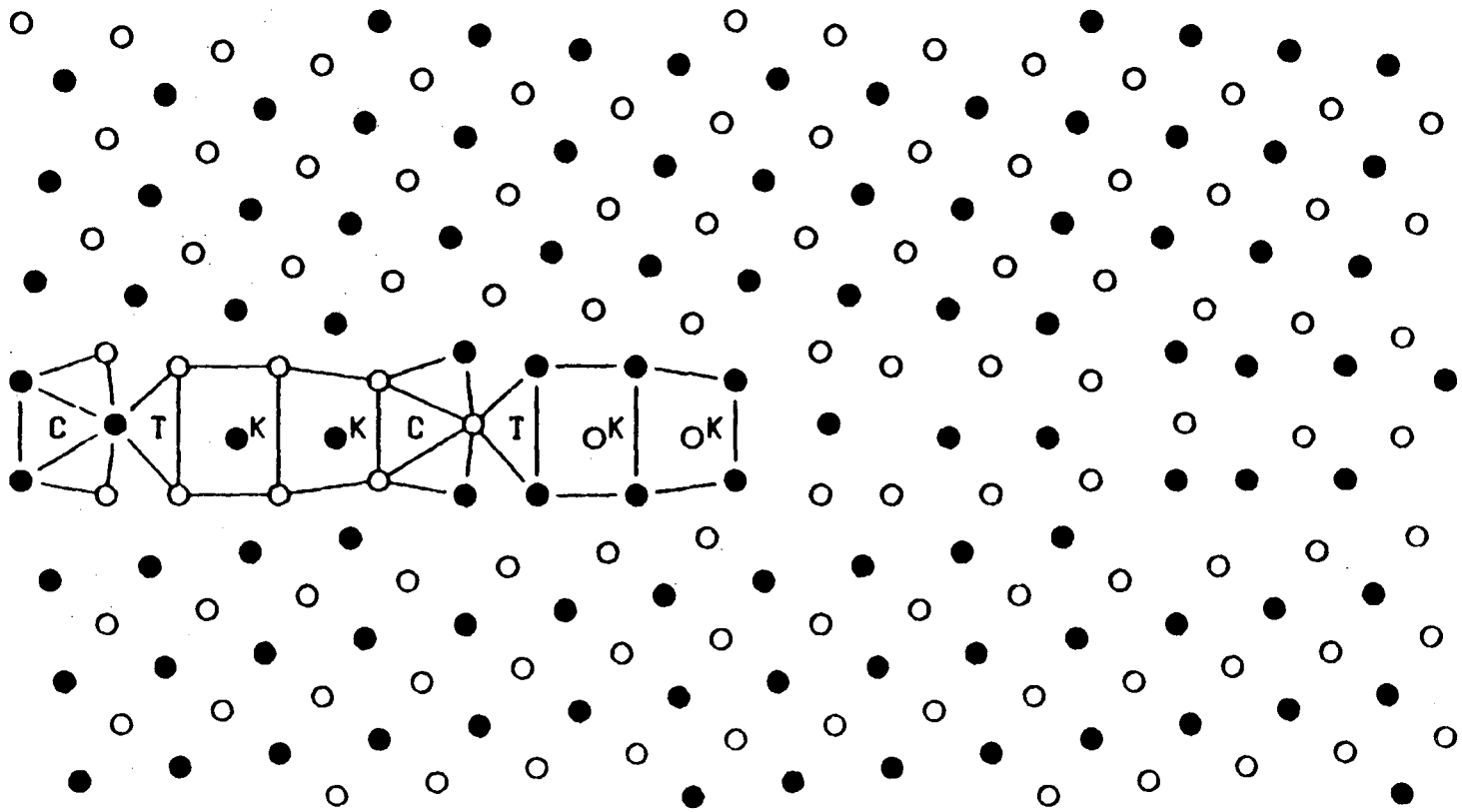

FIGURE 4.2.6 Σ25 STRUCTURAL UNITS

TABLE 4.2.7
GB Translations for a BCC Σ=37 [100]/(016) Tilt Boundary

#	Translations in order of increasing z component (lattice parameter a=1.0)			New atom center at this position is distant to the atom centers indicated † by					
				.866a			a		
1	.4526	.5825	-.4537	1	2	15	-	-	-
2	.5000	.5418	-.4544	1	9	15	-	-	-
3	.5000	.7151	-.4886	2	-	-	1	9	-
4	.2677	1.9452	-.4944	3	13	14	-	-	-
5	.0905	1.7304	-.4977	3	14	-	2	-	-
6	.0895	3.0414	-.4994	5	13	-	4	-	-
				5	-	-	4	12	-
7	.1594	1.8162	-.5079	3	14	-	13	-	-
8	.1127	2.0669	-.5247	3	13	-	14	-	-
9	.5000	.4685	-.5297	1	9	-	2	-	-
10	.1312	1.4828	-.5330	2	14	-	3	-	-
11	.0050	1.9382	-.5365	3	-	-	13	14	-
12	.2709	.6006	-.5621	1	2	-	15	-	-
13	.3800	.7286	-.5699	2	-	-	1	15	-
14	.5000	.4110	-.5754	1	9	-	15	-	-
15	.2342	1.6167	-.5758	14	-	-	2	3	-
16	.3885	1.8047	-.5772	14	-	-	3	13	-
17	.4290	.4771	-.5816	1	-	-	2	15	-
18	.5000	.6366	-.5871	-	-	-	1	9	15
19	.3372	2.0528	-.6092	13	-	-	3	14	-
20	.5000	.6094	-.6153	-	-	-	1	2	9
21	.2223	1.9201	-.6447	-	-	-	3	13	14

† Three atom sets are used in the calculations. If a fourth center is indicated, it is redundant. Only one set is shown; there are other sets of atoms that produce the same translation. These other sets are obvious from the symmetry of the grain boundary.

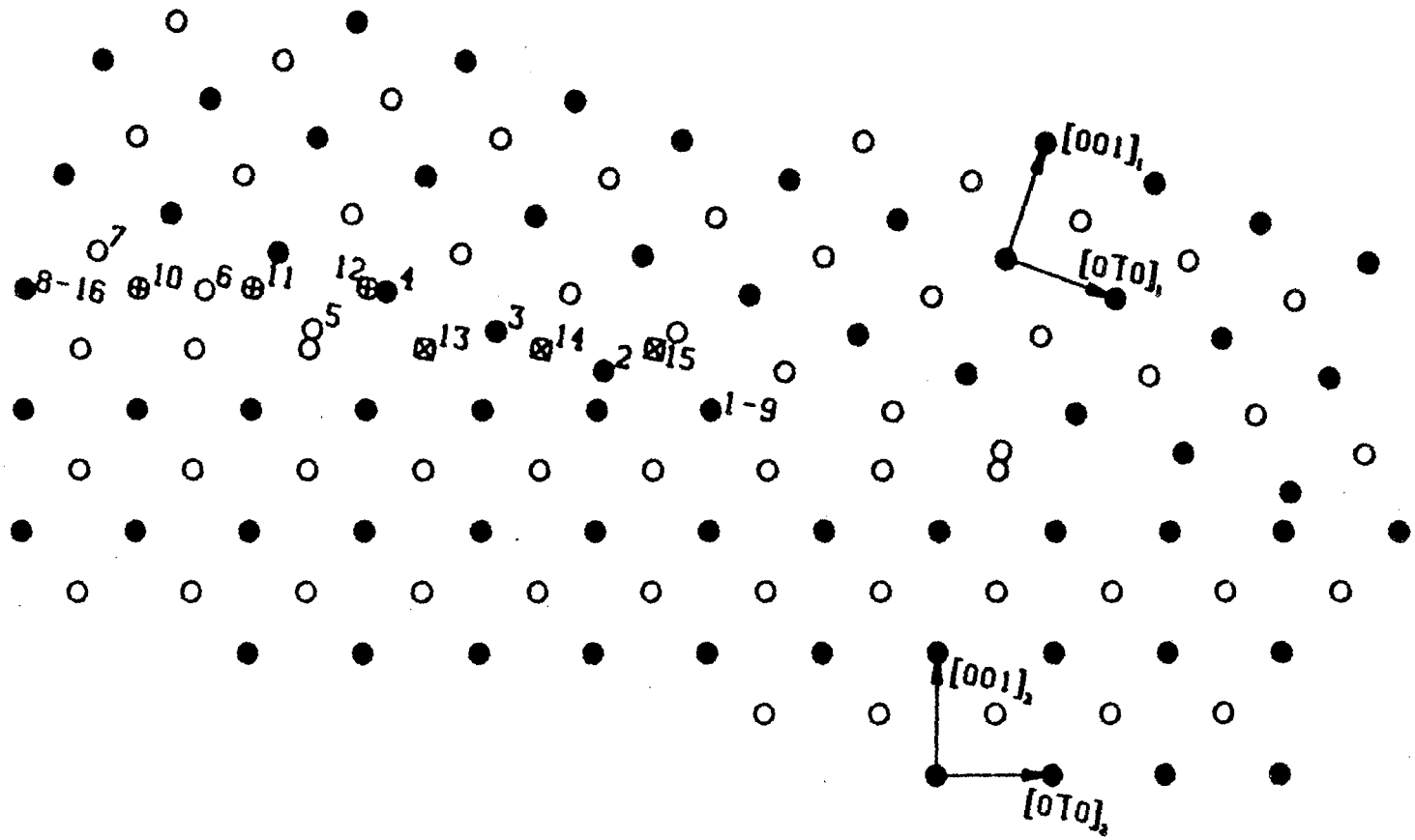

FIGURE 4.2.7 STRUCTURE OF Σ37 CSL BOUNDARY

T_x=0.005 T_y=1.938 T_z=-0.537

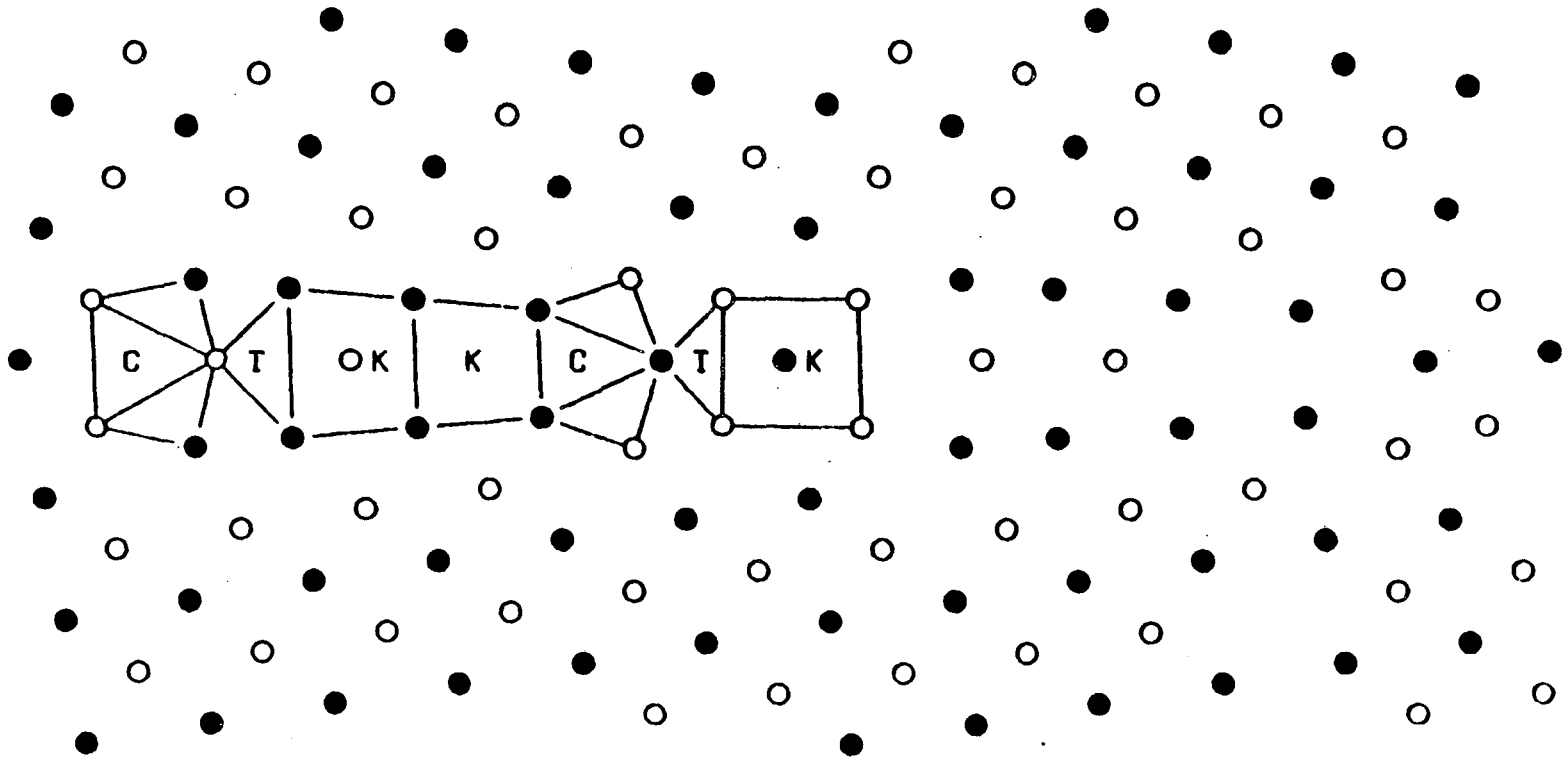

FIGURE4.2.8 Σ37 STRUCTURAL UNITS

TABLE 4.2.8
GB Translations for a BCC Σ=41 [100]/(019) Tilt Boundary

#	Translations in order of increasing z component (lattice parameter a=1.0)			New atom center at this position is distant to the atom centers indicated † by					
				.866a			a		
1	.5000	.5522	-.4417	1	2	7	-	-	-
2	.4763	1.8326	-.4856	4	9	-	3	-	-
3	.2412	1.5642	-.4950	2	3	10	-	-	-
4	.3573	1.6917	-.5104	3	10	-	2	-	-
5	.4517	2.0812	-.5121	3	9	-	4	-	-
6	.3885	1.4414	-.5211	2	10	-	3	-	-
7	.5000	.6874	-.5268	2	-	-	1	7	-
8	.0047	1.5689	-.5371	2	3	-	10	-	-
9	.4727	.6898	-.5484	2	-	-	1	11	-
10	.3618	.5640	-.5486	1	2	-	11	-	-
11	.5000	.6677	-.5516	-	-	-	1	7	11
12	.5000	.4417	-.5522	1	7	-	11	-	-
13	.5000	4389	-.5544	1	7	-	2	-	-
14	.3479	1.9488	-.5713	9	-	-	3	4	-
15	.1312	1.7000	-.5854	3	-	-	2	10	-
16	.1657	1.4508	-.6063	2	-	-	3	10	-
17	.2893	1.5810	-.6456	-	-	-	2	3	10
18	.5000	.5750	-.6476	-	-	-	1	2	7

† Three atom sets are used in the calculations. If a fourth center is indicated, it is redundant. Only one set is shown; there are other sets of atoms that produce the same translation. These other sets are obvious from the symmetry of the grain boundary.

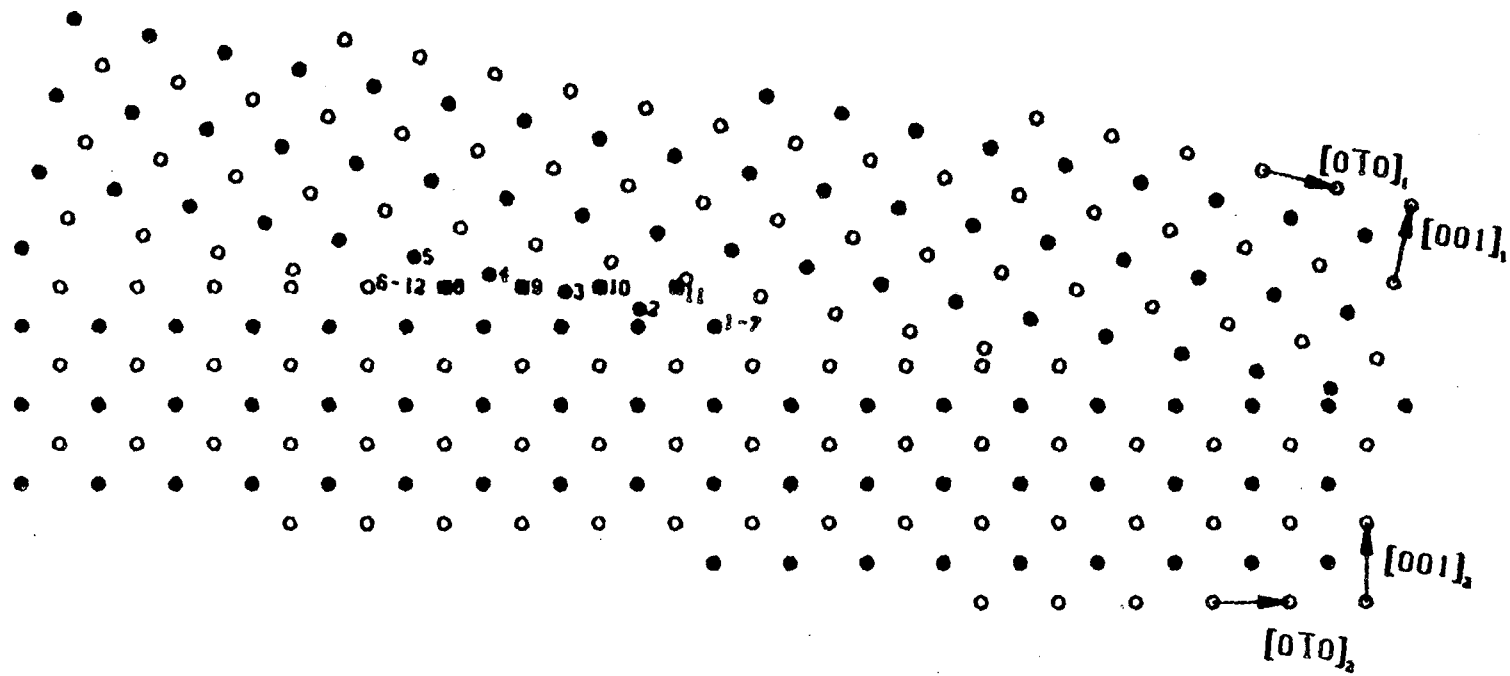

FIGURE 4.2.9 STRUCTURE OF Σ41 CSL BOUNDARY

T_z=0.500 T_r=0.439 T_z=0.554

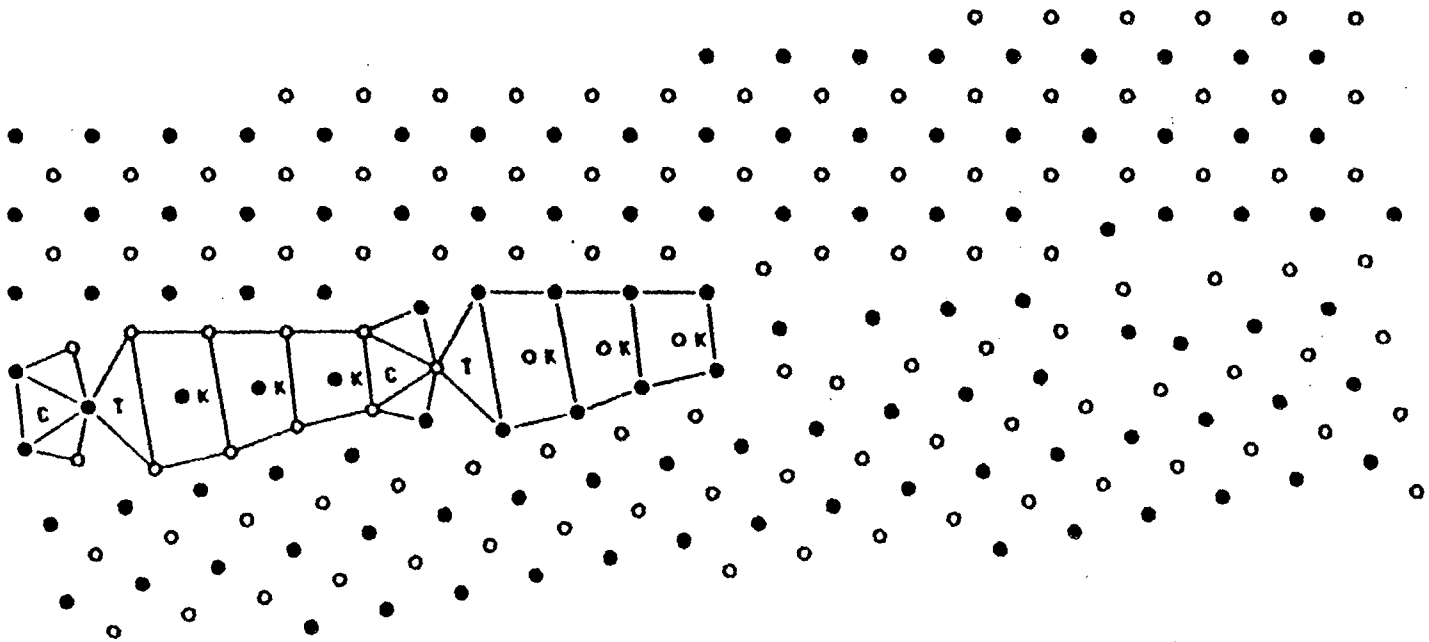

FIGURE . I41 STRUCTURAL UNITS

Fig. 4.2.10

4.3. The Structure of the Twin Boundary

The twin boundary, $\Sigma 3$, which has already been described in chapter 2, plays an important role in the mechanical behavior of BCC materials. Twin boundaries result from a mode of mechanical deformation denominated by twinning or from annealing. Annealing twins occur more frequently in the FCC metals. Twinning occurs under conditions of rapid rate of loading and decrease of temperature. Since twinning is accompanied by very small strains, the important role of twinning is in activating slip systems by putting the twinned grain in a favorable orientation. Twinning occurs on a specific crystallographic plane in a definite direction for each crystal; every atomic plane is involved in this deformation mode. In the case of BCC materials twinning occurs in $\{112\}$ planes in the $<111>$ direction. The usual crystallographic symmetry rule of twinning is that the crystal structure of one grain is the mirror image, about the twinning plane, of the other. The plane of contact between the two grains is called the composition plane. In the case of the BCC structure the composition plane and the twinning plane coincide. The twin structure described above is illustrated in Figure 4.3.1; this structure is usually referred to as the reflection twin, or in CSL notation $\Sigma 3$. Until recently it has been assumed that the twins satisfy the classical orientation relationship and mirror reflection conditions. Recent evidence which is discussed below shows that there might be exceptions to this rule.

The twin boundary was studied in the same manner as previous boundaries. All the possible translations for this boundary are shown in Table 4.3.1. The purpose of studying the possible structures of the twin boundary are twofold. On one hand the period of the twin boundary is very short and thus this boundary is a likely candidate to be a favored boundary in the [110] sequence. In addition, a few atomistic

calculations and TEM studies of the rigid body displacement have been reported, making comparison with experiments possible.

In the reflection twin illustrated in Figure 4.3.1, atom 2 and its mirror image are slightly crowded. A normal displacement equal to the difference between the first nearest neighbor distance and twice the spacing of $\{112\}$ planes would relieve this situation. This expansion is $e_1 = .0495$. The mirror relationship about $(\bar{1}12)$ is preserved. The structural unit for this situation is shown in Figure 4.3.2. The structural unit R is composed of four distorted tetrahedra, or, equivalently, it can be described as an octahedron.

It can be seen from table 4.3.1. that there is a group of translations with $t_y = .433 = 1/4[\bar{1}1\bar{1}]$. The structure for these boundaries is given in Figure 4.3.3 for an equivalent translation. For this equivalent translation there is one atom per period in the lower grain that is at the nearest neighbor distance to atom 2 and at .94 to atoms 1 and 3. This structure is usually referred to as the isosceles twin because in projection the two ligaments mentioned above and the atomic ligament between 1 and 3 form an isosceles triangle. Because the hard-sphere calculations give translations where the interatomic distances are satisfied exactly, a large number of translations appear close to this isosceles translation. However, the atomic arrangements at the isosceles translation can be obtained by simple individual atom relaxations from any of the translations in the cluster. The expansion for this boundary is $e_2 = .038$ which is 75% of e_1. The structural unit I is a distorted octahedron. Both, the R octahedron and the I octahedron, possess eight edges whose length is very close to a first-nearest neighbor distance and four edges whose length is very close to that of the second nearest-neighbor. In both twin structures there are two terminating (001) planes per

structural unit.

The reflection twin and isosceles twin have been studied using molecular statics with the Johnson potential.[9] The results indicate that within the error of the calculations, the energy of both boundaries is equal to 270 $erg\ \ cm^{-2}$. This result can be seen as a consequence of the similarity of the structural units. Since the calculations are carried out at constant volume, the expansion at the boundary was calculated using the extrapolation technique described in section 3.2. The expansion obtained is in good agreement with the hard sphere value for the R twin, and is about half of the hard sphere value for the I twin. The existence of two structures with the same energy, indicate the possibility of dissociation of twinning dislocations. A twinning dislocation has Burgers vector $\frac{1}{6}[\bar{1}1\bar{1}]$ which can dissociate into two isosceles twinning dislocations $\frac{1}{12}[\bar{1}1\bar{1}]$. The displacement of the isosceles dislocation is that which is necessary to transform the reflection twin into an isosceles twin. The structure of the twin in between the partials is then equal to the isosceles twin. To the author's knowledge this disociation has not been observed.

Two groups have investigated the translation at twin boundaries by TEM techniques. The $[\bar{2}2\bar{2}]$ reflection is a common reflection for both grains. Since the electron wave is modified only by displacements that are perpendicular to the reflecting planes, the expansion at the boundary is invisible. However, the displacement along the $[\bar{1}1\bar{1}]$ direction modulates the electron wave. The effect can be evaluated by the phase change in the reflected wave $\alpha = 2\pi \mathbf{g}\cdot\mathbf{R}$ where $\mathbf{g}$ is the reflection vector and $\mathbf{R}$ is the displacement. For the reflection twin $\alpha = 0$ and for the isosceles twin with $\mathbf{R} = \frac{1}{12}[\bar{1}1\bar{1}]$, $\alpha = \pi$. Under these conditions the contrast at the boundary for bright

field and dark field conditions is the same as a stacking fault in an FCC crystal. Using this technique twin boundaries in different BCC materials were studied. Only the in-plane displacement was evaluated in these studies. In an Fe-3.25 wt.%Si alloy the reflection twin was observed,[10] while in Vanadium the displacement observed is a small deviation from the isosceles twin.[11] It appears then that the existence of either structure is strongly material dependent.

TABLE 4.3.1
GB Translations for a BCC Σ=3 [110]/(-112) Tilt Boundary

#	Translations in order of increasing z component (lattice parameter a=1.0)			New atom center at this position is distant to the atom centers indicated † by					
				.866a			a		
1	.6075	.4330	-.4398	1	2	3	-	-	-
2	.7071	.2092	-.4541	1	4	5	-	-	-
3	.7071	.3264	-.4570	2	-	-	1	4	-
4	.0306	.2887	-.4572	2	6	-	1	-	-
5	.6764	.2887	-.4572	1	5	-	3	-	-
6	.7071	.1257	-.4839	1	4	-	2	-	-
7	.0983	.2887	-.5441	1	-	-	2	6	-
8	.6088	.2887	-.5441	3	-	-	5	1	-
9	.7071	.4330	-.5590	-	-	-	3	4	1
10	.2074	.4330	-.5593	1	3	-	5	-	-
11	.4997	.4330	-.5593	1	-	-	2	5	-
12	.7071	.4083	-.5774	-	-	-	1	2	4
13	.6891	.4330	-.5811	-	-	-	1	2	5
14	.1350	.2887	-.5826	6	-	-	1	2	-
15	.5720	.2887	-.5826	1	-	-	3	5	-
16	.7071	.3957	-.5860	-	-	-	1	4	5

† Three atom sets are used in the calculations. If a fourth center is indicated, it is redundant. Only one set is shown; there are other sets of atoms that produce the same translation. These other sets are obvious from the symmetry of the grain boundary.

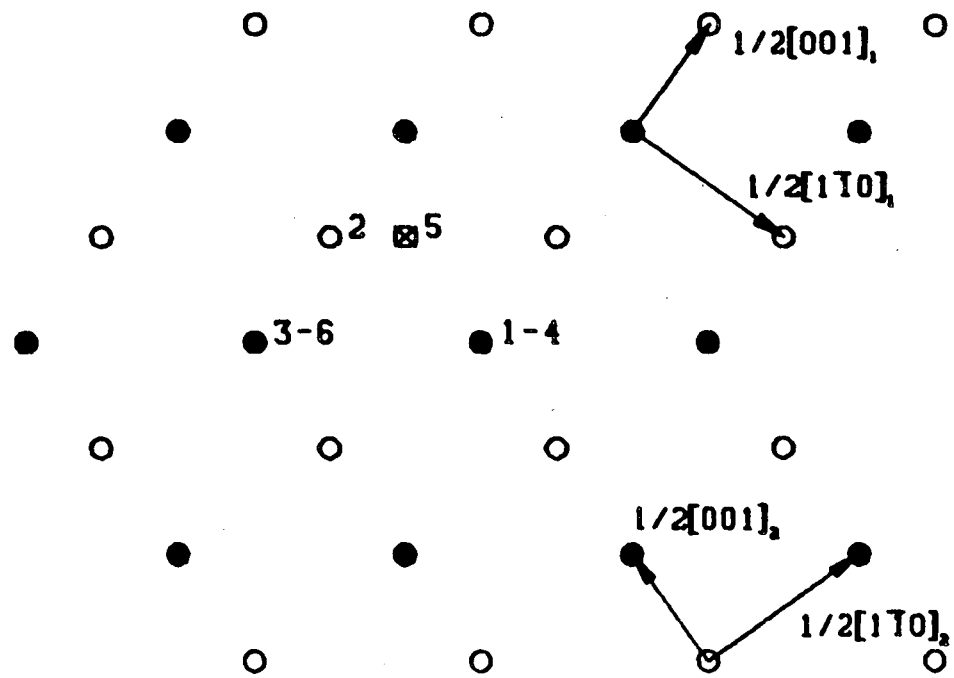

FIGURE 4.3.1 STRUCTURE OF Σ3 CSL BOUNDARY

T_x=0.000 T_y=0.000 T_z= 0.000

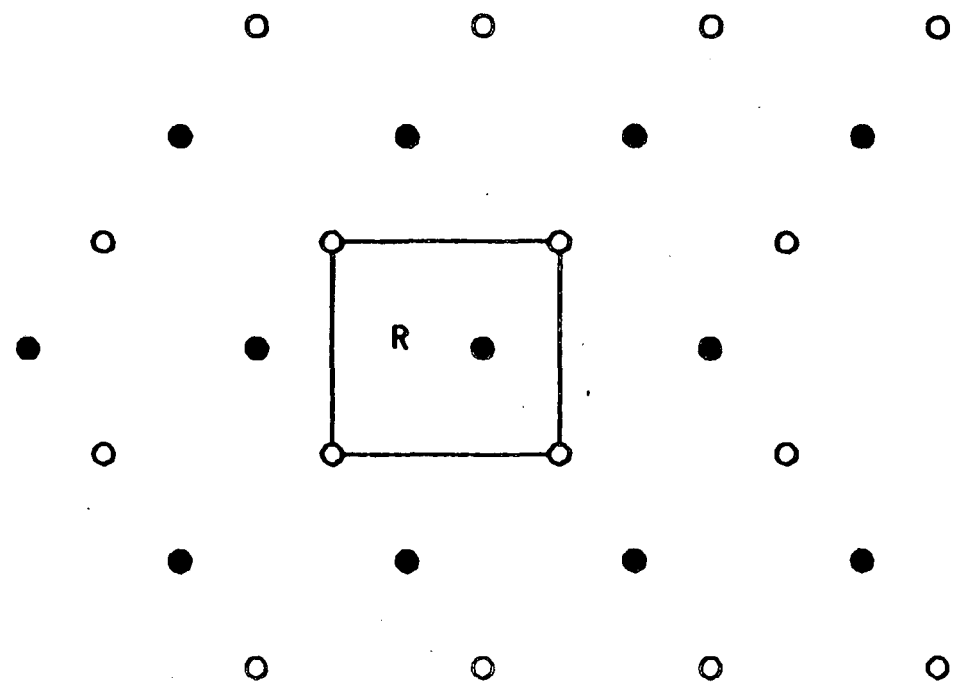

FIGURE 4.3.2Σ3 STRUCTURAL UNITS

T_x=0.707 T_y=0.433 T_z=-0.446

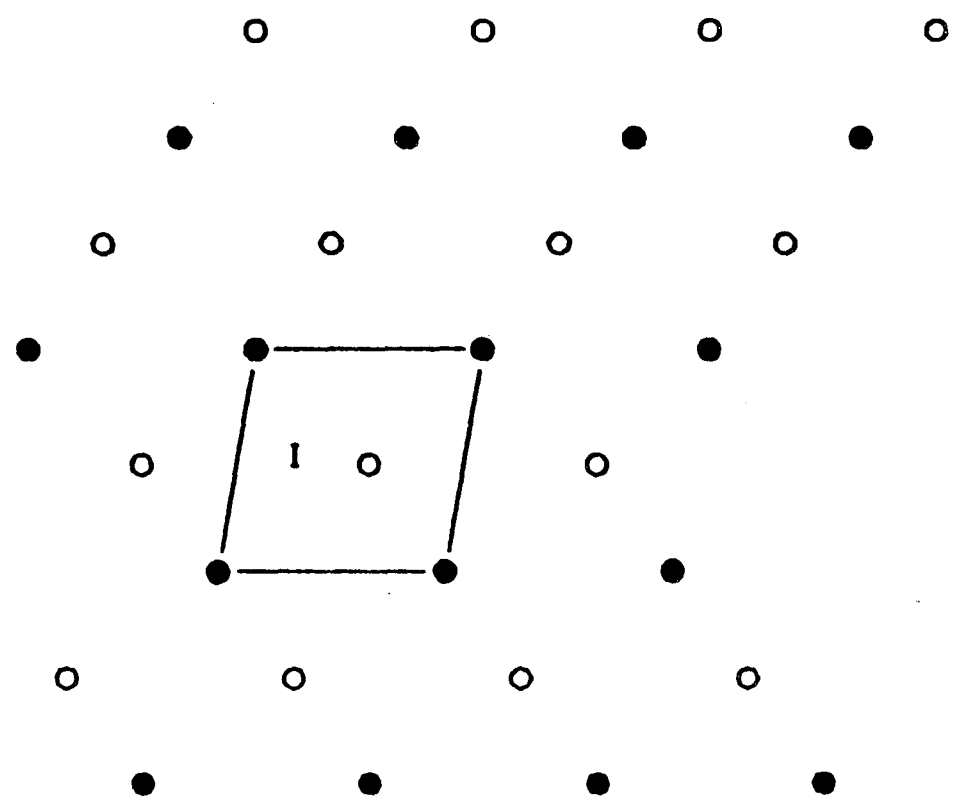

FIGURE4.33 Σ3 STRUCTURAL UNITS

4.4. [110] Symmetrical Tilt Boundaries

The structure of a series of [110] tilt boundaries was studied in the same manner as the previous boundaries. The grain boundary data is included in order of decreasing degree of coincidence. Only the favored structures and 1:1 boundaries were studied. The sequence of structural units for these boundaries is shown in Table 4.4.1.

TABLE 4.4.1
Structural Unit Description of [110] Symmetrical Tilt Boundaries

Σ	*Angle*	*Plane*	*Structural Unit Sequence*
1	0	(001)	L,L,....
19	26.53	$(\bar{1}16)$	PTCT,PTCT,....
9	38.94	$(\bar{1}14)$	PT-PT,PT-PT,....
11	50.48	$(\bar{1}13)$	RPT-RPT,RPT-RPT,....
3	70.53	$(\bar{1}12)$	R,R,....

C = distorted capped triangular prism
L = distorted or perfect crystal structural unit
P = distorted pentagonal bipyramid
R = structural unit of the reflection twin
T = distorted tetrahedron

A striking feature of all of these boundaries is that after individual atom relaxations the colored mirror plane is conserved. The translation in every case is equal to $1/2[00\bar{1}]$ which is also a DSC translation. The z-component is equal to an integral number of planes with the same indices as the boundary plane. Thus, the boundary could be created from the CSL structure simply by layer removal and individual atom relaxations. Because of the conservation of mirror symmetry normal to the boundary, all structural units are oriented so that they have a mirror plane in the boundary plane. The symmetry group of the relaxed boundaries is equal to the holosymmetric color group of the unrelaxed bicrystal.

There are two sequences of boundaries since there are two favored boundaries: $\Sigma 9$ and the twin boundary. The boundary $\Sigma 19$ has a period that decomposes as follows:

$$\frac{1}{2}[\bar{3}3\bar{1}] = \frac{1}{2}[\bar{2}2\bar{1}] + \frac{1}{2}[\bar{1}10] \tag{4.4.1}$$

The first term in the right hand side is half the period of the $\Sigma 9$ boundary since it is a centered boundary. The second term is half the mean period vector. Thus, the structure of $\Sigma 19$ should be equal to one structural unit of the $\Sigma 9$ boundary and one structural unit of perfect crystal. Each pentagonal bipyramid represents two terminating (001) planes. However, as can be seen in Figure 4.4.6, an arrangement of atoms which is equal to one capped trigonal prism and one distorted tetrahedron is observed. The structural arrangement of these two structural units and the tetrahedron that precedes them is equivalent to a distorted unit of perfect crystal. Similarly, the structure of $\Sigma 11$ decomposes as

$$\frac{1}{2}[\bar{3}3\bar{2}] = \frac{1}{2}[\bar{2}2\bar{1}] + \frac{1}{2}[\bar{1}1\bar{1}] \tag{4.4.2}$$

The second term is the period of the twin boundary. Thus, the structure of $\Sigma 11$ is equal to one structural unit of the $\Sigma 9$ boundary and one structural unit of the reflection twin. In this case there are two terminating (001) planes per structural unit. Since these boundaries preserve the color mirror symmetry the structural unit of the reflection twin, rather than the isosceles twin, occurs.

TABLE 4.4.1
GB Translations for a BCC Σ=9 [110]/(-114) Tilt Boundary

#	Translations in order of increasing z component (lattice parameter a=1.0)			New atom center at this position is distant to the atom centers indicated † by					
				.866a			a		
1	.7071	.1667	-.4714	1	2	5	-	-	-
2	.6957	.0069	-.5157	1	-	-	7	2	-
3	.6422	.2536	-.5227	1	2	-	7	-	-
4	.3185	.6015	-.5355	1	2	6	-	-	-
5	.3549	.7443	-.5504	2	6	-	1	-	-
6	.3706	.7420	-.5587	2	-	-	1	8	-
7	.4622	.4610	-.5691	1	2	-	6	-	-
8	.7071	.3949	-.5866	2	-	-	1	5	-
9	.1454	.6169	-.5901	1	6	-	2	-	-
10	.4999	.6208	-.6039	2	-	-	1	6	-
11	.1820	.7278	-.6087	6	-	-	2	1	-
12	.2911	.4854	-.6555	1	-	-	2	6	-
13	.7071	.2357	-.6667	-	-	-	1	2	5
14	.3288	.6457	-.6897	-	-	-	1	2	6

† Three atom sets are used in the calculations. If a fourth center is indicated, it is redundant. Only one set is shown; there are other sets of atoms that produce the same translation. These other sets are obvious from the symmetry of the grain boundary.

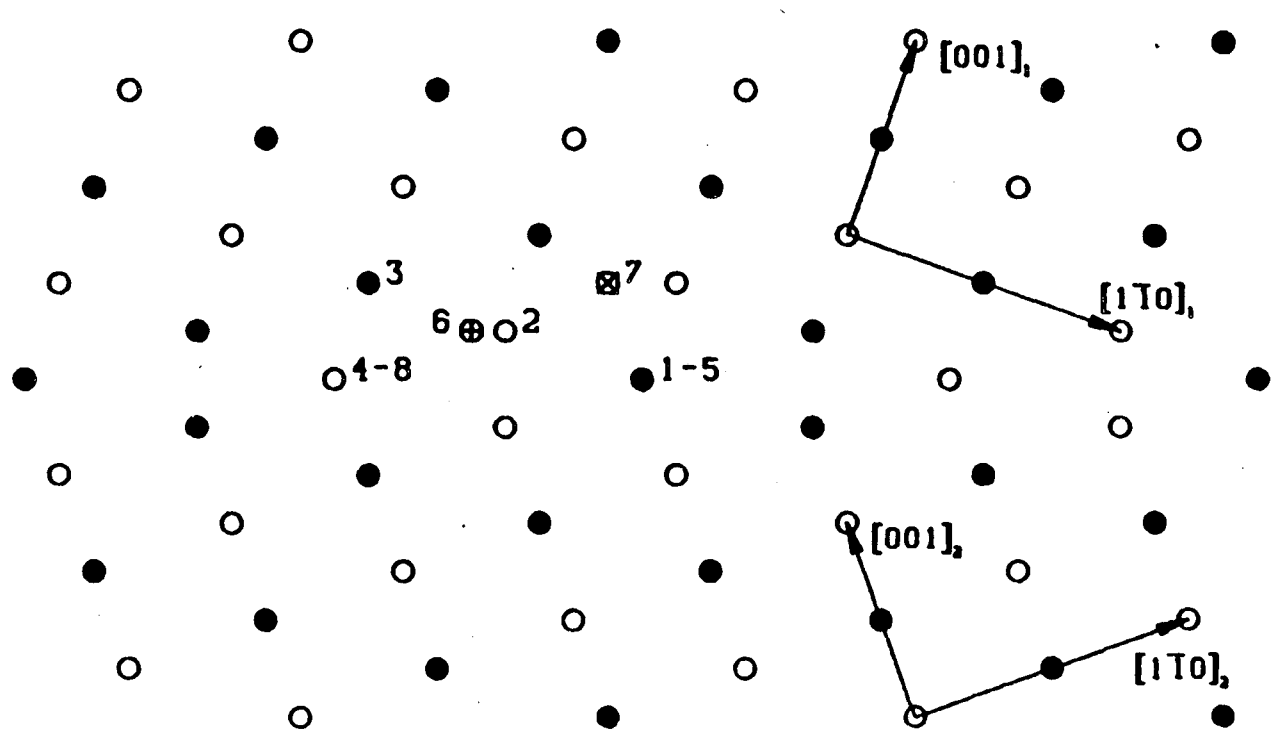

FIGURE 4.4.1 STRUCTURE OF Σ9 CSL BOUNDARY

T_x=0.707 T_y=0.167 T_z=-0.471

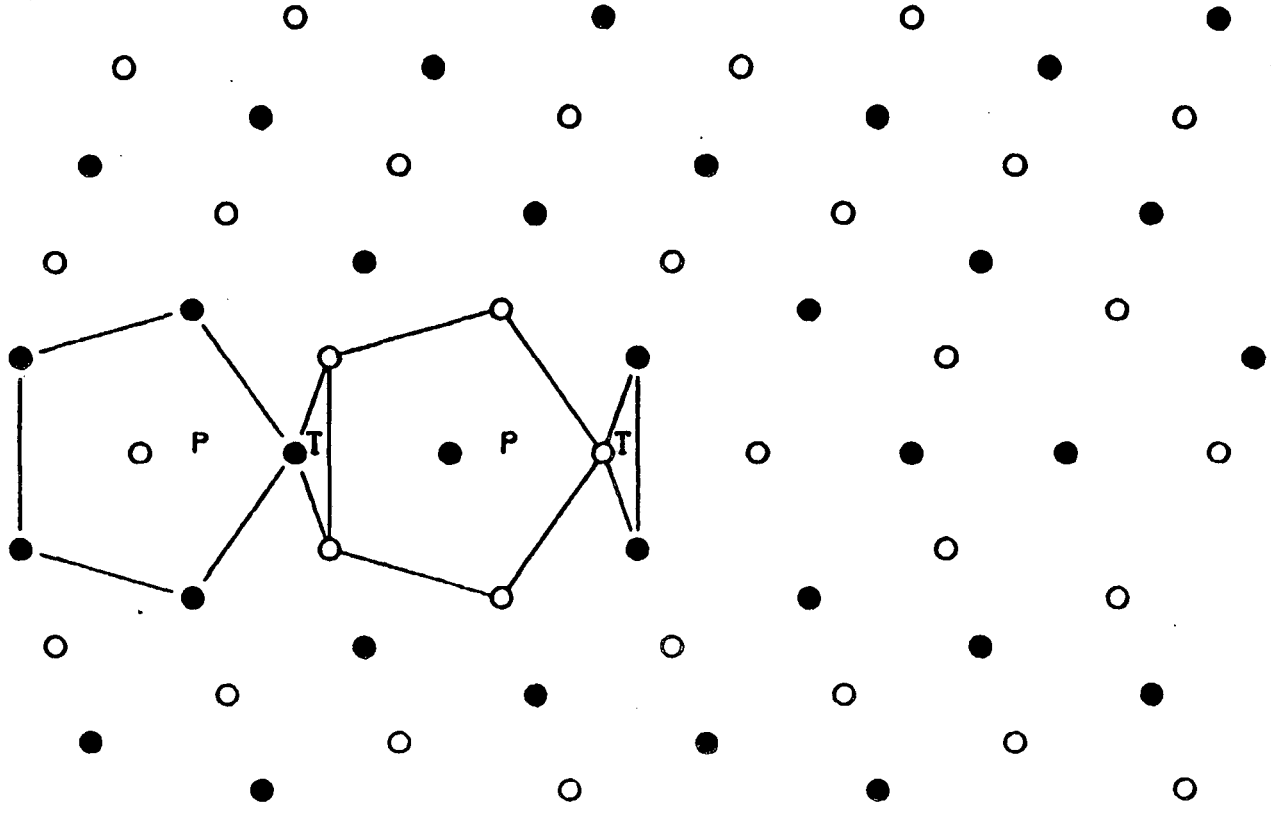

FIGURE4.4.2 Σ9 STRUCTURAL UNITS

TABLE 4.4.2
GB Translations for a BCC Σ=11 [110]/(-113) Tilt Boundary

#	Translations in order of increasing z component (lattice parameter a=1.0)			New atom center at this position is distant to the atom centers indicated † by					
				.866a			a		
1	.7071	.2132	-.4522	1	2	5	-	-	-
2	.7071	.0395	-.4984	1	5	-	2	-	-
3	.5660	.9378	-.4992	2	3	7	-	-	-
4	.5795	.3844	-.5161	2	1	-	7	-	-
5	.4472	.5312	-.5175	1	2	7	-	-	-
6	.5272	.7852	-.5330	7	2	-	3	-	-
7	.4968	.6813	-.5376	2	7	-	1	-	-
8	.7071	.4518	-.5439	2	-	-	5	1	-
9	.7071	.7817	-.5527	2	-	-	7	3	-
10	.6341	.5379	-.5554	2	-	-	7	1	-
11	.6261	1.0667	-.5991	3	-	-	7	2	-
12	.4431	1.0736	-.5598	7	3	-	2	-	-
13	.2936	.5465	-.6042	1	7	-	2	-	-
14	.4070	.9180	-.6109	7	-	-	2	3	-
15	.3442	.6974	-.6286	7	-	-	2	1	-
16	.4334	.4047	-.6312	1	-	-	2	7	-
17	.7071	.3015	-.6396	-	-	-	1	2	5
18	.5907	.9104	-.6541	-	-	-	2	3	7
19	.4881	.5583	-.6708	-	-	-	1	2	7

† Three atom sets are used in the calculations. If a fourth center is indicated, it is redundant. Only one set is shown; there are other sets of atoms that produce the same translation. These other sets are obvious from the symmetry of the grain boundary.

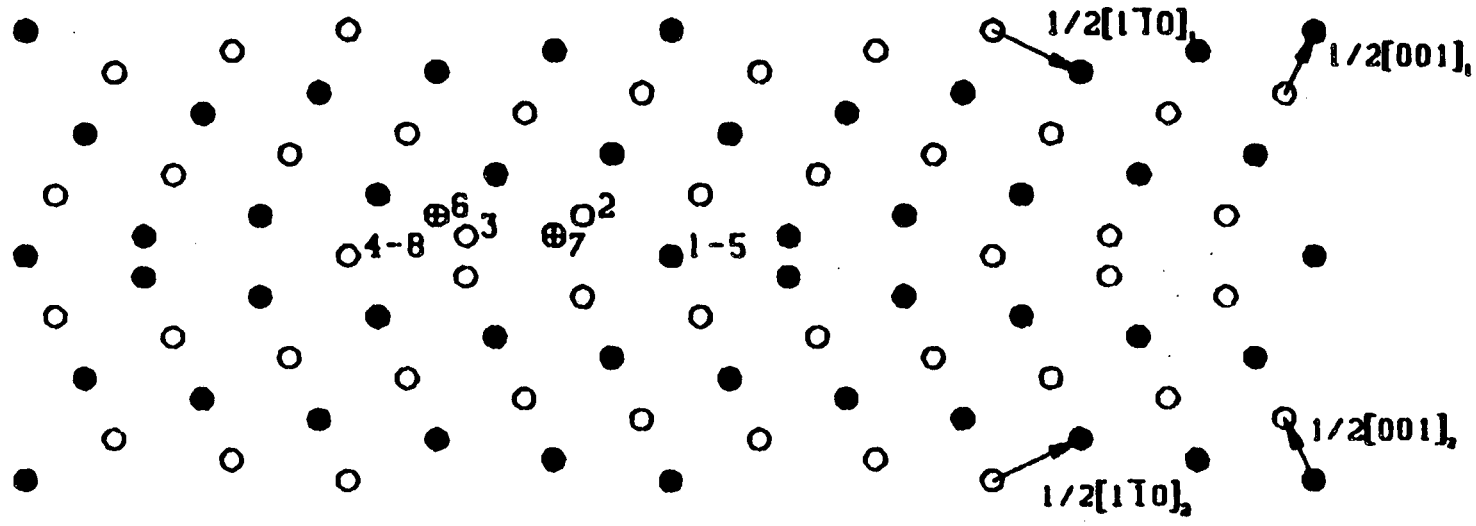

FIGURE 4.4.3 STRUCTURE OF Σ11 CSL BOUNDARY

T_x-0.707 T_y-0.213 T_z--0.452

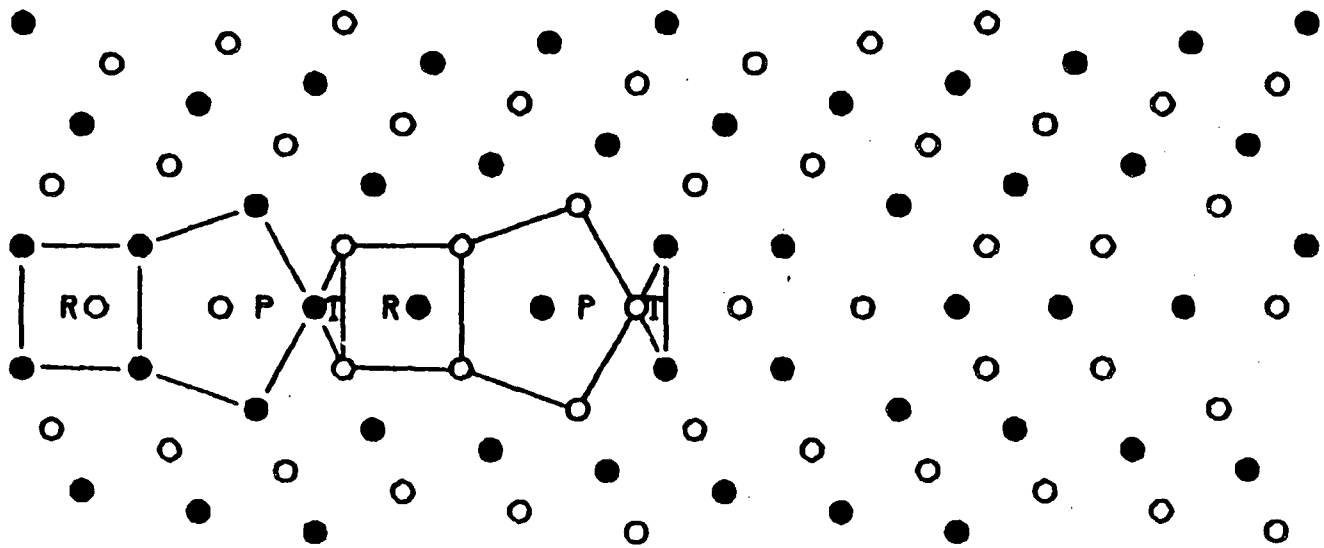

FIGURE 4.4.4 Σ11 STRUCTURAL UNITS

TABLE 4.4.3
GB Translations for a BCC Σ=19 [110]/(-116) Tilt Boundary

#	Translations in order of increasing z component (lattice parameter a=1.0)			New atom center at this position is distant to the atom centers indicated † by					
				.866a			a		
1	.4576	1.0897	-.4537	2	3	7	-	-	-
2	.7071	.1147	-.4866	1	2	16	-	-	-
3	.0643	1.0897	-.4902	3	8	-	2	-	-
4				3	-	-	7	2	-
5	.2125	.9341	-.5048	2	8	-	7	-	-
6	.4946	.9341	-.5048	3	7	-	2	-	-
7	.6826	.1460	-.5126	1	2	-	9	-	-
8	.2000	.8718	-.5154	2	8	-	3	-	-
9	.1681	.6753	-.5155	1	2	8	-	-	-
10	.1927	.8326	-.5194	2	8	-	1	-	-
11	.2561	.9341	-.5350	7	-	-	8	2	-
12	.4510	.9341	-.5350	2	-	-	3	7	-
13	.0179	.8718	-.5388	8	-	-	2	3	-
14	.0124	.8412	-.5401	8	-	-	1	2	-
15	.3081	1.0897	-.5434	7	2	-	3	-	-
16	.4057	1.0897	-.5434	2	-	-	3	8	-
17	.3068	.5511	-.5934	1	2	-	8	-	-
18	.3388	.9341	-.5956	7	-	-	3	2	-
19	.3684	.9341	-.5956	2	-	-	8	7	-
20	.4937	1.0897	-.6094	-	-	-	2	3	7
21	.3284	.7160	-.6161	2	-	-	1	8	-
22	.7071	.3291	-.6258	2	-	-	1	6	-
23	.1223	.5701	-.6403	1	-	-	2	8	-
24	.1439	.7348	-.6628	-	-	-	1	2	8
25	.7071	.1622	-.6883	-	-	-	1	2	6

† Three atom sets are used in the calculations. If a fourth center is indicated, it is redundant. Only one set is shown; there are other sets of atoms that produce the same translation. These other sets are obvious from the symmetry of the grain boundary.

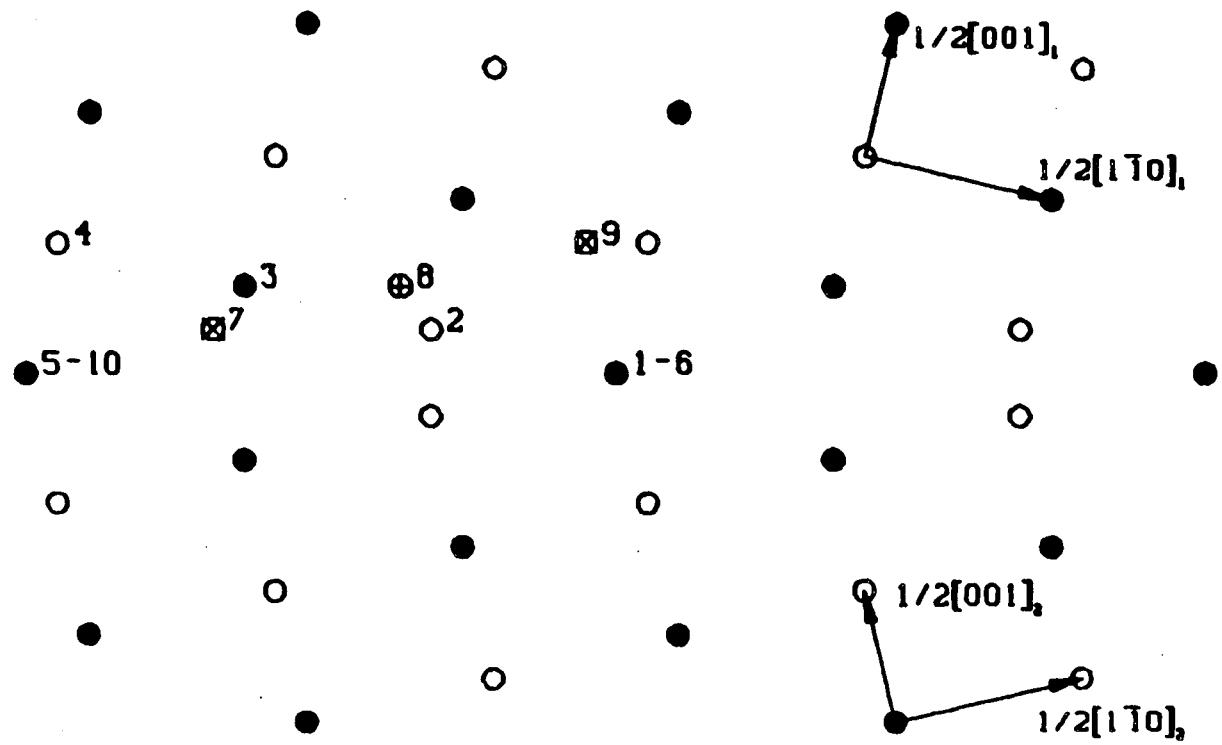

FIGURE 4.45 STRUCTURE OF Σ19 CSL BOUNDARY

T_x=0.707 T_y=0.115 T_z=-0.487

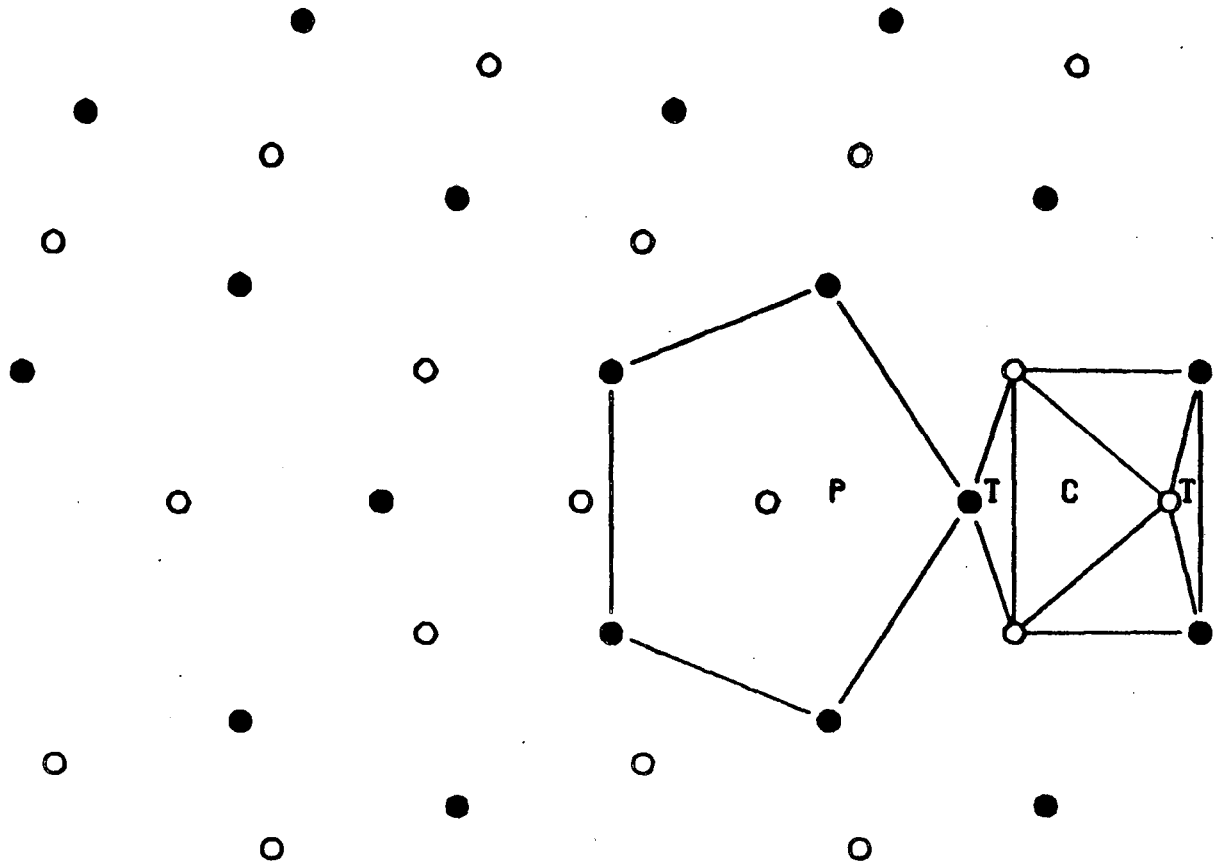

FIGURE 4.4.6 Σ19 STRUCTURAL UNITS

4.5. References

[1] H. B. Aaron and G. F. Bolling, in *Grain Boundary Structure and Properties* , G. A. Chadwick and D. A. Smith (eds.), Academic Press, New York, 1976.

[2] A. P. Sutton, R. W. Balluffi, and V. Vitek, *Scripta Met.* **15** , 989 (1981).

[3] A. P. Sutton and V. Vitek, *Phil. Trans. R. Soc. Lond.* **A309** , 1 (1983).

[4] A. P. Sutton and V. Vitek, *Phil. Trans. R. Soc. Lond.* **A309** , 37 (1983).

[5] A. P. Sutton, *Phil. Mag.* **A46** 171 (1982).

[6] R. W. Balluffi and P. D. Bristowe, *Surf. Sci.* **144** , 28 (1984).

[7] A. Brokman and R. W. Balluffi, *Acta Met.* **29** , 1703 (1981).

[8] V. Vitek, D. A. Smith and R. C. Pond, *Phil.Mag.* **41** , 649 (1980).

[9] P. D. Bristowe and A. G. Crocker, *Phil. Mag.* **31** , 503 (1975).

[10] K. Marukawa, *Phil.Mag.* **36** , 1375 (1977).

[11] G. Nouet and P. Delavignette, *J. Microsc. Spectrosc. Electron.* **3** , 389 (1978).

5. EXPERIMENTAL

5.1. Bicrystal Growth and TEM Specimen Preparation

In order to study the structure of the symmetrical tilt boundaries, bicrystals of controlled structure were prepared. The purpose of growing bicrystals is to prepare specimens with geometrical parameters equal to those of the boundaries studied in Chapter 4. Growing a bicrystal with such a control on the geometry of the boundary requires special equipment and techniques that are described in this section. These bicrystals were grown by Prof. Y. T. Chou using his experimental facilities at Lehigh University. The author is indebted to Prof. Chou for providing these specimens. Different techniques for growing bicrystals have been reviewed by Pande and Chou.[1] All the bicrystals used in this investigation were [100] tilt bicrystals.

It is desirable to obtain bicrystals from the melt so that the grain boundary is representative of grain boundaries in polycrystalline materials. The technique for growing niobium bicrystals has been described by Pande, *et.al.* .[2] The bicrystal seed is prepared as follows. A single crystal cylindrical seed is grown with the [011] axis along the axis of the cylinder. The single crystal was grown at the rate of 10 cm/hr in a vertical floating-zone electron beam melting unit. The top of the single crystal was cut along a center line for one inch in a spark cutter. The two separate parts of the crystal were bent apart to the desired angle so that the two ends are symmetrical with respect to the center line. This Y-shaped seed is illustrated in Figure 5.1.1 together with the rest of the charges used. The seed is chemically etched in order to remove deformed surface layers and annealed to reduce dislocation densities. The bicrystals were grown at the same speed than the seeds.

There are two ways in which [100] tilt boundaries can be grown using this procedure. The crystallography for each type of seed is discussed next. If the axis of the single crystal is [011] the cut plane is $[01\bar{1}]$ as illustrated in Figure 5.1.2. The top part of the figure illustrates the seed itself while the lower part shows the stereographic projection in the direction of the crystal axis. The stereographic projection is divided into two parts corresponding to the two sections of the seed. Notice that all the poles are symmetrical with respect to the cut plane so the chances for symmetrical grow of the boundary plane are maximized. The natural direction of grow for BCC materials is [110]. For small-angle boundaries this direction is very near the bicrystal grow axis. However, for large-angle boundaries any asymmetry in the experimental set-up would disturb the orientation of the boundary plane much more than for small-angle boundaries. Another way to grow [100] tilt boundaries is illustrated in Figure 3.5.3. In this case the single crystal axis is [001] and the cut plane is [010]. The stereographic projection indicates that the poles are symmetrical. However {011} type planes are inclined at large angles to the growth axis which tends to reduce the success in growing this type of bicrystals. All the bicrystals used in these experiments were grown using a [011] single crystal seed.

Using the procedure described above, two symmetrical tilt bicrystals were grown, one with the misorientation of $\Sigma 17$ and another with the misorientation of $\Sigma 13$. Several techniques were tried to prepare thin specimens suitable for high-resolution transmission electron microscopy (HRTEM). The author has not been successful in preparing a HRTEM specimen, and the reasons are detailed below. The bicrystals were oriented using a back-Laue camera. Specimens were cut using a diamond blade. Each cut consumed 200μ of material and gave a slab of 400μ thickness. If a cut was

spaced at less than 600μ the slab curled under the cutting action. The slabs were then thinned down to 150μ. Discs, 3 mm in diameter, were punched from the slabs. The specimens were further thinned to 100μ and a shallow dimple was introduced at the center of the specimen over the grain boundary. The dimple ensures that a hole forms first at the center of the specimen right over the boundary. Several solutions were tried for electropolishing the niobium bicrystals. All of the solutions for polishing niobium have very small polishing plateaus. The solution that gave the best results was a 500 ml CH_3OH – 25 ml H_2SO_4 – 5 ml HF solution. The solution temperature was -30 °C, the voltage was 50V and the current 25 mA. All of the solutions that result in good polishing of a niobium thin film contain small amount of HF which attacks the grain boundary preferentially. Several alternatives were tried to slow this reaction, such as adding glycerol to the solution or raising the solution temperature to 0 °C or room temperature. Unfortunately, the problem remained. Alternative solutions that do not contain HF did not give a good polish of the niobium specimens. An entirely different method of specimen preparation that was tried is ion milling. The gun voltage (4kV) and incidence angle (12°) were kept as low as possible to avoid damage in the specimen. Ion milling gives good specimens with no preferential attack of the boundaries, but the thin areas suitable for HRTEM are amorphous due to the damage to the specimen.

The specimen preparation problems are surmountable. However, due to lack of results at present on the niobium bicrystals, the experimental evidence discussed in section 3 corresponds to a $\Sigma 41$ boundary in molybdenum. These results are included in this thesis by courtesy of Dr. R. Gronsky. The molybdenum bicrystals were prepared by electron beam welding of two single crystals.[3]

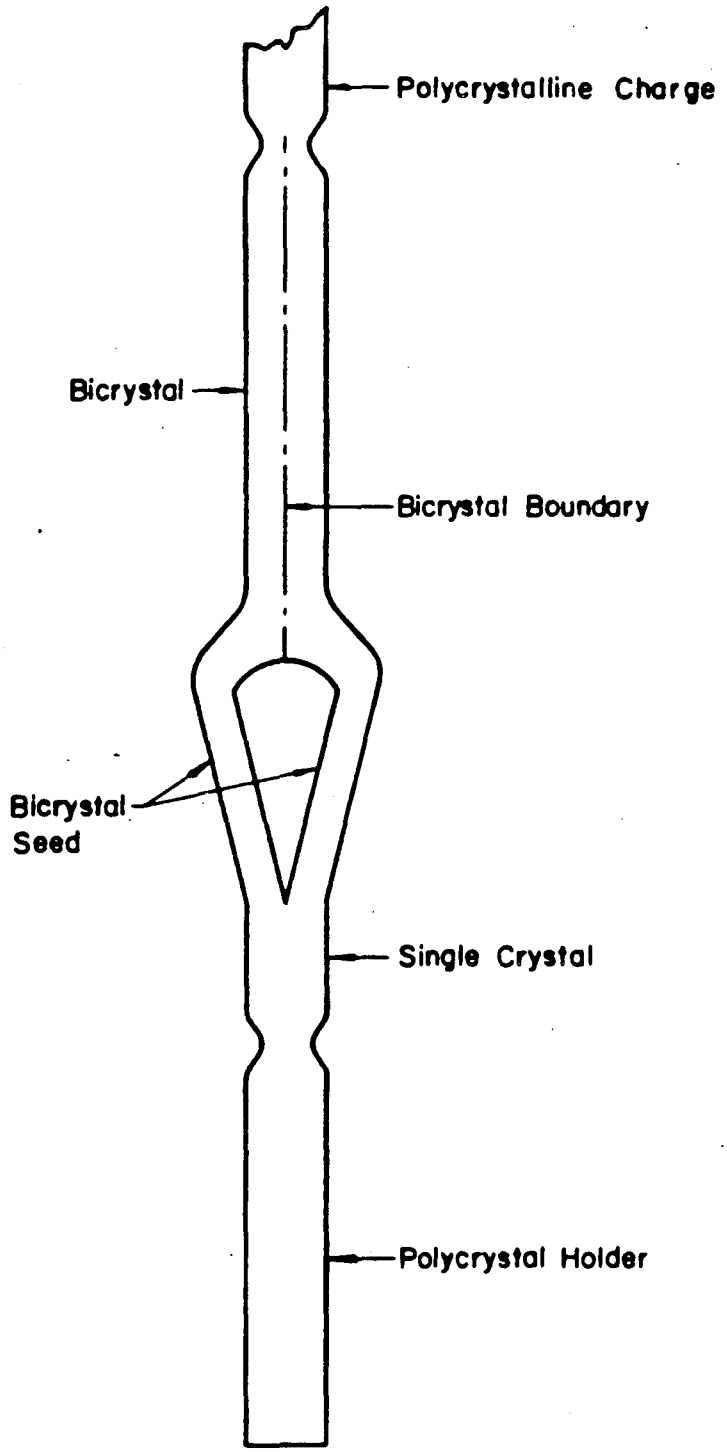

XBL 852-1296

Fig. 5.1.1 Arrangement for growing seeded bicrystals (from C. S. Pande and Y. T. Chou, *op.cit.*).

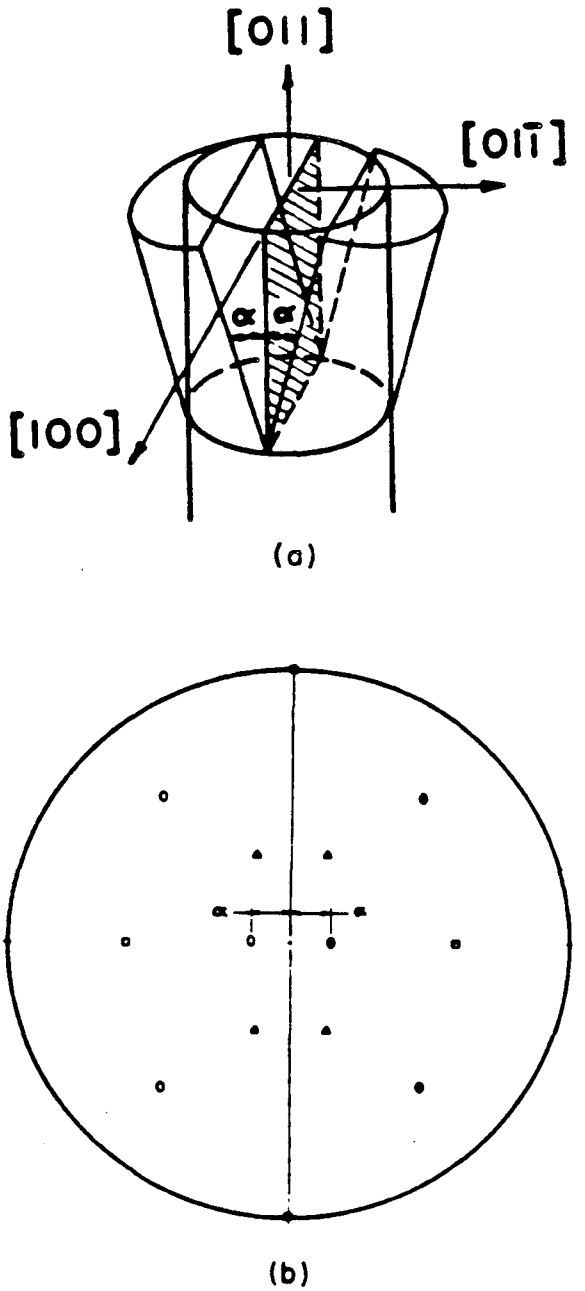

Fig. 5.1.2 A [011] type seed with cut plane (01$\bar{1}$) (from C. S. Pande and Y. T. Chou, *op.cit.*).

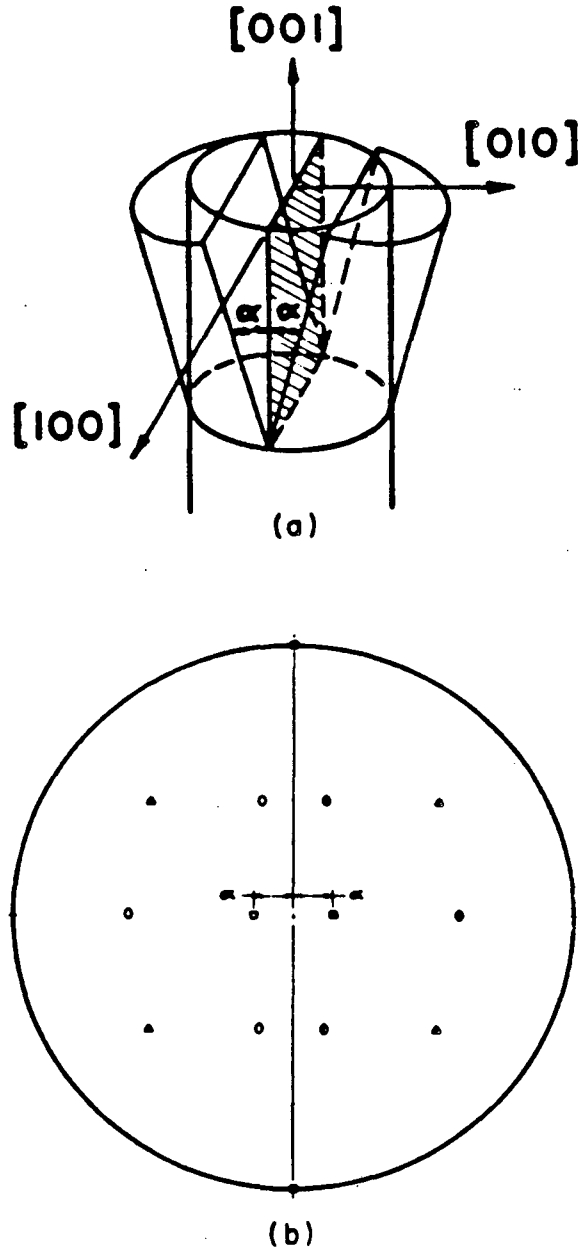

XBL 852-1298

Fig. 5.1.3 A [001] type seed with cut plane (010) (from C. S. Pande and Y. T. Chou, *op. cit.*).

5.2. Image Simulation

Tilt boundaries are ideal for high-resolution transmission electron microscopy (HRTEM) experiments since it is possible to look at the projected atomic structure along low index crystallographic directions with planar spacings within the resolution limits of the microscope. In the simplest approximation the image can be interpreted as a mapping of the projected structure. However, for most experimental conditions the interpretation of the images requires matching them to computed image simulations. To obtain a computed image a set of atom positions is used as input to a program that simulates the operation of the electron microscope under the same conditions than the experimental images obtained. If the computed and experimental images match, the atom positions have been determined. Thus, extensive image simulation is always necessary to study defects in HRTEM. In this investigation image simulation has been used to establish the best experimental conditions for imaging the core of symmetric tilt boundaries. The techniques of HRTEM[4] and image simulation[5] have been reviewed recently. A detailed account of either technique is beyond the scope of this text and thus only those aspects that are particular to the experimental study of tilt boundaries are discussed here.

In order to simulate the structure of the sequence of [100] tilt boundaries, $\Sigma 5$ was chosen as the most suitable boundary. This boundary contains the two structural units that are different from a perfect or distorted BCC unit cell. In addition it is the shortest period boundary, and thus the number of atoms in the computational unit cell is smaller. Since the image simulation programs rely on Fourier techniques periodicity of the computational unit cell is always implied. Figure 5.2.1 shows the projected crystal potential of the computational cell for the $\Sigma 5$ boundary. Notice that there are

two grain boundaries one at 1/4 and the other at 3/4 of the height of the cell. If the cell is constructed with one grain boundary at the center, then additional boundaries occur at the edges of the computational cell. These additional boundaries produce scattering events which are not representative of the actual physical situation. In order to separate scattering from the two boundaries, a large number of atomic layers separate the two defects. In addition, when the periodically continued cell is invariant under a translation through a distance equal to the spacing between the two defects, it can be shown that the scattered waves from each defect are equal.[6]

The simulation cell described above is necessary for multi-slice simulation in reciprocal space. Recently, multi-slice real space image simulation methods have been developed that offer some advantage in the simulation of planar defects such as grain boundaries and interphase interfaces.[7] For the real-space method the computational cell can be divided into patches where the dynamical calculations are performed separately for a thickness increment of one slice. Special considerations are only required at the edge where information on neighboring patches is required. Thus, using the real-space method the computational cell contains only one boundary in the middle of the cell. Simulated images for the $\Sigma 5$ boundary were also obtained by the real-space method. There are no differences between the real space and the reciprocal space multi-slice images. Since more extensive image simulations were carried out using the reciprocal space multi-slice method, these results are discussed next.

The main objective of the image simulation calculations was to establish the best experimental conditions for observing the structure of these boundaries in the Atomic Resolution Microscope (ARM), here at the Lawrence Berkeley Laboratory. The characteristics, operation and recent results on the ARM have been discussed by

Gronsky.[8] ,[9] The resolution of the microscope increases with the operating voltage. One of the objectives of image simulation is to establish the best resolution with the minimum amount of radiation damage. Experimentally it has been determined that for niobium and molybdenum knok-on radiation damage occurs at 800 kV.[10] Figure 5.2.2 illustrates the simulated images for typical ARM parameters at 800 kV and for various thicknesses. Similarly, Figure 5.2.3 illustrates the simulated images at 1000 kV. For 800 kV a direct interpretation of bright spots as atom positions is possible for thicknesses between 100 and 200 . At 1000 kV the image goes through a contrast reversal in between these thicknesses. At 800 kV the structural features of the capped trigonal prism and tetrahedra are visible. Using 1000 kV does not seem to give improvements in the image information while it increases the potential for radiation damage. In addition it has been experimentally determined that the filament brightness is maximized at 800 kV, facilitating experimental work. Thus, it was determined that 800 kV is the optimal voltage for observing the structure of these boundaries.

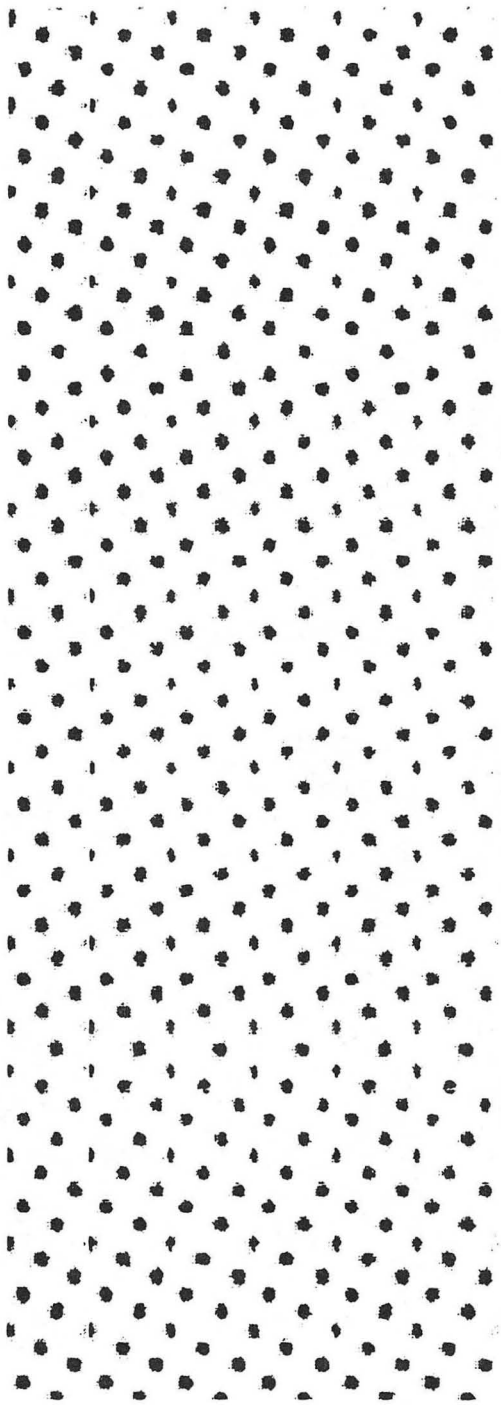

XBL 844-1564

Fig. 5.2.1 Projected potential of the image-simulation computational cell for the $\Sigma 5$ boundary.

SIGMA 5 GRAIN BOUNDARY

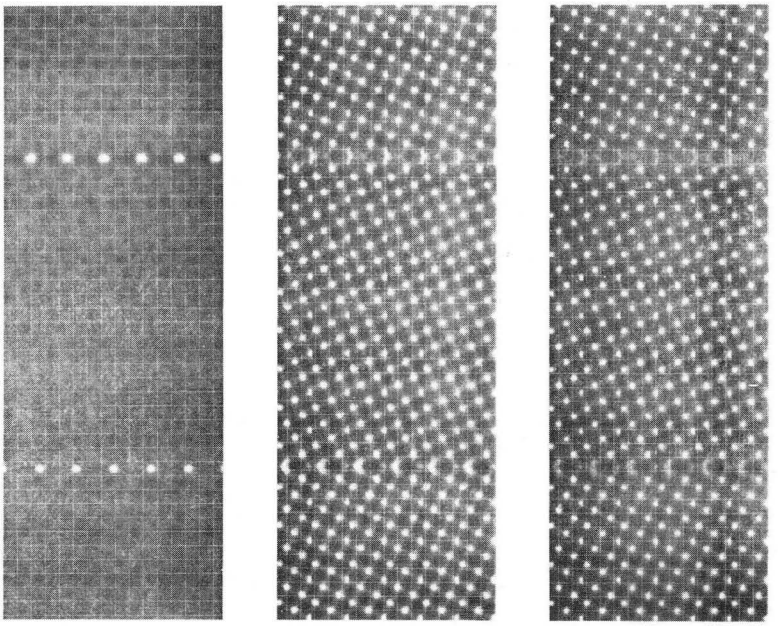

IMAGE AT THICKNESS = 49.6 A

IMAGE AT THICKNESS = 99.2 A

IMAGE AT THICKNESS = 148.8 A

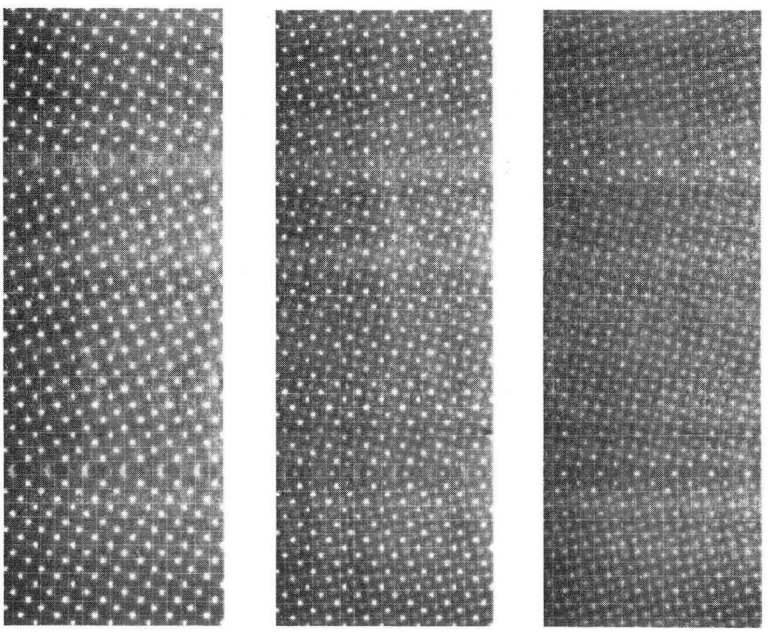

IMAGE AT THICKNESS = 198.4 A

IMAGE AT THICKNESS = 248.0 A

IMAGE AT THICKNESS = 297.6 A

OBJ.LENS-DEFOCUS = -605. A
APERTURE-RADIUS = 80 A-1
SPHER.ABR.CONST = 2.80 MM
DIV.ANGLE(HALF-) = 60 MRAD
DELTA = +00.0 A

CALCULATIONAL METHOD -- FFT --
THE APERTURE CONTAINS -IT BEAMS
FR. CF. OF THE POTENTIAL OUT TO 3.0 A-1

ACCELER.VOLTAGE = 800.0 KVOLT

XBB 844-3035

Figure 5.2.2

SIGMA 5 GRAIN BOUNDARY

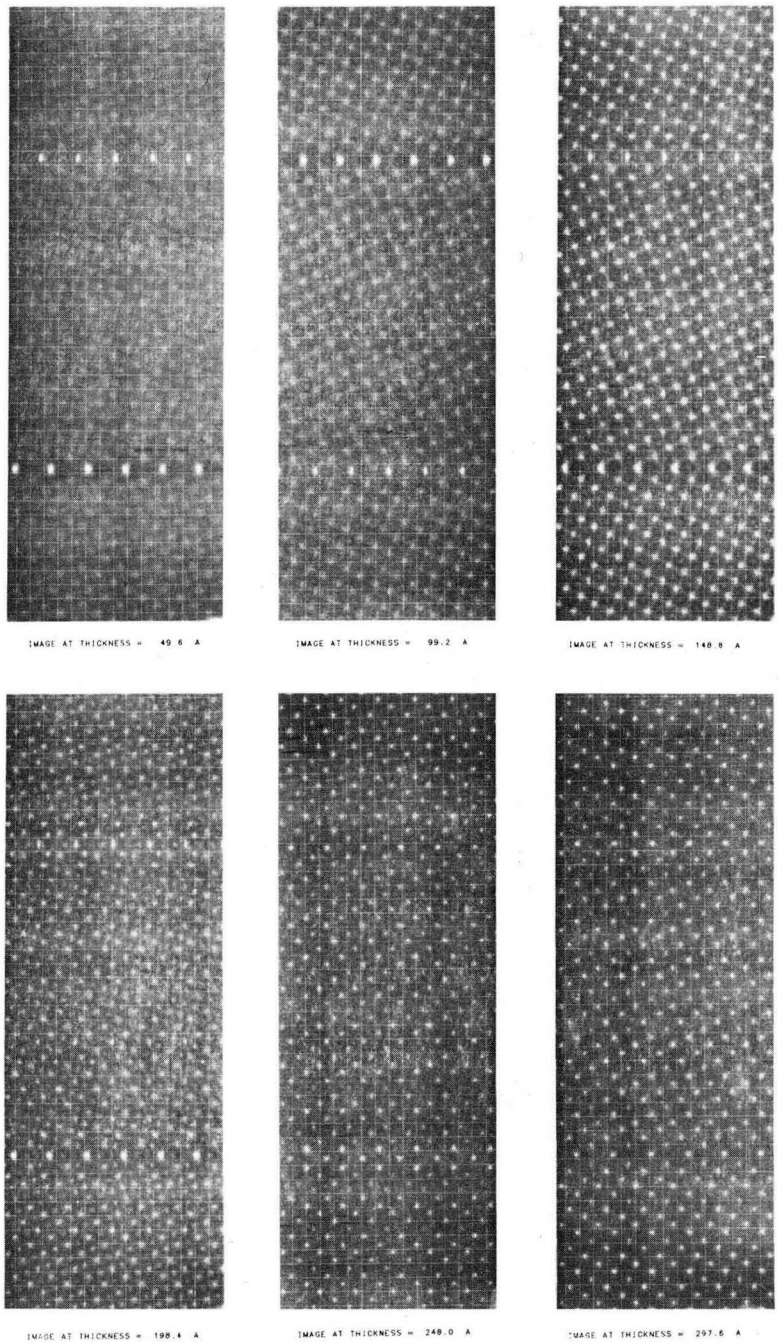

OBJ LENS-DEFOCUS = -605. A
APERTURE-RADIUS = .80 A-1
SPHER.ABR.CONST. = 2.80 MM
DIV ANGLE(HALF-) = .80 MRAD
DELTA = 100.0 A

CALCULATIONAL METHOD -- FFT --
THE APERTURE CONTAINS -1F BEAMS
FR. OF. OF THE POTENTIAL OUT TO 3.0 A-1

ACCELER VOLTAGE = 1000.0 KVOLT

XBB 844-3036

Figure 5.2.3

5.3. The Structure of Σ41 in Molybdenum

The results of an investigation on the structure of a Σ41 boundary in Molybdenum are included in this section by courtesy of Dr. R. Gronsky. Since these results have also been published and discussed in detail,[11] only those aspects that are related to a discussion of the hard-sphere calculations in section 4.2 are presented here. The tilt angle was measured directly by the deviation of the (110) planes across the boundary; it was shown to be equal to $(12\pm1)^\circ$. The misorientation for a Σ41 boundary is 12.68°. In addition, a small twist component of 1.3° was measure by the displacement of the first Laue circle. The structure of this asymmetrical boundary is shown in Figure 5.3.1 together with a projection of the O-lattice along the tilt axis. An enlarged view of one period of the asymmetrical boundary is shown in Figure 5.3.2; the core of the grain boundary dislocations are indicated by a Burgers circuit that also defines the Burgers vector. Each period of the asymmetrical boundary contains four pure edge [100] dislocations and one 1/2 [111] mixed dislocation. However, these two dislocations are sometimes mixed in different proportions indicating that the exact misorientation of the boundary gives an asymmetric boundary of very long period. The mixed dislocation always has the the extra half-plane in the same crystal making the boundary asymmetric as shown in Fig. 5.3.1. The screw component can not be determined from the HRTEM images because only a projection of the crystal structure is obtained. The presence of mixed dislocations leads to a faceted structure of the boundary. Macroscopically the boundary would appear to be asymmetrical. The region of interest for our observations is the region between two [100] dislocations which is equivalent to half the period of a symmetrical tilt Σ41 boundary. This region shows that there are three distorted BCC unit cells separating each dislocation core.

In order to determine the atom position at the dislocation core an extensive program of image simulation is in progress. Since the period of the boundary is relatively large much computational time can be saved by using the real-space methodology that became available over the last year. However, these results already show excellent agreement with the structure of $\Sigma 41$ discussed in section 4.2.

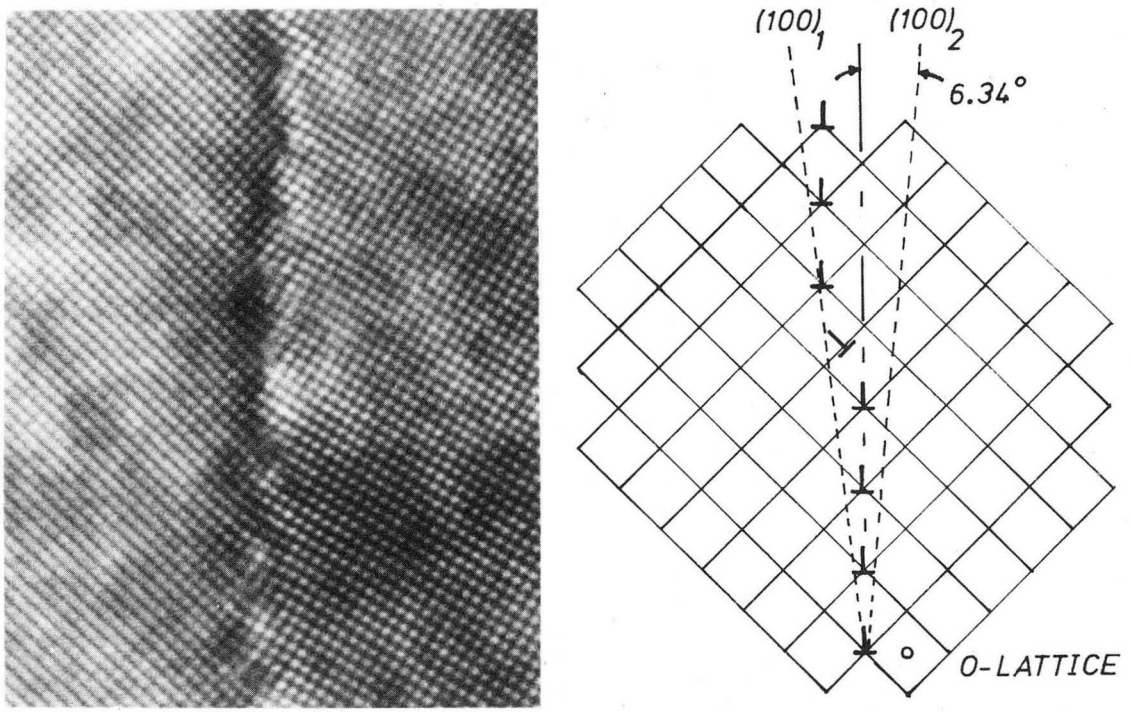

XBB 813-2724

Fig. 5.3.1 HRTEM image of a near Σ41 grain boundary. Projection of the O-lattice along the tilt axis; the grain boundary dislocations are indicated. This figure is included by courtesy of Dr. R. Gronsky.

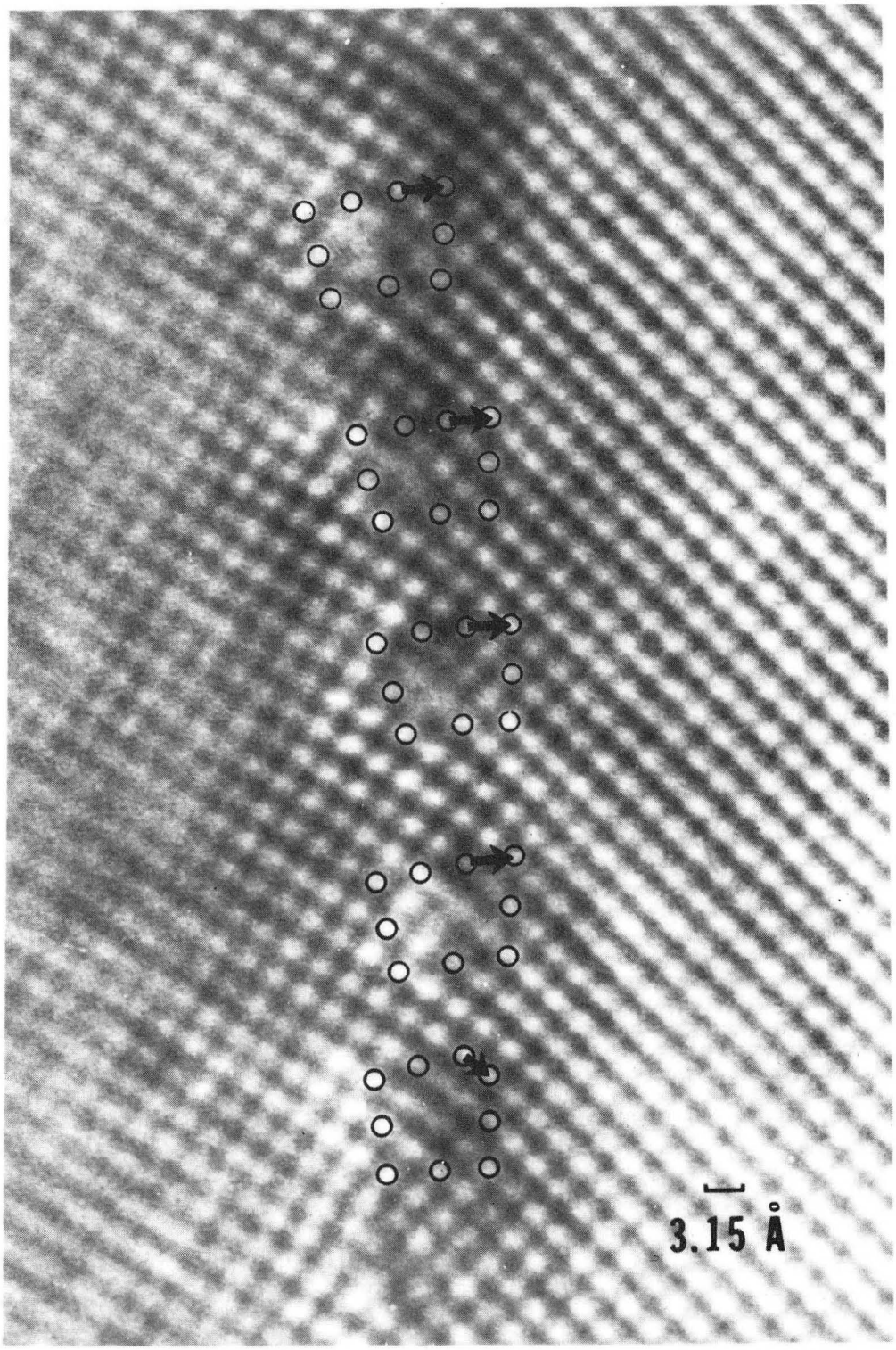

XBB 819-9056

Fig. 5.3.2 HRTEM image of a near Σ41 boundary in Molybdenum. The Burgers vector of the grain boundary dislocations is indicated. This micrograph is included by courtesy of Dr. R. Gronsky.

5.4. References

[20] C. S. Pande and Y. T. Chou, *Treatise on Materials Science and Technology* **8** , H. Herman (ed.), Academic Press, New York, 1975, p.43.

[21] C. S. Pande, L. S. Lin, S. R. Butler and Y. T. Chou, *J. Crytal Growth* **19** ,209 (1973).

[22] A. Kobylanski and C. Goux, *Comptes-Rendus Acad. Sci. Paris* **C272** ,1937 (1971).

[23] R. Gronsky, in *Treatise on Materials Science and Technology: Experimental Techniques* **19B** ,H. Herman (ed.), Academic Press, New York, 1983, p.325.

[24] M. A. O'Keefe, *SEM 1984* , SEM Inc., Chicago, 1984, p.209.

[25] A. R. Wilson and A. E. C. Spargo, *Phil. Mag.* **46A** , 435 (1982).

[26] R. Kilaas and R. Gronsky, *Ultramicroscopy* **11** , 289 (1983).

[27] W. Coene, D. Van Dyck, G. Van Tendeloo and J. Van Landuyt, *Phil. Mag.* **52A,** 127 (1985).

[28] R. Gronsky, in *38th. Annual Proc. Electron Micros. Soc. Amer.* , G.W. Bailey (ed.), 2 (1980).

[29] R. Gronsky, in *Electron Microscopy of Materials* , W. Krakow, D. A. Smith and L. W. Hobbs (eds.), North-Holland, New York, 1984, p.1.

[30] E. P. Butler and K. F. Hale, *Dynamic Experiments in the Electron Microscope* , in *Practical Methods in Electron Micros.* **9** , A. M. Glauert (ed.), North-Holland, New York, 1981.

[31] J. M. Penisson, R. Gronsky, and J. B. Brosse, *Scripta Met.* **16** , 1239 (1982).

6. CONCLUSIONS

6.1. Comments on Grain Boundary Structure

The method that was developed in chapters 3 and 4 is generalized here for the cases of asymmetric and mixed boundaries. The usefulness and limitations of the structural unit model are discussed. In the next section the implications of this model on grain boundary phenomena will be studied. First, the results in section 4 will be compared with the experimental data in section 1.3. Finally, some predictions on physical processes at grain boundaries are discussed.

The computational method presented in section 3.4 can be adapted to study more general boundaries. The procedure of using the first layer of atoms of crystal 2 on the other side of the boundary is particular to the study of symmetrical boundaries. However, the method of obtaining an interlocking group of atoms that retains the proper interatomic distances is general in nature. Thus, in order to study genral boundaries, a method to keep track of the atom positions before and after a displacement is required. By picking groups of three atoms, two in one grain and the third in the other grain, it is possible to modify the equations in section 3.4 to obtain a possible rigid body translation. For example, a new sphere is equidistant from two atoms in grain 1 while an atom position in grain 2, after the translation, retains first or second-nearest neighbor distance with one of the two atoms in grain 1. The individual atom relaxations will be more difficult to visualize than those at symmetrical tilt boundaries with an AB stacking. In the authors view for a number of translations, the structure of the boundaries will consist of octahedra and tetrahedra in no particular order. Thus, for those translations the boundary would resemble a thin amorphous layer. However, for some translations, the structure of the mixed boundaries will

decompose in structural units of tilt and twist boundaries. These structures would have a higher coordination, and thus they will be more likely to occurr according to the criteria developed in section 3.1. In order to distinguish between structures with high coordination the excess volume can be used as a criteria; in this case atom counting inside a volume that goes well into the perfect crystal will be required. Thus, mixtures of capped trigonal prisms and pentagonal bipyramids that are typical of tilt boundaries together with capped Archimedian antiprisms that are typical of twist boundaries, would be observed. It is commonly observed that asymmetrical tilt boundaries facet onto crystallographic planes with low indices. A study of the structural units of asymmetrical tilt boundaries would show that microfaceting occurs by the existence of structural units of the nearest symmetrical boundary and structural units corresponding to other tilt boundaries with crystallographic boundary planes. This type of micro-faceting is shown, for example, by the near $\Sigma 41$ boundary discussed in section 5.3.

The structural unit model has solved a number of the problems that were raised in section 3.1. A polyhedra description of boundary structure is continuous with changes in boundary parameters. Thus, the polyhedra description has an advantage over dislocation models in that the reference states are determined. The only problem remaining has been pointed out in section 4.2. Since the structural units are distorted from their canonical hole form, for some of these units it is hard to decide the favored structure. Consider, for example, the [110] tilt boundaries. A capped trigonal prism if twisted becomes a pentagonal bipyramid. Thus instead of the given sequence of favored boundaries as $\Sigma 1$ - $\Sigma 9$ - $\Sigma 3$ it could be argued that this sequence is simply $\Sigma 1$ - $\Sigma 3$. However, the author prefers the former sequence because the pentagonal bipy-

ramid is a recognizable unit for all the boundaries in the sequence between $\Sigma 1$ and $\Sigma 3$. The favored boundaries are then those short period boundaries that are compossed of one structural unit only. Thus, a study of the short period boundaries in a given range gives all the possible structural units in that range. A structural unit description for a long period boundary can then be predicted by use of decompositions such as those shown in sections 4.2 and 4.4. The decomposition gives the number of structural units from each favored boundary, and their arrangement can be determined by requiring that the distance between minority units be maximized. The structural unit model is a powerful tool for predicting the structure of grain boundaries once the structure of a few short period boundaries is known.

6.2. Comments on Grain Boundary Processes

The structural unit model has some important implications on the physical behavior of grain boundaries. In particular, the problem of grain boundary segregation which causes significant engineering problems is discussed. First, the experimental data in section 1.3 is discussed.

The favored boundaries represent cusps in the energy versus misorientation curve. This arises from the fact that minority units represent stress concentrations in the boundary. Since the favored boundaries are compossed of only type of unit, they have lower energy than the intervening boundaries. It can be predicted then that $\Sigma 5$ should be a minima in the energy versus misorientation curve for [100] tilt boundaries. This agrees with the results in Fig. 1.3.2. Similarly $\Sigma 9$ and $\Sigma 3$ should be energy minima for the [110] boundaries. This agrees with the results discussed in section 1.3; however, the minima at $\Sigma 51$ and $\Sigma 19$ are not predicted by the structural unit model. Other cusps in a property versus misorientation curve can arise because the degree of distortion of the structural units is small. These cannot be predicted by the structural unit model but they usually occur in coincidence boundaries and small-angle boundaries. However, it should be noted that those boundaries that are shown to have special properties by the structural unit model, always satisfy that prediction.

One of the more important aspects that result from this investigation is the existence of structures that are related by the addition or removal of one layer of atoms parallel to the boundary. Although the discussion that follows concentrates on the addition of a layer per period as would occur in grain boundary segregation, the problem of formation of substitutional point defects at the boundary can be described by the inverse phenomenon of removal of one layer per period of the boundary.

Segregation occurs then simply by adding one atom per boundary period. The sequence of structural units for a period without segregation will be indicated by a U, and the sequence of units in a period where segregation has occured by S. The U periods and S periods have the same excess volume. Thus the two structures have different in-plane translations. This implies that at the region where an U unit joins a S unit, a partial grain boundary dislocation with Burgers vector equal to the difference in translations exist. Since this defect has an energy associated with it, segregation would tend to occur in such a way that the number of these defects is minimized. Under non-equilibrium conditions segregation occurs randomly along the boundary as the segregating atom species arrive at the boundary plane. Upon annealing U units and S units will cluster to minimize the energy associated with the partial grain boundary dislocations. This implies that changes in concentration along the boundary plane should occur, and that the clusters of S units are preferential sites for the heterogeneous nucleation of second faces or for crack nucleation due to fragility at the boundary plane induced by the segregating species. The existence of partial grain boundary dislocations has been observed experimentally very recently.[1] Variations of the concentration of a segregating species along the boundary plane have also been reported.[2]

Since grain boundaries are shown to be composed of a small number of different polyhedra, it is possible to study the effect of an impurity atom in an isolated polyhedra. For example, electron densities in a tetragonal dodecahedron of nickel atoms with one sulphur atom show that strong bonds form between the nickel atoms and the sulphur while simultaneously weakening the nickel-nickel bonds.[3] If the weak nickel-nickel bonds occur across the boundary plane the grain boundary would be fragile.

An important aspect that should be treated in future calculations is the influence of the structural unit distortions in the electron densities. The polyhedra model provides a considerable simplification to the problem of studying grain boundary structure and properties.

6.3. References

[1] C. T. Forwood and L. M. Clarebrough, *Phil. Mag.* **51A** , 589 (1985).

[2] J. Briceno-Valero and R. Gronsky, in *Solid-Solid Phase Transformations* , H. I. Aaronson, D. E. Laughlin, R. F. Sekerka, and C. M. Wayman (eds.), The Metallurgical Society of AIME, Warrendale, Pa, 1982, p.439.

[3] C. L. Briant and R. P. Messmer, *Phil. Mag.* **42B** , 569 (1980).

7. ACKNOWLEDGEMENTS

This work is the fruit of many years of education and research. In closing these pages, I would like to acknowledge the contributions, over those years, of many people.

This work would not have been possible without the support, encouragement and scientific guidance of my research supervisor Professor Ron Gronsky. Besides the scientific and technical matters pertaining to this investigation Ron has extended his teachings to other materials science problems, the thought and problem solving processes, and the politics and sociology of doing research.

Professor Russell Chou of Lehigh University has kindly provided me with the bicrystals needed for this research. Unfortunately, it has proven very difficult to get HREM results from the Nb bicrystals. Sorry, Russell. However, since the problems seem surmountable, this work will be retaken in the near future.

I would like to thank all of my associates in the Gronsky group and at the National Center for Electron Microscopy for their friendship and many useful discussions. In particular I would like to thank my friend and former officemate, Jim Howe, for much small talk and many useful scientific discussions, and to Kannan Krishnan for many cups of coffee over science and the politics of science.

To Roar (and Char), Jamie (and Eileen), and Mike and Roseann whose friendship will remain; thanks for all the fun. You are a class apart.

To Mom and Dad just for that. Also for their support and in particular for their wisdom in getting me into that plane to the U.S. And, gee!; a few years later a Ph.D. from Berkeley.

This report was done with support from the Department of Energy. Any conclusions or opinions expressed in this report represent solely those of the author(s) and not necessarily those of The Regents of the University of California, the Lawrence Berkeley Laboratory or the Department of Energy.

LAWRENCE BERKELEY LABORATORY
TECHNICAL INFORMATION DEPARTMENT
UNIVERSITY OF CALIFORNIA
BERKELEY, CALIFORNIA 94720